

**TEMPLATING INORGANIC MATERIALS  
WITH BLOCK POLYMER THIN FILMS  
AND  
CATALYZING MILITARY JET FUEL TO LIQUEFIED PETROLEUM GAS**

by

Michael Kai Mayeda

A dissertation submitted to the Faculty of the University of Delaware in partial fulfillment of the requirements for the degree of Doctor of Philosophy in Chemical Engineering

Summer 2016

© 2016 Michael Kai Mayeda  
All Rights Reserved

ProQuest Number: 10192663

All rights reserved

INFORMATION TO ALL USERS

The quality of this reproduction is dependent upon the quality of the copy submitted.

In the unlikely event that the author did not send a complete manuscript and there are missing pages, these will be noted. Also, if material had to be removed, a note will indicate the deletion.



ProQuest 10192663

Published by ProQuest LLC (2016). Copyright of the Dissertation is held by the Author.

All rights reserved.

This work is protected against unauthorized copying under Title 17, United States Code  
Microform Edition © ProQuest LLC.

ProQuest LLC.  
789 East Eisenhower Parkway  
P.O. Box 1346  
Ann Arbor, MI 48106 - 1346

**TEMPLATING INORGANIC MATERIALS**  
**WITH BLOCK POLYMER THIN FILMS**  
**AND**  
**CATALYZING MILITARY JET FUEL TO LIQUEFIED PETROLEUM GAS**

by

Michael Kai Mayeda

Approved: \_\_\_\_\_  
Abraham M. Lenhoff, Ph.D.  
Chair of the Department of Chemical and Biomolecular Engineering

Approved: \_\_\_\_\_  
Babatunde A. Ogunnaike, Ph.D.  
Dean of the College of Engineering

Approved: \_\_\_\_\_  
Ann L. Ardis, Ph.D.  
Senior Vice Provost for Graduate and Professional Education

I certify that I have read this dissertation and that in my opinion it meets the academic and professional standard required by the University as a dissertation for the degree of Doctor of Philosophy.

Signed:

---

Thomas H. Epps, III, Ph.D.  
Professor in charge of dissertation

I certify that I have read this dissertation and that in my opinion it meets the academic and professional standard required by the University as a dissertation for the degree of Doctor of Philosophy.

Signed:

---

Jochen A. Lauterbach, Ph.D.  
Professor in charge of dissertation

I certify that I have read this dissertation and that in my opinion it meets the academic and professional standard required by the University as a dissertation for the degree of Doctor of Philosophy.

Signed:

---

Raul F. Lobo, Ph.D.  
Member of dissertation committee

I certify that I have read this dissertation and that in my opinion it meets the academic and professional standard required by the University as a dissertation for the degree of Doctor of Philosophy.

Signed:

---

Brian C. Benicewicz, Ph.D.  
Member of dissertation committee

## ACKNOWLEDGMENTS

First and most importantly, I would like to thank my co-advisors Thomas H. Epps, III and Jochen Lauterbach. Their patience, wisdom, and empathy are without parallel. Thomas' favorite question, "why?" has instilled an innate curiosity that will permeate my thought processes, in perpetuity. Jochen's impressive ability to accomplish work-family obligations leaves one believing that there are more than twenty-four hours in a German day. Most students are not fortunate enough to have two advisors, much less three. I thank my life-advisor and wife, Donna. Donna guides me through everything from egg-roll rolling to mother cajoling; without her I would truly be lost.

No dissertation is a one-student effort. I would like to thank current *and* past members of the Epps and Lauterbach research groups; I am standing on the shoulders of giants. A comprehensive list would be exhausting, but a handful of people need to be acknowledged. In no particular order and not limited to the Epps and Lauterbach groups: J. Albert, née Lawson, M. Tureau, O. Young, S. Mastroianni, E. Kelley, W.F. Kuan, J. Seppala, S. Traylor, S. Kim, E. Sasmaz, J. Bedenbaugh, C. Hardy, A. Viswanath, J. Hayat, A. Foster née Palmer, A. Foster, and E. Balogh.

Last and certainly not least, I would like to thank my friends and family from home. "Home" includes Hawai'i, California, Delaware, and South Carolina. Without them, nothing could be possible.

## TABLE OF CONTENTS

LIST OF TABLES .....	x
LIST OF FIGURES .....	xi
ABSTRACT .....	xxi

### Chapter

1	BLOCK POLYMER TEMPLATING AND FUEL CONVERSION CATALYSIS: OVERVIEW AND APPLICATIONS.....	1
1.1	Introduction .....	1
1.1.1	Nanoparticles in Block Polymer Templates .....	1
1.1.1.1	<i>In situ</i> Synthetic Methods .....	2
1.1.1.2	<i>Ex situ</i> Synthetic Methods .....	5
1.1.1.2.1	Enthalpic Considerations .....	6
1.1.1.2.2	Entropic Considerations .....	7
1.1.2	Introduction to Block Polymers.....	9
1.1.2.1	Block Polymer Thin Films .....	14
1.1.3	Templating Inorganics with Block Polymers .....	17
1.1.3.1	<i>In Situ</i> Templating .....	18
1.1.3.2	<i>Ex Situ</i> Templating .....	21
1.1.3.3	Applications in Photocatalysis .....	23
1.1.4	Catalytic Fuel Conversion Applications.....	25
1.1.4.1	Applications in Developing Countries .....	26
1.1.4.2	Defense Applications.....	29
1.1.4.3	Fuel Conversion Devices - Current State .....	30
1.1.4.4	Monomolecular Fuel Conversion .....	31
1.2	Thesis Overview .....	32



3.2.8	TEM Tomography (TEMT) .....	88
3.3	Results .....	89
3.4	Discussion.....	96
3.5	Conclusions .....	102
3.6	Acknowledgements .....	103
REFERENCES .....		104
4	METAL OXIDE ARRAYS FROM BLOCK POLYMER THIN FILM TEMPLATES .....	109
4.1	Introduction .....	109
4.2	Experimental Section.....	112
4.2.1	Materials .....	112
4.2.2	Templating procedure.....	113
4.2.2.1	Spincoating films .....	114
4.2.2.2	Pattern formation .....	115
4.2.2.3	Immersion and metal complexation .....	115
4.2.2.4	EISA TiO <sub>2</sub> .....	116
4.2.2.5	Etching template .....	116
4.2.2.6	Gold nanoparticle addition .....	116
4.2.3	Film characterization .....	116
4.2.4	Photocatalysis experiments .....	117
4.3	Results .....	118
4.4	Conclusions .....	126
4.5	Acknowledgements .....	127
REFERENCES .....		128
5	SUMMARY AND FUTURE WORK FOR NANOSTRUCTURED THIN FILMS .....	133
5.1	Summary.....	133
5.2	Recommendations for Future Work .....	135
5.2.1	Top-Down Metal-assisted Chemical Etching.....	136
5.2.2	Bottom-Up Applications .....	141
5.2.2.1	Seed-mediated Growth .....	142

5.2.2.2	Pattern Propagation .....	144
5.2.3	Pluronic™ Materials in SPICE .....	146
5.2.4	Additional Catalytic Reactions.....	146
5.3	Conclusions .....	148
5.4	Acknowledgements .....	148
REFERENCES .....		149
6	OPTIMIZING A CATALYTIC FUEL CONVERTER .....	156
6.1	Introduction .....	156
6.1.1	Past Project Objectives and Solutions .....	158
6.1.2	Current Project Objectives .....	160
6.2	Experimental Section.....	162
6.3	Results and Construction.....	164
6.4	Discussion.....	170
6.5	Device Construction and Operation .....	173
6.6	Conclusions .....	174
6.7	Acknowledgements .....	176
REFERENCES .....		177
7	SUMMARY AND FUTURE WORK FOR A FUEL CONVERTER .....	181
7.1	Summary.....	181
7.2	Recommendations for Future Work in Commercializing a Fuel Converter .....	182
7.2.1	Customer Segment Development .....	183
7.2.1.1	Tailgating at Sports Events.....	184
7.2.1.2	Disaster Relief Agencies .....	187
7.2.1.3	Military Field Kitchens.....	190
7.2.1.4	Military Portable-Fuel Cell System Integrators .....	195
7.2.1.5	Other Customer Segments .....	198
7.2.2	Future Technical Considerations.....	200
7.2.2.1	Safety .....	200
7.2.2.2	Thermal Management.....	202

7.2.2.3	Military Specifications .....	204
7.2.3	Obstacles and Recommendations for Commercialization.....	205
7.3	Conclusions .....	206
7.4	Acknowledgements .....	207
REFERENCES .....		208
Appendix		
A	SUPPORTING INFORMATION FOR CHAPTER 3 .....	213
A.1	Ligand Exchanges .....	213
A.2	<sup>1</sup> H NMR Spectra.....	214
A.3	<sup>1</sup> H MAS-NMR Spectra.....	215
A.4	Gold Nanoparticle Size Characterization .....	216
A.5	Thermally Annealed Nanocomposites .....	217
A.6	TEM Micrographs .....	219
A.7	Tomogram Movie.....	221
B	SUPPORTING INFORMATION FOR CHAPTER 4 .....	222
B.1	AFM of Metal Oxides .....	222
B.2	XPS of Metal Oxides.....	225
B.3	Titania Loading .....	226
B.4	Methylene Blue Catalysis.....	227
B.5	TiO <sub>2</sub> Dispersion.....	229
C	SUPPORTING INFORMATION FOR CHAPTER 5 .....	231
D	COPYRIGHT PERMISSIONS .....	233

## LIST OF TABLES

Table 1.1:	Reaction constants for chelating Cu <sup>2+</sup> with PVFP or pyridine. Adapted with permission from Nishikawa, H. and Tsuchida, E. <i>J. Phys. Chem.</i> 1975, 79, (19), 2072-2076. Copyright 1975 American Chemical Society. ....	3
Table 1.2:	Flory-Huggins interaction parameters for common block polymer systems. ....	12
Table 2.1:	Molar and mass feed ratios for ligand exchange reactions .....	56
Table 3.1	Hildebrand solubility parameters and surface energies of relevant compounds.....	98
Table 4.1.	Photocatalytic conditions and rate constants.....	125
Table 6.1.	Approximate energy densities and power densities of battlefield power sources and civilian power sources for comparison. ....	157
Table 6.2.	Summary of quantitative objectives for converting JP-8 to C <sub>2</sub> -C <sub>4</sub> hydrocarbons. Adapted with permission from Bedenbaugh, J.E. Ph.D. Dissertation, University of Delaware, Newark, 2012. ....	159
Table 6.3:	Normalized integrated peak areas from <sup>1</sup> H NMR spectra in Figure 6.3. Peak areas were normalized to the methyl proton peak near 0.75 ppm. ....	166
Table A.1.	Molar and mass feed ratios for ligand exchange reactions .....	213
Table B.1.	XPS peak positions and associated full width half maxima (FWHM)..	225

## LIST OF FIGURES

- Figure 1.1: Polymer chains bound to a SiO<sub>2</sub> nanoparticle *via* (top) grafting-to and (bottom) grafting-from. The grafting-to approach is performed using an alkyne-azide click reaction. The grafting-from is performed with a surface-bound initiator that is a precursor to tethered polymer chains. Adapted with permission from Achilleos, D. S.; Vamvakaki, M. *Materials* 2010, 3, (3), 1981-2026. .... 7
- Figure 1.2: Phase diagram for a diblock polymer showing close packed spheres (S<sub>cp</sub>, not shown), body-centered cubic spheres (S), hexagonally packed cylinders (C), continuous gyroid network (G), *Fddd* orthorhombic network (O<sup>70</sup>, not shown), lamellae (L), and their respective inverted structures (O<sup>70'</sup>, G', C', S', S<sub>cp'</sub>). The dot marks a mean-field critical point and the diamonds mark triple points. The phase diagram was adapted with permission from Matsen, M. W. *Macromolecules* 2012, 45(4), 2161-2165. Copyright 2012, American Chemical Society. Unit cell illustrations were adapted with permission from Bates, F. S.; Fredrickson, G. H. *Phys. Today* 1999, 52, (2), 32-38. Copyright 1999, American Institute of Physics..... 13
- Figure 1.3: Schematic of a lamellae-forming diblock polymer (red-blue) thin film, not to scale. For a film of thickness  $t$ , surface relief structures form (a) holes or (c) islands when film thicknesses are incommensurate with the domain spacing,  $L_0$ . Otherwise, commensurate films can exhibit (b) symmetric or (d) asymmetric wetting depending on the block affinities for the substrate and free-surface. .... 15
- Figure 1.4: Substrate effect on thin film orientation and order. (a) The substrate surface chemistry can induce (i) preferential wetting or (ii) a neutral interaction, which would lead to a perpendicular orientation. (b) Patterned substrates direct the self-assembly into (i) well-ordered structures; whereas films on (ii) unpatterned substrates exhibit considerably more grain boundaries and defects. (b) Adapted with permission from Macmillan Publishers Ltd: Nature. Kim, S. O.; Solak, H. H.; Stoykovich, M. P.; Ferrier, N. J.; de Pablo, J. J.; Nealey, P. F. *Nature* 2003, 424, (6947), 411-414. Copyright 2003 ..... 17

Figure 1.5:	(a) Schematic of the evaporation-induced self-assembly process and (b) a transmission electron microscope image of a mesoporous carbon product; inset image is a diffractogram. In both (a) and (b), the cubic phases are shown, but numerous other mesostructures can be formed. (a) was adapted from Pan, J. H.; Zhao, X. S.; Lee, W. I. <i>Chem. Eng. J.</i> 2011, 170, (2-3), 363-380, copyright 2011, with permission from Elsevier. (b) was adapted with permission from Deng, Y. H.; Yu, T.; Wan, Y.; Shi, Y. F.; Meng, Y.; Gu, D.; Zhang, L. J.; Huang, Y.; Liu, C.; Wu, X. J.; Zhao, D. Y. <i>J. Am. Chem. Soc.</i> 2007, 129, (6), 1690-1697. Copyright 2007 American Chemical Society.....	18
Figure 1.6:	Atomic force microscopy images of iron oxide nanoparticles made from (a) a one-pot approach, (b) a solution of homopolymer-iron complexes and block polymer micelles, and (c) gold nanoparticles from a neat block polymer thin film template. Inset images for (a) and (b) show respective auto-covariance functions. (a) and (b) were adapted with permission from Shan, L.; Punniyakoti, S.; Van Bael, M. J.; Temst, K.; Van Bael, M. K.; Ke, X.; Bals, S.; Van Tendeloo, G.; D'Olieslaeger, M.; Wagner, P.; Haenen, K.; Boyen, H.-G. <i>J. Mater. Chem. C</i> 2014, 2, (4), 701-707. Copyright 2014 Royal Society of Chemistry. (c) was adapted with permission from Cho, H.; Park, H.; Russell, T. P.; Park, S. <i>J. Mater. Chem.</i> 2010, 20, (24), 5047-5051. Copyright 2010 Royal Society of Chemistry. ....	20
Figure 1.7:	Gold and silica nanoparticles were templated in an <i>ex situ</i> fashion. Gold nanoparticles segregated to the PS/PEP interface while silica particles segregated to the centers of the PEP domains. Adapted with permission from Bockstaller, M. R.; Lapetnikov, Y.; Margel, S.; Thomas, E. L. <i>J. Am. Chem. Soc.</i> 2003, 125, (18), 5276-5277. Copyright 2003 American Chemical Society.....	23
Figure 1.8:	Liquid and gaseous petroleum production consumption represented as a percentage of the world's respective consumption. Data were obtained from US Energy Information Administration. ....	27
Figure 1.9:	Map of allowable sulfur content in diesel fuel according to government regulations. Reprinted with permission from the United Nations Environment Programme – Partnership for Clean Fuels and Vehicles. <sup>278</sup> .....	28
Figure 2.1:	Tapping mode AFM scans an oscillating tip just above the surface of the sample with a height profile and varying material composition with differing moduli ( <i>i.e.</i> , red or blue). Top axes illustrate the recorded height profile while the bottom axes show the phase profile. ..	65

Figure 2.2:	Path of an electron beam through a sample with varying mass-thickness in a transmission electron microscope. Sample regions with low mass-thickness easily transmit electrons; thus, bright areas are produced. Sample regions with high mass-thickness absorb or scatter incident electrons that may be cut out by the aperture; thus, dark areas are produced. Adapted with permission from Dr. Frank Krumeich, copyright 2012 ETH Zürich. ....	67
Figure 2.3:	Polymer thin film peeling procedure starts with (a) depositing a thin layer of amorphous carbon <i>via</i> thermal evaporation, (b) depositing a droplet of an aqueous solution of poly(acrylic acid) and allowing it to dry in ambient conditions, and (c) peeling the dried poly(acrylic acid) from the substrate and dissolving it in a large volume of water.....	69
Figure 2.4:	Traditional transmission electron micrographs are (a) 2D images of 3D objects, which can lead to (b) ambiguous interpretations regarding out-of-plane orientations. ....	71
Figure 2.5:	Grid shadowing and sample opacity typically limit single-axis tilt acquisitions (left) to $\pm 60^\circ$ . Meanwhile, stage drift and beam-induced sample degradation place an upper limit on the acquisition time and thus a lower limit on the tilt resolution $\Delta\theta$ . The “missing wedge” reduces resolution during tomogram reconstruction. Dual-axis tilt acquisitions result in improved tomograms by minimizing the missing wedge to a “missing pyramid.” .....	72
Figure 2.6:	(a) The 2D projections from the tilted sample are (b) back projected along the same tilt angle. Colors are used to differentiate the super-positioned back projections. (c) A simple summation of the 2D projections yields a tomogram that mimics the original 3D object but with a low-frequency background. (d) A <i>R</i> -weighted scheme is used to reduce the background and enhance the tomogram reconstruction. ....	74
Figure 3.1:	AFM phase images of SIS films (a) as-cast and (b) annealed with THF solvent vapor. Nanocomposite films exhibited similar ordering and grain sizes for as-cast and annealed samples. Bright regions indicated PS-rich domains while dark regions indicated PI-rich domains. Reprinted with permission from Mayeda <i>et al.</i> , <i>Chemistry of Materials</i> , 2012, 24(14), 2627-2634. <sup>1</sup> .....	90

- Figure 3.2:  $^1\text{H}$  NMR spectroscopy of ligand exchange products in deuterated chloroform. Spectra were normalized to integrated areas associated with  $\text{C}_{12}\text{SH}$  between 1 - 1.4 ppm. Peaks between 6.3 - 7.3 ppm, associated with the phenyl group in PS-SH, were compared with the 1 - 1.4 ppm peak, associated with the hydrocarbon chain in  $\text{C}_{12}\text{SH}$ .  $\text{C}_{12}\text{SH}:\text{PS-SH}$  ratios of the spectra shown were calculated to be 2.7:1, 4.8:1, and 5.1:1. Reprinted with permission from Mayeda *et al.*, *Chemistry of Materials*, 2012, 24(14), 2627-2634.<sup>1</sup> ..... 91
- Figure 3.3: TEM micrographs of  $\text{OsO}_4$  stained and unstained (insets) (a) SIS and (b)  $\text{Au}_\infty\text{NP}/\text{SIS}$  thin films after THF annealing. Micrographs of stained samples show PS (light) and PI (dark) domains oriented parallel to the plane of the film. The micrograph in (b) reveals  $\text{Au}_\infty\text{NPs}$  (dark spots) with an affinity for PI over PS domains. The inset of (b) shows inhomogeneous distribution of  $\text{Au}_\infty\text{NPs}$ , which indicates a polymer domain preference. Reprinted with permission from Mayeda *et al.*, *Chemistry of Materials*, 2012, 24(14), 2627-2634.<sup>1</sup> ..... 93
- Figure 3.4: TEM micrographs of  $\text{OsO}_4$  stained nanocomposite films of (a)  $\text{Au}_{5.1}\text{NP}/\text{SIS}$ , (b)  $\text{Au}_{4.8}\text{NP}/\text{SIS}$ , (c)  $\text{Au}_{2.7}\text{NP}/\text{SIS}$ , and (d) mix of  $\text{Au}_\infty\text{NP}/\text{Au}_{2.7}\text{NP}/\text{SIS}$  after annealing with saturated THF vapor. Inset images show corresponding unstained samples at the same magnification. All nanocomposite films contained 0.4 vol% AuNPs; the sample represented in (d) contained approximately equal volume loadings of  $\text{Au}_\infty\text{NPs}$  and  $\text{Au}_{2.7}\text{NPs}$ .  $\text{Au}_{5.1}\text{NPs}$  in (a) exhibit an affinity for the PI domain while  $\text{Au}_{4.8}\text{NPs}$  in (b) and  $\text{Au}_{2.7}\text{NPs}$  in (c) show affinities for the PS domains. Unstained images (see insets) suggest AuNP segregation. The mixture of  $\text{Au}_\infty\text{NPs}$  and  $\text{Au}_{2.7}\text{NPs}$  in (d) shows no visible domain preference, and the unstained image (inset) indicates a well-mixed nanocomposite. Reprinted with permission from Mayeda *et al.*, *Chemistry of Materials*, 2012, 24(14), 2627-2634.<sup>1</sup> ..... 94
- Figure 3.5: x-y plane (a) and x-z plane (b) views of a reconstructed tomogram of unstained  $\text{Au}_{4.5}\text{NP}/\text{SIS}$  after THF annealing. The x-z plane view is taken along the dotted blue line. The sample contains approximately 0.4 vol%  $\text{Au}_{4.5}\text{NP}$  loading. Considered together, (a) and (b) show that the  $\text{Au}_{4.5}\text{NPs}$  show an affinity for one polymer domain and do not segregate to the film interfaces nor the polymer-polymer interfaces. Reprinted with permission from Mayeda *et al.*, *Chemistry of Materials*, 2012, 24(14), 2627-2634.<sup>1</sup> ..... 96

- Figure 3.6: Graphical representation of Au<sub>5</sub>NPs indicating (a) approximate length differences between C<sub>12</sub>SH and PS-SH and (b) effective ligand surface coverage. Reprinted with permission from Mayeda *et al.*, *Chemistry of Materials*, 2012, 24(14), 2627-2634.<sup>1</sup> ..... 100
- Figure 4.1: The spincoat-pattern-immersed-complex-etch (SPICE) templating method decouples polymer annealing from the metal precursor gel incorporation. Traditional methods, represented by EISA, spincoat an all-in-one solution that includes both polymer and metal precursor. Although EISA has fewer steps, it produces irregular arrays of inorganic material. High-humidity annealing was achieved by using standard solvent annealing techniques enclosed in a humidified glove box. Reprinted with permission from Mayeda *et al.*, *Journal of Materials Chemistry A*, 2015, 3(15), 7822-7829 – Published by the Royal Society of Chemistry.<sup>1</sup> ..... 114
- Figure 4.2: Atomic force microscopy height images of PS-*b*-PEO films after solvent vapor annealing with (a) toluene and (b) toluene/water. TiO<sub>2</sub> arrays were templated by (c) EISA and (d) SPICE; and (e) AuNPs were spincoated onto templated SPICE TiO<sub>2</sub>. Inset images are FFTs of the AFM images. Scale bars represent 200 nm. (f) Line scans show height profiles of the TiO<sub>2</sub> made by the SPICE (green, bottom) and EISA (blue, top) methods. Reprinted with permission from Mayeda *et al.*, *Journal of Materials Chemistry A*, 2015, 3(15), 7822-7829 – Published by the Royal Society of Chemistry.<sup>1</sup> ..... 119
- Figure 4.3: Transmission electron micrograph of (a) EISA (Ti precursor) films after annealing with toluene/water vapor and (b) toluene vapor as compared to a (c) SPICE Ti precursor film. Images are unstained; contrast is afforded by the electron density difference between PEO-titanium complex (dark) and PS (light). The scale bars represent 100 nm. Reprinted with permission from Mayeda *et al.*, *Journal of Materials Chemistry A*, 2015, 3(15), 7822-7829 – Published by the Royal Society of Chemistry.<sup>1</sup> ..... 122
- Figure 4.4: Plot of the natural log of MB concentrations against UV irradiation time. Error bars on data points represent standard deviations across three reproducibility studies. The slopes represent rate constants, which are reported in Table 4.1. The magnitude of  $k_{dark}$  was taken to be the error on the rate constants. Reprinted with permission from Mayeda *et al.*, *Journal of Materials Chemistry A*, 2015, 3(15), 7822-7829 – Published by the Royal Society of Chemistry.<sup>1</sup> ..... 124

Figure 5.1: Schematic depicting the use of nanoscale arrays in bottom-up (left) and top-down (right) processes. ....	135
Figure 5.2: Diagram depicting (a, c, e) a noble metal coated on a silicon substrate and the resulting (b) nanopores, (d) nanowires, and (f) nanorods after etching. Adapted with permission from Huang, Z.; Geyer, N.; Werner, P.; de Boor, J.; and Gösele, U. <i>Adv. Mater.</i> , 2011, 23, 285-308. Copyright 2011 Wiley-VCH. ....	137
Figure 5.3: (a) AFM phase image of a toluene-annealed AuNP/SIS film, (b) AFM height image of the film in (a) after PI removal by ozone etching, and AFM height images (c) and (d) of AuNP chains after complete UVO etching. The height scale applies to b-d. The scale bars in a-c represent 200 nm while the scale bar in (d) represents 50 nm. (e) The histogram shows the size distributions of AuNPs before and after UVO treatment of the nanocomposite thin film. ....	138
Figure 5.4: Increasing the molecular weight of the PS- <i>b</i> -PEO template to 25.5 kg/mol (left) increased the resulting radius of the produced TiO <sub>2</sub> nanodots (right) to 11.3 ± 1 nm. ....	142
Figure 5.5: AFM phase image of (a) Fe <sub>2</sub> O <sub>3</sub> arrays, (b) carbon nanotubes grown using (a), (c) SnO <sub>2</sub> arrays, and (d) carbon nanotubes grown from (c). Nanotubes were grown by chemical vapor deposition. Scale bars represent 300 nm. ....	143
Figure 5.6: (a) SPICE-generated features are the basis for (b) an orthogonally self-assembled monolayer. (c) A subsequent BP film with similar domain sizes is cast on the modified substrate and (d) annealed to yield the substrate-propagated pattern through the film. ....	145
Figure 5.7: AFM phase image of a ceria-zirconia dot array made by the SPICE method. The scale bar represents 500 nm. ....	147
Figure 6.1: Flow diagram of jet fuel conversion system. An inert gas used to push the evaporated reactant fuel through a single reactor. Reaction products were separated from the unreacted fuel <i>via</i> condensation. The liquid product was discarded while the gaseous product was analyzed for purity. ....	159

Figure 6.2:	Fuel conversion efficiency as a function of time using a single-pass and a recycling approach. Reactions were performed at 450 °C using a 0.3 mL/h total liquid flowrate ( <i>i.e.</i> , 0.15 mL <sub>JP-8</sub> /h and 0.15 mL <sub>condensed</sub> /h for recycling or 0.3 mL <sub>JP-8</sub> /h for single-pass). The author would like to acknowledge Dr. Sungtak Kim for performing the conversion experiments. ....	165
Figure 6.3:	<sup>1</sup> H NMR spectra of fresh JP-8, post-reaction condensed liquid, and post-recycle reaction condensed liquid. Spectra were normalized to the methyl proton peak near 0.75 ppm. The inset image shows a magnified view of the aromatic region (6.5 – 7.5 ppm). All spectra were vertically offset for comparison purposes. Intensity was measured in arbitrary units. The peak near 7.26 ppm is from the deuterated chloroform used in the measurement. ....	166
Figure 6.4:	GC data of JP-8, condensed liquid after cracking JP-8, and condensed liquid after implementing a recycle loop while cracking JP-8. Spectra were vertically offset. Toluene and C <sub>9</sub> -C <sub>13</sub> <i>n</i> -paraffins are labeled; ▼ symbols mark aromatic hydrocarbons in the condensed and recycled liquid that are distinguishable from nearby linear hydrocarbons in JP-8. ....	167
Figure 6.5:	Fuel conversion efficiency with and without the carrier gas (helium). The author would like to acknowledge Dr. Sungtak Kim for performing the conversion experiments. ....	169
Figure 6.6:	Current-voltage curves for the P250i solid oxide fuel cell stack performance on commercial propane and the gas product from gasoline conversion. The author would like to acknowledge Dr. Tom Westrich for performing the conversion experiments. ....	170
Figure 6.7:	Current block diagram of the prototype fuel converter. Significant changes include the absence of a carrier gas, low-power condenser system, and a recirculating reactant feed. ....	175
Figure 7.1:	Map of the US indicating the responses from state directors of disaster relief. Grey states did not respond, red states indicated “no,” and green states indicated “yes.” ....	189
Figure 7.2:	The M2 military burner viewed from the (a) side and (b) underside, which clearly shows the u-shaped fuel tank. Images are reproduced with permission from the photographer. Images were originally posted on <a href="http://www.spiritburner.com">www.spiritburner.com</a> . ....	192

Figure 7.3:	The modern burner unit produced by Proheat. Image was adapted and reproduced with permission from Marine Canada Acquisition Inc., doing business as SeaStar Solutions.....	193
Figure 7.4:	Commercial SOFC systems have been designed to operate on propane (top). Without propane in the battlefield, a fuel converter would be necessary to utilize field-available JP-8 (bottom). .....	196
Figure A.1:	$^1\text{H}$ NMR spectroscopy of ligand exchange products in deuterated chloroform. Spectra were normalized to integrated areas associated with $\text{C}_{12}\text{SH}$ between 1 - 1.4 ppm. Peaks between 6.3 - 7.3 ppm, associated with the phenyl group in PS-SH, grow with decreasing $\text{C}_{12}\text{SH}:\text{PS-SH}$ ratios while the peak between 1.0 - 1.4 ppm, associated with the $\text{C}_{12}\text{SH}$ hydrocarbon chain, remains relatively constant. $\text{C}_{12}\text{SH}:\text{PS-SH}$ ratios of the spectra shown were 2.7:1, 2.8:1, 3.1:1, 4.1:1, 4.8:1, 5.1:1, and 6.6:1. Reprinted with permission from Mayeda <i>et al.</i> , <i>Chemistry of Materials</i> , 2012, 24(14), 2627-2634.....	214
Figure A.2:	Comparison of $^1\text{H}$ spectra obtained via conventional NMR (black line) and MAS-NMR (red line). Reprinted with permission from Mayeda <i>et al.</i> , <i>Chemistry of Materials</i> , 2012, 24(14), 2627-2634.....	215
Figure A.3:	TEM micrographs of AuNPs (a) as-synthesized and (b) after a typical ligand exchange with PS-SH. The AuNPs were mounted on a lacey carbon grid for imaging. Insets present histograms generated using ImageJ. Histograms indicate that AuNPs do not appreciably change size ( $3.5 \pm 0.6$ nm) following ligand exchange. The scale bar corresponds to 20 nm. Reprinted with permission from Mayeda <i>et al.</i> , <i>Chemistry of Materials</i> , 2012, 24(14), 2627-2634.....	216
Figure A.4:	Transmission electron micrographs of $\text{OsO}_4$ stained and unstained (insets) nanocomposite thin films after thermal annealing at $120^\circ\text{C}$ for 4 hours, (a) $\text{Au}_\infty\text{NP/SIS}$ and (b) $\text{Au}_{2.7}\text{NP/SIS}$ . Scale bars correspond to 100 nm; insets are presented at the same magnification. The micrograph in (a) contain globular gold aggregates with affinities for the PI domains. The micrograph in (b) contains AuNP aggregates ( $4 \pm 2$ nm) that preferentially segregate to the PS domains. Reprinted with permission from Mayeda <i>et al.</i> , <i>Chemistry of Materials</i> , 2012, 24(14), 2627-2634. ....	217

- Figure A.5: TEM micrographs of OsO<sub>4</sub> stained (a) Au<sub>6.6</sub>NP/SIS, (b) Au<sub>5.1</sub>NP/SIS, (c) Au<sub>4.8</sub>NP/SIS, (d) Au<sub>4.5</sub>NP/SIS, (e) Au<sub>4.1</sub>NP/SIS, (f) Au<sub>3.1</sub>NP/SIS, (g) Au<sub>2.8</sub>NP/SIS, (h) Au<sub>2.7</sub>NP/SIS, (i) Au<sub>∞</sub>NP/Au<sub>2.7</sub>NP/SIS. Scale bars correspond to 100 nm. Inset images are unstained and at the same magnification. In micrographs a-h, unstained images confirm AuNP segregation. AuNPs do not show preference for one polymer domain in (i), which highlights the stability of the gold-thiol bond. Reprinted with permission from Mayeda *et al.*, *Chemistry of Materials*, 2012, 24(14), 2627-2634. .... 221
- Figure B.1: AFM height images of metal oxides templated by the SPICE method: (a) MgO, (b) Al<sub>2</sub>O<sub>3</sub>, (c) MnO<sub>2</sub>, (d) Fe<sub>2</sub>O<sub>3</sub>, (e) Co<sub>3</sub>O<sub>4</sub>, (f) NiO, (g) CuO, (h) ZnO, (i) ZrO<sub>2</sub>, (j) SnO<sub>2</sub>, (k) Ce<sub>2</sub>O<sub>3</sub>, and (l) RuO<sub>2</sub>. Insets are FFTs of the entire image. Scale bars represent 200 nm. Reprinted with permission from Mayeda *et al.*, *Journal of Materials Chemistry A*, 2015, 3(15), 7822-7829. .... 224
- Figure B.2: Representative UV-vis spectra of MB photocatalytically degraded by SPICE TiO<sub>2</sub>. MB solutions were exposed to catalyst and UV irradiation in UV-transparent cuvettes. Spectra were collected in two hour intervals. Inset contains the entire UV-vis spectra of a MB aqueous solution. The peaks between 550-750 nm (solid) were used to evaluate the photocatalytic activity of SPICE TiO<sub>2</sub>, EISA TiO<sub>2</sub>, and Au/SPICE-TiO<sub>2</sub> surfaces. Reprinted with permission from Mayeda *et al.*, *Journal of Materials Chemistry A*, 2015, 3(15), 7822-7829. .... 227
- Figure B.3: Size distributions of EISA and SPICE TiO<sub>2</sub> were measured according to the AFM images in Figure 4.2c and Figure 4.2d, respectively. Radii were calculated using ImageJ and binned in 0.5 nm increments. Counts (y-axis) were normalized for the purposes of comparison. Radii ( $r_x$ ) represent the average and standard deviation of each data set. The data represent over 2700 measurements for each AFM image. Reprinted with permission from Mayeda *et al.*, *Journal of Materials Chemistry A*, 2015, 3(15), 7822-7829. .... 229
- Figure C.1: Weight conversions (determined by GC) as a function of reaction cycle. One reaction cycle is 10 h of reaction followed by 1 h of regeneration. Adapted with permission from Bedenbaugh, J.E. Ph.D. Dissertation, University of Delaware, Newark, 2012. .... 231
- Figure C.2: Picture of (left to right) JP-8, condensed liquid, and recycled liquid. JP-8 is shows a light yellow hue whereas condensed liquid is bright yellow and recycled liquid nearly is brown. .... 232

Figure C.3: Overlaid  $^1\text{H}$  NMR spectra for JP-8 (red), condensed liquid after cracking (green), and condensed liquid after recycling (blue). Spectra are normalized to the methyl proton peak (0.75 ppm). All spectra show peaks associated with aromatics (6.5-7.5 ppm), unsaturated bonds (2-2.5 ppm), and aliphatics (0.5-1.5 ppm). ..... 232

## ABSTRACT

Nanometer-scaled materials have instigated an explosion of investigations into their applications as sensors, energy harvesting tools, memory devices, and catalysts. Researchers are intensely focused on the ability to tailor the size, shape, and geometric spacing because performance is inherently tied to nanomaterial structure and assembly. Block polymer thin films, which self-assemble at the nanometer scale, are well-studied systems that can be used to synthesize and orient such nanomaterials. Therefore, to meet the demands of next-generation devices, it is important to develop block polymer composite thin films that the material scientist can manipulate to meet specific performance metrics (*e.g.*, catalytic activity, optical reflectance, or magnetic coercivity to name a few). Herein, two templating methods were used to order inorganic material with block polymer thin films. The first method exploited the polymer-nanoparticle interactions to selectively incorporate gold nanoparticles within a specific domain of a polystyrene-*b*-polyisoprene-*b*-polystyrene triblock polymer thin film. The second method used a self-assembled polystyrene-*b*-poly(ethylene oxide) block polymer thin film to selectively absorb metal precursors into a hexagonal pattern. In both cases, inorganic nanoparticles were positioned according to the self-assembled morphology of the block polymer.

In an unrelated thrust, a fuel converter unit was designed and built around a fuel converting catalyst that was previously developed with the research group. The fuel converter improved upon existing efficiency while minimizing system cost, size,

and complexity. Furthermore, the converter was confirmed to be of substantial interest to commercial solid oxide fuel cell researchers and engineers that were interviewed as a part of the National Science Foundation I-Corps program. Recommendations for future work on the fuel converter and the block polymer composites are discussed.

## Chapter 1

### **BLOCK POLYMER TEMPLATING AND FUEL CONVERSION CATALYSIS: OVERVIEW AND APPLICATIONS**

#### **1.1 Introduction**

In the nascent stages of this thesis, the objective was to utilize self-assembled block polymer nanostructures to dictate the placement of catalytically active metals and supporting metal oxides. It was envisioned that exercising nanometer-scale control in catalyst development would lead to exciting breakthroughs in catalytic activity and selectivity. Indeed, the objective came into fruition when using block polymer templates to create nanostructured metal oxides. However, in addition to polymer-assisted catalyst development, a separate project was undertaken to develop a catalytic fuel converter that cracked military jet fuel into a mixture of hydrocarbons that mimicked liquefied petroleum gas. Therefore, two separate introductions are warranted here. Section 1.1.1 through section 1.1.3 introduces block polymer nanocomposites, while an introduction into fuel conversion is included in section 1.1.4.

##### **1.1.1 Nanoparticles in Block Polymer Templates**

While research continues to develop polymers with improved mechanical,<sup>1-4</sup> chemical,<sup>5,6</sup> and electrical properties,<sup>7,8</sup> composites of nanoparticles in polymers have yielded impressive gains.<sup>9</sup> For example, when inorganic fillers are effectively blended into polymers ( $\sim 0.1$ -10 vol<sub>particle</sub>%),<sup>9</sup> the resulting composites can exhibit dramatically

improved properties such as strength,<sup>10</sup> thermal conductivity,<sup>7,11,12</sup> electrical conductivity,<sup>7,11</sup> or permeability.<sup>13,14</sup> However, without efforts to stabilize the polymer-particle interface,<sup>15</sup> the surface energy mismatch between inorganic particles (relatively high surface energy) and hydrocarbon polymers (relatively low surface energy) usually results in aggregated nanoparticles within the polymer matrix.<sup>15</sup> *In situ* options achieve well-mixed nanocomposites because the nanoparticles are synthesized within the polymer matrix of interest. On the other hand, particle-matrix mixing is achieved in *ex situ* methods *via* ligands (*e.g.*, small molecules or polymers) that shield particle-particle van der Waals attractions.<sup>15</sup> Scaling laws have been developed to adequately blend a nanocomposite with a desired nanoparticle size, ligand molecular weight, ligand grafting density, and matrix polymer molecular weight.<sup>15-17</sup> Broadly speaking, *in situ* and *ex situ* techniques represent the bulk of nanocomposite synthesis methods.

#### **1.1.1.1 *In situ* Synthetic Methods**

The main benefit of the *in situ* approach is a homogeneous distribution of particles.<sup>18-20</sup> Generally, a polymer is loaded with a metal precursor and then undergoes oxidation/reduction<sup>21</sup> or thermal decomposition<sup>22</sup> to yield dispersed nanoparticles. Polymer-metal precursor interactions occupy a large parameter space that covers weak interactions such as coordination bonds,<sup>23,24</sup> hydrogen bonds,<sup>23</sup> charge-transfer interactions,<sup>25</sup> hydrophobic interactions, and  $\pi$ -bonding.<sup>25-28</sup> Furthermore, unlike small-molecule analogs, polymers exhibit conformational changes to accommodate the inter- and intra-chain metal complexes.<sup>29</sup> Here, a brief introduction is provided, which covers coordination bonds with poly(vinyl pyridine) (PVP) and poly(ethylene oxide) (PEO), and the reader is referred to the literature for

more information on polymer-metal complexes.<sup>30-33</sup> Other methods employ polymers with functional groups like alcohols and acids for electrostatic interactions,<sup>34-36</sup> methacrylates for dipole interactions,<sup>37-39</sup> and metallocenes for  $\pi$ -bonding.<sup>20,40,41</sup>

A receptive polymer has functional moieties such as unpaired electrons or polar segments. In block polymers, PVP and PEO are two commonly used blocks for metal incorporation. For example, complex formation between  $\text{Cu}^{2+}$  and PVP or pyridine can be described by the following expressions:



for which  $L$  is PVP or pyridine. Nishikawa and Tsuchida reported the formation constants,  $k_x$ , as shown in Table 1.1.<sup>42</sup>

Table 1.1: Reaction constants for chelating  $\text{Cu}^{2+}$  with PVFP or pyridine. Adapted with permission from Nishikawa, H. and Tsuchida, E. *J. Phys. Chem.* 1975, 79, (19), 2072-2076. Copyright 1975 American Chemical Society.

$L$	$\log k_1$	$\log k_2$	$\log k_3$	$\log k_4$
<b>PVP</b>	2.2	2.3	3.0	3.1
<b>pyridine</b>	2.5	1.9	1.3	0.8

Interestingly, the multidentate (*i.e.*,  $\text{CuL}_{>1}^{2+}$ ) interactions form faster for PVP than for pyridine. In fact, each *successive* polymer interaction forms faster than its predecessor (*i.e.*,  $k_4 > k_3 > k_2 > k_1$ ). By definition of a polymer, the local concentration of functional

monomer is very high; therefore, once the initial complex is formed ( $k_1$ ) polymers can form multidentate complexes ( $k_{>1}$ ) at faster rates than their small-molecule analogs.<sup>42</sup> Stable intra-chain multidentates also form with PEO due to its chain flexibility and electron donor capability of the oxygen atoms along the backbone.<sup>29</sup> Evidence suggests that the PEO chains coordinate with metals by forming crown-ether-like complexes.<sup>43</sup> Furthermore, block polymers containing both PEO and PVP can be used to complex two different salts in an orthogonal manner.<sup>44,45</sup>

Once the complex is formed, nanoparticles are produced by reducing the precursor salt to a metal or reacting the salt with oxygen to form metal oxides. The simplest and most common method is to use the polymer as a reducing agent during thermal annealing.<sup>35,38,46</sup> Additionally, the polymer-metal precursor composite can be chemically reduced using sodium borohydride or hydrazine,<sup>34,39,47</sup> or chemically oxidized using water,<sup>48</sup> ozone,<sup>49</sup> or oxygen plasma.<sup>24,50,51</sup> In all cases, the polymer serves as a host that minimizes aggregation and agglomeration during nanoparticle formation.

Researchers have incorporated complexing polymers into self-assembling block polymers to create a variety of functional inorganic materials.<sup>52,53</sup> The strong affinity between the hydrophilic polymers and the precursors selectively confines the metal into a polymer domain. In particular, the Pluronic® family of block polymers has been extensively used for evaporation-induced self-assembly sol-gel techniques (see section 1.1.1.1).<sup>54,55</sup> Block polymers have been used with the *in situ* process to template inorganics such as gold,<sup>50</sup> silver,<sup>56</sup> platinum,<sup>51</sup> palladium,<sup>51</sup> aluminum,<sup>57,58</sup> iron,<sup>59</sup> silicon,<sup>52</sup> titanium,<sup>58,60</sup> and others.<sup>61,62</sup> Perhaps more importantly, the block polymer morphology persists in the *in situ* inorganic structures such as lamellae,<sup>63,64</sup>

gyroid,<sup>64-66</sup> hexagonally packed cylinders,<sup>64,67,68</sup> and body-centered cubic spheres.<sup>64,67,68</sup> However, when designing nanostructured inorganics, it is important to control the relative quantity and composition of inorganic precursor that is mixed with the polymer template. As the precursor selectively swells a hydrophilic polymer domain, the change in relative volume fractions of the hydrophobic and hydrophilic blocks can result in morphology changes.<sup>69</sup> For example, Cheng and Gutmann used a titania sol and a polystyrene-*b*-poly(ethylene oxide) template to create a wide variety of morphologies including foams, flakes, and wires.<sup>53</sup> Therefore, *in situ* techniques provide an attractive option to create a variety of free-standing inorganic structures or block polymer composites.<sup>52,53</sup>

#### **1.1.1.2 *Ex situ* Synthetic Methods**

Nanoparticle-polymer blends can be made by synthesizing the nanoparticles in a separate process prior to blending with the polymer, which is referred to as an *ex situ* synthetic method. *Ex situ* approaches benefit from a plethora of synthesis techniques, which afford nanoparticles with various compositions,<sup>70,71</sup> sizes,<sup>72,73</sup> and shapes.<sup>74-76</sup> Nanoparticles are typically produced in solution by reducing or oxidizing a metal precursor salt in the presence of capping ligands, which direct the nucleation and growth process.<sup>74,77</sup> The topic of nanoparticle synthesis is beyond the scope of this thesis; the reader is referred to the literature for more background information.<sup>78-81</sup>

Nanoparticle-polymer blending is germane to this thesis. Unlike the *in situ* method, an even particle distribution within the polymer matrix requires a balance of enthalpic and entropic driving forces that encourage phase separation and/or particle agglomeration as briefly discussed below.

### 1.1.1.2.1 Enthalpic Considerations

Enthalpic penalties for mixing occur at the nanoparticle-polymer interface. Researchers have used many different types of nanoparticle capping ligands including alkanes,<sup>74,77,82</sup> functional moieties,<sup>83</sup> polymers,<sup>84,85</sup> or dendrimers to minimize enthalpic penalties and maximize nanoparticle dispersion.<sup>86</sup> Block polymer composites have been used to reveal the importance of tuning ligand chemistry; ligands have been selected to direct nanoparticles into specific polymer domains. Examples include silica and gold in polystyrene-*b*-poly(ethylene propylene),<sup>87</sup> gold or silver in polystyrene-*b*-polyisoprene-*b*-polystyrene,<sup>88,89</sup> gold in polystyrene-*b*-poly(methyl methacrylate),<sup>90</sup> silica-based clays (*i.e.*, sodium montmorillonites) in polystyrene-*b*-polybutadiene-*b*-polystyrene,<sup>91</sup> and palladium in polystyrene-*b*-poly(2-vinyl pyridine).<sup>92,93</sup> Access to a variety of ligands translates to compatibility across many polymer-particle pairs. Enthalpic penalties even can be negated in so-called athermal nanocomposites (*e.g.*, polystyrene-covered gold nanoparticles in a polystyrene matrix).<sup>94-96</sup> However, it should be noted that appropriate scaling laws, which are discussed in section 1.1.1.2.2, must be taken into consideration to avoid autophobic dewetting between the matrix and grafted polymers.<sup>15,97</sup> Polymer-covered particles can be made in a grafting-to<sup>98,99</sup> or grafting-from approach (Figure 1.1).<sup>100,101</sup> A grafting-through approach also exists, wherein particles are decorated with functional moieties (*e.g.*, vinyl or methacrylate groups) that are incorporated into the polymer backbone during polymerization.<sup>102,103</sup> While grafting-through has the potential to achieve higher grafting densities than grafting-to,<sup>102</sup> the method does not match the versatility of either grafting-to or grafting-from.<sup>104,105</sup>

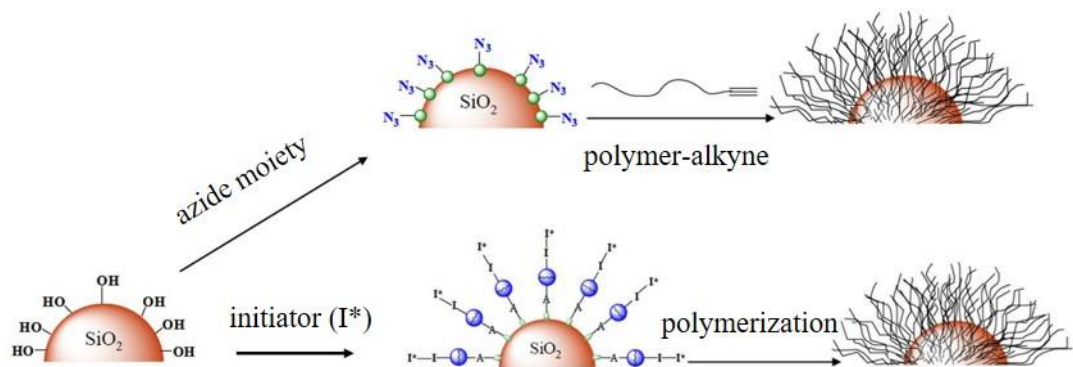


Figure 1.1: Polymer chains bound to a SiO<sub>2</sub> nanoparticle *via* (top) grafting-to and (bottom) grafting-from. The grafting-to approach is performed using an alkyne-azide click reaction. The grafting-from is performed with a surface-bound initiator that is a precursor to tethered polymer chains. Adapted with permission from Achilleos, D. S.; Vamvakaki, M. *Materials* 2010, 3, (3), 1981-2026.

The grafting-to method is simpler, but steric repulsions between attached ligands can limit grafting densities and thus decrease nanoparticle stability.<sup>106,107</sup> The grafting-from method can achieve higher grafting densities while still maintaining control over polymer composition and molecular weight.<sup>94,95</sup> Finally, in addition to achieving good dispersion within a polymer, nanoparticle surfaces can be tuned to mitigate polymer-polymer interfaces for blends and block polymers, which can lead to block polymer order-order transitions or interface stabilization.<sup>108</sup>

### 1.1.1.2.2 Entropic Considerations

While an entropic gain in free energy from polymer-particle mixing encourages dispersion, entropic penalties associated with polymer chain deformation to accommodate nanoparticles and a loss of translational chain entropy can lead to aggregation and phase separation.<sup>94,95</sup> The entropy of mixing ( $S_{mix}$ ) and chain

deformation ( $S_{deformation}$ ) are related to the volume fraction ( $\varphi$ ) of nanoparticles, with a radius of  $R_{NP}$ , in a polymer with a radius of gyration,  $R_g$ , as follows:<sup>109,110</sup>

$$S_{mix} \propto \left( \frac{\varphi}{R_{NP}^3} \right) \ln \varphi \quad 1-5$$

$$S_{deformation} \propto \left( \frac{R_{NP}}{R_g} \right)^2 \quad 1-6$$

It can be seen that smaller particles and larger polymer chains will promote mixing.<sup>111</sup> For block polymers, it has been shown that smaller particles uniformly dispersed within a polymer domain while larger particles segregated towards the domain centers.<sup>16,112</sup>

For athermal nanocomposites, three parameters become increasingly important in avoiding autophobic dewetting: grafted polymer degree of polymerization ( $N$ ), host polymer degree of polymerization ( $P$ ), and grafting density (*i.e.*, chains/nm<sup>2</sup>;  $\sigma$ ). Autophobic dewetting occurs when the tethered polymer chains form dry brushes that exclude interaction with the host matrix. Polymer-grafted nanoparticles can aggregate under the following condition:<sup>110</sup>

$$\sigma\sqrt{N} > \sqrt{\frac{N}{P}} \quad 1-7$$

It should be noted that equation 1-7 is not a definitive rule, and aggregation remains nanoparticle-size dependent.<sup>95</sup> Furthermore, the “aggregate” can be a functional secondary shape, in its own right, that takes on morphologies such as chains or sheets.<sup>94</sup> Therefore, equation 1-7 serves more as a guide when considering entropic contributions to miscibility in particle-polymer blends.

### 1.1.2 Introduction to Block Polymers

Patterns have facilitated natural and man-made phenomena over numerous size scales. For example, honeybees produce a hexagon-patterned honeycomb, which sparingly uses valuable wax to partition storage units that maximize the area-to-perimeter ratio.<sup>113</sup> Other long-studied patterns in phyllotaxis exhibit Fibonacci sequences that optimize leaves' exposure to resources (*i.e.*, light and precipitation) while minimizing occlusion of neighboring leaves.<sup>114,115</sup> On a larger scale, vehicle parking lots commonly exhibit rows of repeated demarcations that maximize the lot's capacity for vehicles while maintaining a safe and intuitively navigable facility.<sup>116,117</sup> On an even larger scale, large agricultural farms sow seeds in tightly packed rows that can increase the yields per acre.<sup>118-120</sup>

At the other end of the spectrum, the semiconductor industry employs patterns to construct ever-smaller transistors that, in turn, lead to faster and smaller electronic devices:<sup>121,122</sup> smartphones that act as personal assistants,<sup>123,124</sup> engine control units that reduce emissions and improve fuel economy,<sup>125,126</sup> glucose monitors for patients self-administering insulin,<sup>127,128</sup> and even circuit-equipped sporting goods that record activity statistics.<sup>129-131</sup> In all cases, defects in the patterns can lead to sub-optimal performance in terms of wax use,<sup>132</sup> plant growth,<sup>133,134</sup> vehicle packing and pedestrian safety,<sup>135</sup> crop yield,<sup>118</sup> or microprocessor performance.<sup>136,137</sup> Therefore, predictable and reproducible patterns are highly desirable.

Just as patterns at the macroscale can have positive impacts on performance, nanoscale patterns show promise for next-generation devices such as solar energy converters,<sup>138,139</sup> separation membranes,<sup>140-142</sup> and lithographic masks.<sup>137,143</sup> Nanoscale patterning approaches can be categorized into top-down or bottom-up processes. Top-down approaches employ lithography with short wavelength photon sources to create

nanoscale shapes such as trenches, dots, wires, and pillars among others.<sup>144</sup> Top-down approaches include optical lithography,<sup>145</sup> e-beam lithography,<sup>146</sup> nanoimprint lithography,<sup>147</sup> and scanning probe lithography.<sup>148,149</sup> The advantage of a top-down process is relatively few defects.<sup>150,151</sup> However, the disadvantage is a compromise between smallest achievable size, cost, and wafer throughput.<sup>146</sup> On the other hand, bottom-up approaches rely on thermodynamics and kinetics to self-assemble patterns of interest. Examples of nanoscale bottom-up products include monolayers,<sup>152,153</sup> zeolites and metal organic frameworks,<sup>154-156</sup> nanoreactors,<sup>157,158</sup> colloidal superstructures,<sup>159-161</sup> and protein meshworks and cages.<sup>162,163</sup> The main advantage of a bottom-up process is the potential for prolific nanoscale manufacturing at relatively low cost.<sup>164</sup>

To realize the benefits of bottom-up processing, considerable effort has focused on using block polymers to create a variety of nanoscale structures with tunable sizes and geometries. Block polymers are macromolecules that are composed of chemically distinct polymer segments, which are covalently bonded together. The covalent bond prevents the blocks from macrophase separating. Therefore, block polymers can exhibit interesting microphase features on the order of nanometers.<sup>165,166</sup> While more intricate structures can be achieved by increasing the number of blocks and/or their architectural complexity (*e.g.*, cyclic or branched),<sup>167</sup> an understanding of linear diblock polymers is sufficient for topics addressed in this thesis.

A linear diblock polymer is composed of two chemically distinct segments: polymer *A* and polymer *B*. In diblock polymers, the equilibrium phase is governed by the degree of polymerization,  $N$ , volume fraction of *A*,  $f_A$  (*i.e.*,  $f_B = 1 - f_A$ ), and *A-B* Flory-Huggins interaction parameter,  $\chi_{AB}$ .<sup>165</sup> For a given diblock polymer system, the

degree of polymerization and volume fractions can be tailored by adjusting the polymer synthesis conditions such as the ratio of monomer to initiator, polymerization time, polymerization temperature, and solvent choice.<sup>168,169</sup> The degree of polymerization typically varies from ~50 to ~1,000, and the volume fractions are tailored to target the microstructure of interest. Together, the degree of polymerization and volume fraction govern the translational and configurational entropy of the polymer chains. Translational entropy describes the degree of mixing (or phase separation) amongst the polymer chains whereas configurational entropy describes chain stretching.<sup>170</sup> The Flory-Huggins interaction parameter encompasses the enthalpic contribution from the Gibbs free energy of mixing between the two polymer blocks (Equation 1-8).<sup>170,171</sup> Flory-Huggins theory extends the thermodynamics of solutions to solutes of linked monomers (*i.e.*, polymer) instead of small molecules.<sup>172,173</sup> The interaction parameter depends on temperature ( $T$ ) and temperature-independent variables  $\alpha$  and  $\beta$ , which govern the enthalpic and entropic contributions, respectively.

$$\chi_{AB} = \frac{\alpha}{T} + \beta \quad 1-8$$

For context, some Flory-Huggins interaction parameters for commonly researched polymers and polymers used in this thesis are provided in Table 1.2.<sup>174</sup>

Table 1.2: Flory-Huggins interaction parameters for common block polymer systems.

Polymer	$\chi_{AB}(T)$ (K)
polystyrene- <i>b</i> -polyisoprene <sup>175</sup>	$26.4/T - 0.0288$
polystyrene- <i>b</i> -poly(ethylene oxide) <sup>175</sup>	$29.8/T - 0.0229$
polystyrene- <i>b</i> -poly(2-vinylpyridine) <sup>176</sup>	$63/T - 0.033$
polystyrene- <i>b</i> -poly(methyl methacrylate) <sup>177</sup>	$3.9/T - 0.028$
poly(ethylene oxide)- <i>b</i> -poly(propylene oxide) <sup>178</sup>	$20.2/T + 0.0221$

Ultimately, the thermodynamically stable morphologies that can be obtained from bulk diblock polymers include close-packed spheres, body-centered cubic spheres, hexagonally packed cylinders, continuous gyroid network, *Fddd* orthorhombic network, and lamellae. Each morphology typically has size features on the order of 10-100 nm (Figure 1.2).<sup>165,179,180</sup>

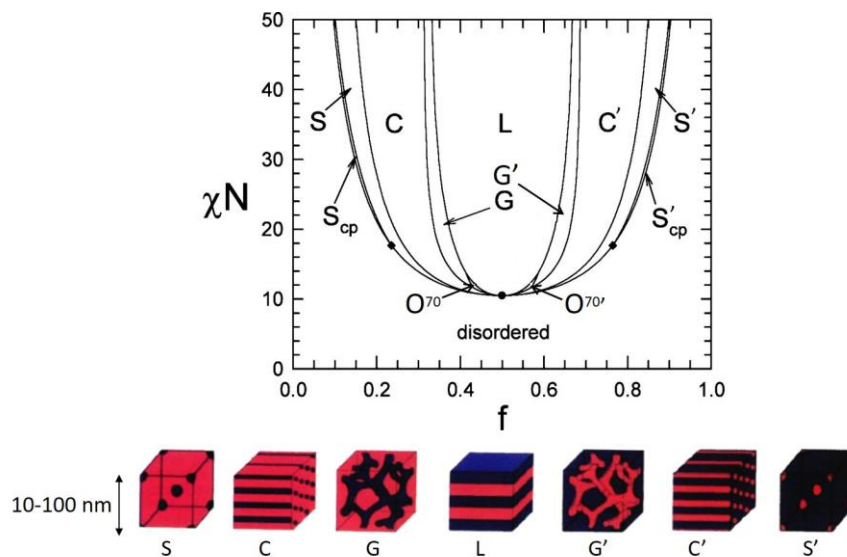


Figure 1.2: Phase diagram for a diblock polymer showing close packed spheres ( $S_{cp}$ , not shown), body-centered cubic spheres (S), hexagonally packed cylinders (C), continuous gyroid network (G),  $Fddd$  orthorhombic network ( $O^{70}$ , not shown), lamellae (L), and their respective inverted structures ( $O^{70'}$ ,  $G'$ ,  $C'$ ,  $S'$ ,  $S_{cp}'$ ). The dot marks a mean-field critical point and the diamonds mark triple points. The phase diagram was adapted with permission from Matsen, M. W. *Macromolecules* 2012, 45(4), 2161-2165. Copyright 2012, American Chemical Society. Unit cell illustrations were adapted with permission from Bates, F. S.; Fredrickson, G. H. *Phys. Today* 1999, 52, (2), 32-38. Copyright 1999, American Institute of Physics.

Researchers have found interesting applications for the various phases: spheres and cylinders for bit-patterned media<sup>181-184</sup> and lamellae-forming phases for wire templating.<sup>185,186</sup> However, the gyroid network remains the most coveted phase because its co-continuous pathways make it attractive for applications requiring electron or mass transport.<sup>187,188</sup> Electron and mass transport is limited by grain boundaries in cylinder- or lamellae-forming phases.<sup>189</sup> While the gyroid phase is obtainable with a diblock polymer system, researchers have pursued more complicated

block polymer systems,<sup>167</sup> which exhibit larger gyroid windows in their respective phase diagrams.<sup>190</sup>

In addition to the interesting applications, the interest in the field of block polymers steadily has increased due to the relative safety and simplicity of new living polymerization techniques such as reversible-addition fragmentation chain-transfer and atom-transfer radical-polymerization.<sup>168,191</sup> Such versatile techniques have lowered the synthesis entry barrier and allowed block polymers to permeate fields from solar energy conversion to drug delivery.<sup>192,193</sup>

### 1.1.2.1 Block Polymer Thin Films

In addition to the variables that affect bulk block polymer phase equilibrium, confinement into thin film geometries introduces three variables: thickness of the film, interaction between the substrate and the film, and interaction between the free-surface and the film.<sup>194</sup> Here, it should be noted that additional non-equilibrium structures can be achieved by manipulating film casting and annealing procedures.<sup>195</sup> The thickness,  $t$ , of a thin film block polymer of domain spacing,  $L_0$ , is approximately  $L_0 < t < 10L_0$  (Figure 1.3). For an AB diblock polymer thin film, symmetric wetting refers to polymer A or B wetting both the substrate and the free-surface (Figure 1.3b); asymmetric wetting refers to polymer A (or B) wetting the substrate and polymer B (or A) wetting the free surface (Figure 1.3d). Film thickness is important vis-à-vis commensurability. Block polymer films are commensurate if Equation 1-9 is true.

$$t/L_0 = \begin{cases} n, & \text{symmetric wetting } \cap n \in \mathbb{N} \\ (n + 1/2), & \text{asymmetric wetting } \cap n \in \mathbb{N} \end{cases} \quad 1-9$$

The enthalpic penalty of mixing blocks causes the polymer domains to behave like discrete layers parallel to the substrate plane (Figure 1.3). Therefore, incommensurate films display surface relief structures, so-called “holes” (Figure 1.3a) and “islands” (Figure 1.3c), that accommodate the deficient or excess volume, respectively.<sup>196</sup>

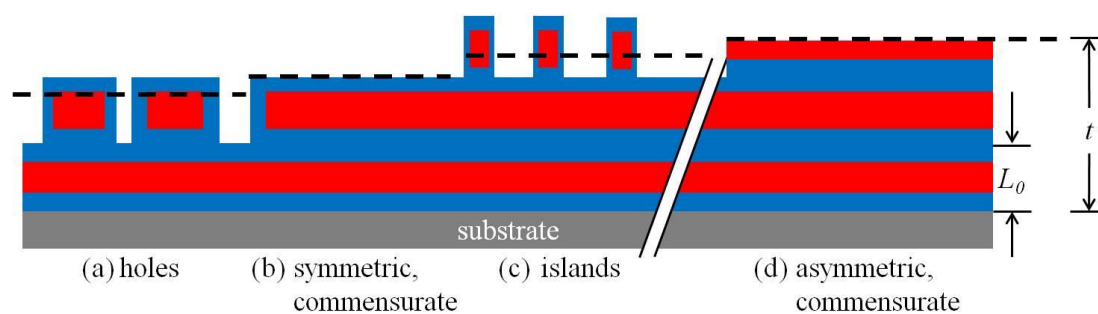


Figure 1.3: Schematic of a lamellae-forming diblock polymer (red-blue) thin film, not to scale. For a film of thickness  $t$ , surface relief structures form (a) holes or (c) islands when film thicknesses are incommensurate with the domain spacing,  $L_0$ . Otherwise, commensurate films can exhibit (b) symmetric or (d) asymmetric wetting depending on the block affinities for the substrate and free-surface.

Although  $L_0$  for block polymers typically is within the range of 15-200 nm, the diameters of the islands and holes can be many microns, depending on the degree of incommensurability and polymer molecular weight.<sup>197</sup> While Figure 1.3 implies that smooth-surface films require commensurate thicknesses for lamellae or cylinders lying parallel to the substrate plane, it has been shown that incommensurate thicknesses can provide a driving force towards perpendicularly oriented morphologies, which is often more desirable.<sup>198,199</sup>

In addition to film thickness, the substrate- and free-surface interfacial areas play important roles in the formation of block polymer thin film structures.<sup>194</sup> The surface energy difference between the two media (*e.g.*, substrate-polymer or polymer-free surface) governs the polymer wetting behavior. The free surface usually is air; therefore, the lowest energy block will create a wetting layer at the free-surface interface.<sup>196</sup> It should be noted that changes to the gas-phase composition (*e.g.*, solvent vapor annealing) can create a driving force to bring higher surface energy materials to the film surface.<sup>200,201</sup>

More research has explored the effect of the substrate surface interaction. Substrates have been chemically modified to control the orientation and degree of order of block polymer thin films.<sup>186,202,203</sup> Regarding orientation, parallel cylinders and lamellae can be achieved by ensuring that the substrate is preferentially wet by one of the blocks (Figure 1.4a(i)).<sup>204</sup> On the other hand, perpendicularly oriented structures are more desirable for applications such as filtration membranes or templates.<sup>205-208</sup> Perpendicular orientations have been shown to be the lowest energy orientation on substrates that are modified so as to be non-preferential (Figure 1.4a(ii)).<sup>201</sup> In addition to influencing the domain orientation, substrates can be modified so as to improve the long-range ordering after annealing. Substrate modifications such as chemical or topographical patterns, which are applied prior to film casting, have been shown to reduce the defect density in annealed polymer films.<sup>186,209-211</sup>

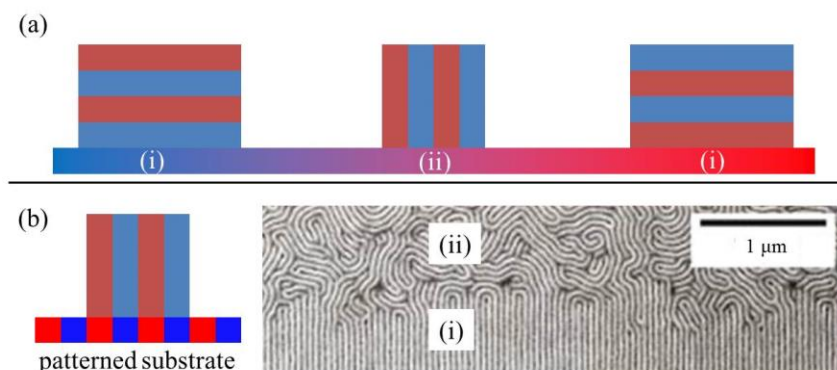


Figure 1.4: Substrate effect on thin film orientation and order. (a) The substrate surface chemistry can induce (i) preferential wetting or (ii) a neutral interaction, which would lead to a perpendicular orientation. (b) Patterned substrates direct the self-assembly into (i) well-ordered structures; whereas films on (ii) unpatterned substrates exhibit considerably more grain boundaries and defects. (b) Adapted with permission from Macmillan Publishers Ltd: *Nature*. Kim, S. O.; Solak, H. H.; Stoykovich, M. P.; Ferrier, N. J.; de Pablo, J. J.; Nealey, P. F. *Nature* 2003, 424, (6947), 411-414. Copyright 2003

In one case, block polymer self-assembly (bottom up) was combined with extreme ultraviolet interferometric lithography (top down) to produce ordered defect-free areas of perpendicularly oriented lamellae (Figure 1.4b(i)); whereas block polymer domains on substrates that were not pre-patterned by interferometric lithography exhibited a poorly-ordered film (Figure 1.4b(ii)).<sup>211</sup> Such patterning is crucial for long-range order applications in the semiconductor industry.<sup>212</sup>

### 1.1.3 Templating Inorganics with Block Polymers

The co-assembly of block polymers and nanoparticles is a research area rich with applications in energy harvesting,<sup>213</sup> magnetic bit patterning,<sup>214</sup> optics,<sup>215</sup> and catalysis. Researchers have taken lessons from creating well-dispersed

nanocomposites in homopolymers and applied them to create analogous block polymer composites using both *ex situ* and *in situ* approaches.<sup>195,216,217</sup>

### 1.1.3.1 *In Situ* Templating

One of the most common applications of block polymer templating is the evaporation-induced self-assembly (EISA) sol-gel process to produce metal oxides.<sup>218-221</sup> The EISA technique is used to make bulk and thin film materials with ordered and size-controlled pores correlated with polymer molecular weight.<sup>222</sup> In a typical process, the metal precursor, block polymer, and solvent(s) are mixed together and cast into a thin film. Solvent evaporation beyond a critical micelle concentration triggers assembly and organization of the structures (Figure 1.5a).

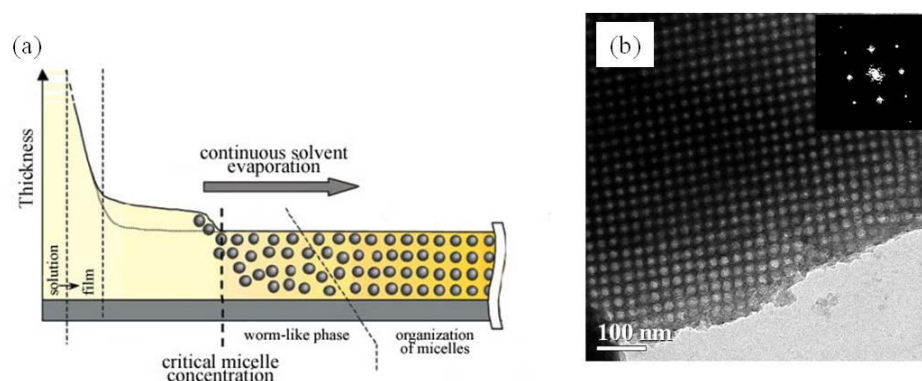


Figure 1.5: (a) Schematic of the evaporation-induced self-assembly process and (b) a transmission electron microscope image of a mesoporous carbon product; inset image is a diffractogram. In both (a) and (b), the cubic phases are shown, but numerous other mesostructures can be formed. (a) was adapted from Pan, J. H.; Zhao, X. S.; Lee, W. I. *Chem. Eng. J.* 2011, 170, (2-3), 363-380, copyright 2011, with permission from Elsevier. (b) was adapted with permission from Deng, Y. H.; Yu, T.; Wan, Y.; Shi, Y. F.; Meng, Y.; Gu, D.; Zhang, L. J.; Huang, Y.; Liu, C.; Wu, X. J.; Zhao, D. Y. *J. Am. Chem. Soc.* 2007, 129, (6), 1690-1697. Copyright 2007 American Chemical Society.

Subsequent polymer removal *via* thermal degradation or oxidation leaves an inorganic fossil of the polymer morphology; isotropic, body-centered cubic spheres, hexagonally packed cylinders, gyroid network, and lamellar morphologies can be synthesized (Figure 1.5b).<sup>219,223</sup> Attractive aspects of EISA include its one-pot simplicity and batch-to-batch reproducibility.<sup>218</sup> However, using block polymer reverse micelles in a similar approach produces nanoparticles with a wide size distribution and irregular nanoparticle arrays (Figure 1.6a).<sup>24</sup> Heterogeneity probably stems from inter-chain complexes that kinetically trap micelles from equilibrating towards a homogeneous-size population.<sup>224</sup> Boyen and coworkers recently published a well-ordered array whereby the metal precursors are coordinated with a homopolymer before being combined in a block polymer micelle solution (Figure 1.6b), thereby giving mobility to the micelle-forming block polymer chains.<sup>24</sup>

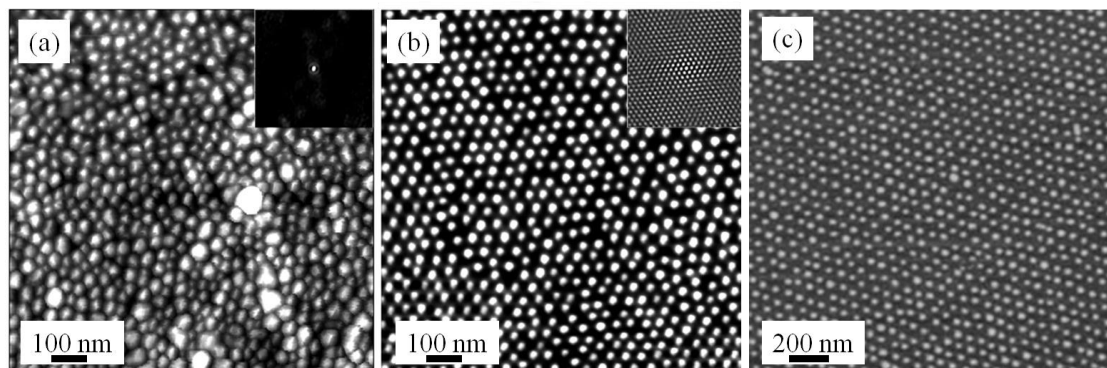


Figure 1.6: Atomic force microscopy images of iron oxide nanoparticles made from (a) a one-pot approach, (b) a solution of homopolymer-iron complexes and block polymer micelles, and (c) gold nanoparticles from a neat block polymer thin film template. Inset images for (a) and (b) show respective auto-covariance functions. (a) and (b) were adapted with permission from Shan, L.; Punniyakoti, S.; Van Bael, M. J.; Temst, K.; Van Bael, M. K.; Ke, X.; Bals, S.; Van Tendeloo, G.; D'Olieslaeger, M.; Wagner, P.; Haenen, K.; Boyen, H.-G. *J. Mater. Chem. C* 2014, 2, (4), 701-707. Copyright 2014 Royal Society of Chemistry. (c) was adapted with permission from Cho, H.; Park, H.; Russell, T. P.; Park, S. *J. Mater. Chem.* 2010, 20, (24), 5047-5051. Copyright 2010 Royal Society of Chemistry.

In a separate *in situ* approach, Russell and coworkers eliminated complexities associated with intra- and inter-chain metal-polymer coordination by using a polystyrene-*b*-poly(2-vinylpyridine) (PS-*b*-P2VP,  $M_{n,PS} = 125 \text{ kg mol}^{-1}$ ;  $M_{n,P2VP} = 59 \text{ kg mol}^{-1}$ ) thin film template to produce gold nanoparticle arrays.<sup>50</sup> Exposure to polar solvents caused the polymer thin film to undergo a surface reconstruction whereby the solvated P2VP domains were drawn to the film's surface, leaving a nanoporous template. Then, the pores were back-filled with precursor solutions of gold, iron oxide, and titanium oxide. After oxygen plasma etching, well-ordered arrays of inorganic nanoparticles with a narrow size distribution were produced (Figure 1.6c).<sup>50</sup>

Templating multiple materials using block copolymers can be accomplished by carefully choosing polymer-precursor pairs. For example, Russell and coworkers used a polystyrene-*b*-poly(2-vinylpyridine)-*b*-poly(ethylene oxide) to form reverse micelles to template concentric spheres of platinum and gold; the H<sub>2</sub>PtCl<sub>6</sub> selectively coordinated with the P2VP while LiAuCl<sub>4</sub> selectively coordinated with PEO.<sup>44</sup> The platinum-shell gold-core nanoparticles are denoted Pt@Au. The approach has been replicated to create a variety of core-shell nanoparticles including Au@Ag,<sup>225</sup> TiO<sub>2</sub>@AuAg,<sup>226</sup> and Au@SiO<sub>2</sub>,<sup>227</sup> Templating multiple materials is particularly relevant to heterogeneous catalysis because a catalyst can have multiple active phases.<sup>228,229</sup>

### 1.1.3.2 *Ex Situ* Templating

When templating particles with block polymers, dispersion considerations remain consistent as with homopolymers (see section 1.1.1.2) with an additional objective: preferentially segregate the particles into one of the polymer blocks.<sup>230</sup> Chemical dissimilarities between blocks allow researchers to preferentially segregate nanoparticles into targeted domains. Larger disparities between blocks decrease the enthalpic driving force towards nanoparticle aggregation; simple ligands can be used in place of grafted polymers. For example, Teranishi and coworkers exploited the repulsive interactions between alkane ligands and PVP to segregate gold nanoparticles into the polystyrene domains of a polystyrene-*b*-poly(vinyl pyridine) (PS-*b*-PVP) film.<sup>231</sup> Similar cases can be found with oxides,<sup>213,232</sup> semiconductors,<sup>233</sup> and nanorods.<sup>234</sup> The ability to segregate nanoparticles into discrete domains is in contrast to the poor segregation, if at all, that is achieved when non-polar ligands are used with non-polar block polymers (*i.e.*, the blocks are similar).<sup>235-237</sup> More control over the

precise location within a particular domain can be achieved using polymer-tethered nanoparticles. Work by Kramer and coworkers with gold nanoparticles and PS-*b*-PVP demonstrated excellent control of gold nanoparticle positions within the center, interfaces, and homogeneously distributed throughout the PVP domains.<sup>108,238-241</sup> Such work exhibits the fine control of enthalpic and entropic contributions in a block polymer composite.

Multiple domains of a diblock polymer can be used to template multiple materials. Thomas and coworkers used a lamellae-forming polystyrene-*b*-poly(ethylene propylene) (PS-*b*-PEP) to template gold and silica nanoparticles in an *ex situ* fashion.<sup>87</sup> While the underlying reason for differential nanoparticle segregation was not explicit (*i.e.*, influence of the ligand, nanoparticle size, or nanoparticle material), the electron microscopy image clearly showed gold nanoparticles located at the polymer domain interfaces and silica nanoparticles located in the centers of the PEP domains (Figure 1.7).

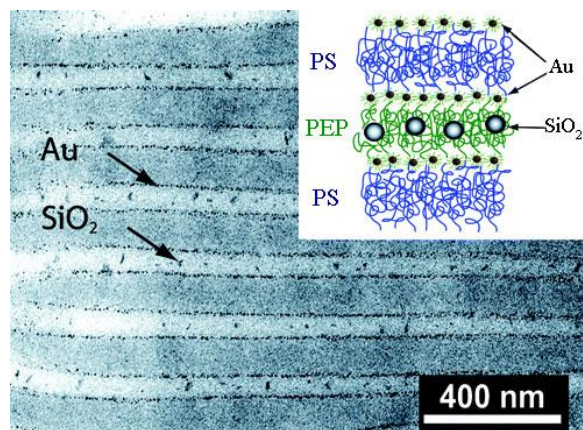


Figure 1.7: Gold and silica nanoparticles were templated in an *ex situ* fashion. Gold nanoparticles segregated to the PS/PEP interface while silica particles segregated to the centers of the PEP domains. Adapted with permission from Bockstaller, M. R.; Lapetnikov, Y.; Margel, S.; Thomas, E. L. *J. Am. Chem. Soc.* 2003, 125, (18), 5276-5277. Copyright 2003 American Chemical Society.

Similarly, Haridas and Basu used a polystyrene-*b*-poly(4-vinylpyridine) (PS-*b*-P4VP) block polymer to simultaneously template PS-covered gold nanoparticles and pyridine-covered CdSe quantum dots into PS and P4VP, respectively.<sup>242</sup> Controlled templating allowed them to tune the photoluminescence of their thin film composites. While adding complexity to the system, templating multiple sets of nanoparticles can add functionality to the composite system.

### 1.1.3.3 Applications in Photocatalysis

Common light-induced processes on heterogeneous surfaces include energy harvesting and catalyzed chemical reactions.<sup>243</sup> Generally, the energy from an incident photon is converted into an electron-hole pair by the semiconductor. If the dissociated electron performs work through an external circuit, the process is harvesting energy in a photovoltaic cell.<sup>244</sup> Otherwise, the electron-hole pair can migrate to the surface of

the semiconductor and catalyze chemical reactions.<sup>245</sup> Titania is one of the most commonly used materials in photocatalysis due to its low cost, low toxicity, and large band gap (3.2 eV for anatase and 3.0 eV for rutile).<sup>246</sup> When light is absorbed by titania, electron-hole pairs produce surface hydroxyl radicals and highly oxidizing holes that make the catalyst a strong oxidizer.<sup>246</sup> The radicals and holes are ideal for degrading organic compounds, which is one of the most popularly studied photocatalytic processes.<sup>243,247</sup>

Generally, researchers improve the photocatalytic efficiency of titania *via* two routes: increasing the surface concentration of reactive species and increasing the absorption band towards the visible range.<sup>246</sup> One way to increase the concentration of reactive species is to increase the overall surface area of the catalyst. Therefore, researchers have used block polymers to synthesize nanoparticles<sup>46,248,249</sup> and porous materials<sup>60,222,249,250</sup> that have smaller features, which result in an increase in the surface area to volume ratio. Ying and coworkers performed chloroform degradation experiments, with titania nanoparticles that were synthesized using a sol-gel hydrolysis technique, and determine that the optimal feature size was approximately 10 nm.<sup>251</sup> They concluded that decreasing the feature size below 10 nm can increase the rate of electron-hole recombination at the surface and thus decrease photocatalytic activity.<sup>252</sup> Meanwhile, van Grieken *et al.* found that 6-7 nm TiO<sub>2</sub> crystals performed best for their cyanide photo-oxidation experiments<sup>253</sup> and Anpo *et al.* reported that 5.5 nm TiO<sub>2</sub> yielded the best results for photocatalyzed hydrolysis of propyne.<sup>254</sup> In all cases, the researchers highlighted the importance of large surface areas in achieving high photocatalytic activity.

Anatase titania, which is the most common phase of titania photocatalysts,<sup>243</sup> absorbs light with wavelengths below 384 nm, which accounts for less than 5% of the air mass 1.5 solar spectrum.<sup>246</sup> To increase the bandwidth of absorption, researchers have modified titania by doping<sup>255,256</sup> or adding plasmon-active nanoparticles.<sup>257-259</sup> While the former process is accomplished by wet impregnation or co-precipitation techniques, the latter can be accomplished by co-templating using two or more polymer blocks.<sup>195</sup> Nanoparticles of gold and silver, which exhibit surface plasmon resonances in the visible light range, can be co-templated with titania.<sup>260,261</sup> The plasmon frequency of the metal nanoparticles can be tuned by changing their size,<sup>262,263</sup> shape,<sup>263,264</sup> and composition.<sup>261,265</sup> Gold-nanoparticle-surface plasmons enhance the photocatalytic activity of titania by either charge transfer (*i.e.*, plasmon-induced injection of electrons from the gold nanoparticle into the titania phase) or local electric field enhancement (*i.e.*, plasmons on the gold surface induce an electron-hole pair in the titania).<sup>260,261</sup> While there is debate on the exact mechanism of synergy, researchers have demonstrated improved photocatalytic efficiency with gold- or silver-decorated titania using block polymer assemblies.<sup>257-259,266,267</sup> Therefore, titania remains one of the most heavily researched photocatalysts. In addition to photocatalysis, the conversion of hydrocarbon fuels is another catalytic process that is relevant to this thesis and will be discussed in the next section.

#### **1.1.4 Catalytic Fuel Conversion Applications**

Previous work in our lab has demonstrated the feasibility of a catalytic cracking reaction that produces a mixture of small hydrocarbons from jet fuel.<sup>268,269</sup> Due to the price inversion (low-value products from high-value reactants), incentives to carry out such a value-detracting reaction exist in microcosms with extreme supply-

demand imbalances. This section will focus on two juxtaposed situations: developing countries (subsection 1.1.4.1) and the defense industry (subsection 1.1.4.2). Finally, a brief summary is provided of the current approaches to fuel conversion (subsection 1.1.4.3) and our lab-developed catalytic cracking reaction (subsection 1.1.4.4).

#### **1.1.4.1 Applications in Developing Countries**

Clean energy remains one of the world's leading problems.<sup>270</sup> In this case, “clean” refers to fuels with reduced sulfurous emissions and/or particulate matter when burned. In particular, distributing clean usable energy to end-users in remote locations remains a non-trivial task.<sup>271</sup> Developed countries consume liquid and gaseous petroleum fuels approximately equally (Figure 1.8, black/grey).<sup>272</sup> On the other hand, developing regions tend to use more primitive fuels (*i.e.*, solids and liquids) because the fuels can be used for a variety of applications including heating, electricity production, transportation, lighting, and cooking.<sup>273,274</sup> Consumption of gaseous hydrocarbons tends to lag that of its liquid counterpart (Figure 1.8).<sup>272</sup>

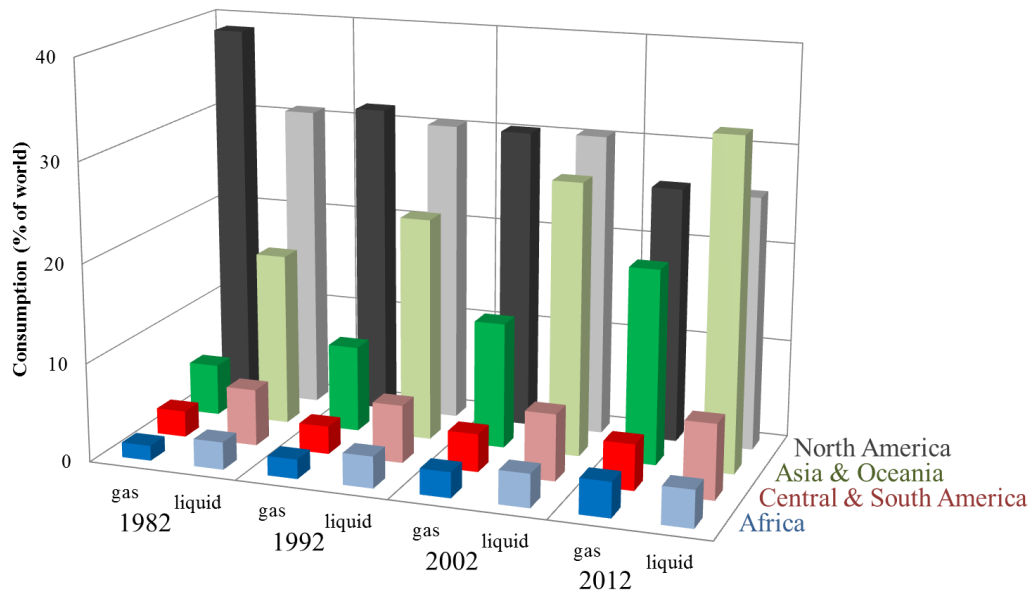


Figure 1.8: Liquid and gaseous petroleum production consumption represented as a percentage of the world's respective consumption. Data were obtained from US Energy Information Administration.

The lag between liquid and gaseous hydrocarbon consumption is probably due to a lack of access more than a lack of demand.<sup>275</sup> Regarding access, using gas pipeline lengths as a proxy for distribution infrastructure prevalence, the top ten countries (from longest to shortest: USA, Russia, Canada, China, Ukraine, Australia, Argentina, UK, Germany, and Iran) possess 86% of the world's 2,865,340 km. The remaining 14% are split by the 115 countries tracked by the Central Intelligence Agency.<sup>276</sup> Access, to modern fuels like natural gas, propane, or liquefied petroleum gas remains limited in developing countries.

Regarding demand for clean-burning fuels, it is estimated that 1.3 million people prematurely die per year due to exposure to indoor air pollution (*i.e.*, from burning unclean fuels for heating and cooking).<sup>275,277</sup> For example, the high sulfur

content of liquid fuels in developing countries result in higher concentrations of toxic SO<sub>x</sub> species upon combustion (Figure 1.9).<sup>278</sup>

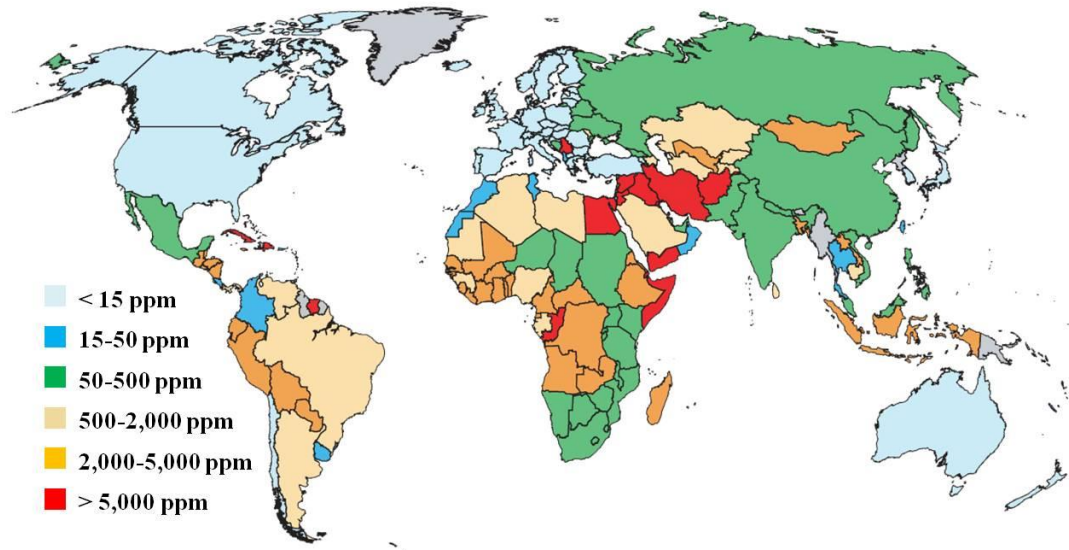


Figure 1.9: Map of allowable sulfur content in diesel fuel according to government regulations. Reprinted with permission from the United Nations Environment Programme – Partnership for Clean Fuels and Vehicles.<sup>278</sup>

In addition to high-sulfur liquid fuels, many residents of developing countries use traditional biomass for heating and cooking fuels.<sup>279,280</sup> To counteract the health concerns, the international community has supported a transition towards cleaner gas-burning appliances.<sup>277</sup> However, unreliable or nonexistent gas distribution networks contribute to the slow adoption of natural gas and liquefied petroleum gas.<sup>275,281</sup> Therefore, converting existing sources of liquid fuels into gaseous fuels at the point of use could increase the adoption rates of natural gas and liquefied petroleum gas appliances.

#### **1.1.4.2 Defense Applications**

Prior to the Single Fuel Policy, variations in fuel quality and distribution reliability adversely affected logistics planning for the North Atlantic Treaty Organization (NATO) forces.<sup>282</sup> The NATO Fuels and Lubricants Working Group elected to use JP-8, which is a kerosene-based jet fuel, as the single battlefield fuel. Homogenizing the fuel type simultaneously simplified sourcing (upstream logistics) and maximized interoperability (downstream logistics); that is, all fuel-consuming devices needed to work with JP-8.<sup>282</sup> While a single-fuel policy offered benefits for logistics, it significantly reduced the types of devices that could be used in the field.

A simple example of the single-fuel problem is the army's field kitchen. A recent Small Business Innovation Research call for proposals criticized current JP-8 appliances for "relying on inefficient burner units that subject cooks to excessive heat, exhaust, and noise." Therefore, the army sought to convert existing JP-8 fuels into a "mixture that can be directly used in commercial gas-fired kitchen appliances with minimal modification."<sup>283</sup> A more advanced example is the desire to replace lithium-ion batteries with energy-dense fuel cells for soldier-wearable portable power in the battlefield.<sup>284,285</sup> Both cases indicate the suboptimal performance of JP-8 in low-to-mid power applications.

The Future Force Warrior project that was initiated by the United States military seeks to equip individual soldiers with technology that improves situational awareness and communications.<sup>286</sup> One of the biggest problems with added technology is the inevitable increased power consumption.<sup>287</sup> Therefore, the military seeks portable power sources that are lightweight and quick to recharge without sacrificing the reliability of current lithium-ion battery systems. Multiple organizations and companies have supported the use of fuel cells (either polyelectrolyte- or solid

oxide-type). However, the lack of fuel cell-compatible fuels in the battlefield (*i.e.*, hydrogen or small molecule hydrocarbons) precludes fuel cell proliferation.<sup>288</sup> Therefore, efforts focus on converting the existing supply of JP-8 into fuel cell-compatible fuels.<sup>288-290</sup> Such a conversion provides added fuel diversification without requiring a reconfigured distribution network.<sup>290</sup>

#### 1.1.4.3 Fuel Conversion Devices - Current State

Fuel cells offer significant energy density advantages over batteries and generators for portable power and backup power, respectively.<sup>284,291</sup> However, because fuel cells typically require hydrogen, fuel storage and transportation are non-trivial problems.<sup>288</sup> To this end, fuel converters offer a method to convert from one fuel to another without requiring intermediate storage and transportation steps.<sup>289</sup> The conversion typically is from large molecules (hydrocarbons) into a mixture of small molecules like syngas or hydrogen, with the help of a water gas shift reaction.<sup>292,293</sup> Therefore, fuel cell systems can leverage the existing solutions to hydrocarbon storage and transportation while still having access to hydrogen.

There are three popular catalytic fuel conversion reactions: steam reformation (SR, Equation 1-10), catalytic partial oxidation (CPOX, Equation 1-11), and autothermal reformation (ATR, Equation 1-12).<sup>289</sup>



SR is an endothermic reaction that operates at high temperatures and thus high energy inputs.<sup>294</sup> CPOX is an exothermic reaction that can create hotspots that result in

catalyst sintering.<sup>291</sup> ATR combines SR and CPOX in an attempt to balance the thermal energy.<sup>295,296</sup> In all cases, the reactions require an additional reactant (*e.g.*, steam and/or oxygen) and produce syngas.<sup>289</sup> Furthermore, catalyst deactivation due to sintering and fuel-sulfur poisoning remains a large concern.<sup>296-299</sup> To mitigate the deleterious effects of sintering and poisoning, researchers have pursued heat management technologies (*e.g.*, Precision Combustion's *Microlith*<sup>TM</sup> technology) and desulfurization processes,<sup>300</sup> respectively. While the fuel conversion community improves technology associated with ATR reactors and desulfurizers, our group has shown the potential of low-temperature sulfur-tolerant zeolites for fuel conversion.<sup>268</sup> This approach mitigates the two main concerns with fuel conversion: sulfur-induced poisoning and temperature-induced sintering. Furthermore, the product gas is a mixture of small hydrocarbons (C<sub>2</sub>-C<sub>5</sub> species), which is easier to store and transport than hydrogen or syngas.

#### **1.1.4.4 Monomolecular Fuel Conversion**

Zeolites can be tailored to exhibit desired porosity, composition, and acidity for applications in catalysis.<sup>154</sup> While materials with nanometer-scaled features can be templated by block polymers,<sup>195</sup> the 5-50 Å scaled zeolites are synthesized using small-molecule structure-directing agents.<sup>301</sup> Also, the ability to decorate the pores with catalytically active sites makes zeolites amenable to catalytic reactions in the petrochemical industry.<sup>302,303</sup> Indeed, previous work from our group used a ZSM-5 catalyst to convert JP-8 into a mixture of hydrocarbons that resembled liquefied petroleum gas *via* a fuel cracking reaction.<sup>268</sup> Also, subsequent work proved that the cracking reaction effectively converted gasoline and diesel. Unlike the existing fuel conversion devices, the catalytic cracking process was effective at low temperatures (<

500 °C) and avoided catalyst sintering associated with CPOX or ATR (600-1200 °C)<sup>304</sup> and the large energetic inputs associated with SR (950°C).<sup>289,293</sup> Furthermore, the catalyst was remarkably tolerant to sulfur-containing species in the fuels. Perhaps more surprising was the apparent absence of sulfurous compounds in the resulting gas-phase product (< 10 ppm). Although the catalyst and reaction conditions satisfied the goals that were set by the Defense Advanced Research Projects Agency, improvements to the balance of plant are required to advance the so-called total readiness level. Work by Lauterbach and coworkers optimized the zeolite catalyst composition in the packed-bed reactor.<sup>268</sup> However, when considering field-use, the system cannot realistically source an inert carrier gas without incurring significant parasitic losses. Furthermore, energetic parasitic losses need to be minimized for heating the reactor, cooling the effluent, and all of the associated pumps, valves, and controllers. Finally, the conversion efficiency was found to be approximately 15-20 wt%. Given the economic value of the input fuel, higher conversion efficiencies near 60 wt% need to be achieved.

## **1.2 Thesis Overview**

This thesis describes two separate, though tangentially related, thrusts towards improving catalytic methods: (1) using block polymers to template inorganic materials and (2) engineering a catalytic fuel conversion device, which uses a zeolite catalyst that was templated using non-polymeric structure-directing agents.

Chapter 2 contains a detailed description of the synthesis and characterization methods used throughout the thesis. Although all of the methods are multi-purpose in nature, they are described with relevance to the two aforementioned thrusts. Chapter 3 describes how gold nanoparticles with varying surface chemistries were synthesized

and templated (*ex situ*) into aligned columns using a cylinder-forming polystyrene-*b*-polyisoprene-*b*-polystyrene triblock polymer. Chapter 4 describes the effort to employ an *in situ* technique to template arrays of metal oxides using pre-formed polystyrene-*b*-poly(ethylene oxide) thin films. Chapter 5 describes future directions to take with polymer-templated nanopatterns. Chapter 6 switches to the second thrust and describes the work on a fuel conversion device. Finally, Chapter 7 describes anticipated future directions on both the block polymer catalyst templating and the fuel conversion device.

## REFERENCES

1. Omenetto, F. G.; Kaplan, D. L. *Science* **2010**, 329(5991), 528-531.
2. Galeski, A. *Prog. Polym. Sci.* **2003**, 28(12), 1643-1699.
3. Ravati, S.; Beaulieu, C.; Zolali, A. M.; Favis, B. D. *AIChE J.* **2014**, 60(8), 3005-3012.
4. Kmetty, A.; Barany, T.; Karger-Kocsis, J. *Prog. Polym. Sci.* **2010**, 35(10), 1288-1310.
5. Roziere, J.; Jones, D. J. *Annu. Rev. Mater. Res.* **2003**, 33(1), 503-555.
6. Ulbricht, M. *Polymer* **2006**, 47(7), 2217-2262.
7. He, M.; Qiu, F.; Lin, Z. Q. *Energy Environ. Sci.* **2013**, 6(5), 1352-1361.
8. Sun, K.; Zhang, S. P.; Li, P. C.; Xia, Y. J.; Zhang, X.; Du, D. H.; Isikgor, F. H.; Ouyang, J. Y. *J. Mater. Sci. - Mater. Electron.* **2015**, 26(7), 4438-4462.
9. Kickelbick, G. *Prog. Polym. Sci.* **2003**, 28(1), 83-114.
10. Tjong, S. C. *Mater. Sci. Eng., R* **2006**, 53(3-4), 73-197.
11. Grossiord, N.; Loos, J.; van Laake, L.; Maugey, M.; Zakri, C.; Koning, C. E.; Hart, A. J. *Adv. Funct. Mater.* **2008**, 18(20), 3226-3234.
12. Han, Z. D.; Fina, A. *Prog. Polym. Sci.* **2011**, 36(7), 914-944.
13. Choudalakis, G.; Gotsis, A. D. *Eur. Polym. J.* **2009**, 45(4), 967-984.
14. Vaia, R. A.; Maguire, J. F. *Chem. Mater.* **2007**, 19(11), 2736-2751.
15. Li, Y.; Krentz, T. M.; Wang, L.; Benicewicz, B. C.; Schadler, L. S. *ACS Appl. Mater. Interfaces* **2014**, 6(9), 6005-6021.
16. Jeon, S. J.; Yang, S. M.; Kim, B. J.; Petrie, J. D.; Jang, S. G.; Kramer, E. J.; Pine, D. J.; Yi, G. R. *Chem. Mater.* **2009**, 21(16), 3739-3741.
17. Kim, B. J.; Fredrickson, G. H.; Kramer, E. J. *Macromolecules* **2008**, 41(2), 436-447.

18. Yu, L. Y.; Xu, Z. L.; Shen, H. M.; Yang, H. *J. Membr. Sci.* **2009**, *337*(1-2), 257-265.
19. Taurozzi, J. S.; Arul, H.; Bosak, V. Z.; Burban, A. F.; Voice, T. C.; Bruening, M. L.; Tarabara, V. V. *J. Membr. Sci.* **2008**, *325*(1), 58-68.
20. Ramesh, G. V.; Porel, S.; Radhakrishnan, T. P. *Chem. Soc. Rev.* **2009**, *38*(9), 2646-2656.
21. Hamley, I. W. *Nanotechnology* **2003**, *14*(10), R39-R54.
22. Orilall, M. C.; Wiesner, U. *Chem. Soc. Rev.* **2011**, *40*(2), 520-535.
23. Pomogailo, A.; Dzhardimalieva, G., Physics and Chemistry of Sol-Gel Nanocomposites Formation. In *Nanostructured Materials Preparation via Condensation Ways*, Springer Netherlands: 2014; pp 141-203.
24. Shan, L.; Punniyakoti, S.; Van Bael, M. J.; Temst, K.; Van Bael, M. K.; Ke, X.; Bals, S.; Van Tendeloo, G.; D'Olieslaeger, M.; Wagner, P.; Haenen, K.; Boyen, H.-G. *J. Mater. Chem. C* **2014**, *2*(4), 701-707.
25. Rabek, J. F.; Lucki, J.; Qu, B. J.; Shi, W. F. *Macromolecules* **1991**, *24*(4), 836-843.
26. Kaliyappan, T.; Kannan, P. *Prog. Polym. Sci.* **2000**, *25*(3), 343-370.
27. Bronstein, L. H.; Sidorov, S. N.; Valetsky, P. M.; Hartmann, J.; Colfen, H.; Antonietti, M. *Langmuir* **1999**, *15*(19), 6256-6262.
28. Kaczmarek, H.; Sionkowska, A.; Kaminska, A.; Kowalonek, J.; Swiatek, M.; Szalla, A. *Polym. Degrad. Stabil.* **2001**, *73*(3), 437-441.
29. Ciardelli, F.; Tsuchida, E.; Wöhrle, D., *Macromolecule-Metal Complexes*. Springer: New York, 1996; p 318.
30. Cao, K.; Murshid, N.; Wang, X. S. *Macromol. Rapid Commun.* **2015**, *36*(7), 586-596.
31. Biradha, K.; Sarkar, M.; Rajput, L. *Chemical Communications* **2006**, (40), 4169-4179.
32. Whittell, G. R.; Hager, M. D.; Schubert, U. S.; Manners, I. *Nat. Mater.* **2011**, *10*(3), 176-188.

33. Rivas, B. L.; Pereira, E. D.; Moreno-Villoslada, I. *Prog. Polym. Sci.* **2003**, 28(2), 173-208.
34. Khanna, P. K.; Gokhale, R.; Subbarao, V.; Vishwanath, A. K.; Das, B. K.; Satyanarayana, C. V. V. *Mater. Chem. Phys.* **2005**, 92(1), 229-233.
35. Fritzsche, W.; Porwol, H.; Wiegand, A.; Bornmann, S.; Kohler, J. M. *Nanostruct. Mater.* **1998**, 10(1), 89-97.
36. Biondi, I.; Laurency, G.; Dyson, P. J. *Inorg. Chem.* **2011**, 50(17), 8038-8045.
37. Deshmukh, R. D.; Buxton, G. A.; Clarke, N.; Composto, R. J. *Macromolecules* **2007**, 40(17), 6316-6324.
38. Deshmukh, R. D.; Composto, R. J. *Chem. Mater.* **2007**, 19(4), 745-754.
39. Liu, Y.; Liu, X. H.; Wang, X.; Yang, J. Z.; Yang, X. J.; Lu, L. D. *J. Appl. Polym. Sci.* **2010**, 116(5), 2617-2625.
40. Hardy, C. G.; Ren, L.; Ma, S.; Tang, C. *Chem. Commun.* **2013**, 49(39), 4373-4375.
41. Whittell, G. R.; Manners, I. *Adv. Mater.* **2007**, 19(21), 3439-3468.
42. Nishikawa, H.; Tsuchida, E. *J. Phys. Chem.* **1975**, 79(19), 2072-2076.
43. Rey, I.; Lassègues, J. C.; Grondin, J.; Servant, L. *Electrochim. Acta* **1998**, 43(10-11), 1505-1510.
44. Koh, H. D.; Park, S.; Russell, T. P. *ACS Nano* **2010**, 4(2), 1124-1130.
45. Aizawa, M.; Buriak, J. M. *J. Am. Chem. Soc.* **2006**, 128(17), 5877-5886.
46. Sun, Z. C.; Kim, D. H.; Wolkenhauer, M.; Bumbu, G. G.; Knoll, W.; Gutmann, J. S. *ChemPhysChem* **2006**, 7(2), 370-378.
47. Li, J. B.; Shi, L. Q.; An, Y. L.; Li, Y.; Chen, X.; Dong, H. J. *Polymer* **2006**, 47(26), 8480-8487.
48. Kim, D. H.; Kim, S. H.; Lavery, K.; Russell, T. P. *Nano Lett.* **2004**, 4(10), 1841-1844.

49. Lee, D. H.; Park, S.; Gu, W. Y.; Russell, T. P. *ACS Nano* **2011**, 5(2), 1207-1214.
50. Cho, H.; Park, H.; Russell, T. P.; Park, S. *J. Mater. Chem.* **2010**, 20(24), 5047-5051.
51. Spatz, J. P.; Mossmer, S.; Hartmann, C.; Moller, M.; Herzog, T.; Krieger, M.; Boyen, H. G.; Ziemann, P.; Kabius, B. *Langmuir* **2000**, 16(2), 407-415.
52. Soler-Illia, G.; Crepaldi, E. L.; Grosso, D.; Sanchez, C. *Curr. Opin. Colloid Interface Sci.* **2003**, 8(1), 109-126.
53. Cheng, Y. J.; Gutmann, J. S. *J. Am. Chem. Soc.* **2006**, 128(14), 4658-4674.
54. Pluronic®.  
<http://worldaccount.basf.com/wa/NAFTA/Catalog/ChemicalsNAFTA/pi/BASF/Brand/pluronic> (July 17, 2014).
55. Mahoney, L.; Koodali, R. T. *Materials* **2014**, 7(4), 2697-2746.
56. Clay, R. T.; Cohen, R. E. *Supramol. Sci.* **1995**, 2(3-4), 183-191.
57. Peng, Q.; Tseng, Y. C.; Darling, S. B.; Elam, J. W. *ACS Nano* **2011**, 5(6), 4600-4606.
58. Kamcev, J.; Germack, D. S.; Nykypanchuk, D.; Grubbs, R. B.; Nam, C. Y.; Black, C. T. *ACS Nano* **2013**, 7(1), 339-346.
59. Akcora, P.; Briber, R. M.; Kofinas, P. *Polymer* **2006**, 47(6), 2018-2022.
60. Ortel, E.; Fischer, A.; Chuenchom, L.; Polte, J.; Emmerling, F.; Smarsly, B.; Kraehnert, R. *Small* **2012**, 8(2), 298-309.
61. Ciebien, J. F.; Clay, R. T.; Sohn, B. H.; Cohen, R. E. *New J. Chem.* **1998**, 22(7), 685-691.
62. Brautigam, M.; Weyell, P.; Rudolph, T.; Dellith, J.; Kriek, S.; Schmalz, H.; Schacher, F. H.; Dietzek, B. *J. Mater. Chem. A* **2014**, 2(17), 6158-6166.
63. Sundstrom, L.; Krupp, L.; Delenia, E.; Rettner, C.; Sanchez, M.; Hart, M. W.; Kim, H. C.; Zhang, Y. *Appl. Phys. Lett.* **2006**, 88(24), 1-3.

64. Garcia, B. C.; Kamperman, M.; Ulrich, R.; Jain, A.; Gruner, S. M.; Wiesner, U. *Chem. Mater.* **2009**, *21*(22), 5397-5405.
65. Toombes, G. E. S.; Finnefrock, A. C.; Tate, M. W.; Ulrich, R.; Wiesner, U.; Gruner, S. M. *Macromolecules* **2007**, *40*(25), 8974-8982.
66. Hsueh, H. Y.; Chen, H. Y.; She, M. S.; Chen, C. K.; Ho, R. M.; Gwo, S.; Hasegawa, H.; Thomas, E. L. *Nano Lett.* **2010**, *10*(12), 4994-5000.
67. Freer, E. M.; Krupp, L. E.; Hinsberg, W. D.; Rice, P. M.; Hedrick, J. L.; Cha, J. N.; Miller, R. D.; Kim, H. C. *Nano Lett.* **2005**, *5*(10), 2014-2018.
68. Crepaldi, E. L.; Soler-Illia, G.; Grosso, D.; Cagnol, F.; Ribot, F.; Sanchez, C. *J. Am. Chem. Soc.* **2003**, *125*(32), 9770-9786.
69. Ivanova, R.; Lindman, B.; Alexandridis, P. *Adv. Colloid Interface Sci.* **2001**, *89*(SI), 351-382.
70. Costi, R.; Saunders, A. E.; Banin, U. *Angew. Chem. Int. Ed.* **2010**, *49*(29), 4878-4897.
71. Toshima, N.; Yonezawa, T. *New J. Chem.* **1998**, *22*(11), 1179-1201.
72. Brown, K. R.; Walter, D. G.; Natan, M. J. *Chem. Mater.* **2000**, *12*(2), 306-313.
73. Zhao, P. X.; Li, N.; Astruc, D. *Coord. Chem. Rev.* **2013**, *257*(3-4), 638-665.
74. Cozzoli, P. D.; Kornowski, A.; Weller, H. *J. Am. Chem. Soc.* **2003**, *125*(47), 14539-14548.
75. Peng, X. G.; Manna, L.; Yang, W. D.; Wickham, J.; Scher, E.; Kadavanich, A.; Alivisatos, A. P. *Nature* **2000**, *404*(6773), 59-61.
76. Tao, A. R.; Habas, S.; Yang, P. D. *Small* **2008**, *4*(3), 310-325.
77. Brust, M.; Walker, M.; Bethell, D.; Schiffrin, D. J.; Whyman, R. *J. Chem. Soc., Chem. Comm.* **1994**, (7), 801-802.
78. Daniel, M. C.; Astruc, D. *Chem. Rev.* **2004**, *104*(1), 293-346.
79. Murray, C. B.; Kagan, C. R.; Bawendi, M. G. *Annu. Rev. Mater. Sci.* **2000**, *30*, 545-610.

80. DeLorey, G. T.; Kestell, A. E., *Nanoparticles : Properties, Classification, Characterization, and Fabrication*. Nova Science Publishers: New York, 2010.
81. Varma, R. S.; Luque, R., *Sustainable Preparation of Metal Nanoparticles : Methods and Applications*. Royal Society of Chemistry: Cambridge, 2012.
82. Peng, Z. A.; Peng, X. G. *J. Am. Chem. Soc.* **2002**, *124*(13), 3343-3353.
83. White, M. A.; Maliakal, A.; Turro, N. J.; Koberstein, J. *Macromol. Rapid Commun.* **2008**, *29*(18), 1544-1548.
84. Shan, J.; Tenhu, H. *Chem. Commun.* **2007**, (44), 4580-4598.
85. Zhang, Q. L.; Gupta, S.; Emrick, T.; Russell, T. P. *J. Am. Chem. Soc.* **2006**, *128*(12), 3898-3899.
86. Crooks, R. M.; Zhao, M. Q.; Sun, L.; Chechik, V.; Yeung, L. K. *Acc. Chem. Res.* **2001**, *34*(3), 181-190.
87. Bockstaller, M. R.; Lapetnikov, Y.; Margel, S.; Thomas, E. L. *J. Am. Chem. Soc.* **2003**, *125*(18), 5276-5277.
88. Mayeda, M. K.; Kuan, W.-F.; Young, W.-S.; Lauterbach, J. A.; Epps III, T. H. *Chem. Mater.* **2012**, *24*(14), 2627-2634.
89. Peponi, L.; Tercjak, A.; Torre, L.; Kenny, J. M.; Mondragon, I. *J. Nanosci. Nanotechnol.* **2009**, *9*(3), 2128-2139.
90. Hu, S. W.; Brittain, W. J.; Jacobson, S.; Balazs, A. C. *Eur. Polym. J.* **2006**, *42*(9), 2045-2052.
91. Ha, Y. H.; Kwon, Y.; Breiner, T.; Chan, E. P.; Tzianetopoulou, T.; Cohen, R. E.; Boyce, M. C.; Thomas, E. L. *Macromolecules* **2005**, *38*(12), 5170-5179.
92. Shin, W. J.; Kim, J. Y.; Lee, J. S. *Macromol. Res.* **2010**, *18*(8), 742-746.
93. Haryono, A.; Binder, W. H. *Small* **2006**, *2*(5), 600-611.
94. Akcora, P.; Liu, H.; Kumar, S. K.; Moll, J.; Li, Y.; Benicewicz, B. C.; Schadler, L. S.; Acehan, D.; Panagiotopoulos, A. Z.; Pryamitsyn, V.; Ganesan, V.; Ilavsky, J.; Thiyagarajan, P.; Colby, R. H.; Douglas, J. F. *Nature Mater.* **2009**, *8*(4), 354-359.

95. Kumar, S. K.; Jouault, N.; Benicewicz, B.; Neely, T. *Macromolecules* **2013**, *46*(9), 3199-3214.
96. Harton, S. E.; Kumar, S. K. *J. Polym. Sci. Pt. B-Polym. Phys.* **2008**, *46*(4), 351-358.
97. Borukhov, I.; Leibler, L. *Macromolecules* **2002**, *35*(13), 5171-5182.
98. Korth, B. D.; Keng, P.; Shim, I.; Bowles, S. E.; Tang, C.; Kowalewski, T.; Nebesny, K. W.; Pyun, J. *J. Am. Chem. Soc.* **2006**, *128*(20), 6562-6563.
99. Corbierre, M. K.; Cameron, N. S.; Lennox, R. B. *Langmuir* **2004**, *20*(7), 2867-2873.
100. Radhakrishnan, B.; Ranjan, R.; Brittain, W. J. *Soft Matter* **2006**, *2*(5), 386-396.
101. Li, C.; Han, J.; Ryu, C. Y.; Benicewicz, B. C. *Macromolecules* **2006**, *39*(9), 3175-3183.
102. Chinthamanipeta, P. S.; Kobukata, S.; Nakata, H.; Shipp, D. A. *Polymer* **2008**, *49*(26), 5636-5642.
103. Ngo, V. G.; Bressy, C.; Leroux, C.; Margaillan, A. *Polymer* **2009**, *50*(14), 3095-3102.
104. Lowes, B. J.; Bohrer, A. G.; Tran, T.; Shipp, D. A. *Polym. Bull.* **2009**, *62*(3), 281-289.
105. Achilleos, D. S.; Vamvakaki, M. *Materials* **2010**, *3*(3), 1981-2026.
106. Oyerokun, F. T.; Vaia, R. A. *Macromolecules* **2012**, *45*(18), 7649-7659.
107. Balazs, A. C.; Emrick, T.; Russell, T. P. *Science* **2006**, *314*(5802), 1107-1110.
108. Kim, B. J.; Fredrickson, G. H.; Hawker, C. J.; Kramer, E. J. *Langmuir* **2007**, *23*(14), 7804-7809.
109. Béziel, W.; Reiter, G.; Drockenmuller, E.; Ostaci, R.-V.; Akhrass, S. A.; Cousin, F.; Sferrazza, M. *Europhys. Lett.* **2010**, *90*(2), 1-6.
110. Arceo, A.; Meli, L.; Green, P. F. *Nano Lett.* **2008**, *8*(8), 2271-2276.

111. Mackay, M. E.; Tuteja, A.; Duxbury, P. M.; Hawker, C. J.; Van Horn, B.; Guan, Z. B.; Chen, G. H.; Krishnan, R. S. *Science* **2006**, *311*(5768), 1740-1743.
112. Thompson, R. B.; Ginzburg, V. V.; Matsen, M. W.; Balazs, A. C. *Science* **2001**, *292*(5526), 2469-2472.
113. Hales, T. C. *Discret. Comput. Geom.* **2001**, *25*(1), 1-22.
114. Shipman, P. D.; Newell, A. C. *Phys. Rev. Lett.* **2004**, *92*(16), 1-4.
115. Jean, R. V., *Phyllotaxis: a systematic study in plant morphogenesis*. Cambridge University Press: Cambridge, 1994; p 386.
116. Young, W. *Transp. Rev.* **1988**, *8*(2), 161-181.
117. Iranpour, R.; Tung, D. *Transport. Eng. - J. ASCE* **1989**, *115*(2), 139-160.
118. Soratto, R. P.; Souza-Schlick, G. D.; Fernandes, A. M.; Zanotto, M. D.; Crusciol, C. A. C. *Ind. Crop. Prod.* **2012**, *35*(1), 244-249.
119. Henderson, T. L.; Johnson, B. L.; Schneiter, A. A. *Agron. J.* **2000**, *92*(2), 329-336.
120. Bedane, G. M.; Gupta, M. L.; George, D. L. *Ind. Crop. Prod.* **2009**, *29*(1), 139-144.
121. Moore, G. *Electronics* **1965**, *38*(8), 114-117.
122. Moore, G. *Electron Devices Meeting, 1975 International* **1975**, *12*, 11-13.
123. Fontecha, J.; Navarro, F. J.; Hervas, R.; Bravo, J. *Pers. Ubiquit. Comput.* **2013**, *17*(6), 1073-1083.
124. Rawassizadeh, R.; Tomitsch, M.; Wac, K.; Tjoa, A. M. *Pers. Ubiquit. Comput.* **2013**, *17*(4), 621-637.
125. Gonzalez, E. G.; Florez, J. A.; Arab, S. *Mech. Syst. Signal Process.* **2008**, *22*(6), 1356-1373.
126. Drmic, A.; Burkardt, D. *VDI Berichte* **2008**, (2009), 245-254.

127. Norris, S. L.; Engelgau, M. M.; Narayan, K. M. V. *Diabetes Care* **2001**, *24*(3), 561-587.
128. Karter, A. J.; Ackerson, L. M.; Darbinian, J. A.; D'Agostino, R. B.; Ferrara, A.; Liu, J.; Selby, J. V. *Am. J. Med.* **2001**, *111*(1), 1-9.
129. Babolat Babolat Play Pure Drive.  
[www.babolat.us/product/tennis/racket/babolat-play-pure-drive-102188](http://www.babolat.us/product/tennis/racket/babolat-play-pure-drive-102188) (25 February).
130. Kane, N. A.; Simmons, M. C.; John, D.; Thompson, D. L.; Basset, D. R. *Int. J. Sports Med.* **2010**, *31*(2), 101-105.
131. Trautmann, C.; Martinelli, N.; Rosenbaum, D. *J. Sports Sci.* **2011**, *29*(15), 1585-1592.
132. Hepburn, H. R. *J. Entomol. Soc. South. Afr.* **1983**, *46*(1), 87-101.
133. Takahashi, T.; Matsuhara, S.; Abe, M.; Komeda, Y. *Plant Cell* **2002**, *14*(9), 2085-2093.
134. Coen, E. S.; Meyerowitz, E. M. *Nature* **1991**, *353*(6339), 31-37.
135. Ben-Joseph, E., *ReThinking a Lot: The Design and Culture of Parking*. The MIT Press: Cambridge, MA, 2012; p 184.
136. Ye, Z. M.; Luo, K.; Lu, X. M.; Fletcher, B.; Liu, W. J.; Xu, F.; LaBrake, D.; Resnick, D. J.; Sreenivasan, S. V. *J. Micro Nanolithogr. MEMS MOEMS* **2012**, *11*(3), 1-6.
137. Levinson, H. J. *J. Micro Nanolithogr. MEMS MOEMS* **2009**, *8*(4), 1-9.
138. Law, M.; Greene, L. E.; Johnson, J. C.; Saykally, R.; Yang, P. *Nature Mater.* **2005**, *4*(6), 455-459.
139. Peng, K. Q.; Lee, S. T. *Adv. Mater.* **2011**, *23*(2), 198-215.
140. Stroeve, P.; Ileri, N. *Trends Biotechnol.* **2011**, *29*(6), 259-266.
141. Cohen-Tanugi, D.; Grossman, J. C. *Nano Lett.* **2012**, *12*(7), 3602-3608.
142. Shah, M.; McCarthy, M. C.; Sachdeva, S.; Lee, A. K.; Jeong, H. K. *Ind. Eng. Chem. Res.* **2012**, *51*(5), 2179-2199.

143. Sanchez, C.; Boissière, C.; Grosso, D.; Laberty, C.; Nicole, L. *Chem. Mater.* **2008**, *20*(3), 682-737.
144. Tseng, A. A., *Nanofabrication : Fundamentals and Applications*. World Scientific: Singapore, 2008.
145. Sanders, D. P. *Chem. Rev.* **2010**, *110*(1), 321-360.
146. Tennant, D. M. *J. Vac. Sci. Technol. A* **2013**, *31*(5), 1-9.
147. Zhou, W. M.; Min, G. Q.; Zhang, J.; Liu, Y. B.; Wang, J. H.; Zhang, Y. P.; Sun, F. *Nano-Micro Lett.* **2011**, *3*(2), 135-140.
148. Garcia, R.; Knoll, A. W.; Riedo, E. *Nature Nanotech.* **2014**, *9*(8), 577-587.
149. Bratton, D.; Yang, D.; Dai, J. Y.; Ober, C. K. *Polym. Adv. Technol.* **2006**, *17*(2), 94-103.
150. Okoroanyanwu, U.; Kye, J.; Yamamoto, N.; Cummings, K. *Microlithogr. World* **2005**, *14*(4), 4-6.
151. Liang, T.; Stivers, A.; Livengood, R.; Yan, P. Y.; Zhang, G. J.; Lo, F. C. *J. Vac. Sci. Technol. B* **2000**, *18*(6), 3216-3220.
152. Vericat, C.; Vela, M. E.; Benitez, G.; Carro, P.; Salvarezza, R. C. *Chem. Soc. Rev.* **2010**, *39*(5), 1805-1834.
153. Haensch, C.; Hoepfner, S.; Schubert, U. S. *Chem. Soc. Rev.* **2010**, *39*(6), 2323-2334.
154. Chal, R.; Gerardin, C.; Bulut, M.; van Donk, S. *ChemCatChem* **2011**, *3*(1), 67-81.
155. Zhu, K.; Wang, D. G.; Liu, J. *Nano Res.* **2009**, *2*(1), 1-29.
156. Czaja, A. U.; Trukhan, N.; Muller, U. *Chem. Soc. Rev.* **2009**, *38*(5), 1284-1293.
157. Vriezema, D. M.; Aragonés, M. C.; Elemans, J.; Cornelissen, J.; Rowan, A. E.; Nolte, R. J. M. *Chem. Rev.* **2005**, *105*(4), 1445-1489.

158. Koblenz, T. S.; Wassenaar, J.; Reek, J. N. H. *Chem. Soc. Rev.* **2008**, 37(2), 247-262.
159. Furst, E. M. *Nature Mater.* **2015**, 14(1), 19-20.
160. Zhang, J. H.; Li, Y. F.; Zhang, X. M.; Yang, B. *Adv. Mater.* **2010**, 22(38), 4249-4269.
161. Pelaz, B.; Jaber, S.; de Aberasturi, D. J.; Wulf, V.; Aida, T.; de la Fuente, J. M.; Feldmann, J.; Gaub, H. E.; Josephson, L.; Kagan, C. R.; Kotov, N. A.; Liz-Marzan, L. M.; Mattoussi, H.; Mulvaney, P.; Murray, C. B.; Rogach, A. L.; Weiss, P. S.; Willner, I.; Parak, W. J. *ACS Nano* **2012**, 6(10), 8468-8483.
162. Pum, D.; Toca-Herrera, J. L.; Sleytr, U. B. *Int. J. Mol. Sci.* **2013**, 14(2), 2484-2501.
163. Uchida, M.; Klem, M. T.; Allen, M.; Suci, P.; Flenniken, M.; Gillitzer, E.; Varpness, Z.; Liepold, L. O.; Young, M.; Douglas, T. *Adv. Mater.* **2007**, 19(8), 1025-1042.
164. Santos, A.; Deen, M. J.; Marsal, L. F. *Nanotechnology* **2015**, 26(4), 042001.
165. Bates, F. S.; Fredrickson, G. H. *Phys. Today* **1999**, 52(2), 32-38.
166. Hadjersi, T.; Gabouze, N.; Kooij, E. S.; Zinine, A.; Ababou, A.; Chergui, W.; Cheraga, H.; Belhousse, S.; Djeghri, A. *Thin Solid Films* **2004**, 459(1-2), 271-275.
167. Bates, F. S.; Hillmyer, M. A.; Lodge, T. P.; Bates, C. M.; Delaney, K. T.; Fredrickson, G. H. *Science* **2012**, 336(6080), 434-440.
168. Braunecker, W. A.; Matyjaszewski, K. *Prog. Polym. Sci.* **2007**, 32(1), 93-146.
169. Moad, G.; Rizzardo, E.; Thang, S. H. *Aust. J. Chem.* **2009**, 62(11), 1402-1472.
170. Bates, F. S. *Science* **1991**, 251(4996), 898-905.
171. Young, R. J.; Lovell, P. A., *Introduction to Polymers*. 2nd ed.; CRC Press: New York, 1991.
172. Flory, P. I. *J. Chem. Phys.* **1942**, 10(1), 51-61.
173. Huggins, M. L. *J. Chem. Phys.* **1942**, 46(1), 151-158.

174. Russell, T. P.; Tsui, O. K. C., *Polymer Thin Films*. World Scientific: Singapore, 2008.
175. Frielinghaus, H.; Hermsdorf, N.; Almdal, K.; Mortensen, K.; Messe, L.; Corvazier, L.; Fairclough, J. P. A.; Ryan, A. J.; Olmsted, P. D.; Hamley, I. W. *Europhys. Lett.* **2001**, *53*(5), 680-686.
176. Dai, K. H.; Kramer, E. J. *Polymer* **1994**, *35*(1), 157-161.
177. Russell, T. P.; Hjelm, R. P.; Seeger, P. A. *Macromolecules* **1990**, *23*(3), 890-893.
178. Patrick, J.; Fairclough, A.; Yu, G. E.; Mai, S. M.; Crothers, M.; Mortensen, K.; Ryan, A. J.; Booth, C. *Phys. Chem. Chem. Phys.* **2000**, *2*(7), 1503-1507.
179. Matsen, M. W. *Macromolecules* **2012**, *45*(4), 2161-2165.
180. Cochran, E. W.; Garcia-Cervera, C. J.; Fredrickson, G. H. *Macromolecules* **2006**, *39*(7), 2449-2451.
181. Chuang, V. P.; Cheng, J. Y.; Savas, T. A.; Ross, C. A. *Nano Lett.* **2006**, *6*(10), 2332-2337.
182. Xiao, S. G.; Yang, X. M.; Hwu, J. J.; Lee, K. Y.; Kuo, D. J. *Polym. Sci. Pt. B-Polym. Phys.* **2014**, *52*(5), 361-367.
183. Tang, C.; Lennon, E. M.; Fredrickson, G. H.; Kramer, E. J.; Hawker, C. J. *Science* **2008**, *322*(5900), 429-432.
184. Xiao, S. G.; Yang, X. M.; Edwards, E. W.; La, Y. H.; Nealey, P. F. *Nanotechnology* **2005**, *16*(7), S324-S329.
185. Yang, X. M.; Peters, R. D.; Nealey, P. F.; Solak, H. H.; Cerrina, F. *Macromolecules* **2000**, *33*(26), 9575-9582.
186. Liu, C. C.; Ramirez-Hernandez, A.; Han, E.; Craig, G. S. W.; Tada, Y.; Yoshida, H.; Kang, H. M.; Ji, S. X.; Gopalan, P.; de Pablo, J. J.; Nealey, P. F. *Macromolecules* **2013**, *46*(4), 1415-1424.
187. Crossland, E. J. W.; Kamperman, M.; Nedelcu, M.; Ducati, C.; Wiesner, U.; Smilgies, D. M.; Toombes, G. E. S.; Hillmyer, M. A.; Ludwigs, S.; Steiner, U.; Snaith, H. J. *Nano Lett.* **2009**, *9*(8), 2807-2812.

188. Hsueh, H. Y.; Yao, C. T.; Ho, R. M. *Chem. Soc. Rev.* **2015**, *44*(7), 1974-2018.
189. Park, C.; Yoon, J.; Thomas, E. L. *Polymer* **2003**, *44*(22), 6725-6760.
190. Tureau, M. S.; Kuan, W. F.; Rong, L. X.; Hsiao, B. S.; Epps, T. H. *Macromolecules* **2012**, *45*(11), 4599-4605.
191. Web of Science v.5.14. Thomson Reuters: New York, 2014.
192. Mastroianni, S. E.; Patterson, J. P.; O'Reilly, R. K.; Epps, T. H. *Soft Matter* **2013**, *9*(42), 10146-10154.
193. Kelley, E. G.; Albert, J. N. L.; Sullivan, M. O.; Epps, T. H. *Chemical Society Reviews* **2013**, *42*(17), 7057-7071.
194. Albert, J. N. L.; Epps III, T. H. *Mater. Today* **2010**, *13*(6), 24-33.
195. Segalman, R. A. *Mater. Sci. Eng., R* **2005**, *48*(6), 191-226.
196. Kim, S.; Bates, C. M.; Thio, A.; Cushen, J. D.; Ellison, C. J.; Willson, C. G.; Bates, F. S. *ACS Nano* **2013**, *7*(11), 9905-9919.
197. Smith, A. P.; Douglas, J. F.; Meredith, J. C.; Amis, E. J.; Karim, A. *J. Polym. Sci. Pt. B-Polym. Phys.* **2001**, *39*(18), 2141-2158.
198. Huang, E.; Mansky, P.; Russell, T. P.; Harrison, C.; Chaikin, P. M.; Register, R. A.; Hawker, C. J.; Mays, J. *Macromolecules* **1999**, *33*(1), 80-88.
199. Pickett, G. T.; Balazs, A. C. *Macromolecules* **1997**, *30*(10), 3097-3103.
200. Xuan, Y.; Peng, J.; Cui, L.; Wang, H.; Li, B.; Han, Y. *Macromolecules* **2004**, *37*(19), 7301-7307.
201. Albert, J. N. L.; Baney, M. J.; Stafford, C. M.; Kelly, J. Y.; Epps III, T. H. *ACS Nano* **2009**, *3*(12), 3977-3986.
202. Ruiz, R.; Kang, H. M.; Detcheverry, F. A.; Dobisz, E.; Kercher, D. S.; Albrecht, T. R.; de Pablo, J. J.; Nealey, P. F. *Science* **2008**, *321*(5891), 936-939.
203. Liu, G.; Detcheverry, F.; Ramírez-Hernández, A.; Yoshida, H.; Tada, Y.; de Pablo, J. J.; Nealey, P. F. *Macromolecules* **2012**, *45*(9), 3986-3992.

204. Xu, T.; Hawker, C. J.; Russell, T. P. *Macromolecules* **2005**, *38*(7), 2802-2805.
205. Yin, J.; Yao, X. P.; Liou, J. Y.; Sun, W.; Sun, Y. S.; Wang, Y. *ACS Nano* **2013**, *7*(11), 9961-9974.
206. Phillip, W. A.; Hillmyer, M. A.; Cussler, E. L. *Macromolecules* **2010**, *43*(18), 7763-7770.
207. Luo, M.; Epps III, T. H. *Macromolecules* **2013**, *46*(19), 7567-7579.
208. Olayo-Valles, R.; Guo, S.; Lund, M. S.; Leighton, C.; Hillmyer, M. A. *Macromolecules* **2005**, *38*(24), 10101-10108.
209. Kang, H.; Craig, G. S. W.; Han, E.; Gopalan, P.; Nealey, P. F. *Macromolecules* **2011**, *45*(1), 159-164.
210. Dessí, R.; Pinna, M.; Zvelindovsky, A. V. *Macromolecules* **2013**, *46*(5), 1923-1931.
211. Kim, S. O.; Solak, H. H.; Stoykovich, M. P.; Ferrier, N. J.; de Pablo, J. J.; Nealey, P. F. *Nature* **2003**, *424*(6947), 411-414.
212. Bates, C. M.; Maher, M. J.; Janes, D. W.; Ellison, C. J.; Willson, C. G. *Macromolecules* **2014**, *47*(1), 2-12.
213. Yen, W.-C.; Lee, Y.-H.; Lin, J.-F.; Dai, C.-A.; Jeng, U. S.; Su, W.-F. *Langmuir* **2010**, *27*(1), 109-115.
214. Dai, Q.; Berman, D.; Virwani, K.; Frommer, J.; Jubert, P. O.; Lam, M.; Topuria, T.; Imaino, W.; Nelson, A. *Nano Lett.* **2010**, *10*(8), 3216-3221.
215. Kim, S. Y.; Gwyther, J.; Manners, I.; Chaikin, P. M.; Register, R. A. *Adv. Mater.* **2014**, *26*(5), 791-795.
216. Forster, S.; Antonietti, M. *Adv. Mater.* **1998**, *10*(3), 195-217.
217. Lin, Y.; Boker, A.; He, J. B.; Sill, K.; Xiang, H. Q.; Abetz, C.; Li, X. F.; Wang, J.; Emrick, T.; Long, S.; Wang, Q.; Balazs, A.; Russell, T. P. *Nature* **2005**, *434*(7029), 55-59.
218. Brinker, C. J. *MRS Bull.* **2004**, *29*(9), 631-640.

219. Urade, V. N.; Wei, T. C.; Tate, M. P.; Kowalski, J. D.; Hillhouse, H. W. *Chem. Mater.* **2007**, *19*(4), 768-777.
220. Wan, Y.; Shi, Y.; Zhao, D. *Chem. Commun.* **2007**, (9), 897-926.
221. Deng, Y. H.; Yu, T.; Wan, Y.; Shi, Y. F.; Meng, Y.; Gu, D.; Zhang, L. J.; Huang, Y.; Liu, C.; Wu, X. J.; Zhao, D. Y. *J. Am. Chem. Soc.* **2007**, *129*(6), 1690-1697.
222. Pan, J. H.; Zhao, X. S.; Lee, W. I. *Chem. Eng. J.* **2011**, *170*(2-3), 363-380.
223. Holmqvist, P.; Alexandridis, P.; Lindman, B. *J. Phys. Chem. B* **1998**, *102*(7), 1149-1158.
224. Lee, D. H.; Kim, H. Y.; Kim, J. K.; Huh, J.; Ryu, D. Y. *Macromolecules* **2006**, *39*(6), 2027-2030.
225. Seo, E.; Ko, S.-J.; Min, S. H.; Kim, J. Y.; Kim, B.-S. *Chem. Mater.* **2015**, *27*(13), 4789-4798.
226. Li, N.; Zhang, X.; Yuan, S.; Zhang, X.; Yuan, Y.; Li, X. *Phys. Chem. Chem. Phys.* **2015**, *17*(18), 12023-12030.
227. Bastakoti, B. P.; Guragain, S.; Yusa, S.-i.; Nakashima, K. *RSC Adv.* **2012**, *2*(14), 5938-5940.
228. Shang, C.; Liu, Z. P. *J. Phys. Chem. C* **2010**, *114*(40), 16989-16995.
229. Wang, X. D.; Mitchell, D. R. G.; Prince, K.; Atanacio, A. J.; Caruso, R. A. *Chem. Mater.* **2008**, *20*(12), 3917-3926.
230. Pavan, M. J.; Shenhar, R. *J. Mater. Chem.* **2011**, *21*(7), 2028-2040.
231. Sohn, B. H.; Choi, J. M.; Yoo, S. I.; Yun, S. H.; Zin, W. C.; Jung, J. C.; Kanehara, M.; Hirata, T.; Teranishi, T. *J. Am. Chem. Soc.* **2003**, *125*(21), 6368-6369.
232. Kashem, M. M. A.; Perlich, J.; Diethert, A.; Wang, W. N.; Memesa, M.; Gutmann, J. S.; Majkova, E.; Capek, I.; Roth, S. V.; Petry, W.; Muller-Buschbaum, P. *Macromolecules* **2009**, *42*(16), 6202-6208.
233. Zou, S.; Hong, R.; Emrick, T.; Walker, G. C. *Langmuir* **2007**, *23*(4), 1612-1614.

234. Thorkelsson, K.; Mastroianni, A. J.; Ercius, P.; Xu, T. *Nano Lett.* **2012**, *12*(1), 498-504.
235. Park, M. J.; Park, J.; Hyeon, T.; Char, K. *J. Polym. Sci. Pt. B-Polym. Phys.* **2006**, *44*(24), 3571-3579.
236. Kalra, V.; Lee, J.; Lee, J. H.; Lee, S. G.; Marquez, M.; Wiesner, U.; Joo, Y. L. *Small* **2008**, *4*(11), 2067-2073.
237. Peponi, L.; Tercjak, A.; Martin, L.; Mondragon, I.; Kenny, J. M. *Express Polym. Lett.* **2011**, *5*(2), 104-118.
238. Kim, B. J.; Fredrickson, G. H.; Kramer, E. J. *Macromolecules* **2007**, *41*(2), 436-447.
239. Kim, B. J.; Fredrickson, G. H.; Bang, J.; Hawker, C. J.; Kramer, E. J. *Macromolecules* **2009**, *42*(16), 6193-6201.
240. Kim, B. J.; Chiu, J. J.; Yi, G. R.; Pine, D. J.; Kramer, E. J. *Adv. Mater.* **2005**, *17*(21), 2618-2622.
241. Kim, B. J.; Bang, J.; Hawker, C. J.; Chiu, J. J.; Pine, D. J.; Jang, S. G.; Yang, S.-M.; Kramer, E. J. *Langmuir* **2007**, *23*(25), 12693-12703.
242. Haridas, M.; Basu, J. K. *Nanotechnology* **2010**, *21*(41), 1-6.
243. Carp, O.; Huisman, C. L.; Reller, A. *Prog. Solid State Chem.* **2004**, *32*(1-2), 33-177.
244. Moulé, A. J.; Neher, D.; Turner, S. T., P3HT-Based Solar Cells: Structural Properties and Photovoltaic Performance. In *P3HT Revisited – From Molecular Scale to Solar Cell Devices*, Ludwigs, S., Ed. Springer Berlin Heidelberg: 2014; Vol. 265, pp 181-232.
245. Gaya, U. I., Principles of Heterogeneous Photocatalysis. In *Heterogeneous Photocatalysis Using Inorganic Semiconductor Solids*, Springer Netherlands: 2014; pp 1-41.
246. Fujishima, A.; Zhang, X. T.; Tryk, D. A. *Surf. Sci. Rep.* **2008**, *63*(12), 515-582.
247. Yan, X. L.; Ohno, T.; Nishijima, K.; Abe, R.; Ohtani, B. *Chem. Phys. Lett.* **2006**, *429*(4-6), 606-610.

248. Koh, J. H.; Park, J. T.; Roh, D. K.; Seo, J. A.; Kim, J. H. *Colloids Surf., A* **2008**, 329(1-2), 51-57.
249. Peng, J.; Li, X.; Kim, D. H.; Knoll, W. *Macromol. Rapid Commun.* **2007**, 28(21), 2055-2061.
250. Niedermeier, M. A.; Gro; Muller-Buschbaum, P. *J. Mater. Chem. A* **2013**, 1(43), 13399-13403.
251. Wang, C. C.; Zhang, Z. B.; Ying, J. Y. *Nanostruct. Mater.* **1997**, 9(1-8), 583-586.
252. Zhang, Z. B.; Wang, C. C.; Zakaria, R.; Ying, J. Y. *J. Phys. Chem. B* **1998**, 102(52), 10871-10878.
253. van Grieken, R.; Aguado, J.; Lopez-Munoz, M. J.; Marugan, J. *J. Photochem. Photobiol., A* **2002**, 148(1-3), 315-322.
254. Anpo, M.; Shima, T.; Kodama, S.; Kubokawa, Y. *J. Phys. Chem.* **1987**, 91(16), 4305-4310.
255. Serpone, N. *J. Phys. Chem. B* **2006**, 110(48), 24287-24293.
256. Liu, G.; Wang, L. Z.; Yang, H. G.; Cheng, H. M.; Lu, G. Q. *J. Mater. Chem.* **2010**, 20(5), 831-843.
257. Primo, A.; Corma, A.; Garcia, H. *Phys. Chem. Chem. Phys.* **2011**, 13(3), 886-910.
258. Kowalska, E.; Mahaney, O. O. P.; Abe, R.; Ohtani, B. *Phys. Chem. Chem. Phys.* **2010**, 12(10), 2344-2355.
259. Awazu, K.; Fujimaki, M.; Rockstuhl, C.; Tominaga, J.; Murakami, H.; Ohki, Y.; Yoshida, N.; Watanabe, T. *J. Am. Chem. Soc.* **2008**, 130(5), 1676-1680.
260. Du, L. C.; Furube, A.; Hara, K.; Katoh, R.; Tachiya, M. *J. Photochem. Photobiol. C-Photochem. Rev.* **2013**, 15, 21-30.
261. Hou, W. B.; Cronin, S. B. *Adv. Funct. Mater.* **2013**, 23(13), 1612-1619.
262. Kolwas, K.; Derkachova, A.; Shopa, M. *J. Quant. Spectrosc. Radiat. Transfer* **2009**, 110(14-16), 1490-1501.

263. Kim, K. H.; Husakou, A.; Herrmann, J. *Opt. Express* **2010**, *18*(7), 7488-7496.
264. Mock, J. J.; Barbic, M.; Smith, D. R.; Schultz, D. A.; Schultz, S. *J. Chem. Phys.* **2002**, *116*(15), 6755-6759.
265. Zeng, S. W.; Yong, K. T.; Roy, I.; Dinh, X. Q.; Yu, X.; Luan, F. *Plasmonics* **2011**, *6*(3), 491-506.
266. Arabatzis, I. M.; Stergiopoulos, T.; Andreeva, D.; Kitova, S.; Neophytides, S. G.; Falaras, P. *J. Catal.* **2003**, *220*(1), 127-135.
267. Cha, M. A.; Shin, C.; Kannaiyan, D.; Jang, Y. H.; Kochuveedu, S. T.; Ryu, D. Y.; Kim, D. H. *J. Mater. Chem.* **2009**, *19*(39), 7245-7250.
268. Bedenbaugh, J. E.; Kim, S.; Sasmaz, E.; Lauterbach, J. *ACS Comb. Sci.* **2013**, *15*(9), 491-497.
269. Bedenbaugh, J. E. Investigation of Catalytic Materials for Cracking of Military Aviation Fuel to Liquefied Petroleum Gas: High Throughput Experimentation. University of Delaware, Newark, 2012.
270. Smalley, R., Top Ten Problems for next 50 Years. Smalley Institute: 2003.
271. Doukas, A.; Ballesteros, A. In *Clean Energy Access in Developing Countries: Perspectives on Policy and Regulation*, World Resources Institute, 2012; World Resources Institute: 2012.
272. International Energy Statistics. US EIA: 2014.
273. Smith, K. R. *Annu. Rev. Energy Env.* **1993**, *18*(1), 529-566.
274. Smith, K. R.; Rogers, J.; Cowlin, S. C.; World, L. P. G. A., *Household fuels and ill-health in developing countries : what improvements can be brought by LP gas?* World LP Gas Association: Paris, France, 2005.
275. Energy for Cooking in Developing Countries. In *World Energy Outlook 2006*, Priddle, R., Ed. OECD/IEA: Paris, 2006.
276. *The World Factbook 2013-14*. Central Intelligence Agency: Washington, DC, 2013.

277. Bruce, N.; Rehfuess, E.; Mehta, S.; Hutton, G.; Smith, K., Indoor Air Pollution. In *Disease Control Priorities in Developing Countries* 2nd ed.; Jamison, D.; Breman, J.; Measham, A.; Alleyne, G.; Claeson, M.; Evans, D.; Prabhath, J.; Mills, A.; Musgrove, P., Eds. World Bank: Washington DC, 2006; p 1452.
278. *Opening the Door to Cleaner Vehicles in Developing and Transition Countries: The Role of Lower Sulfur Fuels*; United Nations Environment Programme: Nairobi, 2014.
279. Grieshop, A. P.; Marshall, J. D.; Kandlikar, M. *Energy Policy* **2011**, 39(12), 7530-7542.
280. Bacon, R.; Bhattacharya, S.; Kojima, M., Expenditure of Low-Income Households on Energy: Evidence from Africa and Asia. Oil, G., and Mining Policy, Ed. The World Bank: 2010; Vol. 16.
281. McDade, S. *Energy Sustain. Dev.* **2004**, 8(3), 74-81.
282. NATO Logistics Handbook. Support, P., Ed. NATO: Brussels, 2012.
283. Battle Fuel Conditioner (BFC) for Commercial Gas Appliances in Field Kitchens.  
[http://www.dodsbir.net/sitis/archives\\_display\\_topic.asp?Bookmark=43187](http://www.dodsbir.net/sitis/archives_display_topic.asp?Bookmark=43187)  
(Dec 2013).
284. Thampan, T.; Shah, D.; Cook, C.; Novoa, J.; Shah, S. *J. Power Sources* **2014**, 259, 276-281.
285. Shaw, L.; Pratt, J.; Klebanoff, L.; Johnson, T.; Arienti, M.; Moreno, M. *Int. J. Hydrogen Energy* **2013**, 38(6), 2810-2823.
286. Comstock, J. J. M.; Freeborg, C. D.; Martinez, B. J.; Turner, C. P.; Wilson, D. L.; Rippert, M. T. In *Future Force Warrior*, IEEE Systems and Information Engineering Design Symposium, Charlottesville, VA, United states, 2006; Institute of Electrical and Electronics Engineers Computer Society: Charlottesville, VA, United states, 2006; pp 234-238.
287. Meredith, S. P.; Bergmann, D. *Infantry* **2013**, 5-8.
288. Patil, A. S.; Dubois, T. G.; Sifer, N.; Bostic, E.; Gardner, K.; Quah, M.; Bolton, C. *J. Power Sources* **2004**, 136(2), 220-225.

289. Xu, X. H.; Li, P. W.; Shen, Y. S. *Appl. Energy* **2013**, *108*, 202-217.
290. Roychoudhury, S.; Lyubovsky, M.; Walsh, D.; Chu, D.; Kallio, E. *J. Power Sources* **2006**, *160*(1), 510-513.
291. Schwank, J. W.; Tadd, A. R., Catalytic reforming of liquid hydrocarbons for on-board solid oxide fuel cell auxiliary power units. In *Catalysis: Volume 22*, The Royal Society of Chemistry: 2010; Vol. 22, pp 56-93.
292. Brown, L. F. *Int. J. Hydrogen Energy* **2001**, *26*(4), 381-397.
293. Ahmed, S.; Krumpelt, M. *Int. J. Hydrogen Energy* **2001**, *26*(4), 291-301.
294. Walluk, M. R.; Bradley, M. A.; Trabold, T. A.; Smith, D. F.; Junaedi, C.; Roychoudhury, S. *Fuel* **2015**, *139*, 35-39.
295. Scenna, R.; DuBois, T. G.; Nieh, S. *Fuel* **2013**, *108*, 731-739.
296. Klinghoffer, N. B.; Barraï, F.; Castaldi, M. J. *J. Power Sources* **2011**, *196*(15), 6374-6381.
297. Sehested, J.; Larsen, N. W.; Falsig, H.; Hinnemann, B. *Catal. Today* **2014**, *228*, 22-31.
298. Sehested, J. *Catal. Today* **2006**, *111*(1-2), 103-110.
299. Lee, I. C.; Ubanyionwu, H. C. *Fuel* **2008**, *87*(3), 312-318.
300. Song, C. S. *Catal. Today* **2003**, *86*(1-4), 211-263.
301. Cundy, C. S.; Cox, P. A. *Chem. Rev.* **2003**, *103*(3), 663-701.
302. Lee, J.; Farha, O. K.; Roberts, J.; Scheidt, K. A.; Nguyen, S. T.; Hupp, J. T. *Chem. Soc. Rev.* **2009**, *38*(5), 1450-1459.
303. Davis, M. E. *Acc. Chem. Res.* **1993**, *26*(3), 111-115.
304. Gould, B. D.; Tadd, A. R.; Schwank, J. W. *J. Power Sources* **2007**, *164*(1), 344-350.

## **Chapter 2**

### **EXPERIMENTAL METHODS AND CHARACTERIZATION TECHNIQUES**

Chapter 2 details the experimental methods and characterization techniques for investigating nanoparticle synthesis, block polymer composite thin film casting and templating, and designing a fuel converter. Each technique serves multiple functions; applications to block polymer thin films and catalysis are discussed here. Specific details are reserved for the respective experimental sections in later chapters.

#### **2.1 Gold Nanoparticle Preparation**

##### **2.1.1 Gold Nanoparticle Synthesis**

Gold nanoparticles (AuNPs) have a variety of applications in catalysis, energy harvesting, drug delivery, and sensors.<sup>1</sup> Correspondingly, researchers have developed numerous nanoparticle synthetic procedures to control the size,<sup>2,3</sup> size dispersity,<sup>3</sup> and shape.<sup>4,5</sup> In general, synthetic techniques create nanoparticles by reducing a precursor gold salt in the presence of ligands that direct the nucleation and growth process.<sup>1</sup> Ligands can be small molecules,<sup>6</sup> polymers,<sup>7</sup> or dendrimers.<sup>8</sup>

The most popular method for AuNP synthesis is the Brust-Schiffrin method, which uses an alkanethiol capping ligand to control the growth of nanoparticles during a hydrochloroaurate reduction reaction.<sup>6</sup> Specifically, a beaker of an aqueous phase and a toluene phase was used as a reactor. Hydrogen tetrachloroaurate, which was dissolved in the aqueous phase (30 mL, 30 mM), was extracted into the toluene phase by the addition of tetraoctylammonium bromide (80 mL, 50 mM). The

tetrachloroaurate ion was then reduced by titrating an aqueous solution of sodium borohydride ( $\approx 25$  mL, 400 mM). Growth of AuNPs was limited by the attachment of the dodecanethiol molecules ( $C_{12}SH$ , 170 mg) that were present in the organic phase. Washing was done with excess ethanol and separation was performed with centrifugation (23,000 relative centripetal force). The resulting nanoparticles ( $\approx 4$  nm diameter) could be processed in organic solvents and incorporated into polymer thin films.<sup>9-11</sup> Within the limits of the Brust-Schiffrin method, the sizes of AuNPs could be tuned by varying the thiol:gold reactant molar ratio; for example, tuning the thiol:gold ratio from 0:1 to 2:1 changed the AuNP size from 8 nm to 2 nm.<sup>12</sup> Beyond the Brust-Schiffrin method exists a plethora of procedures that varied the reducing agent, solution pH, reaction temperature, capping ligands, and post-processing.<sup>1,13</sup> Furthermore, the gold-thiol bond was weak enough to allow thiol ligand exchanges, which was an effective way to change the surface chemistry of the nanoparticles.<sup>14,15</sup>

### **2.1.2 Ligand Exchanges**

Post-synthesis ligand exchanges on AuNPs can be done to improve their compatibility with block polymer domains.<sup>10,16,17</sup> To perform ligand exchanges, as-synthesized AuNPs were dispersed in chloroform and a desired amount of thiol-functionalized polystyrene (PS-SH) was added and stirred for three days. For example, to produce AuNPs with a  $C_{12}SH:PS-SH$  molar ratio of  $4.8 \pm 0.2$ , 10.1 mg of as-synthesized AuNPs and 3.9 mg of polystyrene-thiol were stirred in 5 mL of dichloromethane. The mass feed ratios and resulting  $C_{12}SH:PS-SH$  molar ratios used in this thesis are given in the table below.

Table 2.1: Molar and mass feed ratios for ligand exchange reactions

Au <sub>∞</sub> NP:PS-SH mass feed ratio	C <sub>12</sub> SH:PS-SH molar ratio
0.70 ± 0.05	2.7 ± 0.2
1.31 ± 0.05	2.8 ± 0.2
1.38 ± 0.05	3.1 ± 0.2
2.20 ± 0.05	4.1 ± 0.2
2.4 ± 0.1	4.5 ± 0.2
2.6 ± 0.1	4.8 ± 0.2
2.8 ± 0.1	5.1 ± 0.2
3.4 ± 0.1	6.6 ± 0.2

Washing and separation was performed as previously described. Characterization of ligand exchanged AuNPs was done using nuclear magnetic resonance spectroscopy.

## 2.2 Nuclear Magnetic Resonance Spectroscopy

Nuclear magnetic resonance (NMR) spectroscopy is a powerful method to characterize the product and product purity of organic compounds such as oligomers and ligands.<sup>18</sup> NMR spectra were used to identify the chemical composition of grafted ligands on AuNP surfaces. More specifically, <sup>1</sup>H magic angle spinning nuclear magnetic resonance experiments were performed in order to corroborate the chemical shifts observed from standard NMR measurements. However, before introducing MAS NMR spectroscopy, a brief introduction to NMR spectroscopy is discussed.

NMR spectroscopy yields detailed information on a selected set of nuclei such as neighboring nuclei, structural information, and chemical bonding. NMR experiments in this thesis utilized <sup>1</sup>H nuclei. Elemental isotopes with a nuclear spin quantum number  $I = 1/2$  are commonly used (*e.g.*, <sup>1</sup>H, <sup>13</sup>C, <sup>19</sup>F, <sup>31</sup>P). In the absence of a magnetic field, <sup>1</sup>H nuclei can occupy one of two degenerate ground states: +1/2 and -1/2. When placed in a magnetic field, the <sup>1</sup>H nucleus will experience Zeeman splitting,

which describes the separation of the  $+1/2$  and  $-1/2$  states into low and high energy levels, and precess at the Larmor frequency.<sup>19</sup> The Larmor frequency depends on the strength of the applied magnetic field and the gyromagnetic constant, which is  $2.675 \times 10^8 \text{ s}^{-1}\cdot\text{T}^{-1}$  for  $^1\text{H}$ . For example, a proton in a 9.4 T magnetic field will precess at a resonant frequency near 400 MHz. The effect of the applied magnetic field on  $^1\text{H}$  nuclei is succinctly described by the Hamiltonian, which is a second-rank Cartesian tensor. The full NMR Hamiltonian,  $H$ , encompasses contributions from the chemical shift,  $J$ -coupling, dipolar coupling, and quadrupolar coupling interactions and can be summarized by the following equation.

$$H = H_{Zeeman} + H_{chemical\ shift} + H_{J-coupling} + H_{dipolar} + H_{quadrupolar} \quad 2-1$$

Subtle changes in the local electron density of each  $^1\text{H}$  nuclei will alter the effective strength of the magnetic field and “shift” the Larmor frequency. Thus  $H_{chemical\ shift}$  includes the effect from neighboring nuclei and their chemical bonds that can shield or deshield the  $^1\text{H}$  from the applied magnetic field and shift the Larmor frequency to higher or lower resonances, respectively.  $J$ -coupling interactions capture the influence of a nucleus’ spin-induced magnetic field influencing the local magnetic field of chemically dissimilar nuclei.  $J$ -coupling results in a NMR peak signal splitting into  $N+1$  peak signals with  $N$  active nuclei that are within three chemical bond lengths. Dipolar coupling interactions can be understood by considering nuclei as classical bar magnets. The interaction between the two magnets depends on their proximity to each other and the strength of the externally applied magnetic field. Dilute solutions or quick and random movement associated with molecular tumbling will minimize spectral line broadening caused by dipolar interactions (*i.e.*,  $H_{dipolar} \approx 0$ ). However, such quick and random movement cannot be assumed when analyzing ligands that are

attached to nanomaterials because the nanoparticles can be hundreds of times larger than their grafted ligands. Nanomaterials should be analyzed by  $^1\text{H}$  magic angle spinning NMR, which is a more rigorous analysis technique and is briefly discussed in section 2.3. Finally, quadrupolar interactions result from aspherical charge distributions of a nucleus with spin quantum numbers larger than  $\frac{1}{2}$ . As previously stated,  $^1\text{H}$  nuclei have a spin quantum number of  $\frac{1}{2}$  and have a spherical charge distribution without quadrupolar coupling.<sup>19-21</sup> While not necessary, *a priori* knowledge about the analyte and the influence of each interaction greatly expedites peak assignment during NMR spectra analysis.

As a Fourier spectroscopic technique, NMR uses a time-domain radio frequency pulse to simultaneously excite a broad band of frequencies, which include the Larmor frequencies of interest. After the pulse is emitted, excited nuclei relax to the ground state by dissipating energy to the environment in the form of photon emission or heat loss. Equilibration of the energetic distribution of nuclei follows an exponential decay, which is recorded in the time domain. The NMR spectrum of intensity *versus* frequency is achieved by calculating the Fourier transformation of the exponential decay. It is common to see spectra plotted as intensity *versus* a chemical shift in units of ppm, which is normalized to the Larmor frequency of a standard molecule such as trimethylsilane.

In a typical measurement, the analyte was dissolved in deuterated chloroform and passed through a 0.45  $\mu\text{m}$  filter to remove unwanted dust and debris. The solution was placed in a 7 in x 5 mm  $\varnothing$  borosilicate NMR tube with a polyethylene cap. Measurements were taken with either a Bruker AV-400 NMR at the University of Delaware or a Bruker Avance III HD 300 at the University of South Carolina.

### 2.3 $^1\text{H}$ Magic Angle Nuclear Magnetic Resonance Spectroscopy

NMR spectra become difficult to resolve when the analytes are tethered to a surface because the spectral line signals broaden due to confinement effects.<sup>22,23</sup> While line broadening is especially pronounced with large solids (*e.g.*, resins),<sup>22</sup> broadening also can be observed when organics are attached to nanomaterials.<sup>23</sup> Molecular reorientation may not happen at a fast enough rate to eliminate anisotropic line broadening. Magic angle spinning nuclear magnetic resonance (MAS NMR) spectroscopy was developed to improve spectral resolution by minimizing line broadening.

The main sources of anisotropic broadening are dipolar interactions and the chemical shift.<sup>24</sup> The time-averaged Hamiltonians,  $H$ , of both interactions depend on the angle,  $\theta$ , between the spinning axis and the magnetic field according to the following expressions.<sup>24</sup>

$$\begin{aligned} H_{dipolar} &\propto (1 - 3 \cos^2 \theta) \\ H_{CS} &\propto (3 \cos^2 \theta - 1) \end{aligned} \quad 2-2$$

Therefore, the anisotropic contributions to the Hamiltonian are zeroed when the probe head is adjusted such that the spinning axis is oriented at  $54.74^\circ$ , which is the magic angle with respect to the magnetic field.<sup>25</sup> In addition to aligning the magic angle, it is important to suppress spinning sidebands by increasing the sample rotation rate.<sup>24</sup> For a sample that is spinning at a rate of  $\omega_r$  with a chemical shift located at a frequency  $\omega_{CS}$ , sidebands would appear at the following frequencies.

$$\omega_{CS} \pm n\omega_r; n = 1, 2, 3, \dots \quad 2-3$$

$^1\text{H}$  MAS NMR experiments were performed on a 500 MHz instrument with a sample spinning at 1 kHz.<sup>10</sup> The resulting spectra exhibited no spinning sidebands that convoluted the peak interpretation.

## 2.4 Thin Film Deposition

Thin films are commonly deposited on flat substrates, such as glass slides and crystalline wafers, from solvent solutions.<sup>26</sup> Relevant solution deposition techniques include spin coating,<sup>27</sup> flow coating,<sup>28,29</sup> dip coating,<sup>30</sup> droplet pinning,<sup>31</sup> and spray coating.<sup>32-34</sup> Samples prepared throughout this thesis were made by spin coating and flow coating onto silicon and silicon oxide wafers.

During spin coating, a solution is syringed onto a spinning substrate (*e.g.*, 2 wt% polymer in a toluene solution onto a silicon wafer fragment spinning at a rate of 4,000 revolutions per minute). Polymer film thicknesses can be controlled by changing the polymer concentration, solvent, and rotation rate.<sup>27</sup> Spin coaters are used widely because they are commercially available and simple and safe to operate.

Flow coating is an alternative technique that uses a blade to coat a droplet of solution onto a substrate.<sup>28,29</sup> One of the main benefits of flow coating over spin coating is the ability to generate thickness gradients in a continuous fashion.<sup>29</sup> In flow coating, a polymer solution is spread onto a substrate by a suspended blade. Gradient-thickness films are generated by accelerating or decelerating the blade during deposition, while constant-thickness films are generated using a constant velocity. To control the film thickness profiles, Stafford *et al.* demonstrated the importance of the blade height, blade angle (pitch, roll, and yaw), blade velocity, solution concentration, and blade acceleration for gradient thicknesses.<sup>29</sup> Furthermore, Davis *et al.* experimentally verified that flow coating follows Landau-Levich flow, which is based on a lubrication approximation.<sup>28</sup> When adjusting flow coating parameters to target a specific film thickness, the blade velocity usually was the first parameter to be changed because altering the blade profile or polymer solution concentration required precise adjustments to the blade mount or making a new polymer solution,

respectively. Because flow coating is a linear process, as opposed to a rotational process, it is more amenable to high throughput roll-to-roll processes.<sup>35</sup>

## 2.5 Thermal and Solvent Vapor Annealing

Except for special film casting techniques like droplet pinning,<sup>31</sup> as-cast polymer films exhibit kinetically-trapped poor ordering due to the short solvent evaporation timescale ( $\sim$  s) during film deposition. Therefore, polymer films need to be annealed to achieve long-range ordered features.<sup>36,37</sup> Generally, annealing processes impart mobility to the polymer chains to promote self-assembly into a thermodynamic equilibrium or metastable state.<sup>26,37,38</sup> Specifically, thermal annealing imparts polymer chain mobility by heating the polymer film above the polymer glass transition temperature while remaining below the polymer degradation temperature. The temperature, time, and atmospheric composition (*e.g.*, inert or vacuum) are the typical annealing parameters that can be altered to improve ordering. Films are not annealed in air so as to avoid temperature-induced oxidation. For example, a film could be annealed at 150 °C for 24 h under vacuum ( $10^{-3}$  torr).

Long exposure to high temperatures can thermally degrade the polymer films. Solvent vapor annealing is a common alternative method to annealing polymer thin films.<sup>36,39-41</sup> In a typical annealing step, a beaker of solvent and the polymer film were enclosed in a sealed container and allowed to equilibrate, at room temperature, for a period of minutes to hours. As the solvent evaporated from the beaker into the environment of the sealed container, it diffused into the polymer film and induced polymer chain mobility even at temperatures below the polymer glass transition temperature.<sup>42</sup> The solvent was selected to be compatible with all blocks of the block polymer; in some cases, multiple solvents were used;<sup>43,44</sup> in one case, toluene vapor

annealing in a high-humidity chamber was used to improve the ordering of a polystyrene-*b*-poly(ethylene oxide) block polymer thin film.<sup>43</sup> More elaborate solvent annealing techniques controlled the rate of vapor introduction and evacuation or the method of vapor delivery.<sup>39,40,45</sup> Ultimately, solvent vapor annealing techniques could be used to control the morphology and orientation of block polymer thin films.<sup>36,43</sup>

## 2.6 Spectral Reflectance

Spectral reflectance is a fast and simple method to measure a large range of polymer film thicknesses; depending on the wavelengths that are employed, films from 3 nm to 3000  $\mu\text{m}$  can be measured.<sup>46,47</sup> The non-destructive characterization method requires that the polymer film be on an optically reflective and flat substrate. Common substrates include silicon wafers and metal-coated wafers (*e.g.*, gold, silver, aluminum, etc.). Light with wavelength,  $\lambda$ , is spectrally reflected at a normal incidence angle. Constructive and destructive interferences caused by Fresnel reflections from the top and bottom surfaces of the film, which is of thickness  $d$  and refractive index  $n$ , create a spectrum of reflectivity intensity,  $I$ , that can be numerically modeled according to the following expression.<sup>48</sup>

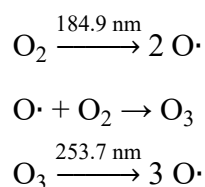
$$I \propto \cos\left(\frac{4\pi}{\lambda}nd\right) \quad 2-4$$

The equation shows that the reflectance will oscillate with wavelength and the frequency of the oscillation will increase with the thickness or refractive index of the film.<sup>48</sup> The model can accommodate multi-layer films, each with varying thicknesses and optical constants. However, because there is no closed-form solution for multi-layered films, the measurement precision decreases with increasing number of layers.<sup>48</sup> Also, while the technique is well-suited for transparent passive materials (*i.e.*,

negligible extinction coefficient), spectral reflectance is not well-suited to characterize opaque thin films (*e.g.*, metal films, carbon black, nanocomposites with loading volumes over ~10%) and requires additional film characterization for use with light-absorbing films (*e.g.*, dyes, photovoltaic materials, and materials with a nonzero extinction coefficient).<sup>48</sup> Spectral reflectance is a fast and non-destructive method for measuring polymer thin film thicknesses.

## 2.7 Polymer Etching with Ultraviolet-Ozone

Ozone exposure is an effective way to degrade organic material. For safety reasons, it is advantageous to generate and extinguish the needed ozone at the point of use.<sup>49</sup> Therefore, ultraviolet ozone (UVO) cleaners are safe and effective instruments for oxidizing polymer thin films.<sup>50</sup> A Jelight 42 was used throughout these experiments and several alternatives are available (*e.g.*, UVOCS T10X10/OES, UVFAB ProCleaner, SAMCO UV-1, or Novascan PSD), but all work on the same principle. Two wavelengths of ultraviolet light (184.9 nm and 253.7 nm) are used to simultaneously dissociate molecular oxygen and ozone into atomic oxygen according to the following reactions.



As a strong oxidizer, atomic oxygen reacted with the hydrocarbon polymer to produce water and carbon dioxide.<sup>50</sup> The 253.7 nm wavelength also accelerated polymer thin film etching by degrading the polymer. Etching rates decreased with distance from the UV lamp. In one experiment, samples were placed 5 mm and 800 mm away from the UV lamp; the former was cleaned within 90 s while the latter took 13 min.<sup>49</sup> To ensure

complete organic removal, the samples were placed within 10 mm of the lamp and were irradiated for 30 min. For safety purposes, the UVO product gas was exhausted into a secondary chamber that functioned as an “ozone killer.” The residual ozone in the exhaust gas was dissociated by a 253.7 nm lamp. It was important that the so-called “ozone killer” was properly operational to remove the toxic ozone, which had a lifetime of 3 days at 20 °C.<sup>51</sup>

## **2.8 Atomic Force Microscopy**

Surface features of block polymer thin films can be imaged in a scanning fashion using atomic force microscopy (AFM).<sup>52</sup> Tapping mode AFM scans a sharp tip across the sample surface to detect topography and material stiffness contrast. The tip deflections are optically detected by reflecting a laser beam from the tip to a photodiode; the sensitive optics can detect features as small as 1-10 nm, which is enough resolution to detect the domains of a block polymer.<sup>53</sup> Therefore, AFM is a powerful technique that can identify the nanoscale ordering of block copolymer thin films.<sup>54</sup>

In tapping mode AFM, which is a common method that is used for imaging polymer thin films, the tip is made to oscillate near its resonance frequency (~ 100-300 kHz) using piezoelectrics.<sup>53</sup> The scanning tip creates a raster by simultaneously recording height and phase images (Figure 2.1). The height image is generated by monitoring the amplitude of the oscillating tip. A proportional-integral-derivative controller maintains a constant tip-amplitude by adjusting the tip height in response to height changes in film topography.<sup>53</sup> On the other hand, the phase image is generated by observing the phase lag between the input sinusoidal signal (*i.e.*, electronic signal

from the piezoelectric to the cantilever tip) and output sinusoidal signal (*i.e.*, tip oscillation as recorded by the aforementioned photodiode).<sup>53</sup>

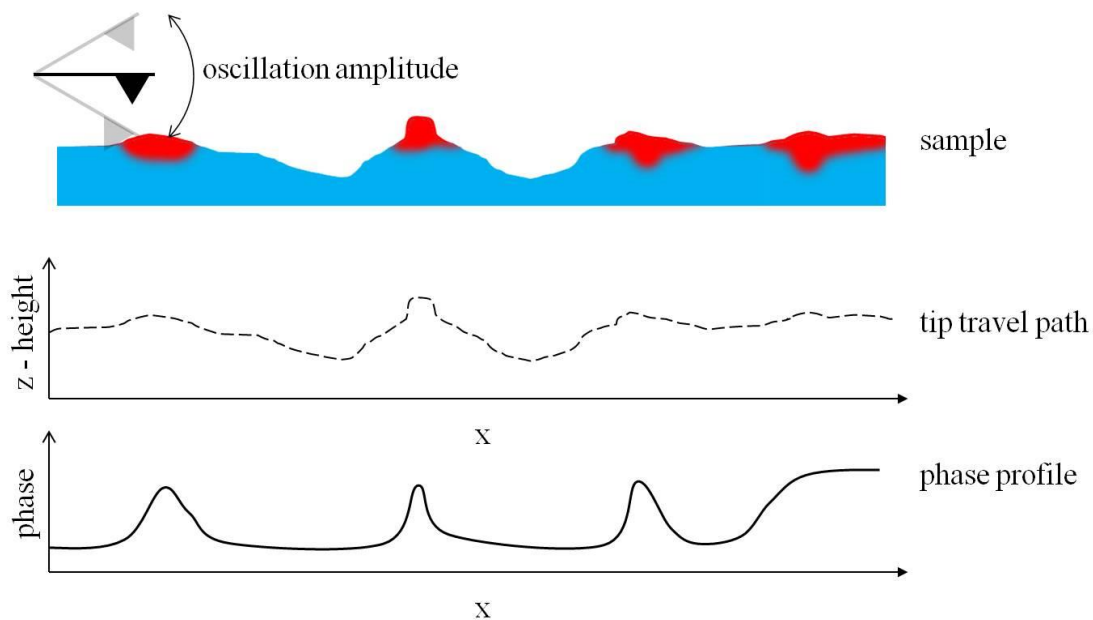


Figure 2.1: Tapping mode AFM scans an oscillating tip just above the surface of the sample with a height profile and varying material composition with differing moduli (*i.e.*, red or blue). Top axes illustrate the recorded height profile while the bottom axes show the phase profile.

The phase lag is caused by attractive and repulsive forces between the tip and sample, which can retard the tip oscillation.<sup>54</sup> Therefore, in block polymer films that have a significant difference in block moduli (*e.g.*, polystyrene-*b*-polyisoprene-*b*-polystyrene or polystyrene-*b*-poly(ethylene oxide) used in this thesis),<sup>10</sup> the phase image often is clearer and more informative than the height image.

## 2.9 Transmission Electron Microscopy

Transmission electron microscopy (TEM) is an imaging technique that can achieve magnifications anywhere from  $5,000 \times$  to over  $1,000,000 \times$ . Therefore, TEM is a powerful method to characterize the nanostructures of block polymers and their composites.<sup>10,55,56</sup> In a typical TEM measurement, electrons are produced by thermionic emission from a lanthanum hexaboride ( $\text{LaB}_6$ ) filament. Once generated, the electrons are driven through the TEM column by an accelerating voltage, which is typically between 50 kV - 500 kV. A series of pole-piece electromagnetic lenses collimate the electron beam, which is transmitted through a thin sample and subsequently projected onto a camera or fluorescent screen for imaging. The reader is referred to an introductory book for a working knowledge of TEM.<sup>57</sup> The mechanisms to adjust image contrast are particularly relevant to this thesis.

TEM exploits electron density differences in multi-phase material, so-called “mass-thickness contrast,” to produce a real-space image.<sup>58</sup> Incident electrons will be scattered more by phases with larger electron density (*e.g.*, metals or metal oxides) than phases with smaller mass density (*e.g.*, polymers or biological material). Similarly, thicker samples will cause more electron scattering than thinner samples (Figure 2.2).

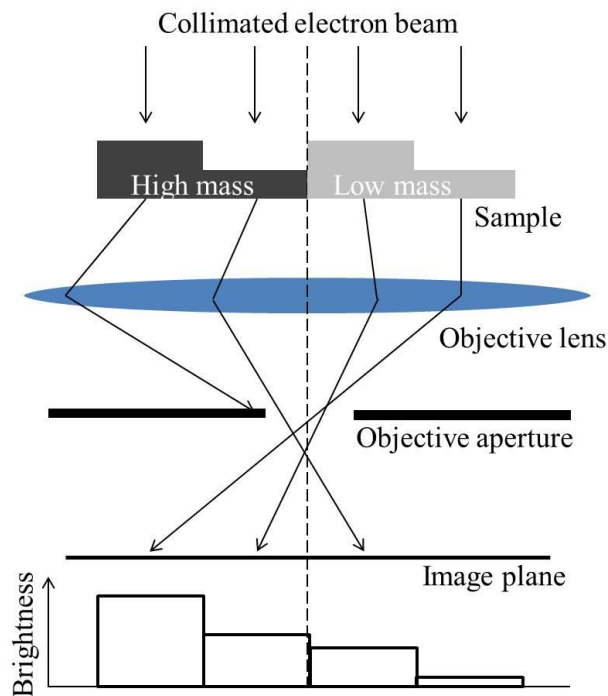


Figure 2.2: Path of an electron beam through a sample with varying mass-thickness in a transmission electron microscope. Sample regions with low mass-thickness easily transmit electrons; thus, bright areas are produced. Sample regions with high mass-thickness absorb or scatter incident electrons that may be cut out by the aperture; thus, dark areas are produced. Adapted with permission from Dr. Frank Krumeich, copyright 2012 ETH Zürich.

Typically, block polymer analysis by TEM takes advantage of mass contrast. However, because typical polymers are composed primarily of hydrocarbons, the masses or electron densities are very similar. Therefore, contrast between blocks usually is enhanced by selectively staining one block with a high-mass molecule such as ruthenium tetroxide or osmium tetroxide; the stained block shows up as dark regions in the TEM image.<sup>56</sup>

If mass-thickness contrast is insufficient and the samples are not amenable to staining, adjustments to the TEM accelerating voltage and aperture size can improve image contrast. Decreasing the accelerating voltage decreases the energy of the incident electrons and thus increases the possibility of interacting (*i.e.*, scattering) with sample atoms.<sup>59</sup> Indeed, microscopes with low accelerating voltages of 10 kV or less can analyze soft materials without staining. However, as the energy of the electron decreases, the resolving power decreases due to a decrease in the de Broglie wavelength of the incident electron.<sup>57</sup> Therefore, decreasing the accelerating voltage can improve the image contrast at the cost of image resolution. On the other hand, reducing the objective aperture size can screen highly scattered electrons and thus increase image contrast.<sup>59</sup> However, a small aperture screens the majority of the transmitted electrons, which results in a dim image that is difficult to see on the fluorescent screen.<sup>57,59</sup> Therefore, the user needs to find an optimum TEM accelerating voltage and aperture size for each sample.

In all cases, TEM analysis requires thin samples to allow electron transmission. Bulk samples are prepared into thin slices (50-200 nm) using microtomy.<sup>60</sup> However, the thin block polymer films used in this thesis are sufficiently thin enough to avoid microtoming. Therefore, the silicon wafer-supported thin films needed to be peeled and transferred to an appropriate TEM grid.<sup>61,62</sup>

### **2.9.1 Thin Film Characterization**

Glass slides, silicon wafers, and mica are too thick for TEM analysis; electrons cannot pass through the substrate to the detector. Therefore, block polymer thin films needed to be transferred from the aforementioned substrates to a TEM grid. Film transfer was an added processing step; thus, care must be taken so as to retain the

sample morphology. If the film was cast on a silica support, a common transfer method was to use a hydrofluoric acid solution to dissolve the underlying silica. After silica dissolution, the floating hydrocarbon film can be “scooped” onto a TEM grid and dried for subsequent TEM analysis.<sup>63-65</sup> Alternatively, a “non-HF” technique was described by Faselka *et al.* (Figure 2.3).<sup>61</sup>

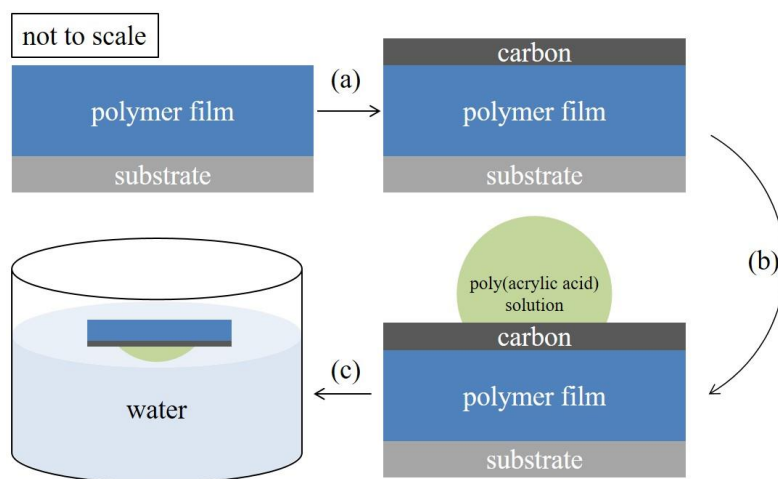


Figure 2.3: Polymer thin film peeling procedure starts with (a) depositing a thin layer of amorphous carbon *via* thermal evaporation, (b) depositing a droplet of an aqueous solution of poly(acrylic acid) and allowing it to dry in ambient conditions, and (c) peeling the dried poly(acrylic acid) from the substrate and dissolving it in a large volume of water.

A thin ( $\approx 10\text{-}20$  nm) coating of amorphous carbon was thermally evaporated onto the polymer film so as to reinforce the mechanical integrity of the film. Then a droplet ( $\approx 50$   $\mu\text{L}$ ) of a 25 wt% poly(acrylic acid) (PAA) aqueous solution was deposited onto the multi-layer stack and allowed to dry overnight in ambient conditions. The remaining solid PAA was peeled from the substrate; the peeled section removed the carbon and polymer film together. The PAA-carbon-polymer section was then placed upside-

down in a large volume (~ 100 mL) of water to dissolve the PAA. The remaining floating film was picked up using a standard copper mesh TEM grid.<sup>61,62</sup> It should be noted that both techniques required polymer films that are not soluble in water. To avoid using hydrofluoric acid, the latter technique was used throughout this thesis.

### **2.9.2 Nanoparticle Characterization by TEM**

Because of its ability to provide real-space images of nanoscale features, TEM is a popular choice for characterizing the size and shape of nanoparticles.<sup>66</sup> Nanoparticles were suspended in the electron beam using TEM grids with support films (*e.g.*, Formvar®), which were commercially available. The support films were designed to have a low electron density so as to minimize the background noise that would obfuscate the final micrograph.<sup>67</sup> A droplet ( $\approx 20 \mu\text{L}$ ) of the nanoparticle solution was drop cast onto the grid. The solvent was allowed to evaporate prior to TEM analysis due to the strict vacuum requirements of the instrumentation.<sup>57</sup>

### **2.9.3 Tilt Tomography**

An illustration demonstrates the inherent ambiguity of using two-dimensional (2D) images to obtain information on three-dimensional (3D) objects (Figure 2.4). Whereas traditional TEM images are 2D projections of 3D objects, weighted back-projections of tilted-sample TEM images produces a real-space tomogram,<sup>68</sup> which is particularly helpful when characterizing block polymers,<sup>60</sup> catalysts,<sup>69</sup> and biological material.<sup>70</sup> Producing a tomogram is a multi-step process: tilt-series acquisition, image alignment, and tomogram construction.<sup>68,69</sup>

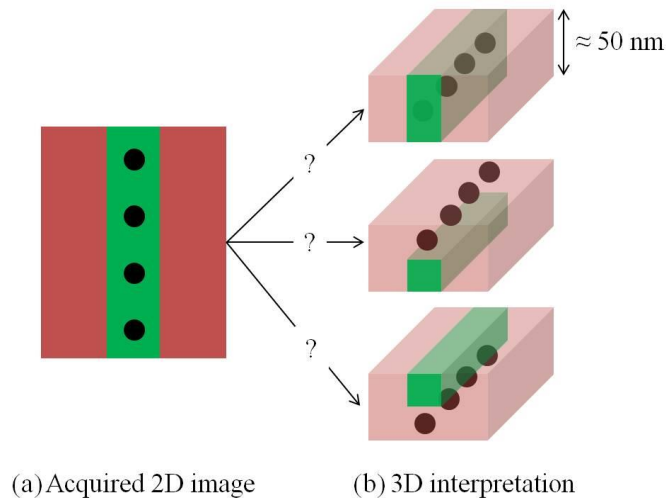


Figure 2.4: Traditional transmission electron micrographs are (a) 2D images of 3D objects, which can lead to (b) ambiguous interpretations regarding out-of-plane orientations.

### 2.9.3.1 Tilt-Series Image Acquisition

Electron tomography relies on the central slice theorem as described by Bracewell.<sup>71</sup> The central slice theorem states that when analyzing a 3D object rotated at an angle,  $\theta$ , the Fourier transform of its 2D projection corresponds to a slice through the 3D Fourier transform's center, along angle  $\theta$ . Therefore, a perfectly constructed tomogram would require images acquired over a  $\pm 90^\circ$  range about any given axis with infinitely small angular resolution  $\Delta\theta$  (Figure 2.5).<sup>71</sup> However, the thicknesses of the copper mesh grid and grid holder produce unavoidable shadows that limit the tilt range<sup>72</sup> and the mass-thickness of a high-tilt sample severely minimizes electron beam transmission.<sup>58</sup> In an electron tomography measurement, tilt angles are realistically limited to  $\pm 60^\circ$ . The result is the so-called “missing wedge” problem: the missing images between  $60^\circ$  and  $90^\circ$  prevent a complete tomogram construction (Figure 2.5).<sup>72</sup> A part of the missing wedge can be recovered by performing dual-tilt series

acquisitions of  $\pm 60^\circ$  along orthogonal axes.<sup>71,73</sup> The resulting “missing pyramid” maximizes the experimentally achievable sampling within the Fourier space (Figure 2.5). However, using dual-tilt measurements increases acquisition time and series-stitching complexity.<sup>74</sup> Increased acquisition time causes sample degradation from the beam and reduced image alignment due to stage drift. In addition to problems associated with data acquisition, two orthogonal sets that are misaligned with respect to each other will compromise voxel stitching during data analysis.<sup>74</sup> Therefore, single-tilt series remains a popular acquisition method.<sup>56,60</sup>

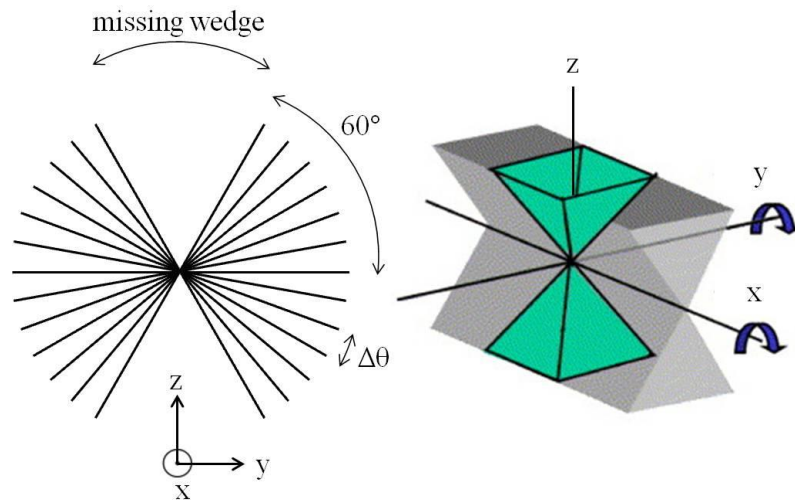


Figure 2.5: Grid shadowing and sample opacity typically limit single-axis tilt acquisitions (left) to  $\pm 60^\circ$ . Meanwhile, stage drift and beam-induced sample degradation place an upper limit on the acquisition time and thus a lower limit on the tilt resolution  $\Delta\theta$ . The “missing wedge” reduces resolution during tomogram reconstruction. Dual-axis tilt acquisitions result in improved tomograms by minimizing the missing wedge to a “missing pyramid.”

### **2.9.3.2 Image Alignment Using Fiducial Markers**

Fiducial markers, such as AuNPs,<sup>74-76</sup> are commonly used to align the tilt-series images; however, marker-free cross-correlation methods also have been developed.<sup>77,78</sup> By tracking the fiducial markers through known rotation angles, translational and rotational shifts can be calculated using a least-squares minimization.<sup>79</sup> The images are shifted so as to share the same tilt axis. Once aligned, non-overlapping edges of the images are cropped; therefore, minimal stage drift is necessary to minimize cropped areas. After the images have been aligned around a common tilt axis, the tomogram can be constructed using one of three methods: Fourier reconstruction, iterative real space, or weighted back projection.<sup>79</sup> The weighted back projection method was used in this thesis and will be described in the following section.

### **2.9.3.3 Tomogram Construction - Weighted Back Projection Method**

A back projection is simply a smearing of the acquired image along the same angle as the sample tilt. When the back projections are super-positioned, the 3D sample can be reconstructed. A simplified example, which uses three spheres along a line, is shown in Figure 2.6. Projections from Figure 2.6a are smeared along the acquisition angle and super-positioned with other projections in Figure 2.6b.

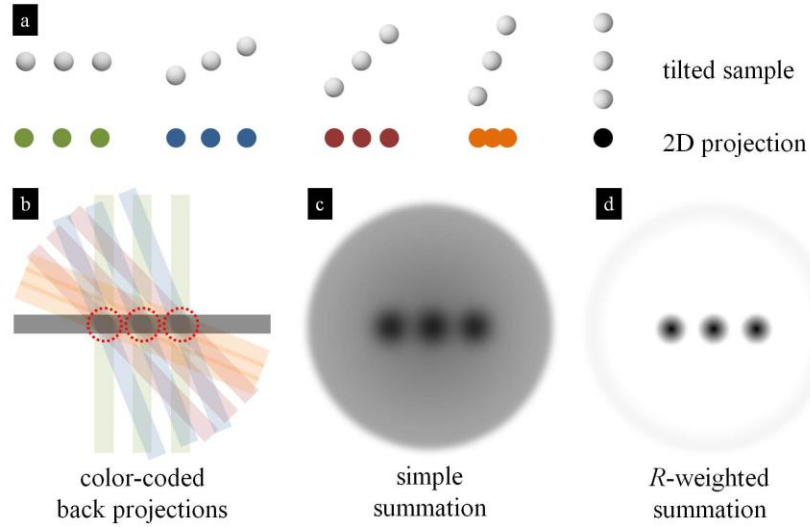


Figure 2.6: (a) The 2D projections from the tilted sample are (b) back projected along the same tilt angle. Colors are used to differentiate the super-positioned back projections. (c) A simple summation of the 2D projections yields a tomogram that mimics the original 3D object but with a low-frequency background. (d) A  $R$ -weighted scheme is used to reduce the background and enhance the tomogram reconstruction.

Although the summation of projections from all angles results in a faithful replication (Figure 2.6c), real tilt acquisitions would run into problems with tilt-range limitations and sample-contrast variations.<sup>72</sup> The problems with real acquisitions would result in significantly lower signal-to-noise tomograms. Therefore, a weighting scheme that reduces the intensity of the low-frequency background is used to improve the tomogram reconstruction.<sup>80</sup>

Numerous weighting schemes exist for the various tilt-acquisition methods; it is common to use the  $R$ -weighted scheme for single-tilt series with equal angular increments, which was the acquisition method used in this thesis.<sup>75</sup> In the  $R$ -weighting scheme, each 2D image is multiplied in Fourier space by the Fourier radius,  $R$ . After weighting, an inverse Fourier Transform brings the weighted image back to real space

for back projection and subsequent summation (Figure 2.6d, *R*-weighted summation).<sup>79</sup> The resulting tomogram has reduced low-frequency background, which more accurately reflects the measured sample.

## 2.10 Gas Chromatography

Gas chromatography (GC) is one of the most powerful techniques that can be used to separate and quickly characterize mixtures of small molecules.<sup>81</sup> The sample is analyzed by first separating the sample mixture into its components and then using a detector to identify the component and its concentration. To separate the sample using GC, the mixture is vaporized and passed through a column, with an inert gas, where the individual components of the sample are separated based on their affinity for the column material. Therefore, the column needs to be chosen for the specific analytes.<sup>81</sup> The liquefied petroleum gas-like mixture produced in this thesis was separated using a HayeSep-D fused silica capillary-type column (30 m x 0.53 mm ID, 20  $\mu$ m film thickness), which is well-suited for separating the C<sub>1</sub>-C<sub>5</sub> hydrocarbon products that were expected from the fuel cracking reaction.<sup>82</sup>

Component identification is commonly done by using a mass spectrometer as a detector.<sup>83</sup> However, if the components of the eluent are known *a priori* and only concentration is of interest, simpler flame ionization or thermal conductivity detectors can be used.<sup>83</sup> The improvements to the fuel converter, which are outlined in Chapter 6, build upon previous work in the Lauterbach research group.<sup>84,85</sup> Components of the eluent were known, so a mass spectrometer was not needed. Concentrations could be monitored by comparing the signal intensity from a flame ionization detector with the response from a mixture of calibration gases.

## REFERENCES

1. Daniel, M. C.; Astruc, D. *Chem. Rev.* **2004**, *104*(1), 293-346.
2. Kimling, J.; Maier, M.; Okenve, B.; Kotaidis, V.; Ballot, H.; Plech, A. *J. Phys. Chem. B* **2006**, *110*(32), 15700-15707.
3. Jana, N. R.; Gearheart, L.; Murphy, C. J. *Chem. Mater.* **2001**, *13*(7), 2313-2322.
4. Huang, X. H.; Neretina, S.; El-Sayed, M. A. *Adv. Mater.* **2009**, *21*(48), 4880-4910.
5. Grzelczak, M.; Perez-Juste, J.; Mulvaney, P.; Liz-Marzan, L. M. *Chem. Soc. Rev.* **2008**, *37*(9), 1783-1791.
6. Brust, M.; Walker, M.; Bethell, D.; Schiffrin, D. J.; Whyman, R. *J. Chem. Soc., Chem. Comm.* **1994**, (7), 801-802.
7. Shan, J.; Tenhu, H. *Chem. Commun.* **2007**, (44), 4580-4598.
8. Crooks, R. M.; Zhao, M. Q.; Sun, L.; Chechik, V.; Yeung, L. K. *Acc. Chem. Res.* **2001**, *34*(3), 181-190.
9. Sohn, B. H.; Choi, J. M.; Yoo, S. I.; Yun, S. H.; Zin, W. C.; Jung, J. C.; Kanehara, M.; Hirata, T.; Teranishi, T. *J. Am. Chem. Soc.* **2003**, *125*(21), 6368-6369.
10. Mayeda, M. K.; Kuan, W.-F.; Young, W.-S.; Lauterbach, J. A.; Epps III, T. H. *Chem. Mater.* **2012**, *24*(14), 2627-2634.
11. Bockstaller, M. R.; Lapetnikov, Y.; Margel, S.; Thomas, E. L. *J. Am. Chem. Soc.* **2003**, *125*(18), 5276-5277.
12. Perala, S. R. K.; Kumar, S. *Langmuir* **2013**, *29*(31), 9863-9873.
13. Jimenez-Ruiz, A.; Perez-Tejeda, P.; Grueso, E.; Castillo, P. M.; Prado-Gotor, R. *Chem.-Eur. J.* **2015**, *21*(27), 9596-9609.
14. Templeton, A. C.; Hostetler, M. J.; Kraft, C. T.; Murray, R. W. *J. Am. Chem. Soc.* **1998**, *120*(8), 1906-1911.

15. Hostetler, M. J.; Templeton, A. C.; Murray, R. W. *Langmuir* **1999**, *15*(11), 3782-3789.
16. Kim, B. J.; Bang, J.; Hawker, C. J.; Chiu, J. J.; Pine, D. J.; Jang, S. G.; Yang, S.-M.; Kramer, E. J. *Langmuir* **2007**, *23*(25), 12693-12703.
17. Kim, B. J.; Fredrickson, G. H.; Kramer, E. J. *Macromolecules* **2008**, *41*(2), 436-447.
18. Cheng, H. N.; Tetsuo, A.; Alan, D. E., Innovative NMR Strategies for Complex Macromolecules. In *NMR Spectroscopy of Polymers: Innovative Strategies for Complex Macromolecules*, American Chemical Society: 2011; Vol. 1077, pp 3-16.
19. Mueller, L. J., Spin and the Nuclear Magnetic Resonance Phenomenon. In *How Does MRI Work?*, Springer Berlin Heidelberg: 2006; pp 1-5.
20. Mueller, L. J. *Concepts in Magnetic Resonance Part A* **2011**, *38A*(5), 221-235.
21. Carbajo, R., Springer Netherlands: 2013.
22. Espinosa, J. F. *Curr. Top. Med. Chem.* **2011**, *11*(1), 74-92.
23. Zhou, H. Y.; Du, F. F.; Li, X.; Zhang, B.; Li, W.; Yan, B. *J. Phys. Chem. C* **2008**, *112*(49), 19360-19366.
24. Popov, A. I.; Hallenga, K., *Modern NMR Techniques and Their Application in Chemistry*. Marcel Dekker, Inc.: New York, 1991; Vol. 11.
25. Braun, S.; Kalinowski, H.-O.; Berger, S., *150 and More Basic NMR Experiments*. 2nd ed.; Wiley-VCH: New York, 1998.
26. Fasolka, M. J.; Mayes, A. M. *Annu. Rev. Mater. Res.* **2001**, *31*, 323-355.
27. Hall, D. B.; Underhill, P.; Torkelson, J. M. *Polym. Eng. Sci.* **1998**, *38*(12), 2039-2045.
28. Davis, R. L.; Jayaraman, S.; Chaikin, P. M.; Register, R. A. *Langmuir* **2014**, *30*(19), 5637-5644.
29. Stafford, C. M.; Roskov, K. E.; Epps, T. H., III; Fasolka, M. J. *Rev. Sci. Instrum.* **2006**, *77*(2), 023908.

30. Grosso, D. *J. Mater. Chem.* **2011**, *21*(43), 17033-17038.
31. Kimura, M.; Misner, M. J.; Xu, T.; Kim, S. H.; Russell, T. P. *Langmuir* **2003**, *19*(23), 9910-9913.
32. Steirer, K. X.; Reese, M. O.; Rupert, B. L.; Kopidakis, N.; Olson, D. C.; Collins, R. T.; Ginley, D. S. *Sol. Energy Mater. Sol. Cells* **2009**, *93*(4), 447-453.
33. Giroto, C.; Rand, B. P.; Genoe, J.; Heremans, P. *Sol. Energy Mater. Sol. Cells* **2009**, *93*(4), 454-458.
34. Krebs, F. C. *Sol. Energy Mater. Sol. Cells* **2009**, *93*(4), 394-412.
35. Singh, G.; Batra, S.; Zhang, R.; Yuan, H.; Yager, K. G.; Cakmak, M.; Berry, B.; Karim, A. *ACS Nano* **2013**, *7*(6), 5291-5299.
36. Albert, J. N. L.; Epps III, T. H. *Mater. Today* **2010**, *13*(6), 24-33.
37. Marencic, A. P.; Register, R. A., Controlling Order in Block Copolymer Thin Films for Nanopatterning Applications. In *Annual Review of Chemical and Biomolecular Engineering, Vol 1*, Prausnitz, J. M.; Doherty, M. F.; Segalman, M. A., Eds. Annual Reviews: Palo Alto, 2010; Vol. 1, pp 277-297.
38. Segalman, R. A. *Mater. Sci. Eng., R* **2005**, *48*(6), 191-226.
39. Albert, J. N. L.; Young, W. S.; Lewis, R. L.; Bogart, T. D.; Smith, J. R.; Epps III, T. H. *ACS Nano* **2012**, *6*(1), 459-466.
40. Albert, J. N. L.; Bogart, T. D.; Lewis, R. L.; Beers, K. L.; Fasolka, M. J.; Hutchison, J. B.; Vogt, B. D.; Epps III, T. H. *Nano Lett.* **2011**, *11*(3), 1351-1357.
41. Jung, Y. S.; Ross, C. A. *Adv. Mater.* **2009**, *21*(24), 2540-2545.
42. Sinturel, C.; Vayer, M.; Morris, M.; Hillmyer, M. A. *Macromolecules* **2013**, *46*(14), 5399-5415.
43. Kim, S. H.; Misner, M. J.; Xu, T.; Kimura, M.; Russell, T. P. *Adv. Mater.* **2004**, *16*(3), 226-231.
44. Park, S.; Wang, J. Y.; Kim, B.; Xu, J.; Russell, T. P. *ACS Nano* **2008**, *2*(4), 766-772.

45. Seppala, J. E.; Lewis, R. L.; Epps III, T. H. *ACS Nano* **2012**, 6(11), 9855-9862.
46. Reizman, F.; Vangelde, W. *Solid State Electron.* **1967**, 10(7), 625-632.
47. Filmetrics Product Filter. <http://www.filmetrics.com/productfilter> (June 30, 2014).
48. About Thin Film Measurements. Filmetrics, I., Ed. Filmetrics, Inc.: San Diego, 2012.
49. Vig, J. R. *J. Vac. Sci. Technol., A* **1985**, 3(3), 1027-1034.
50. Bolon, D. A.; Kunz, C. O. *Polym. Eng. Sci.* **1972**, 12(2), 109-111.
51. *Matheson Gas Data Book*. 6th ed.; Matheson Gas Products Co.: East Rutherford, 1980.
52. Albert, J. N. L.; Baney, M. J.; Stafford, C. M.; Kelly, J. Y.; Epps III, T. H. *ACS Nano* **2009**, 3(12), 3977-3986.
53. Voigtländer, B., Technical Aspects of Scanning Probe Microscopy. In *Scanning Probe Microscopy*, Springer Berlin Heidelberg: 2015; pp 31-63.
54. Haugstad, G., *Atomic Force Microscopy: Understanding Basic Modes and Advanced Applications*. John Wiley & Sons: Somerset, 2012; p 488.
55. Park, H.-W.; Im, K.; Chung, B.; Ree, M.; Chang, T.; Sawa, K.; Jinnai, H. *Macromolecules* **2007**, 40(7), 2603-2605.
56. Jinnai, H.; Spontak, R. J.; Nishi, T. *Macromolecules* **2010**, 43(4), 1675-1688.
57. Flegler, S. L.; John W. Heckman, J.; Klomparens, K. L., *Scanning and Transmission Electron Microscopy: An Introduction*. Oxford University Press: New York, 1993.
58. Electron-Specimen Interactions. In *Transmission Electron Microscopy*, Springer New York: 2008; Vol. 36, pp 139-192.
59. Scattering and Phase Contrast. In *Transmission Electron Microscopy*, Springer New York: 2008; Vol. 36, pp 193-269.

60. Jinnai, H.; Tsuchiya, T.; Motoki, S.; Kaneko, T.; Higuchi, T.; Takahara, A. *J. Electron Microsc.* **2013**, 62(2), 243-258.
61. Faselka, M. J.; Harris, D. J.; Mayes, A. M.; Yoon, M.; Mochrie, S. G. J. *Phys. Rev. Lett.* **1997**, 79(16), 3018-3021.
62. Epps III, T. H.; DeLongchamp, D. M.; Faselka, M. J.; Fischer, D. A.; Jablonski, E. L. *Langmuir* **2007**, 23(6), 3355-3362.
63. Huang, S.; Dai, L.; Mau, A. W. H. *The Journal of Physical Chemistry B* **1999**, 103(21), 4223-4227.
64. Tang, C. B.; Bang, J.; Stein, G. E.; Fredrickson, G. H.; Hawker, C. J.; Kramer, E. J.; Sprung, M.; Wang, J. *Macromolecules* **2008**, 41(12), 4328-4339.
65. Lin, Z. Q.; Kim, D. H.; Wu, X. D.; Boosahda, L.; Stone, D.; LaRose, L.; Russell, T. P. *Advanced Materials* **2002**, 14(19), 1373-1376.
66. Yacaman, M. J.; Ascencio, J. A.; Liu, H. B.; Gardea-Torresdey, J. J. *Vac. Sci. Technol. B* **2001**, 19(4), 1091-1103.
67. Nottbohm, C. T.; Beyer, A.; Sologubenko, A. S.; Ennen, I.; Hutten, A.; Rosner, H.; Eck, W.; Mayer, J.; Golzhauser, A. *Ultramicroscopy* **2008**, 108(9), 885-892.
68. Saghi, Z.; Midgley, P. A. *Annu. Rev. Mater. Res.* **2012**, 42(1), 59-79.
69. Friedrich, H.; de Jongh, P. E.; Verkleij, A. J.; de Jong, K. P. *Chem. Rev.* **2009**, 109(5), 1613-1629.
70. Lucic, V.; Forster, F.; Baumeister, W., Structural studies by electron tomography: From cells to molecules. In *Annual Review of Biochemistry*, Annual Reviews: Palo Alto, 2005; Vol. 74, pp 833-865.
71. Bracewell, R. N. *Aus. J. Phys.* **1956**, 9(3), 297-314.
72. Arslan, I.; Tong, J. R.; Midgley, P. A. *Ultramicroscopy* **2006**, 106(11-12), 994-1000.
73. Penczek, P.; Marko, M.; Buttle, K.; Frank, J. *Ultramicroscopy* **1995**, 60(3), 393-410.
74. Mastrorarde, D. N. *J. Struct. Biol.* **1997**, 120(3), 343-352.

75. Kremer, J. R.; Mastronarde, D. N.; McIntosh, J. R. *J. Struct. Biol.* **1996**, *116*(1), 71-76.
76. Ress, D.; Harlow, M. L.; Schwarz, M.; Marshall, R. M.; McMahan, U. J. *J. Electron Microsc.* **1999**, *48*(3), 277-287.
77. Winkler, H.; Taylor, K. A. *Ultramicroscopy* **2006**, *106*(3), 240-254.
78. Brandt, S.; Heikkonen, J.; Engelhardt, P. *J. Struct. Biol.* **2001**, *136*(3), 201-213.
79. Frank, J., *Electron Tomography: Methods for Three-Dimensional Visualization of Structures in the Cell*. 2nd ed.; Springer: New York, 2006.
80. Gilbert, P. F. C. *Proc. R. Soc. London, Ser. B* **1972**, *182*(1066), 89-102.
81. Lundanes, E.; Reubsaet, L.; Greibrokk, T., *Chromatography : Basic Principles, Sample Preparations and Related Methods*. John Wiley & Sons: Somerset, NJ, USA, 2013.
82. VP-HayeSep D PLOT columns. <http://www.vici.com/columns/vphs-d.php> (December 24, 2015).
83. McNair, H. M.; Miller, J. M., *Basic Gas Chromatography*. 2nd ed.; Wiley-Interscience: Hoboken, 2009.
84. Bedenbaugh, J. E.; Kim, S.; Sasmaz, E.; Lauterbach, J. *ACS Comb. Sci.* **2013**, *15*(9), 491-497.
85. Bedenbaugh, J. E. Investigation of Catalytic Materials for Cracking of Military Aviation Fuel to Liquefied Petroleum Gas: High Throughput Experimentation. University of Delaware, Newark, 2012.

## Chapter 3

### NANOPARTICLES IN BLOCK POLYMER THIN FILMS

This chapter investigates the segregation behavior of gold nanoparticles (AuNPs) in polystyrene-*b*-polyisoprene-*b*-polystyrene (SIS) thin films as a function of the AuNP surface chemistry. 2- and 3-dimensional AuNP segregation was confirmed using transmission electron microscopy and transmission electron microtomography, respectively. The AuNP surface chemistry was quantified with nuclear magnetic resonance spectroscopy (NMR) with corroboration from solid-state magic angle NMR. Analysis of polystyrene- and polyisoprene-preferential AuNPs revealed that the interface between nanoparticle-grafted ligands and the polymer matrix was an important factor in determining segregation behavior. Text and figures are reproduced and adapted with permission from Mayeda *et al.*, *Chemistry of Materials*, 2012, 24(14), 2627-2634.<sup>1</sup>

#### 3.1 Introduction

Composite materials that contain nanostructured filler media find applications in optics, electronics, and mechanics,<sup>2,3</sup> and chains of metal nanoparticles have been proposed as waveguides in integrated optics circuits.<sup>4,5</sup> Such chains have been synthesized using electrostatic interactions between DNA or polyelectrolyte molecules and metal precursors<sup>6,7</sup> or pre-synthesized nanoparticles.<sup>8</sup> Electrostatic interactions also have been used to build well-defined layer-by-layer thin films of polyelectrolyte and semiconductor nanoparticles, which have potential applications as filtration

membranes or electrode coatings.<sup>9</sup> In solar cell applications, localization of TiO<sub>2</sub> nanoparticles in the poly(2-vinyl pyridine) domains of a poly(3-hexylthiophene)-*b*-poly(2-vinyl pyridine) (P3HT-*b*-P2VP) block polymer improved charge transport and exciton separation as compared to a P3HT/P2VP/TiO<sub>2</sub> blend.<sup>10</sup> Further, organized structures of nanoparticles have been used to improve mechanical properties of polymer composites. Computer simulations predicted significant increases in the shear moduli of polymeric materials containing “honeycomb” or “web-like” structures of particles as compared to randomly distributed or hexagonally packed particles.<sup>11</sup> Improved mechanical properties with ordered nanoparticles experimentally were confirmed with ZnO nanorods in polyurethane,<sup>12</sup> layered silicates in epoxy,<sup>13</sup> and carbon nanotubes in epoxy.<sup>14</sup> In addition to performance characteristics, ordered assemblies have promising applications in templating small-scale features to compete with or complement current lithographic techniques.<sup>15</sup>

Block polymers (BPs) are well-suited as matrix materials in nanostructured composites due to their self-assembled and nanometer-scale features, ease of processing, and tunable parameters (molecular weight, architecture, composition, etc.).<sup>16-18</sup> Methods for incorporating nanoparticles into BPs include *in situ* reaction of a metal precursor and particle-polymer blending.<sup>18</sup> The former method typically requires a polymer domain that is capable of complexing with the metal precursor.<sup>19-22</sup> The latter method has been explored using nanoparticles of metals, metal oxides, and semiconductors.<sup>15,23,24</sup> In particular, the popularity of Brust’s AuNP synthesis procedure has increased interest in studying AuNP behavior in polymer composites.<sup>25-27</sup> The as-synthesized AuNPs are stabilized by alkanethiol ligands, which make the nanoparticles soluble in many common organic solvents used in polymer synthesis and

processing. Furthermore, work by Murray and coworkers demonstrated an increase in AuNP functionality and versatility by performing “place-exchange” reactions through an associative pathway to replace the attached thiol ligands.<sup>28,29</sup> Brust’s versatile AuNP synthetic scheme enabled Kramer and coworkers to synthesize batches of AuNPs, covered with various polymer-thiols, to take advantage of the enthalpic interactions with the domains of a polystyrene-*b*-poly(2-vinyl pyridine) block polymer.<sup>30,31</sup> AuNP incorporation also was found to induce order-order transformations by preferentially swelling one domain of the block polymer.<sup>32,33</sup> Furthermore, AuNPs with mixed A/B surface functionalities behaved like surfactants: segregating to interfaces of block polymers to alleviate unfavorable interactions between domains.<sup>31,34,35</sup> Entropic interactions of block polymer nanocomposites were theoretically investigated by Lee *et al.* by incorporating a bimodal size distribution of particles; larger particles were centered in their preferred domains while smaller particles migrated to domain interfaces.<sup>36</sup> This phenomenon was demonstrated experimentally by Bockstaller *et al.* with nanoparticles in polystyrene-*b*-poly(ethylene propylene).<sup>37</sup> However, the two types of nanoparticles used by Bockstaller *et al.* differed in their composition (gold and silica) as well as their attached ligands; size was not the only variable. Indeed, follow up experiments reported on small (3.5 nm diameter) polystyrene-covered AuNPs that preferentially segregated to the polystyrene domains of a block polymer, thus highlighting the complex interplay of entropic and enthalpic interactions.<sup>38,39</sup> In addition to segregation within block polymers, nanoparticles have been found to induce nanostructure reorientation in thin films by mitigating film-substrate and polymer-polymer interactions.<sup>34,40-42</sup> The quantity and quality of polymer-particle studies illustrate the growing interest and understanding of

block polymer nanocomposite behavior as well as progress towards applications in sensors, circuitry, and coatings.

Despite the aforementioned investigations, minimal work on the segregation behavior of ligand-capped AuNPs in the absence of specific ligand-polymer polar interactions has been reported. The methods reported in this chapter control the placement of AuNPs in a symmetric cylinder-forming SIS block polymer by tuning the surface chemistry of the filler particles, *via* thiol ligand exchanges, while holding particle size constant. Because the polystyrene (PS) cylinders have a propensity to lay parallel to the plane of the substrate,<sup>16</sup> characterizing the 3D system with 2D micrographs results in an inherent loss of information. Although viewing the sample at a 90° rotation using ultramicrotomy is a feasible option, the shearing forces could alter the nanoparticles' locations in the original composite film and cutting sections thin enough to observe structures only perpendicular to the cut is challenging. Therefore, transmission electron microtomography (TEMT) was employed to characterize the 3-dimensional location of the AuNPs within the polymer thin films.<sup>43,44</sup> 1-dodecanethiol (C<sub>12</sub>SH) covered AuNPs were found to preferentially segregate to the polyisoprene (PI) domains. To improve versatility in tailoring nanocomposites, AuNP placement in either domain was desired. Instead of synthesizing a new batch of AuNPs using polystyrene-SH (PS-SH) in place of C<sub>12</sub>SH, a simple “place-exchange” reaction was completed to change the AuNP surface chemistry prior to nanoparticle incorporation into the SIS polymer. Increasing PS-SH coverage on the AuNP surface eventually led to AuNPs that preferentially segregated to the PS domains. The segregation behavior was rationalized in terms of area-averaged enthalpic interactions of the capping ligand and polymer chain stretching entropic arguments. This investigation into templating

AuNPs using block polymer thin films is an important step towards improving surface-enhanced spectroscopic methods or biochemical sensor development by creating aggregation-resistant arrays of AuNPs.<sup>45,46</sup>

## 3.2 Experimental Section

### 3.2.1 Materials

All chemicals were used as received. SIS (*DEXCO v4211*,  $M_n = 118$  kg/mol,  $D = 1.09$ ), with block volume fractions of  $f_S = 0.134$ ,  $f_I = 0.732$ , and  $f_S = 0.134$ , respectively, was used to make the nanocomposite thin films. The bulk morphology was hexagonally packed PS cylinders in a PI matrix with a domain spacing of 29 nm as determined by small-angle X-ray scattering. Toluene (certified ACS grade), tetrahydrofuran (THF) (Optima), dichloromethane (ACS stabilized), methanol (certified ACS grade), deuterated chloroform (0.2 vol% trimethylsilane), and poly(acrylic acid) (25 wt% in water,  $M_n = 240$  kg/mol,  $D = 1.09$ ) were purchased from Fisher Scientific and used as received. Hydrogen tetrachloroaurate trihydrate, sodium borohydride, tetra-*n*-octylammonium bromide, and C<sub>12</sub>SH for gold particle synthesis also were purchased from Fisher Scientific. Aqueous solutions of OsO<sub>4</sub> (4 wt%) were purchased from EMS Diatome. PS-SH ( $M_n = 860$  g/mol,  $D = 1.3$ ) was purchased from Polymer Source, Inc. Silicon wafers (N <100>, Wafer World, Inc.) were cleaned using the following procedure: the wafers were rinsed with toluene and dried with nitrogen gas, placed in an ultraviolet ozone cleaner (model 42, Jelight Co., Inc.) for 1 h, and then re-rinsed with toluene and dried with nitrogen gas prior to film casting.

### 3.2.2 Gold Nanoparticle Synthesis

Gold nanoparticles (AuNPs) were synthesized according to the Brust-Schiffrin method.<sup>25</sup> The gold nanoparticle synthetic procedure was described in section 2.1.1.

### 3.2.3 Ligand Exchange

Thiol ligand exchanges were used to tune the surface chemistry of the AuNPs. The ligand exchange procedure was described in section 2.1.2. Mass feed ratios and their resulting molar ratios for each ligand exchange reaction can be found in Appendix A (Table A.1). The degree of ligand exchange was characterized by proton nuclear magnetic resonance (<sup>1</sup>H NMR) spectroscopy. Hereafter, gold nanoparticle products of ligand exchanges are denoted Au<sub>x</sub>NPs with *x* representing the ratio of C<sub>12</sub>SH to PS-SH (C<sub>12</sub>SH:PS-SH). As-synthesized gold nanoparticles have no PS-SH ligands attached and are therefore designated Au<sub>∞</sub>NPs (*i.e.*, C<sub>12</sub>SH:PS-SH = ∞).

### 3.2.4 Proton Nuclear Magnetic Resonance Spectroscopy

<sup>1</sup>H NMR spectra were recorded on a Bruker AV400. Samples were dissolved in deuterated chloroform with 0.2 vol% trimethylsilane as a reference. Analysis and plotting were performed with MestReNova NMR software.

### 3.2.5 Thin Film Preparation

Solutions of Au<sub>x</sub>NPs and SIS were dissolved in toluene at a total of 1 wt% solids composed of 0.4 vol<sub>Au</sub>/vol<sub>polymer</sub>%. Polymer films, 30-35 nm thick, were coated onto cleaned silicon wafers using either a spin-coating or flow-coating method.<sup>47</sup> Nanoscale morphologies did not vary between either of the deposition techniques. In spin-coating, thin films were made by quickly dispensing 20 μL of solution onto substrates rotating at approximately 3000 rpm; substrates were allowed to spin for 30 s

to remove excess solvent. In flow-coating,<sup>47</sup> thin films were made by casting solutions with a blade angle of 20°, gap height of 200 µm, and blade velocity of 10-14 mm/s. Film thicknesses were measured using a Filmetrics F20 spectrometer by fitting spectral data from 400 nm to 900 nm with a constant refractive index of 1.54 for both pure and composite thin films. Before TEM imaging, films were annealed in saturated THF vapor for 1 h to improve domain ordering and nanoparticle segregation compared to as-cast films.

### **3.2.6 Atomic Force Microscopy (AFM)**

AFM micrographs were recorded with a Veeco Dimension 3100 with a Nanoscope V control unit in tapping mode. Tap150-G silicon probes were used with a nominal force constant of 5 N/m and tuning frequency of 150 kHz.

### **3.2.7 Transmission Electron Microscopy (TEM)**

Micrographs were recorded using a JEOL JEM-2000FX TEM operated at 200 kV. Polymer films were peeled off of the silicon substrates as described in the literature and section 2.9.1.<sup>48-50</sup>

### **3.2.8 TEM Tomography (TEMT)**

A 30 nm thick film of Au<sub>4.5</sub>NPs in SIS (0.4 vol<sub>Au</sub>/vol<sub>polymer</sub>%, unstained, THF annealed) was mounted on a TEM grid as described above. Single tilt series were taken using a Gatan High Tilt Tomography sample holder in a Tecnai G2 12 Twin microscope operated at 120 kV. Tilted micrographs were recorded in 2° increments between -30° and 30° and in 1° increments up to -55° and 55°. Image tracking and focusing were performed manually between each image acquisition. Micrographs were aligned using a fiducial tracking model. Tomograms were reconstructed using a

weighted back projection method. All processing was done in the IMOD software suite; eTomo was used for tomogram reconstruction, and 3DMOD was used for image processing.<sup>51,52</sup>

### 3.3 Results

SIS films and nanocomposite Au<sub>0</sub>NP/SIS films were cast at thicknesses of 30-35 nm (approximately one domain spacing) to avoid multilayer domain convolution during TEM imaging. AFM phase images of as-cast SIS films showed microphase separation but with poor ordering due to quick solvent evaporation (Figure 3.1a). The brighter regions in the AFM images correspond to the PS-rich domains, and the darker regions correspond to the PI-rich domains. Discerning polymer domains and AuNP location in TEM micrographs of as-cast samples (not shown) was difficult. Thus, all films were annealed with saturated THF vapor to improve domain ordering (Figure 3.1b); and in the case of nanocomposite films, to allow kinetically trapped particles to segregate into an energetically favored domain. Annealing the SIS film created larger ordered grains, which were approximately 0.5 - 1.0  $\mu\text{m}^2$  in area. Annealing for longer than 1 h increased polymer domain ordering but often resulted in film dewetting (not shown).<sup>53</sup> Long-range order was not the desired result; instead, the improved ordering helped in characterizing AuNP segregation behavior within the nanocomposite thin film by TEM.

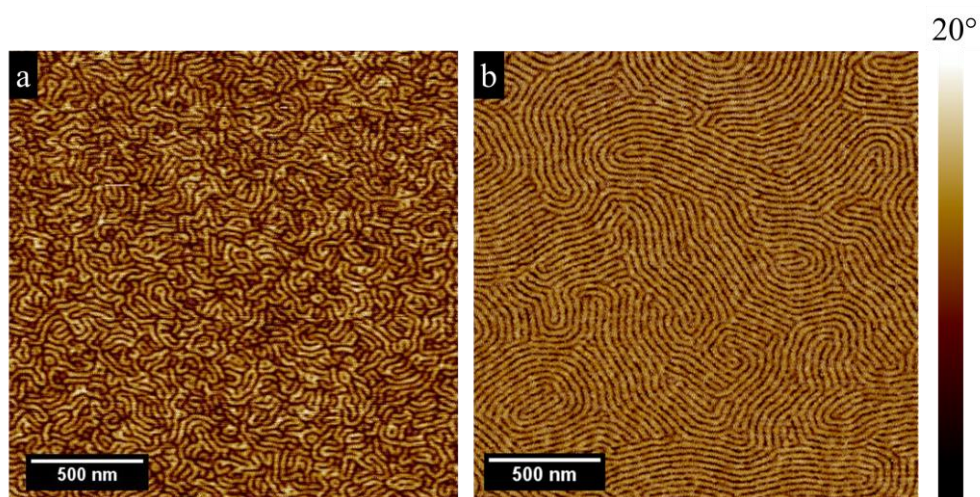


Figure 3.1: AFM phase images of SIS films (a) as-cast and (b) annealed with THF solvent vapor. Nanocomposite films exhibited similar ordering and grain sizes for as-cast and annealed samples. Bright regions indicated PS-rich domains while dark regions indicated PI-rich domains. Reprinted with permission from Mayeda *et al.*, *Chemistry of Materials*, 2012, 24(14), 2627-2634.<sup>1</sup>

The surface chemistry of AuNPs was tuned prior to incorporation into the SIS polymer thin film. The surface chemistry of AuNPs was controlled by varying the ratio of PS-SH to Au<sub>n</sub>NPs stirring in solution. The end products were separated by centrifugation and characterized by <sup>1</sup>H NMR spectroscopy (Figure 3.2).

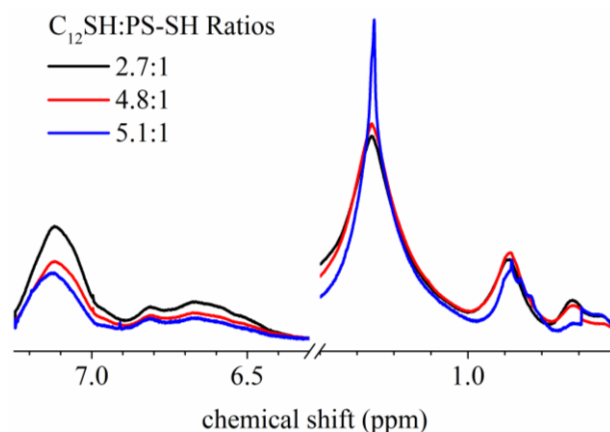


Figure 3.2:  $^1\text{H}$  NMR spectroscopy of ligand exchange products in deuterated chloroform. Spectra were normalized to integrated areas associated with  $\text{C}_{12}\text{SH}$  between 1 - 1.4 ppm. Peaks between 6.3 - 7.3 ppm, associated with the phenyl group in PS-SH, were compared with the 1 - 1.4 ppm peak, associated with the hydrocarbon chain in  $\text{C}_{12}\text{SH}$ .  $\text{C}_{12}\text{SH}:\text{PS-SH}$  ratios of the spectra shown were calculated to be 2.7:1, 4.8:1, and 5.1:1. Reprinted with permission from Mayeda *et al.*, *Chemistry of Materials*, 2012, 24(14), 2627-2634.<sup>1</sup>

Spectra were normalized with respect to  $\text{C}_{12}\text{SH}$  peak areas (1 - 1.4 ppm) to compare PS-SH content (6.3 - 7.3 ppm). Magic angle spinning  $^1\text{H}$  NMR experiments were used to ensure line broadening between 1 - 1.4 ppm was caused by bound ligand confinement and not inhomogeneous magnetic fields (Appendix A, Figure A.1). The three samples, plotted in Figure 3.2, were representative products of place-exchange reactions whereby the  $\text{C}_{12}\text{SH}$  ligands that initially were attached to the AuNP surface were replaced by PS-SH ligands.<sup>28,29</sup> Increasing PS-SH coverage caused integrated peak areas associated with PS-SH to increase relative to integrated areas associated with  $\text{C}_{12}\text{SH}$ . Eight ligand exchange reactions were performed; corresponding NMR spectra can be found in the supporting information (Appendix A, Figure A.1). PS-SH peak areas increased with increasing reactant feed;  $\text{C}_{12}\text{SH}:\text{PS-SH}$  molar ratios based

on peak areas were calculated to be 2.7:1, 2.8:1, 3.1:1, 4.1:1, 4.5:1, 4.8:1, 5.1:1, and 6.6:1 ( $\pm 0.2$ ). Exploring a range of C<sub>12</sub>SH:PS-SH molar ratios on AuNP surfaces was important for identifying the transition between PI- and PS-segregated AuNPs.

The domain preference of AuNPs in SIS was characterized by TEM. Unlike AFM, TEM resolution allowed identification of the AuNPs ( $3.5 \pm 1.0$  nm diameter, Figure A.3) and their in-plane location regardless of AuNP depth within the thin film. TEM micrographs of AuNPs before and after a typical ligand exchange are shown in the Appendix A (Figure A.3). TEM micrographs are presented in Figure 3.3, which include stained and unstained (insets) samples of THF vapor annealed SIS (Figure 3.3a) and Au<sub>∞</sub>/SIS films (Figure 3.3b). Unlike solvent vapor annealing, thermal annealing resulted in AuNP aggregation and smaller grain sizes, thus samples were only annealed with solvent vapor (Appendix A, Figure A.4). Domain size measurements taken from TEM micrographs ( $32 \pm 3$  nm) (Figure 3.3a) and AFM images ( $33 \pm 3$  nm) (Figure 3.1b) were in agreement. Grain sizes also were comparable; thus, the film peeling procedure was deemed satisfactory in transferring films from silicon wafers to TEM mesh grids. An inhomogeneous distribution of Au<sub>∞</sub>NPs in the SIS polymer can be identified in the inset of Figure 3.3b; columns of Au<sub>∞</sub>NPs were indicative of preferential segregation to one polymer domain. OsO<sub>4</sub> stained specimens (OsO<sub>4</sub> chemically binds to PI)<sup>54</sup> showed that Au<sub>∞</sub>NPs preferentially segregated to the PI domains (Figure 3.3b).

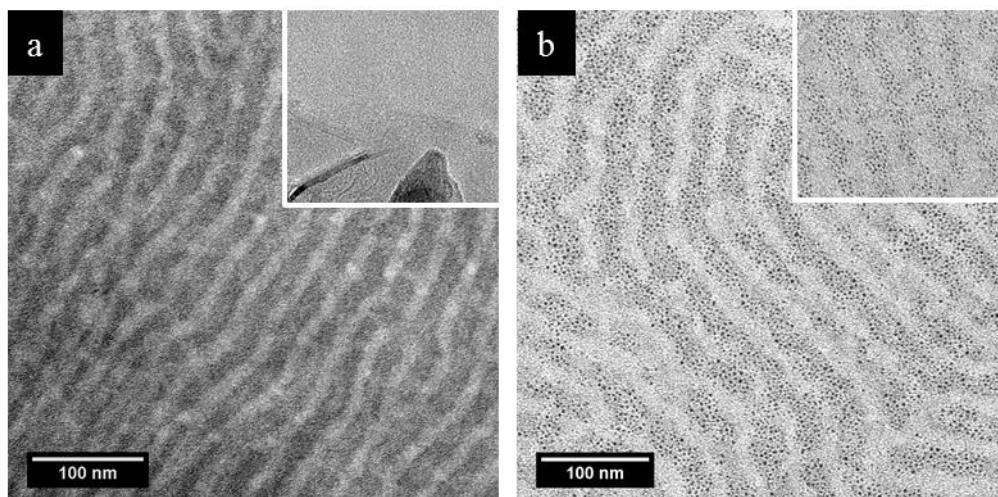


Figure 3.3: TEM micrographs of OsO<sub>4</sub> stained and unstained (insets) (a) SIS and (b) Au<sub>∞</sub>NP/SIS thin films after THF annealing. Micrographs of stained samples show PS (light) and PI (dark) domains oriented parallel to the plane of the film. The micrograph in (b) reveals Au<sub>∞</sub>NPs (dark spots) with an affinity for PI over PS domains. The inset of (b) shows inhomogeneous distribution of Au<sub>∞</sub>NPs, which indicates a polymer domain preference. Reprinted with permission from Mayeda *et al.*, *Chemistry of Materials*, 2012, 24(14), 2627-2634.<sup>1</sup>

Upon determining the PI-preference of Au<sub>∞</sub>NPs, products of the ligand exchanges were incorporated into SIS films. Representative TEM micrographs of the nanocomposite films, which contained the products of ligand exchanges, are shown in Figure 3.4. TEM micrographs of all samples can be found in the Appendix A (Figure A.5).

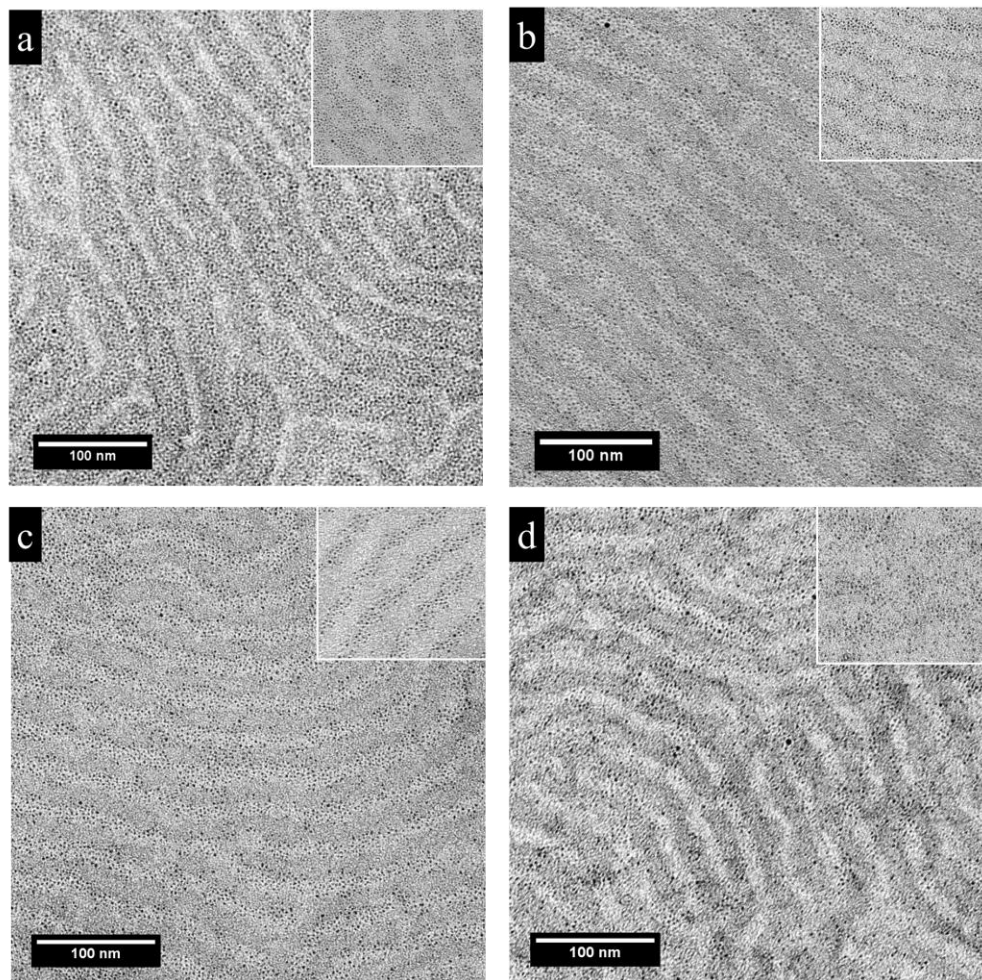


Figure 3.4: TEM micrographs of  $\text{OsO}_4$  stained nanocomposite films of (a)  $\text{Au}_{5.1}\text{NP/SIS}$ , (b)  $\text{Au}_{4.8}\text{NP/SIS}$ , (c)  $\text{Au}_{2.7}\text{NP/SIS}$ , and (d) mix of  $\text{Au}_{\infty}\text{NP/Au}_{2.7}\text{NP/SIS}$  after annealing with saturated THF vapor. Inset images show corresponding unstained samples at the same magnification. All nanocomposite films contained 0.4 vol% AuNPs; the sample represented in (d) contained approximately equal volume loadings of  $\text{Au}_{\infty}\text{NPs}$  and  $\text{Au}_{2.7}\text{NPs}$ .  $\text{Au}_{5.1}\text{NPs}$  in (a) exhibit an affinity for the PI domain while  $\text{Au}_{4.8}\text{NPs}$  in (b) and  $\text{Au}_{2.7}\text{NPs}$  in (c) show affinities for the PS domains. Unstained images (see insets) suggest AuNP segregation. The mixture of  $\text{Au}_{\infty}\text{NPs}$  and  $\text{Au}_{2.7}\text{NPs}$  in (d) shows no visible domain preference, and the unstained image (inset) indicates a well-mixed nanocomposite. Reprinted with permission from Mayeda *et al.*, *Chemistry of Materials*, 2012, 24(14), 2627-2634.<sup>1</sup>

AuNP positions indicated preference for the PI domains in Figure 3.4a and the PS domains in Figure 3.4b and 3.4c. AuNP location was most easily located by identifying their presence or absence in the unstained PS domain. Columns of AuNPs, shown in Figure 3.4 insets, confirm preferential domain segregation. The TEM micrographs indicated that a transition from PI-segregated to PS-segregated AuNPs occurred at a C<sub>12</sub>SH:PS-SH ratio between 5.1:1 (Figure 3.4a) and 4.8:1 (Figure 3.4b). A combination of Au<sub>2.7</sub>NPs and Au<sub>∞</sub>NPs were incorporated into the nanocomposite imaged in Figure 3.4d, which showed a well-mixed dispersion of AuNPs in the SIS polymer.

A TEM micrograph tilt series of Au<sub>4.5</sub>NP/SIS (unstained, THF annealed) was recorded and used for tomogram reconstruction, which was done using a weighted back projection method.<sup>51,52</sup> The tilt series images elucidated the Au<sub>4.5</sub>NP position in three dimensions. An x-y plane view micrograph is shown at a z-slice located near the middle of the film (Figure 3.5a); a cross-sectional (x-z plane) micrograph, corresponding to the dotted blue line in Figure 3.5a, exhibits Au<sub>4.5</sub>NPs clustered together (Figure 3.5b). A video, scanning through z-slices, of the full tomogram can be viewed in the Supporting Information. White regions to the left and right of each Au<sub>4.5</sub>NP in Figure 3.5a are artifacts of the tomogram reconstruction process.<sup>52</sup>

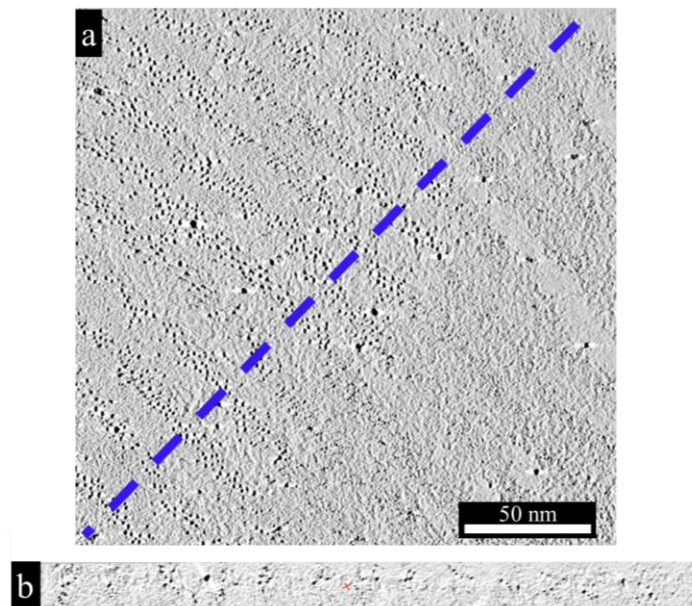


Figure 3.5: x-y plane (a) and x-z plane (b) views of a reconstructed tomogram of unstained Au<sub>4.5</sub>NP/SIS after THF annealing. The x-z plane view is taken along the dotted blue line. The sample contains approximately 0.4 vol% Au<sub>4.5</sub>NP loading. Considered together, (a) and (b) show that the Au<sub>4.5</sub>NPs show an affinity for one polymer domain and do not segregate to the film interfaces nor the polymer-polymer interfaces. Reprinted with permission from Mayeda *et al.*, *Chemistry of Materials*, 2012, 24(14), 2627-2634.<sup>1</sup>

### 3.4 Discussion

As-cast nanocomposite films required annealing in order to adequately discern polymer domains and nanoparticle location in TEM micrographs. THF vapor annealed films exhibited good domain ordering compared to as-cast films (Figure 3.1). THF was chosen because of its ability to solubilize ligand-capped AuNPs and also impart chain mobility to both polymer domains.<sup>55</sup> Well-ordered nanocomposite films were further characterized by TEM to determine AuNP segregation behavior.

TEM micrographs of stained composite films suggest that as-synthesized Au<sub>∞</sub>NPs prefer PI domains of the SIS block polymer (3.3). Ansari *et al.* found that

surface energy drives the affinity of bare Au for OsO<sub>4</sub>-stained PI domains over unstained PS domains.<sup>56</sup> However, the ligand-capped AuNPs used throughout this report do not have a significant area of bare gold exposed to its surroundings, suggested by the nanoparticles' long-term stability in organic solvents.<sup>25</sup> Furthermore, unstained transmission electron microscopy images show Au<sub>∞</sub>NPs with an affinity for one domain (Figure 3.3b). Instead, it was rationalized that the preferential segregation of AuNPs based on Hildebrand solubility and surface energy parameters of their ligands. Hildebrand solubility parameters are related to the enthalpy of mixing and have been used to investigate polymer-solvent mixing of nonpolar and slightly polar systems.<sup>57</sup> Enthalpic interaction penalties increase with increasing disparity between components' solubility parameters. Hildebrand solubility parameters of relevant compounds are summarized in Table 3.1. Based on AFM phase images, Peponi *et al.* concluded that the presence of C<sub>12</sub>SH encouraged segregation of nanoparticles to PS domains in SIS due to similarities in solubility parameters [*i.e.*,  $(\delta_{PS} - \delta_{C_{12}SH})^2 = 0.36 \text{ MPa} < 5.76 \text{ MPa} = (\delta_{PI} - \delta_{C_{12}SH})^2$ ].<sup>58,59</sup> Despite these findings, the results indicated that Au<sub>∞</sub>NPs, Au<sub>6,6</sub>NPs, and Au<sub>5,1</sub>NPs preferentially segregated to PI domains in the SIS polymer (Figure 3.3b and Figure 3.4a). The unexpected AuNP segregation can be explained by considering the small radius of curvature inherent in nanoparticles. The high degree of surface curvature creates a radial gradient in monolayer density that shields ligand atoms closest to the nanoparticle surface from interacting with the surroundings.<sup>60,61</sup> As such, it would be reasonable to conclude that atoms nearest to the Au core, such as the sulfur atom, contribute less to the solubility parameter of the ligand. Thus, the solubility parameter for dodecane is more representative of the solubility parameter for C<sub>12</sub>SH on the AuNP surface, and Hildebrand solubility

parameters predict a switch in Au<sub>∞</sub>NPs segregation from PS- to PI-preferential [*i.e.*,  $(\delta_{PS} - \delta_{C12})^2 = 5.29 \text{ MPa} > 0.25 \text{ MPa} = (\delta_{PI} - \delta_{C12})^2$ ]. Reported surface energies also suggest that Au<sub>∞</sub>NPs would be PI-preferential (see Table 3.1). AuNPs preferentially would segregate to a polymer domain to minimize the surface energy difference between the surrounding polymer and the AuNP ligand. Dodecane and C<sub>12</sub>SH both have lower surface energies, compared to PS and PI, which likely will produce a more favorable interaction with the PI domains than the PS domains. Based on solubility parameters and surface energies, the results suggest that the innermost sulfur atom is shielded on Au<sub>∞</sub>NPs thus allowing preferential segregation to PI domains.

Table 3.1 Hildebrand solubility parameters and surface energies of relevant compounds.

Compound	Hildebrand Solubility $\delta$ , (MPa <sup>1/2</sup> )	Surface Energy (mJ/m <sup>2</sup> )
polyisoprene	16.7 <sup>62</sup> <sup>◇</sup>	32 <sup>62</sup>
polystyrene	18.5 <sup>62</sup> <sup>◇</sup>	40.7 <sup>62</sup>
1-dodecanethiol	19.1 <sup>63</sup>	25.4 <sup>64</sup>
dodecane	16.2 <sup>62</sup>	25.4 <sup>65</sup>

<sup>◇</sup> Represents averages of reported values

Exchanging C<sub>12</sub>SH ligands with PS-SH ligands on the AuNP induces preferential segregation into the PS domains below C<sub>12</sub>SH:PS-SH ratios near 5:1. Using molecular averages, solubility parameters would predict PS-segregated AuNPs below ratios of 0.8:1 (61 mol% PS-SH surface coverage) and surface energies would predict ratios below 0.4:1 (72 mol% PS-SH surface coverage). Based on a C<sub>12</sub>SH:PS-SH ratio of 5:1, only 17 mol% of the AuNP surface must be covered by PS-SH to render the surface PS preferential (Figure 3.4 and Figure 3.5). Differences in required

PS-SH surface coverage can be attributed to the size difference between the C<sub>12</sub>SH and PS-SH ligands<sup>30</sup> and entropic losses due to the architecture of the triblock polymer,<sup>37</sup> as described below.

With regard to size differences, the larger PS-SH ligand (24-carbon backbone) will extend beyond the edges of the C<sub>12</sub>SH ligand (12-carbon backbone) (Figure 3.6a) thus contributing more to domain solubility. Ligand length has been shown to be important in directing nanoparticle segregation in block polymers; larger ligands with lower surface coverage could cause the same segregation behavior as shorter ligands with higher surface coverage.<sup>30</sup> Ellipsometry experiments have shown that the thickness of a C<sub>12</sub>SH capping layer on a planar gold surface is 20 Å,<sup>66</sup> and further characterization of these adsorbed alkanethiols on planar gold with electron diffraction revealed a thiol footprint of 21.4 Å<sup>2</sup>.<sup>67</sup> Surface spectroscopy studies on AuNPs by Hostetler *et al.* suggested that a transition from 3-dimensional to 2-dimensional C<sub>12</sub>SH packing on the surface occurs for nanoparticles with a diameter larger than 3 nm.<sup>68</sup> Therefore, applying the thickness and footprint values for the C<sub>12</sub>SH capping layer is reasonable for the 3.5 nm diameter AuNPs used in this study.

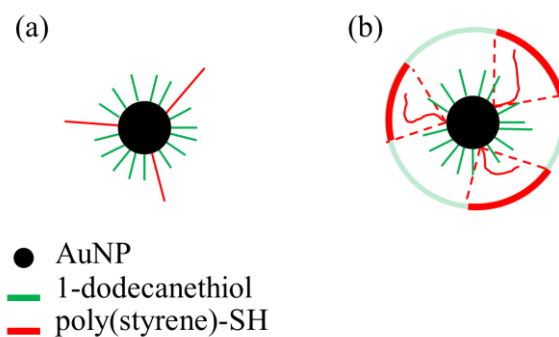


Figure 3.6: Graphical representation of Au<sub>5</sub>NPs indicating (a) approximate length differences between C<sub>12</sub>SH and PS-SH and (b) effective ligand surface coverage. Reprinted with permission from Mayeda *et al.*, *Chemistry of Materials*, 2012, 24(14), 2627-2634.<sup>1</sup>

In comparison, the PS-SH ligand size normally is described by its radius of gyration. However, short-chain PS has been shown to adopt an almost fully stretched conformation when grafted to nanoparticles.<sup>60</sup> In this case, the contour length of the PS-SH ligand used in this study (30 Å) is a more appropriate characteristic length, which is only slightly larger than that of the C<sub>12</sub>SH. Therefore, the length of the PS-SH ligand does not account for the unexpected transition from PI- to PS-segregated AuNPs at high C<sub>12</sub>SH:PS-SH ratios. Instead, the area occupied by a ligand may be a better representation of its size. Corbierre *et al.* found that a 1.9 kg/mol PS-SH ligand occupied a surface area of 29 Å<sup>2</sup> at the Au/ligand interface and an expanded coverage of 240 Å<sup>2</sup> at the ligand/THF interface.<sup>69</sup> Despite high grafting densities, attached polymer ligands avoid a fully stretched conformation by expanding into the “void volumes”, while alkanethiols remain well-packed on the facets, of the AuNP truncated octahedra.<sup>60</sup> If Corbierre’s measurements radially are scaled in accordance with the molecular weight of the PS-SH ligands used in this study, an 860 g/mol PS-SH ligand should occupy a THF/ligand interface surface area of approximately 110 Å<sup>2</sup>. The

expanded occupied area of the PS-SH ligand is particularly applicable during the THF solvent annealing step of the nanocomposite film preparation. The ratio of the interface surface area occupied by a PS-SH ligand to the area occupied by a C<sub>12</sub>SH ligand (5.1:1) is similar to the C<sub>12</sub>SH:PS-SH ratio (5:1) upon which AuNPs transition from PI- to PS-preferential segregation. Therefore, a gold nanoparticle surface with a C<sub>12</sub>SH:PS-SH ratio of 5:1 (17 mol% PS-SH ligands) is predicted to have 50 area% PS-SH coverage at the matrix/ligand interface (Figure 3.6b). The similarity between the ligand ratio that produces 50 area% PS-SH coverage and the ratio at which the transition from PI- to PS-preferential segregation occurs suggests that the matrix/ligand interface is a dominant factor in determining domain preference. Furthermore, the characteristic size of a ligand should be based on the area it occupies at an interface rather than its length.

In addition to enthalpic interactions between ligands and the polymer matrix, the SIS triblock architecture necessitates some entropic losses due to PI segment stretching to accommodate AuNPs. On the other hand, AuNPs segregating to PS domains may reduce polymer chain entropic losses by situating in between the PS chain ends.<sup>70,71</sup> More recent modeling efforts using self-consistent mean field theory in dilute particle loading cases reported that small particles segregate to the A/B interface in a lamellae diblock polymer even when the particles were A-domain preferential.<sup>72</sup> Entropic contributions to nanoparticle segregation were illustrated by Bockstaller *et al.* when they reported on size-dependent particle segregation.<sup>37</sup> Entropic arguments support PS-segregating AuNPs and may, in part, account for the AuNPs that segregated to PS domains at unexpectedly high C<sub>12</sub>SH:PS-SH ratios. However, conclusive remarks cannot be made based on the studies herein.

Besides ligand size influence and entropic contributions, ligand rearrangement on the surface of AuNPs to create Janus-like particles also has been suggested to account for unexpected segregation to the polymer-polymer interface in a PS-*b*-P2VP block polymer.<sup>31</sup> However, the absence of AuNPs segregating to the S/I interface, as shown in the tomogram cross-section (Figure 3.5b), in SIS does not support this idea. One possible explanation for the apparent discrepancy is that the SIS polymeric system is composed of two hydrophobic non-polar components; thus there is a lower driving force for segregation between the C<sub>12</sub>SH and PS-SH ligands bound to the Au surface. Also, the AuNPs are never exposed to the elevated temperatures that have been shown to induce thiol ligand mobility on (and possible dissociation from) the gold surface.<sup>73</sup>

When PS-segregating Au<sub>2.7</sub>NPs and PI-segregating Au<sub>∞</sub>NPs were incorporated into the SIS block polymer, the result was a mixture of particles across both domains. Stained and unstained TEM micrographs show well-ordered PS and PI domains; however, AuNPs occupied both domains (3.4d). The mixture result further illustrates the versatility and control of surface thiols on AuNPs, which may be particularly important in engineering nanocomposites for emerging applications.

### 3.5 Conclusions

This chapter reports on the ability to control segregation of AuNPs to either PI or PS domains of a SIS triblock polymer. By using a short-chain hydrophobic hydrocarbon polymer and capping ligands, on ligand-polymer enthalpic interactions were emphasized without the influence of other polar interactions. Results indicated that as-synthesized AuNPs with C<sub>12</sub>SH ligands preferentially segregate to the PI domains, which is supported by Hildebrand solubility and surface energy arguments.

Simple, post-synthesis, ligand exchanges were performed on the AuNPs to alter their surface chemistry. AuNP segregation preference changes to PS domains below C<sub>12</sub>SH:PS-SH ligand molar ratios of 5:1, which is about an order of magnitude higher ratio than that expected based on molecular average calculations. Transmission electron microtomography was used to elucidate the spatial arrangement of AuNPs in a composite film. Tomography results corroborate micrographs from traditional TEM measurements. The segregation behavior of AuNPs is attributed to area-averaged enthalpic interactions between ligands and their respective polymer domains and entropic contributions from the SIS triblock polymer architecture. This work illustrates the ease of making nanocomposites and tailoring their phase behavior for application-specific designs such as sensors or catalytic coatings.

### **3.6 Acknowledgements**

The author kindly acknowledges Dr. Perry Pellechia (University of South Carolina) for assistance with the <sup>1</sup>H-MAS NMR measurements.

## REFERENCES

1. Mayeda, M. K.; Kuan, W.-F.; Young, W.-S.; Lauterbach, J. A.; Epps III, T. H. *Chem. Mater.* **2012**, *24*(14), 2627-2634.
2. Tang, Z.; Kotov, N. A. *Adv. Mater.* **2005**, *17*(8), 951-962.
3. Fendler, J. H. *Chem. Mater.* **1996**, *8*(8), 1616-1624.
4. Quinten, M.; Leitner, A.; Krenn, J. R.; Aussenegg, F. R. *Opt. Lett.* **1998**, *23*(17), 1331-1333.
5. Takahara, J.; Yamagishi, S.; Taki, H.; Morimoto, A.; Kobayashi, T. *Opt. Lett.* **1997**, *22*(7), 475-477.
6. Keren, K.; Krueger, M.; Gilad, R.; Ben-Yoseph, G.; Sivan, U.; Braun, E. *Science* **2002**, *297*(5578), 72-75.
7. Minko, S.; Kiriya, A.; Gorodyska, G.; Stamm, M. *J. Am. Chem. Soc.* **2002**, *124*(34), 10192-10197.
8. Warner, M. G.; Hutchison, J. E. *Nature Mater.* **2003**, *2*(4), 272-277.
9. Wang, Y.; Angelatos, A. S.; Caruso, F. *Chem. Mater.* **2008**, *20*(3), 848-858.
10. Yen, W.-C.; Lee, Y.-H.; Lin, J.-F.; Dai, C.-A.; Jeng, U. S.; Su, W.-F. *Langmuir* **2010**, *27*(1), 109-115.
11. Gusev, A. A.; Rozman, M. G. *Comput. Theor. Polym. Sci.* **1999**, *9*(3-4), 335-337.
12. Koerner, H.; Kelley, J.; George, J.; Drummy, L.; Mirau, P.; Bell, N. S.; Hsu, J. W. P.; Vaia, R. A. *Macromolecules* **2009**, *42*(22), 8933-8942.
13. Zilg, C.; Mulhaupt, R.; Finter, J. *Macromol. Chem. Phys.* **1999**, *200*(3), 661-670.
14. Camponeschi, E.; Vance, R.; Al-Haik, M.; Garmestani, H.; Tannenbaum, R. *Carbon* **2007**, *45*(10), 2037-2046.
15. Segalman, R. A. *Mater. Sci. Eng., R* **2005**, *48*(6), 191-226.
16. Albert, J. N. L.; Epps III, T. H. *Mater. Today* **2010**, *13*(6), 24-33.

17. Lin, H.-Y.; Chen, H.-A.; Lin, H.-N. *Anal. Chem.* **2008**, *80*(6), 1937-1941.
18. Forster, S.; Antonietti, M. *Adv. Mater.* **1998**, *10*(3), 195-217.
19. Clay, R. T.; Cohen, R. E. *Supramol. Sci.* **1997**, *4*(1-2), 113-119.
20. Dai, C.-A.; Wu, Y.-L.; Lee, Y.-H.; Chang, C.-J.; Su, W.-F. *J. Cryst. Growth* **2006**, *288*(1), 128-136.
21. Horiuchi, S.; Fujita, T.; Hayakawa, T.; Nakao, Y. *Langmuir* **2003**, *19*(7), 2963-2973.
22. Sohn, B. H.; Seo, B. H. *Chem. Mater.* **2001**, *13*(5), 1752-1757.
23. Haryono, A.; Binder, W. H. *Small* **2006**, *2*(5), 600-611.
24. Vaia, R. A.; Maguire, J. F. *Chem. Mater.* **2007**, *19*(11), 2736-2751.
25. Brust, M.; Walker, M.; Bethell, D.; Schiffrin, D. J.; Whyman, R. *J. Chem. Soc., Chem. Comm.* **1994**, (7), 801-802.
26. Shan, J.; Tenhu, H. *Chem. Commun.* **2007**, (44), 4580-4598.
27. Daniel, M. C.; Astruc, D. *Chem. Rev.* **2004**, *104*(1), 293-346.
28. Templeton, A. C.; Hostetler, M. J.; Kraft, C. T.; Murray, R. W. *J. Am. Chem. Soc.* **1998**, *120*(8), 1906-1911.
29. Hostetler, M. J.; Templeton, A. C.; Murray, R. W. *Langmuir* **1999**, *15*(11), 3782-3789.
30. Kim, B. J.; Fredrickson, G. H.; Kramer, E. J. *Macromolecules* **2008**, *41*(2), 436-447.
31. Kim, B. J.; Bang, J.; Hawker, C. J.; Chiu, J. J.; Pine, D. J.; Jang, S. G.; Yang, S.-M.; Kramer, E. J. *Langmuir* **2007**, *23*(25), 12693-12703.
32. Kim, B. J.; Fredrickson, G. H.; Hawker, C. J.; Kramer, E. J. *Langmuir* **2007**, *23*(14), 7804-7809.
33. Kim, B. J.; Chiu, J. J.; Yi, G. R.; Pine, D. J.; Kramer, E. J. *Adv. Mater.* **2005**, *17*(21), 2618-2622.

34. Li, Q. F.; He, J. B.; Glogowski, E.; Li, X. F.; Wang, J.; Emrick, T.; Russell, T. P. *Adv. Mater.* **2008**, *20*(8), 1462-1466.
35. Jeon, S.-J.; Yang, S.-M.; Kim, B. J.; Petrie, J. D.; Jang, S. G.; Kramer, E. J.; Pine, D. J.; Yi, G.-R. *Chem. Mater.* **2009**.
36. Lee, J. Y.; Thompson, R. B.; Jasnow, D.; Balazs, A. C. *Faraday Discuss.* **2003**, *123*, 121-131.
37. Bockstaller, M. R.; Lapetnikov, Y.; Margel, S.; Thomas, E. L. *J. Am. Chem. Soc.* **2003**, *125*(18), 5276-5277.
38. Bockstaller, M. R.; Thomas, E. L. *Phys. Rev. Lett.* **2004**, *93*(16).
39. Chiu, J. J.; Kim, B. J.; Yi, G.-R.; Bang, J.; Kramer, E. J.; Pine, D. J. *Macromolecules* **2007**, *40*(9), 3361-3365.
40. Lin, Y.; Boker, A.; He, J. B.; Sill, K.; Xiang, H. Q.; Abetz, C.; Li, X. F.; Wang, J.; Emrick, T.; Long, S.; Wang, Q.; Balazs, A.; Russell, T. P. *Nature* **2005**, *434*(7029), 55-59.
41. He, J. B.; Tangirala, R.; Emrick, T.; Russell, T. P.; Boker, A.; Li, X. F.; Wang, J. *Adv. Mater.* **2007**, *19*(3), 381-385.
42. Chang, C.-C.; Lo, C.-T. *J. Phys. Chem. B* **2011**, *115*(11), 2485-2493.
43. Dohi, H.; Kimura, H.; Kotani, M.; Kaneko, T.; Kitaoka, T.; Nishi, T.; Jinnai, H. *Polym. J.* **2007**, *39*(8), 749-758.
44. Jinnai, H.; Spontak, R. J.; Nishi, T. *Macromolecules* **2010**, *43*(4), 1675-1688.
45. Stewart, M. E.; Anderton, C. R.; Thompson, L. B.; Maria, J.; Gray, S. K.; Rogers, J. A.; Nuzzo, R. G. *Chem. Rev.* **2008**, *108*(2), 494-521.
46. Saha, K.; Agasti, S. S.; Kim, C.; Li, X.; Rotello, V. M. *Chem. Rev.* **2012**, *112*(5), 2739-2779.
47. Stafford, C. M.; Roskov, K. E.; Epps, T. H., III; Fasolka, M. J. *Rev. Sci. Instrum.* **2006**, *77*(2), 023908.
48. Fasolka, M. J.; Harris, D. J.; Mayes, A. M.; Yoon, M.; Mochrie, S. G. *J. Phys. Rev. Lett.* **1997**, *79*(16), 3018-3021.

49. Epps III, T. H.; DeLongchamp, D. M.; Faselka, M. J.; Fischer, D. A.; Jablonski, E. L. *Langmuir* **2007**, *23*(6), 3355-3362.
50. Roskov, K. E.; Epps, T. H., III; Berry, B. C.; Hudson, S. D.; Tureau, M. S.; Faselka, M. J. *J. Comb. Chem.* **2008**, *10*(6), 966-973.
51. Kremer, J. R.; Mastronarde, D. N.; McIntosh, J. R. *J. Struct. Biol.* **1996**, *116*(1), 71-76.
52. Mastronarde, D. N. *J. Struct. Biol.* **1997**, *120*(3), 343-352.
53. Albert, J. N. L.; Baney, M. J.; Stafford, C. M.; Kelly, J. Y.; Epps III, T. H. *ACS Nano* **2009**, *3*(12), 3977-3986.
54. Smith, D. R.; Meier, D. J. *Polymer* **1992**, *33*(18), 3777-3782.
55. Albert, J. N. L.; Bogart, T. D.; Lewis, R. L.; Beers, K. L.; Faselka, M. J.; Hutchison, J. B.; Vogt, B. D.; Epps III, T. H. *Nano Lett.* **2011**, *11*(3), 1351-1357.
56. Ansari, I. A.; Hamley, I. W. *J. Mater. Chem.* **2003**, *13*(10), 2412-2413.
57. Romdhane, I. H.; Plana, A.; Hwang, S.; Danner, R. P. *J. Appl. Polym. Sci.* **1992**, *45*(11), 2049-2056.
58. Peponi, L.; Tercjak, A.; Gutierrez, J.; Cardinali, M.; Mondragon, I.; Valentini, L.; Kenny, J. M. *Carbon* **2010**, *48*(9), 2590-2595.
59. Peponi, L.; Tercjak, A.; Torre, L.; Kenny, J. M.; Mondragon, I. *J. Nanosci. Nanotechnol.* **2009**, *9*(3), 2128-2139.
60. Corbierre, M. K.; Cameron, N. S.; Lennox, R. B. *Langmuir* **2004**, *20*(7), 2867-2873.
61. Smart, T. P.; Mykhaylyk, O. O.; Ryan, A. J.; Battaglia, G. *Soft Matter* **2009**, *5*(19), 3607-3610.
62. Brandrup, J.; Immergut, E. H.; Grulke, E. A., *Polymer Handbook*. 4th ed. ed.; Wiley: New York, 1999.
63. Peponi, L.; Tercjak, A.; Martin, L.; Mondragon, I.; Kenny, J. M. *Express Polym. Lett.* **2011**, *5*(2), 104-118.

64. Meli, L.; Green, P. F. *ACS Nano* **2008**, *2*(6), 1305-1312.
65. Jasper, J. J. *J. Phys. Chem. Ref. Data* **1972**, *1*(4), 841-1114.
66. Porter, M. D.; Bright, T. B.; Allara, D. L.; Chidsey, C. E. D. *J. Am. Chem. Soc.* **1987**, *109*(12), 3559-3568.
67. Strong, L.; Whitesides, G. M. *Langmuir* **1988**, *4*(3), 546-558.
68. Hostetler, M. J.; Wingate, J. E.; Zhong, C. J.; Harris, J. E.; Vachet, R. W.; Clark, M. R.; Londono, J. D.; Green, S. J.; Stokes, J. J.; Wignall, G. D.; Glish, G. L.; Porter, M. D.; Evans, N. D.; Murray, R. W. *Langmuir* **1998**, *14*(1), 17-30.
69. Corbierre, M. K.; Cameron, N. S.; Sutton, M.; Laaziri, K.; Lennox, R. B. *Langmuir* **2005**, *21*(13), 6063-6072.
70. Thompson, R. B.; Ginzburg, V. V.; Matsen, M. W.; Balazs, A. C. *Science* **2001**, *292*(5526), 2469-2472.
71. Listak, J.; Hakem, I. F.; Ryu, H. J.; Rangou, S.; Politakos, N.; Misichronis, K.; Avgeropoulos, A.; Bockstaller, M. R. *Macromolecules* **2009**, *42*(15), 5766-5773.
72. Matsen, M. W.; Thompson, R. B. *Macromolecules* **2008**, *41*(5), 1853-1860.
73. Ionita, P.; Volkov, A.; Jeschke, G.; Chechik, V. *Anal. Chem.* **2008**, *80*(1), 95-106.

## Chapter 4

### METAL OXIDE ARRAYS FROM BLOCK POLYMER THIN FILM TEMPLATES

This chapter details the use of polystyrene-*b*-poly(ethylene oxide) thin films to template arrays of metal oxides including MgO, Al<sub>2</sub>O<sub>3</sub>, TiO<sub>2</sub>, MnO<sub>2</sub>, Fe<sub>2</sub>O<sub>3</sub>, Co<sub>3</sub>O<sub>4</sub>, NiO, CuO, ZnO, ZrO<sub>2</sub>, RuO<sub>2</sub>, SnO<sub>2</sub>, and Ce<sub>2</sub>O<sub>3</sub>. Templates and resulting arrays were characterized with atomic force microscopy and transmission electron microscopy. Superior nanoarray uniformity and control was highlighted by comparing templated titania to traditional sol-gel-synthesized titania in photodegradation reactions, which were monitored by UV-vis spectroscopy. The increase in photocatalytic activity of templated titania was attributed to fine control of size and dispersity of the nanoparticles within the templated array, which had a larger surface area than traditionally synthesized titania. Text and figures are reproduced with permission from Mayeda *et al.*, *Journal of Materials Chemistry A*, 2015, 3(15), 7822-7829 – Published by the Royal Society of Chemistry.<sup>1</sup>

#### 4.1 Introduction

The development of Mobil's zeolites in the 1960s sparked an avalanche of research on the design of structured materials with nanometer-scale features (> 1 nm) for applications in catalysis and separations.<sup>2</sup> Innovative uses of structure directing agents can yield nanomaterials with improved catalytic activity. Whereas small-molecule surfactants have proven to be excellent sub-nanometer structure directing agents,<sup>3</sup> block polymers (BPs) offer a macromolecular analog with tunable molecular

weights, block choices, and compositions.<sup>4,5</sup> When implemented in thin film environments (< 100 nm in thickness), BPs can serve as ideal organic templates, whose nanostructure can be controlled through processing techniques.<sup>6-11</sup> BP organic templates can be used to direct the nanoscale structure of inorganic materials for catalysts, sensors, and optics applications.<sup>12</sup> Improved ordering of the thin film morphology, to  $\sim\text{cm}^2$  grain sizes, is important for applications in competition (or in concert) with lithography and could be achieved by implementing complementary techniques that employ topographical patterning or external fields.<sup>9,13-17</sup>

BP-templated metal oxide arrays facilitate a variety of exciting applications in magnetic bit patterned media, seed-mediated nanotube growth, energy harvesting, and heterogeneous catalysis.<sup>18-23</sup> The vast majority of previous investigations involving BP templating follow two routes: (1) segregating preformed nanoparticles or (2) using *in situ* sol-gel methods. The former approach benefits from advances in nanoparticle synthesis, which allows researchers to tune particle size, shape, crystallinity, and composition.<sup>24</sup> Additionally, templating preformed nanoparticles is a convenient route to ensure that the inorganic material retains the desired properties of interest. Previous work that was detailed in Chapter 3 templated pre-synthesized gold nanoparticles in a polystyrene-*b*-polyisoprene-*b*-polystyrene thin film by tuning the particles' surface energies using ligand exchanges.<sup>25</sup> Kramer and coworkers also have investigated gold nanoparticle segregation in polystyrene-*b*-poly(2-vinyl pyridine) (PS-*b*-P2VP) BPs by manipulating ligand chemistry, density, and molecular weight.<sup>26-29</sup> Several reviews succinctly describe efforts to incorporate particles with varying composition, size, and shape into BPs.<sup>30-33</sup> In all cases, preformed nanoparticle miscibility and templating

generally were dominated by the particle-polymer entropic (particle size and shape) and enthalpic (ligand chemistry) interactions.

*In situ* sol-gel methods use a sacrificial BP to arrange metal salt precursors into nanoscale features and subsequently reduce, oxidize, or calcine the composite to simultaneously form the templated material and remove the polymer.<sup>34,35</sup> Sol-gel methods can be used to create many types of industrially relevant crystals, powders, and films. Within sol-gel techniques, evaporation induced self-assembly (EISA) is a popular method for templating inorganic materials.<sup>3</sup> In short, the polymer and metal precursor are combined in a single solution and a thin film is coated onto a substrate. The evaporation of solvent creates a concentration gradient that acts as an ordering front that produces the nanoscale features. Features can be tuned by adjusting the polymer molecular weight,<sup>36</sup> sol-gel concentration,<sup>34,37,38</sup> and coating procedure.<sup>39</sup> Researchers have used the EISA-templating method to produce arrays of gold, cobalt, and cobalt oxide, but ordering remains poor (grain size  $< 1 \mu\text{m}^2$ ).<sup>40-44</sup> Poor ordering likely was due to polymer/metal inter- and intra-molecular interactions that inhibit polymer chain mobility and prevent BP ordering.<sup>45</sup> To maximize BP chain mobility, Boyen and coworkers modified the EISA method by complexing Fe and Nb salts with homopolymer P2VP (h2PVP) prior to blending with the PS-*b*-P2VP solution.<sup>46</sup> Thin films of salt/h2VP/PS-*b*-P2VP produced well-ordered arrays with  $\approx 1 \mu\text{m}^2$  grain sizes. However, the modification of the traditional EISA method was limited to metal loading ratios of  $\text{mol}_{\text{metal}}:\text{mol}_{2\text{VP-monomer}} \leq 0.2$  to avoid macrophase separation. On the other hand, Russell and co-workers employed a preformed BP template to create well-ordered Au/Ag arrays for surface plasmon resonance studies.<sup>47</sup> Morris and coworkers have used the method to produce metal oxides with superparamagnetic and

ferroelectric properties.<sup>48-50</sup> Although the method was proven,<sup>51-55</sup> researchers have yet to use it for catalysis applications.

The preformed BP template method, hereafter referred to as spincoat-pattern-immersed-complex-etch (SPICE), was used to produce thin films of well-ordered arrays that were otherwise difficult to achieve *via* the EISA/dip-coating approach. The experimental results presented herein build upon previous investigations<sup>47,54</sup> by creating well-ordered hexagonally packed arrays of MgO, Al<sub>2</sub>O<sub>3</sub>, TiO<sub>2</sub>, MnO<sub>2</sub>, Fe<sub>2</sub>O<sub>3</sub>, Co<sub>3</sub>O<sub>4</sub>, NiO, CuO, ZnO, ZrO<sub>2</sub>, RuO<sub>2</sub>, SnO<sub>2</sub>, and Ce<sub>2</sub>O<sub>3</sub>. Furthermore, an improvement in photocatalytic activity of SPICE TiO<sub>2</sub> and Au/TiO<sub>2</sub> over EISA TiO<sub>2</sub> was demonstrated. In addition to photocatalysis, it is anticipated that this method will be critical to developing advanced materials for sensors, environmental catalysis, and lithography applications.

## 4.2 Experimental Section

### 4.2.1 Materials

All materials were used as received. Polystyrene-*b*-poly(ethylene oxide) (PS-*b*-PEO;  $D = 1.04$ ,  $\bar{M}_{n,styrene} = 16 \text{ kg mol}^{-1}$ ,  $\bar{M}_{n,ethylene\ oxide} = 5 \text{ kg mol}^{-1}$ ) was purchased from Polymer Source, Inc. Iron(III) nitrate nonahydrate (ACS reagent) was purchased from Sigma-Aldrich. Titanium(IV) tetraisopropoxide (98+%) and poly(acrylic acid) (25 wt% aqueous solution,  $\bar{M}_w = 240 \text{ kg mol}^{-1}$ ) was purchased from Acros Organics. Aluminum(III) nitrate nonahydrate (98%), cerium(III) nitrate hexahydrate (REacton®, 99.5%), cobalt(II) nitrate hexahydrate (ACS reagent), copper(II) nitrate hemipentahydrate (98%), magnesium(II) nitrate hexahydrate (98%), manganese(II) nitrate hydrate (99.98%), nickel(II) nitrate hexahydrate (98%), tin(II) chloride

dihydrate (ACS reagent), zinc(II) nitrate hexahydrate (99%), zirconium(IV) dichloride oxide octahydrate (98%), and methylene blue (high purity biological stain) were purchased from Alfa Aesar. ACS grade toluene, tetrahydrofuran, ethanol, and 2-propanol were purchased from BDH. Deionized water was obtained from a Millipore Milli-Q Direct 8 system. Hydrochloric acid (37% in water, technical) was purchased from Fisher Scientific. Silicon and silicon oxide (500 nm on silicon) wafers were purchased from Wafer World. Both types of wafers were rinsed with toluene, dried with a nitrogen stream, and cleaned in a Jelight Model 42 UVO-cleaner for 30 min prior to polymer spincoating.

#### **4.2.2 Templating procedure**

The SPICE method is depicted in Figure 4.1. Each of the sub-processes are explained in detail; however, it should be noted that sub-processes can be substituted (*e.g.*, thermal annealing instead of solvent vapor annealing, dip-coating instead of spincoating, calcination instead of ozone etching, *etc.*)

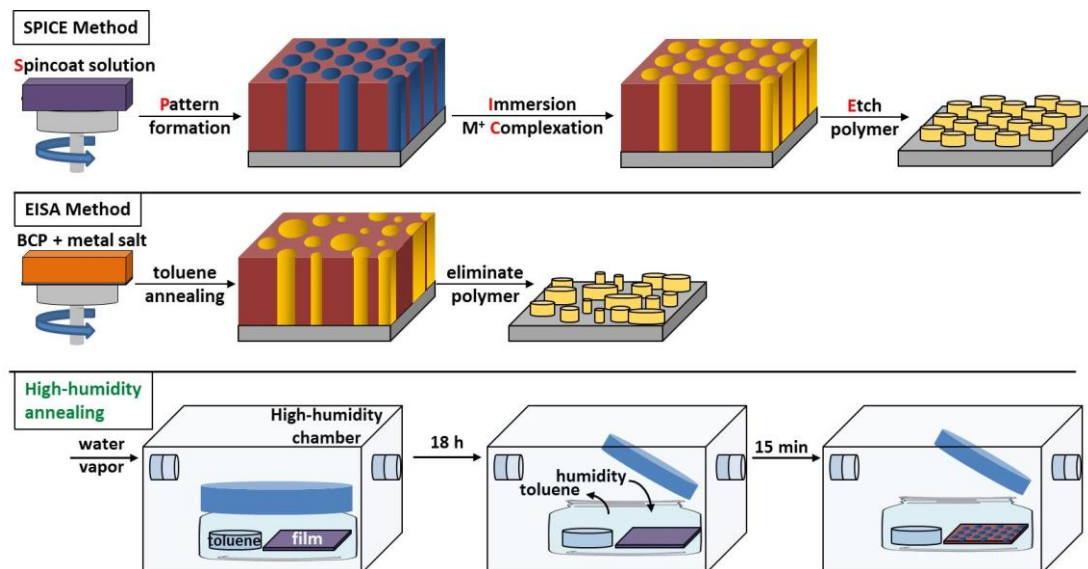


Figure 4.1: The spincoat-pattern-immersed-complex-etch (SPICE) templating method decouples polymer annealing from the metal precursor gel incorporation. Traditional methods, represented by EISA, spincoat an all-in-one solution that includes both polymer and metal precursor. Although EISA has fewer steps, it produces irregular arrays of inorganic material. High-humidity annealing was achieved by using standard solvent annealing techniques enclosed in a humidified glove box. Reprinted with permission from Mayeda *et al.*, *Journal of Materials Chemistry A*, 2015, 3(15), 7822-7829 – Published by the Royal Society of Chemistry.<sup>1</sup>

#### 4.2.2.1 Spincoating films

Films were made using a Laurell WS400-6NPP-Lite spincoater. Toluene solutions of PS-*b*-PEO (1 wt%) were stirred for 1 h and subsequently syringe filtered (0.2  $\mu\text{m}$ , PTFE) prior to film casting. Approximately 40  $\mu\text{L}$  of solution quickly were syringed onto substrates spinning at 3000 RPM for 30 s. Films were further dried under nitrogen. Thicknesses of as-cast films were analyzed using a Filmetrics F20 instrument.

#### 4.2.2.2 Pattern formation

Perpendicularly oriented hexagonally packed array patterns of PEO domains in a PS matrix were made by solvent annealing PS-*b*-PEO films with toluene/water in a high humidity chamber.<sup>56</sup> Films were placed in a bell jar with a beaker of 4 mL of toluene. The bell jar was positioned within a high humidity chamber. Humidity was controlled by bubbling nitrogen through deionized water that was maintained at 60 °C. After exposure to saturated toluene vapor at room temperature for 18 h, the bell jar was opened to simultaneously allow toluene evaporation and humidity exposure. Films were exposed to the high humidity environment for 15 min before being removed from the chamber. It should be noted that although arrays of perpendicular PEO domains were achieved by toluene solvent annealing alone, the addition of high humidity (>90% RH) increased grain sizes from less than 1  $\mu\text{m}^2$  to greater than 4  $\mu\text{m}^2$ .

#### 4.2.2.3 Immersion and metal complexation

Annealed PS-*b*-PEO films were immersed in a 1.0 M precursor (Mg, Al, Mn, Fe, Co, Ni, Cu, Zn, Sn, or Ce) in ethanol solution for 15 min. Different solutions were mixed for Zr and Ti precursors. For Zr solutions, 0.5 M solutions in ethanol/water (equal volume) were mixed to adequately dissolve the precursor. For Ti solutions, 0.25 g HCl solution, 0.7 g titanium(IV) tetraisopropoxide, and 5 mL 2-propanol were stirred for 30 min. Immersion allowed the metal ions to selectively complex with the PEO domains. After submerging the BP film in the precursor solution, excess precursor solution was removed by rinsing with 2-propanol and drying in a nitrogen stream.

#### 4.2.2.4 EISA TiO<sub>2</sub>

For comparison purposes, a film was made using the EISA method. After stirring, 0.2 mL of the titania solution was combined with 0.8 mL of the PS-*b*-PEO toluene solution (1 wt%), and a film was spincoated as previously described. Cast films were annealed in saturated toluene vapor (2 h) *without* water, which undesirably would have hydrolyzed the titanium precursor.

#### 4.2.2.5 Etching template

For all films, template etching and metal oxidation simultaneously were achieved using a UVO cleaner for 30 min. Residual carbon was removed by rinsing with toluene and drying under a dry nitrogen stream.

#### 4.2.2.6 Gold nanoparticle addition

To demonstrate additional modularity of SPICE, gold nanoparticles (AuNP) were spincoated onto the SPICE-templated TiO<sub>2</sub> after polymer removal to enhance the photocatalytic degradation of MB. AuNPs were synthesized according to the Brust-Schiffrin method.<sup>57</sup> AuNPs (3.5 ± 1.0 nm diameter) were stabilized in toluene solutions with dodecanethiol.<sup>25</sup>

#### 4.2.3 Film characterization

Atomic force microscopy (AFM) images were recorded with a Bruker Multimode Nanoscope V system. AppNano ACL tips (190 kHz resonant frequency, 58 N m<sup>-1</sup> spring constant) were used in tapping mode. Image processing and fast Fourier transforms (FFTs) of micrographs were performed with ImageJ.

X-Ray photoelectron spectroscopy (XPS) measurements were performed on a Kratos Axis Ultra DLD instrument equipped with a monochromated Al K $\alpha$  X-ray

source and a hemispherical analyzer. All analyzed metal oxide arrays were deposited on silicon oxide wafers. Binding energies were calibrated using Si 2p at 103.3 eV.

Transmission electron microscopy (TEM) images were taken with a Hitachi H8000 operated at 150 kV. PS-*b*-PEO films containing titania precursor were peeled and mounted onto copper mesh grids according to a method previously described in the literature.<sup>58</sup> The composite film was prepared for peeling by depositing a thin layer of carbon (< 10 nm) using a Hitachi carbon evaporator. A droplet (< 1 mL) of 25 wt% poly(acrylic acid) (PAA) was drop-cast and allowed to dry overnight at atmospheric conditions. A razor blade was used to remove the resulting solid, which adhered to the polymer composite film. The PAA was dissolved in a large volume of water. The resulting floating films were mounted onto copper mesh grids and allowed to air dry for 15 min before imaging.

#### **4.2.4 Photocatalysis experiments**

SPICE-templated titania were used to catalyze the photodegradation reaction of methylene blue (MB), which is an industrial pollutant commonly found in textile waste streams.<sup>21</sup> An aqueous solution of  $1 \times 10^{-5}$  M MB was stirred for 2 days and then stored in a dark environment for later use. Wafer fragments ( $\sim 2$  cm<sup>2</sup>) and 3.3 mL of MB solution were placed in Brandtech UV cuvettes (220-900 nm transparency). The surface areas of the samples were hard to measure when the wafer fragments were shaped irregularly. Therefore, degradation rates were normalized by the weights of the wafer fragments. UV irradiation was accomplished with a UVP XX-15S lamp (15 watt, 254 nm); samples were placed on the top tray, which was 5 cm from the source. UV-vis spectra were recorded with a Shimadzu UV2450 instrument. The 665 nm peak was monitored during time-lapse studies; peak integrations from 550-740 nm

were calculated using UVProbe 2.32. Photocatalytic experiments were reproduced three times for each sample.

### **4.3 Results**

In heterogeneous catalysis, ordered and narrowly dispersed features made by bottom-up processes are critical for applications requiring maximum active surface area. Thus, grain size and narrow structural dispersity inherent in BP films is an important aspect of the SPICE method. To this end, perpendicularly oriented and hexagonally packed domains of PEO cylinders in PS-*b*-PEO films (30 nm thick) were obtained by toluene vapor annealing in a high-humidity chamber, as depicted in Figure 4.1.<sup>56</sup>

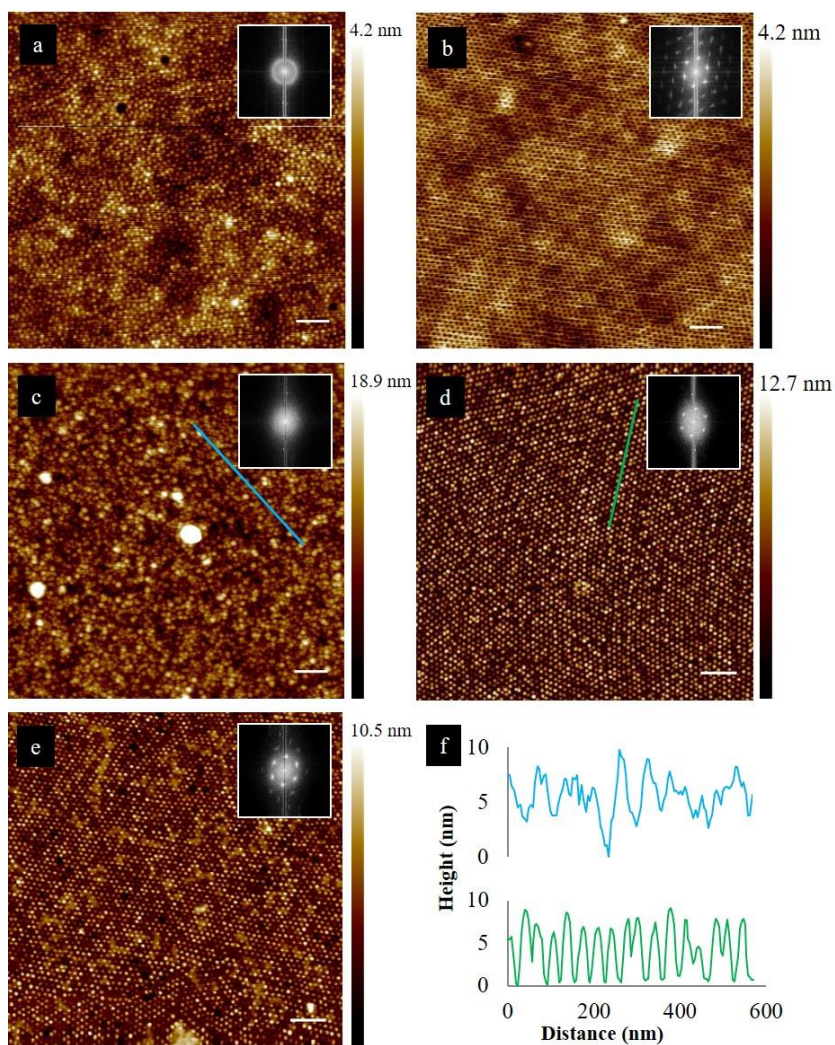


Figure 4.2: Atomic force microscopy height images of PS-b-PEO films after solvent vapor annealing with (a) toluene and (b) toluene/water. TiO<sub>2</sub> arrays were templated by (c) EISA and (d) SPICE; and (e) AuNPs were spincoated onto templated SPICE TiO<sub>2</sub>. Inset images are FFTs of the AFM images. Scale bars represent 200 nm. (f) Line scans show height profiles of the TiO<sub>2</sub> made by the SPICE (green, bottom) and EISA (blue, top) methods. Reprinted with permission from Mayeda *et al.*, *Journal of Materials Chemistry A*, 2015, 3(15), 7822-7829 – Published by the Royal Society of Chemistry.<sup>1</sup>

The average radius of the PEO domains in a toluene/water annealed neat polymer film was  $8.7 \pm 0.8$  nm (>2500 measurements) (Figure 4.2b). The inset FFT exhibits 4<sup>th</sup> order peaks, which corroborate the excellent order and large grain sizes achieved by high-humidity annealing. Grain sizes of toluene/water vapor annealed PS-*b*-PEO films were greater than  $4 \mu\text{m}^2$ . The PS-*b*-PEO films were used to template SPICE TiO<sub>2</sub> (Figure 4.2d) and Au on SPICE TiO<sub>2</sub> (Figure 4.2e) samples. On the other hand, films that were annealed by only toluene or tetrahydrofuran vapor contained grains that were less than  $1 \mu\text{m}^2$  (Figure 4.2a). Subsequently templated TiO<sub>2</sub> exhibited large size distributions and poor order (Figure 4.2c). The disparities in grain sizes highlighted the importance of using high-humidity during the annealing step.

Some metal precursors, such as the titanium(IV) tetraisopropoxide and tin(II) chloride, are susceptible to hydrolysis and cannot be processed in humid or aqueous environments. By separating template formation and metal precursor inclusion into two decoupled steps, the SPICE method can take advantage of annealing techniques (using high humidity in this case) that otherwise would be precluded by the presence of the metal precursor. To further extend this idea, the authors envision bolstering the SPICE method with supplementary annealing techniques that employ external fields, shear fields, or patterned substrates. Achieving wafer-sized areas of templated material is industrially relevant for magnetic storage media and energy harvesting.<sup>59,60</sup>

Metal oxides were templated into the annealed PS-*b*-PEO films by a simple immersion process. BP films were submerged in a metal precursor solution to allow the metal ions to selectively complex with the ethylene oxide monomer units. A typical loading ratio of 0.38 was achieved, which is almost twice that achieved by Boyen and coworkers (calculations are found in Appendix B).<sup>46</sup> Metal oxide formation

and polymer removal were achieved simultaneously using an ultraviolet ozone (UVO) oven. The versatility of the SPICE procedure was exemplified by templating commonly used metal oxides: MgO, Al<sub>2</sub>O<sub>3</sub>, TiO<sub>2</sub>, MnO<sub>2</sub>, Fe<sub>2</sub>O<sub>3</sub>, Co<sub>3</sub>O<sub>4</sub>, NiO, CuO, ZnO, ZrO<sub>2</sub>, RuO<sub>2</sub>, SnO<sub>2</sub>, and Ce<sub>2</sub>O<sub>3</sub>. Empirical formulas for the metal oxides were determined using high resolution XPS scans to identify the oxidation states of the metals.<sup>61</sup> Figure 4.2a-e show AFM images of selected metal oxide arrays as well as corresponding FFTs in the insets. Height images of the remaining metal oxides (Figure B.1) and XPS peak positions of all metal oxides (Table B.1) can be found in Appendix B. Hexagonally packed metal oxide dots are noted in Figure 4.2b, Figure 4.2d-e, and Figure B.1; all corresponding FFTs reveal reflections that are characteristic of hexagonal packing. 2<sup>nd</sup> order reflections are noted for Co<sub>3</sub>O<sub>4</sub>, Fe<sub>2</sub>O<sub>3</sub>, MgO, MnO<sub>2</sub>, ZnO, SnO<sub>2</sub> and TiO<sub>2</sub> samples. After polymer removal, the height of the templated materials ranged between 1-7 nm. For TiO<sub>2</sub>, a 30 nm thick BP film template produced an average oxide dot height of  $5.4 \pm 1.4$  nm. The height reduction was attributed to the significant mass loss during polymer template removal and was used to calculate the average oxide loading. The average radius of a templated dot was  $8.5 \pm 1.9$  nm, which closely matches the initial PEO domain size after solvent annealing ( $8.7 \pm 0.8$  nm).<sup>47</sup> The similarity in PEO domain size and the SPICE dot size suggests that templated metal oxide size can be controlled by tuning the polymer molecular weight and volume fraction.<sup>62</sup> Highly ordered PS-*b*-PEO films led to highly ordered metal oxide dots, supporting the efficacy and simplicity of the SPICE templating method.

The EISA-templating method was applied to the same polymer and titania precursor solution for the purpose of comparison. Because the titania precursor was highly sensitive to water, toluene/water solvent vapor undesirably hydrolyzed the

titania precursor in the EISA film (Figure 4.3a). Thus, only toluene vapor was used to anneal EISA films. Despite efforts to anneal the EISA composite with toluene vapor, the resulting titania were poorly ordered and disperse in diameter (Figure 4.3b). On the other hand, the SPICE method allowed the use of high-humidity annealing conditions and produced highly-ordered PEO domains, which preferentially absorbed the titania precursor (Figure 4.3c). The TEM images illustrate the superiority of the SPICE method.

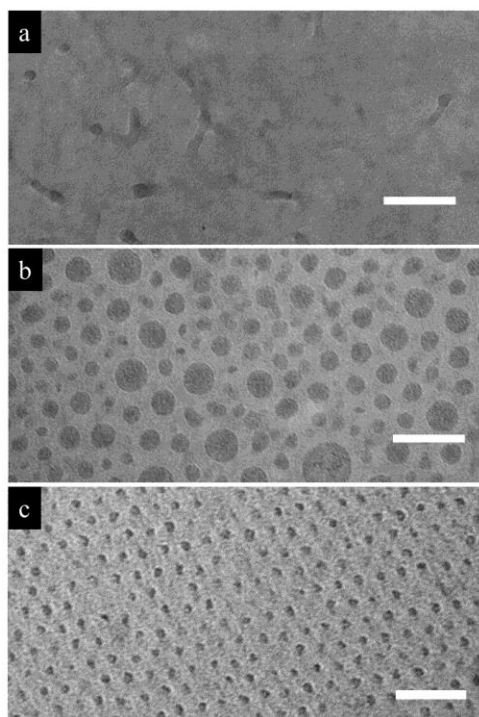


Figure 4.3: Transmission electron micrograph of (a) EISA (Ti precursor) films after annealing with toluene/water vapor and (b) toluene vapor as compared to a (c) SPICE Ti precursor film. Images are unstained; contrast is afforded by the electron density difference between PEO-titanium complex (dark) and PS (light). The scale bars represent 100 nm. Reprinted with permission from Mayeda *et al.*, *Journal of Materials Chemistry A*, 2015, 3(15), 7822-7829 – Published by the Royal Society of Chemistry.<sup>1</sup>

The EISA method produced an average TiO<sub>2</sub> dot radius of  $9.8 \pm 4.4$  nm. Decreased morphology control was evidenced by the line scan in Figure 4.2f, AFM image (Figure 4.2c), and TEM image (Figure 4.3b). Dispersion calculations are available in the Appendix B. The FFT of EISA micrographs showed no spots or rings, indicating the absence of any significant ordering. Poor ordering of annealed EISA films was attributed to hydrolytic oligomerization of titania and reduced polymer chain mobility caused by coordination bonds between the titania precursor and PEO domains.<sup>38,63,64</sup> Huh and coworkers studied the effect of Cd coordination with poly(4-vinylpyridine) (P4VP) and found that increasing the salt loading increased gelation and decreased ordering of their Cd/PS-b-P4VP system.<sup>45</sup> Similarly, it is expected that PEO-metal complexes hinder polymer chain mobility during solvent vapor annealing. By decoupling the polymer-ordering from the metal-coordinating, the SPICE method produced narrow size distributions and highly ordered arrays.

Au was expected to further improve the light absorption efficiency,<sup>65</sup> and thus the photocatalytic activity of TiO<sub>2</sub>.<sup>66,67</sup> Therefore, as a further validation of the approach, gold nanoparticles ( $3.5 \pm 1.0$  nm diameter) in a toluene solution were spincoated onto SPICE-templated TiO<sub>2</sub>. The resulting Au/TiO<sub>2</sub> catalyst was 5 mol% Au as determined by XPS survey scans (not shown). SPICE-templated TiO<sub>2</sub> arrays maintained their high degree of ordering and dispersity after Au addition (Figure 4.2e).

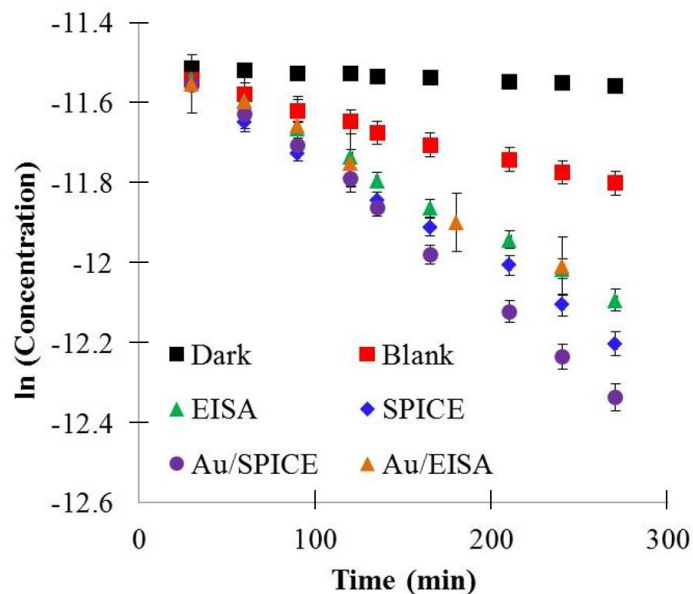


Figure 4.4: Plot of the natural log of MB concentrations against UV irradiation time. Error bars on data points represent standard deviations across three reproducibility studies. The slopes represent rate constants, which are reported in Table 4.1. The magnitude of  $k_{dark}$  was taken to be the error on the rate constants. Reprinted with permission from Mayeda *et al.*, *Journal of Materials Chemistry A*, 2015, 3(15), 7822-7829 – Published by the Royal Society of Chemistry.<sup>1</sup>

Photocatalytic studies were used to demonstrate the increased activity of SPICE TiO<sub>2</sub> compared to EISA TiO<sub>2</sub>. Aqueous solutions of MB were photocatalyzed under UV irradiation with EISA TiO<sub>2</sub>, SPICE TiO<sub>2</sub>, and SPICE TiO<sub>2</sub> coated with gold nanoparticles (Figure 4.4). Vials with SiO<sub>2</sub> wafers, no catalyst (blank), and MB stored in the dark were used as controls. UV-vis spectra were collected every two hours, and peak areas were integrated between 550-750 nm (Figure B.2). MB photodegradation was presumed to follow first order kinetics.<sup>21</sup>

$$\frac{-d[MB]}{dt} = k[MB] \quad 4-1$$

The first order rate constants ( $k$ ) were determined by fitting linear regressions of the MB concentrations as a function of irradiation time as shown in Figure 4.4. The reaction rate constants followed  $k_{Au/SPICE} > k_{SPICE} > k_{EISA} > k_{substrate} > k_{blank} > k_{dark}$  and are listed in Table 4.1.

Table 4.1. Photocatalytic conditions and rate constants

Sample	UV light	Catalyst	Rate constant <sup>a</sup> ( $\times 10^3 \text{ min}^{-1}$ )
<b>Dark</b>	no	N/A	0.2
<b>Blank</b>	yes	N/A	1.1
<b>EISA</b>	yes	TiO <sub>2</sub>	2.3
<b>Au/EISA</b>	yes	Au/TiO <sub>2</sub>	2.3
<b>SPICE</b>	yes	TiO <sub>2</sub>	2.6
<b>Au/SPICE</b>	yes	Au/TiO <sub>2</sub>	3.3

<sup>a</sup> Error values for the rate constants are given by the magnitude of the Dark rate constant.

The absolute value of  $k_{dark}$  was used as the error associated with the determination of rate constants. SPICE TiO<sub>2</sub> showed a 17% increase in photocatalytic activity over EISA TiO<sub>2</sub> during MB degradation experiments. The addition of gold nanoparticles to the SPICE TiO<sub>2</sub> samples (Au/TiO<sub>2</sub>) improved the photocatalytic activity by 22% over EISA TiO<sub>2</sub>.

Photocatalytic activity has been shown to depend on catalyst surface area, crystallinity, and surface hydroxyl concentration.<sup>68</sup> Because the EISA and SPICE methods share the same materials and polymer removal process, it is expected that crystallinity and surface hydroxyl groups remain similar. Therefore, the improved

photocatalytic efficiency was attributed to increased surface area, as the SPICE-templated TiO<sub>2</sub> surface area was increased by minimizing the TiO<sub>2</sub> size distribution (Figure B.3). Exposed surface area was estimated to be 25% larger for SPICE TiO<sub>2</sub> over EISA TiO<sub>2</sub>; uncertainty in the measurement stems from the variations in EISA dot sizes. In addition to an improvement over EISA TiO<sub>2</sub>, experimental results demonstrated a 6% activity gain between SPICE Au/TiO<sub>2</sub> over SPICE TiO<sub>2</sub>. The improvement in efficiency possibly indicates that the templated TiO<sub>2</sub> can be optimized and augmented in a similar manner to other previously reported titania samples.<sup>65,67</sup>

#### **4.4 Conclusions**

In conclusion, the SPICE templating method (spincoat-pattern-immersion-complex-etch) was used to produce arrays of a variety of metal oxides. The method decoupled metal-PEO complexation from BP ordering and thus enabled both exceptionally well-ordered arrays and simple sol-gel templating. The arrays exhibited the same high degree of ordering as their sacrificial BP thin film template. In particular, TiO<sub>2</sub> arrays exhibited a high degree of ordering and narrow size dispersion, which could not be achieved using standard EISA methods. Finally, MB photodegradation studies showed that the SPICE TiO<sub>2</sub> (1) showed a 17% increase in photocatalytic activity over EISA TiO<sub>2</sub> and (2) could be augmented with gold nanoparticles to further improve photocatalytic activity. The SPICE method opens exciting pathways for thin films of ordered metal oxides in sensors, magnetic bit storage media, and energy harvesting.

#### **4.5 Acknowledgements**

The author gratefully acknowledges Professor Chuanbing Tang (University of South Carolina) for use of the atomic force microscope, Professor Miao Yu (University of South Carolina) for use of the solar simulator, and Professor Brian Benicewicz (University of South Carolina) for use of the UV-visible spectrometer instrument.

## REFERENCES

1. Mayeda, M. K.; Hayat, J.; Epps, T. H.; Lauterbach, J. *J. Mat. Chem. A* **2015**, 3(15), 7822-7829.
2. Soler-Illia, G. J. d. A. A.; Sanchez, C.; Lebeau, B.; Patarin, J. *Chem. Rev.* **2002**, 102(11), 4093-4138.
3. Brinker, C. J. *MRS Bull.* **2004**, 29(9), 631-640.
4. Bates, F. S.; Hillmyer, M. A.; Lodge, T. P.; Bates, C. M.; Delaney, K. T.; Fredrickson, G. H. *Science* **2012**, 336(6080), 434-440.
5. Bates, F. S.; Fredrickson, G. H. *Phys. Today* **1999**, 52(2), 32-38.
6. Rawolle, M.; Niedermeier, M. A.; Kaune, G.; Perlich, J.; Lellig, P.; Memesa, M.; Cheng, Y. J.; Gutmann, J. S.; Muller-Buschbaum, P. *Chem. Soc. Rev.* **2012**, 41(15), 5131-5142.
7. Koo, K.; Ahn, H.; Kim, S.-W.; Ryu, D. Y.; Russell, T. P. *Soft Matter* **2013**, 9(38), 9059-9071.
8. Sinturel, C.; Vayer, M.; Morris, M.; Hillmyer, M. A. *Macromolecules* **2013**, 46(14), 5399-5415.
9. Luo, M.; Epps III, T. H. *Macromolecules* **2013**, 46(19), 7567-7579.
10. Albert, J. N. L.; Young, W. S.; Lewis, R. L.; Bogart, T. D.; Smith, J. R.; Epps III, T. H. *ACS Nano* **2012**, 6(1), 459-466.
11. Seppala, J. E.; Lewis, R. L.; Epps III, T. H. *ACS Nano* **2012**, 6(11), 9855-9862.
12. Segalman, R. A. *Mater. Sci. Eng., R* **2005**, 48(6), 191-226.
13. Park, C.; Yoon, J.; Thomas, E. L. *Polymer* **2003**, 44(22), 6725-6760.
14. Bates, C. M.; Maher, M. J.; Janes, D. W.; Ellison, C. J.; Willson, C. G. *Macromolecules* **2014**, 47(1), 2-12.
15. Herr, D. J. C. *J. Mater. Res.* **2011**, 26(2), 122-139.
16. Angelescu, D. E.; Waller, J. H.; Adamson, D. H.; Deshpande, P.; Chou, S. Y.; Register, R. A.; Chaikin, P. M. *Adv. Mater.* **2004**, 16(19), 1736-1740.

17. Kim, S. O.; Solak, H. H.; Stoykovich, M. P.; Ferrier, N. J.; de Pablo, J. J.; Nealey, P. F. *Nature* **2003**, *424*(6947), 411-414.
18. Quan, X.; Yang, S.; Ruan, X.; Zhao, H. *Environ. Sci. Technol.* **2005**, *39*(10), 3770-3775.
19. Zhuang, H. F.; Lin, C. J.; Lai, Y. K.; Sun, L.; Li, J. *Environ. Sci. Technol.* **2007**, *41*(13), 4735-4740.
20. Li, Y.; Sasaki, T.; Shimizu, Y.; Koshizaki, N. *J. Am. Chem. Soc.* **2008**, *130*(44), 14755-14762.
21. Houas, A.; Lachheb, H.; Ksibi, M.; Elaloui, E.; Guillard, C.; Herrmann, J.-M. *Appl. Catal., B* **2001**, *31*(2), 145-157.
22. Syoufian, A.; Nakashima, K. *J. Colloid Interface Sci.* **2008**, *317*(2), 507-512.
23. Acharya, H.; Sung, J.; Bae, I.; Kim, T.; Kim, D. H.; Park, C. *Chem. Eur. J.* **2012**, *18*(46), 14695-14701.
24. Daniel, M. C.; Astruc, D. *Chem. Rev.* **2004**, *104*(1), 293-346.
25. Mayeda, M. K.; Kuan, W.-F.; Young, W.-S.; Lauterbach, J. A.; Epps III, T. H. *Chem. Mater.* **2012**, *24*(14), 2627-2634.
26. Kim, B. J.; Bang, J.; Hawker, C. J.; Chiu, J. J.; Pine, D. J.; Jang, S. G.; Yang, S.-M.; Kramer, E. J. *Langmuir* **2007**, *23*(25), 12693-12703.
27. Kim, B. J.; Fredrickson, G. H.; Kramer, E. J. *Macromolecules* **2007**, *41*(2), 436-447.
28. Chiu, J. J.; Kim, B. J.; Kramer, E. J.; Pine, D. J. *J. Am. Chem. Soc.* **2005**, *127*(14), 5036-5037.
29. Kim, B. J.; Chiu, J. J.; Yi, G. R.; Pine, D. J.; Kramer, E. J. *Adv. Mater.* **2005**, *17*(21), 2618-2622.
30. Balazs, A. C.; Emrick, T.; Russell, T. P. *Science* **2006**, *314*(5802), 1107-1110.
31. Haryono, A.; Binder, W. H. *Small* **2006**, *2*(5), 600-611.

32. Bockstaller, M. R.; Mickiewicz, R. A.; Thomas, E. L. *Adv. Mater.* **2005**, *17*(11), 1331-1349.
33. Kao, J.; Thorkelsson, K.; Bai, P.; Rancatore, B. J.; Xu, T. *Chem. Soc. Rev.* **2013**, *42*(7), 2654-2678.
34. Sun, Z. C.; Kim, D. H.; Wolkenhauer, M.; Bumbu, G. G.; Knoll, W.; Gutmann, J. S. *ChemPhysChem* **2006**, *7*(2), 370-378.
35. Orilall, M. C.; Wiesner, U. *Chem. Soc. Rev.* **2011**, *40*(2), 520-535.
36. Ortel, E.; Fischer, A.; Chuenchom, L.; Polte, J.; Emmerling, F.; Smarsly, B.; Kraehnert, R. *Small* **2012**, *8*(2), 298-309.
37. Urade, V. N.; Bollmann, L.; Kowalski, J. D.; Tate, M. P.; Hillhouse, H. W. *Langmuir* **2007**, *23*(8), 4268-4278.
38. Cheng, Y. J.; Gutmann, J. S. *J. Am. Chem. Soc.* **2006**, *128*(14), 4658-4674.
39. Grosso, D. *J. Mater. Chem.* **2011**, *21*(43), 17033-17038.
40. Kastle, G.; Boyen, H. G.; Weigl, F.; Lengl, G.; Herzog, T.; Ziemann, P.; Riethmuller, S.; Mayer, O.; Hartmann, C.; Spatz, J. P.; Moller, M.; Ozawa, M.; Banhart, F.; Garnier, M. G.; Oelhafen, P. *Adv. Funct. Mater.* **2003**, *13*(11), 853-861.
41. Boyen, H. G.; Kastle, G.; Zurn, K.; Herzog, T.; Weigl, F.; Ziemann, P.; Mayer, O.; Jerome, C.; Moller, M.; Spatz, J. P.; Garnier, M. G.; Oelhafen, P. *Adv. Funct. Mater.* **2003**, *13*(5), 359-364.
42. Polleux, J.; Rasp, M.; Louban, I.; Plath, N.; Feldhoff, A.; Spatz, J. P. *ACS Nano* **2011**, *5*(8), 6355-6364.
43. Spatz, J. P.; Mossmer, S.; Hartmann, C.; Moller, M.; Herzog, T.; Krieger, M.; Boyen, H. G.; Ziemann, P.; Kabius, B. *Langmuir* **2000**, *16*(2), 407-415.
44. Palmer, R. E.; Pratontep, S.; Boyen, H. G. *Nature Mater.* **2003**, *2*(7), 443-448.
45. Lee, D. H.; Han, S. H.; Joo, W.; Kim, J. K.; Huh, J. *Macromolecules* **2008**, *41*(7), 2577-2583.

46. Shan, L.; Punniyakoti, S.; Van Bael, M. J.; Temst, K.; Van Bael, M. K.; Ke, X.; Bals, S.; Van Tendeloo, G.; D'Olieslaeger, M.; Wagner, P.; Haenen, K.; Boyen, H.-G. *J. Mater. Chem. C* **2014**, *2*(4), 701-707.
47. Mistark, P. A.; Park, S.; Yalcin, S. E.; Lee, D. H.; Yavuzcetin, O.; Tuominen, M. T.; Russell, T. P.; Achermann, M. *ACS Nano* **2009**, *3*(12), 3987-3992.
48. Ghoshal, T.; Maity, T.; Godsell, J. F.; Roy, S.; Morris, M. A. *Adv. Mater.* **2012**, *24*(18), 2390-2397.
49. Ghoshal, T.; Maity, T.; Senthamarai kannan, R.; Shaw, M. T.; Carolan, P.; Holmes, J. D.; Roy, S.; Morris, M. A. *Sci. Rep.* **2013**, *3*, 1-8.
50. Varghese, J.; Ghoshal, T.; Deepak, N.; O'Regan, C.; Whatmore, R. W.; Morris, M. A.; Holmes, J. D. *Chem. Mater.* **2013**, *25*(8), 1458-1463.
51. Wu, L. L.; Leng, B.; Bisht, A. *Appl Phys A* **2014**, *116*(3), 893-900.
52. Lu, J. Q. *J. Phys. Chem. C* **2008**, *112*(28), 10344-10351.
53. Ghoshal, T.; Shaw, M. T.; Bolger, C. T.; Holmes, J. D.; Morris, M. A. *J. Mater. Chem.* **2012**, *22*(24), 12083-12089.
54. Cho, H.; Park, H.; Russell, T. P.; Park, S. *J. Mater. Chem.* **2010**, *20*(24), 5047-5051.
55. Roulet, M.; Vayer, M.; Sinturel, C. *Eur. Polym. J.* **2013**, *49*(12), 3897-3903.
56. Kim, S. H.; Misner, M. J.; Xu, T.; Kimura, M.; Russell, T. P. *Adv. Mater.* **2004**, *16*(3), 226-231.
57. Brust, M.; Walker, M.; Bethell, D.; Schiffrin, D. J.; Whyman, R. *J. Chem. Soc., Chem. Comm.* **1994**, (7), 801-802.
58. Epps III, T. H.; DeLongchamp, D. M.; Fasolka, M. J.; Fischer, D. A.; Jablonski, E. L. *Langmuir* **2007**, *23*(6), 3355-3362.
59. Terris, B. D.; Thomson, T. *J. Phys. D-Appl. Phys.* **2005**, *38*(12), R199-R222.
60. Peng, K. Q.; Lee, S. T. *Adv. Mater.* **2011**, *23*(2), 198-215.
61. NIST X-ray Photoelectron Spectroscopy Database, Version 4.1. National Institute of Standards and Technology: Gaithersburg, 2012.

62. Yang, P.; Zhao, D.; Margolese, D. I.; Chmelka, B. F.; Stucky, G. D. *Chem. Mater.* **1999**, *11*(10), 2813-2826.
63. Peng, J.; Li, X.; Kim, D. H.; Knoll, W. *Macromol. Rapid Commun.* **2007**, *28*(21), 2055-2061.
64. Bailey, F. E.; Koleske, J. V., *Alkylene oxides and their polymers*. Dekker: New York, 1991.
65. Kowalska, E.; Mahaney, O. O. P.; Abe, R.; Ohtani, B. *Phys. Chem. Chem. Phys.* **2010**, *12*(10), 2344-2355.
66. Arabatzis, I. M.; Stergiopoulos, T.; Andreeva, D.; Kitova, S.; Neophytides, S. G.; Falaras, P. *J. Catal.* **2003**, *220*(1), 127-135.
67. Primo, A.; Corma, A.; Garcia, H. *Phys. Chem. Chem. Phys.* **2011**, *13*(3), 886-910.
68. Nagaveni, K.; Sivalingam, G.; Hegde, M. S.; Madras, G. *Appl. Catal., B* **2004**, *48*(2), 83-93.

## Chapter 5

### SUMMARY AND FUTURE WORK FOR NANOSTRUCTURED THIN FILMS

#### 5.1 Summary

Investigations into the design and characterization of nanocomposite block polymer (BP) thin films and BP thin film templates are presented in this dissertation. Polystyrene-*b*-polyisoprene-*b*-polystyrene (SIS) and polystyrene-*b*-poly(ethylene oxide) (PS-*b*-PEO) thin films were used to template gold and metal oxide nanoparticles, respectively, into nanostructured patterns. By building upon previous investigations that employed BP thin films to organize inorganic nanomaterials,<sup>1,2</sup> the objective was to apply BP templating to create catalysts that maximized the three-phase interface between active metal, catalyst support, and reactant(s). In one study, alkylthiol-protected gold nanoparticles (AuNPs) were synthesized *ex situ* and subsequently blended into SIS thin films.<sup>3</sup> The nanoparticle surface chemistry was tailored with mixtures of *n*-dodecanethiol and polystyrene-thiol to modulate the nanoparticles' affinity for the polystyrene or the polyisoprene domains of the SIS thin film. It was found that the effective interfacial surface area between the nanoparticle-grafted alkylthiols and the matrix polymer played an important role in determining the nanoparticles' segregation behavior and should be considered in the design and synthesis of other nanoparticle-polymer nanocomposites.

In another study, PEO domains of a PS-*b*-PEO thin film template were infused with metal oxide precursors and subsequently oxidized to produce long-range ordered metal oxide arrays.<sup>4</sup> In contrast, the standard approach employed evaporation

induced self-assembly (EISA) methods.<sup>5-8</sup> While EISA was powerful and simple, the results commonly produced poorly organized or heterogeneous arrays.<sup>7</sup> The poorly ordered arrays had a variety of inter-particle geometries and particle sizes, both of which contributed to decreased exposed surface area. Well-ordered PS-*b*-PEO thin films, which were produced by dual-solvent vapor annealing, were important precursors to the large surface area templated metal oxides. PS-*b*-PEO films selectively complexed various water-soluble metal oxide precursors into the hydrophilic PEO domains. Upon oxidation of the precursor-infused PS-*b*-PEO, the remaining metal oxide array mimicked the hexagonal pattern of the BP thin film template to a high degree. When the arrays were used in photocatalytic reactions, they exhibited superior performance compared to metal oxide thin films that were produced without a template. Perhaps more appealing than the template versatility is the potential to use bottom-up and top-down methods to create interesting high-aspect ratio arrays.<sup>9,10</sup>

The nanocomposite thin films and nanostructured metal oxides presented in this dissertation represent progress towards designing nanostructured catalysts. Section 5.2 outlines recommendations that apply the developed nanostructured templates to create nanomaterials with high aspect ratios for use in catalysis and energy harvesting.<sup>9,10</sup> Separately, the use of commercially available BPs in the templating process would accelerate the adoption of the aforementioned nanomaterial fabrication. Finally, recommendations for additional catalytic reactions are presented: CO-oxidation and three-way catalytic reactions in automotive exhaust.

## 5.2 Recommendations for Future Work

It is now known that nanomaterials exhibit properties that differ from their bulk properties because of an increase in the ratio of surface-to-bulk atoms.<sup>11,12</sup> Nanoparticles have led to a range of next-generation products including membranes,<sup>13</sup> catalysts,<sup>14</sup> biofuels,<sup>15</sup> cancer therapeutics,<sup>16</sup> and even food.<sup>17,18</sup> A burst in nanomaterial synthetic techniques has emerged where the figures of merit include size,<sup>12</sup> shape,<sup>19</sup> structure/composition,<sup>20,21</sup> and processibility.<sup>22-24</sup> To these ends, BPs have been used to guide nanomaterial growth and assembly so as to decrease size and shape dispersity and increase reproducibility and versatility.<sup>25-27</sup> Size- and regio-regularity have placed templated nanomaterials in exciting applications in energy harvesting,<sup>28</sup> gas sorbents,<sup>29</sup> plasmonics,<sup>30</sup> and catalysis.<sup>31</sup>

BPs have been proposed to work with existing lithographic techniques to achieve ever-smaller features.<sup>32</sup> It is envisioned that BP-templated inorganics will be a stepping-stone in top-down and bottom-up strategies for synthesizing advanced nanomaterials (Figure 5.1).

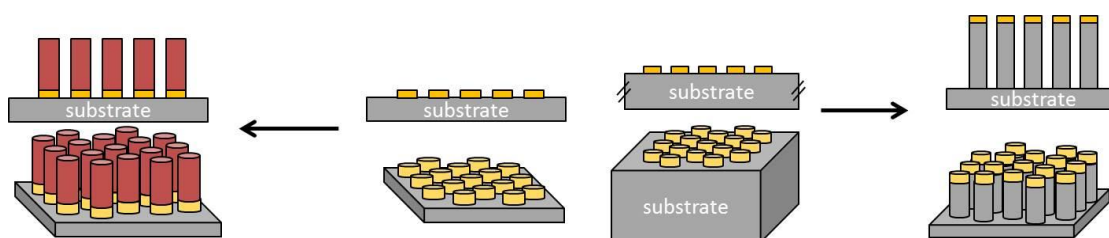


Figure 5.1: Schematic depicting the use of nanoscale arrays in bottom-up (left) and top-down (right) processes.

In a bottom-up approach, the templated materials can be used as a seed to nucleate growth and crystallization of a deposited material like carbon<sup>33</sup> or zinc

oxide.<sup>34</sup> In a top-down approach, the templated materials can be either an etch mask<sup>35,36</sup> (Figure 5.1, right) or an etch catalyst.<sup>37</sup> Furthermore, using the existing method (Section 4.2) is proposed to produce other functional arrays of metal oxides as catalysts, pattern transfer media, and seeds for carbon nanotube growth.

### **5.2.1 Top-Down Metal-assisted Chemical Etching**

Metal nanoparticles can be used in a top-down fashion in metal-assisted etching of silicon.<sup>10,38-41</sup> Nanoparticles of gold,<sup>42-46</sup> silver,<sup>42,47-51</sup> platinum,<sup>42,47,52</sup> copper,<sup>47</sup> or palladium<sup>42,51</sup> reduce an oxidant (*e.g.*, hydrogen peroxide) and simultaneously inject holes into the immediately underlying silicon substrate. The holes oxidize the silicon, which is then dissolved away (*i.e.*, etched) by hydrofluoric acid. The technique has been used to etch crystalline silicon wafers to yield silicon nanopores or vertically-aligned nanorods (Figure 5.2).

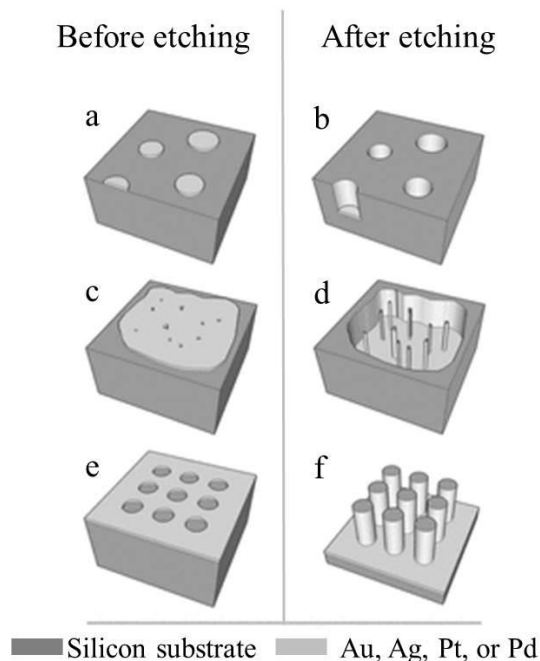


Figure 5.2: Diagram depicting (a, c, e) a noble metal coated on a silicon substrate and the resulting (b) nanopores, (d) nanowires, and (f) nanorods after etching. Adapted with permission from Huang, Z.; Geyer, N.; Werner, P.; de Boor, J.; and Gösele, U. *Adv. Mater.*, 2011, 23, 285-308. Copyright 2011 Wiley-VCH.

The vast majority of previous metal-assisted chemical etching techniques that have created ordered silicon nanostructures hinged on the use of polystyrene nanosphere lithography,<sup>49,53-57</sup> interference nanolithography,<sup>58</sup> or an anodized alumina hard mask to control the size and position of the metal.<sup>46</sup> However, the methods that were described in sections 3.2 and 4.2 represent simpler wet-chemistry methods that use the self-assembling BPs to create inorganic patterns. To this end the SIS template was removed in an ultraviolet ozone (UVO) cleaner to yield columns of AuNPs (Figure 5.3).

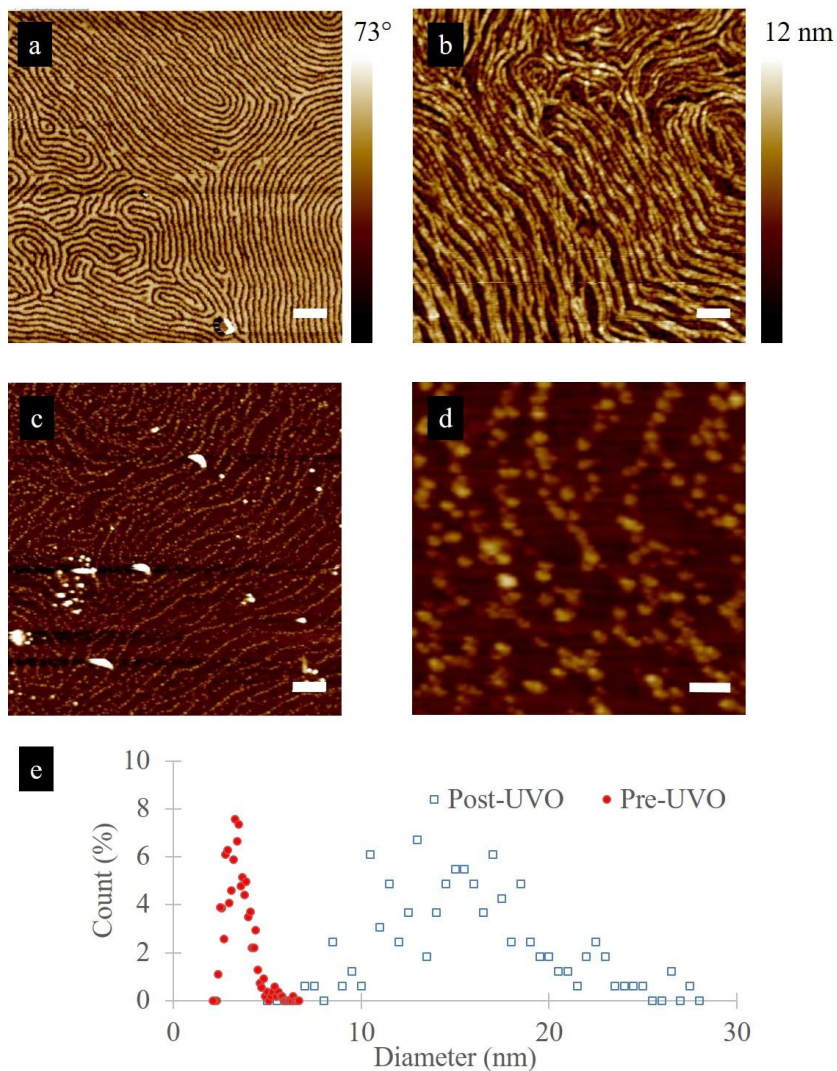


Figure 5.3: (a) AFM phase image of a toluene-annealed AuNP/SIS film, (b) AFM height image of the film in (a) after PI removal by ozone etching, and AFM height images (c) and (d) of AuNP chains after complete UVO etching. The height scale applies to b-d. The scale bars in a-c represent 200 nm while the scale bar in (d) represents 50 nm. (e) The histogram shows the size distributions of AuNPs before and after UVO treatment of the nanocomposite thin film.

Although the columns of AuNPs (Figure 5.3c and Figure 5.3d) mimic the pattern of the AuNP/SIS composite (Figure 5.3a), the template-removal step induced significant

deviations in the form of intra- or inter-column AuNP aggregation. In the case of intra-column aggregation, AuNPs grow from  $3.5 \pm 1.0$  nm to  $17 \pm 5$  nm in diameter (Figure 5.3e). Growth likely was induced by the increased temperature within the UVO chamber (60-90 °C).<sup>59,60</sup> In the case of inter-column aggregation, the original PS-to-PS domain distance ( $35 \pm 2$  nm) yielded columns of AuNPs that were separated by  $60 \text{ nm} \pm 22 \text{ nm}$  as calculated from the image in Figure 5.3c. From Figure 5.3b, it is apparent that inter-column aggregation occurs even when using only ozone to selectively etch the PI domains. To fully exploit the pattern generated by the SIS polymer, the inter- and intra-column aggregation needs to be limited. Inter-column aggregation can be limited by including a UVO-resistant block between gold-containing domains (*e.g.*, polydimethylsiloxane) while intra-column aggregation can be limited by reducing the temperature during oxidation. Examples of reduced-temperature UVO treatments include using (1) cycles that allow cool-down periods (UVO turned off) or (2) floating the substrate on an ice bath within the UVO chamber. Further use of UVO or ozone etching would require investigations into the effects of temperature, time, polymer molecular weight, and polymer architecture.

Although the methods to template well-ordered inorganic materials are established, modifications to the method need to be investigated so as to improve versatility. In the case of the SPICE method, questions include: (1) can the benefits of homopolymer-BP blends still create inorganic templates, (2) can the selective etching of PI (and, eventually, the whole polymer) be better controlled by reducing the UVO chamber temperature, and (3) can a mixture of silver and gold nanoparticles be templated and subsequently used to produce a bimodal distribution of porous structures after metal-assisted etching?

Polymer blends are attractive strategies to access different BP morphologies and domain sizes while avoiding the costs associated with synthesizing new polymers.<sup>61</sup> But in the case of the SPICE method, the polymer blend may not be amenable to the metal precursor immersion and complexation process because the homopolymer PEO would dissolve into solution. Therefore, blends may only work if the blended homopolymer is within the insoluble matrix. Although not strictly a BP - homopolymer blend, it should be noted that Shan *et al.* cleverly used homopolymer solutions to incorporate their metal precursor.<sup>62</sup> However, the homopolymer was not used to alter the morphology of the template. Even if the method is limited to blending hydrophobic polymers, the ability to access varying morphologies and spacing could prove valuable.

In the case of ozone etching to remove PI, inter-domain PS aggregation diminished the integrity of the original fingerprint pattern. Part of the reason for PS domain aggregation could be temperature-induced mobility during etching. The temperature of the UVO chamber (*i.e.*, Jelight model 42) can reach up to 90 °C within 15 min of operation, according to the manufacturer. Decreasing the substrate temperature could lead to etched films that better mimic the original BP film. For safety reasons, the UVO instrument will not operate with the door partially open. Therefore, a cooling coil fed by a recirculating chiller could not be implemented. **No attempts should be made to disengage the safety mechanism that automatically stops the UVO instrument when the chamber door is opened.** Instead, the substrate temperature could be lowered by floating the substrate in an ice water bath that is placed within the UVO chamber. **Care should be taken when introducing water to the internal workings of the UVO apparatus. Water can damage electronics and**

**induce premature corrosion which can lead to instrument failure and safety concerns.** Because small substrates are typically used ( $< 1 \text{ in}^2$ ), a water-filled glass Petri dish should be sufficient. Optimizations in the procedure to maintain low-temperature substrates could reduce the intra- and inter-chain aggregation of gold nanoparticles and polystyrene domains, respectively.

Metal-assisted etching could then be used to create pores in the underlying silicon substrate according to the parent polymer template. In the same way that thiols can be used to modify gold nanoparticles in section 3.2, thiols can be used to direct the self-assembly of BP composites with silver, copper, platinum, and palladium nanoparticles.<sup>63</sup> The size and structure of the etched pores largely depend on the nanoparticle size and material. Therefore, variations in the polymer template, nanoparticle type, and nanoparticle alignment within the template can create a rich array of porous silicon substrates. Dual templating nanoparticles also could be used to create a bimodal distribution of metal-assisted pores in the underlying silicon substrate.<sup>64</sup>

### **5.2.2 Bottom-Up Applications**

Bottom-up strategies require a guide that directs the growth of a material. A macroscopic example of bottom-up construction is the use of a garden trellis to manipulate the growth of a shrub into an aesthetic or functional shape. By carefully establishing the initial conditions for growth (*i.e.*, trellis shape and placement and plant type), the resulting full-grown shrub can reasonably be expected to mimic the desired shape. This section will briefly discuss the use of BP-templated inorganics in seed-mediated growth processes and potential use in pattern propagation in subsequently cast BP films.

### 5.2.2.1 Seed-mediated Growth

Seed-mediated growth is a bottom-up method that has been used to create non-spherical nanoparticles with high surface area-to-volume ratios.<sup>65-67</sup> Surface-bound seeds can nucleate the growth of aligned zinc oxide nanorods, silicon nanowires, and carbon nanotubes.<sup>34,68-72</sup> It has been shown that carbon nanotube quality can depend on seed material,<sup>73,74</sup> size,<sup>33,75</sup> and spacing. Therefore, the SPICE method would be an ideal platform that can generate the commonly used catalysts (*e.g.*, iron and nickel). For example, by increasing the molecular weight of the template polymer, the size of the PEO dots and resulting oxides can be increased (Figure 5.4).

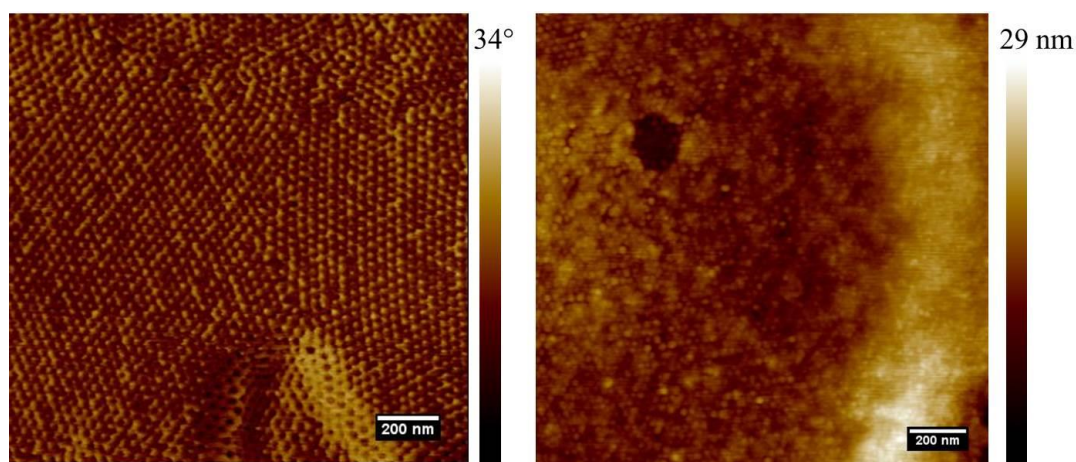


Figure 5.4: Increasing the molecular weight of the PS-*b*-PEO template to 25.5 kg/mol (left) increased the resulting radius of the produced TiO<sub>2</sub> nanodots (right) to  $11.3 \pm 1$  nm.

Whereas previous studies have shown the ability to nucleate aligned arrays of zinc oxide and carbon nanotubes, the nucleating seeds typically lacked order.<sup>76</sup> The lack of order resulted in perpendicular nanostructures that formed bundles, which may have hindered mass transfer, charge separation, or electron conductivity. Therefore, the

well-ordered (*i.e.*, well-spaced) results from the SPICE method may be able to produce structures that resist bundling. Preliminary results on carbon nanotube growth by chemical vapor deposition suggested that a minority of the SPICE-Fe<sub>2</sub>O<sub>3</sub> and -SnO<sub>2</sub> nanodots were active (Figure 5.5). Growth conditions were taken from Cassell *et al.* Briefly, methane (750 mL/min) was passed over the catalyst, which was preheated to 900°C in a furnace, for 20 min.<sup>77</sup> Samples were allowed to cool before imaging with AFM (Figure 5.5b and Figure 5.5d).

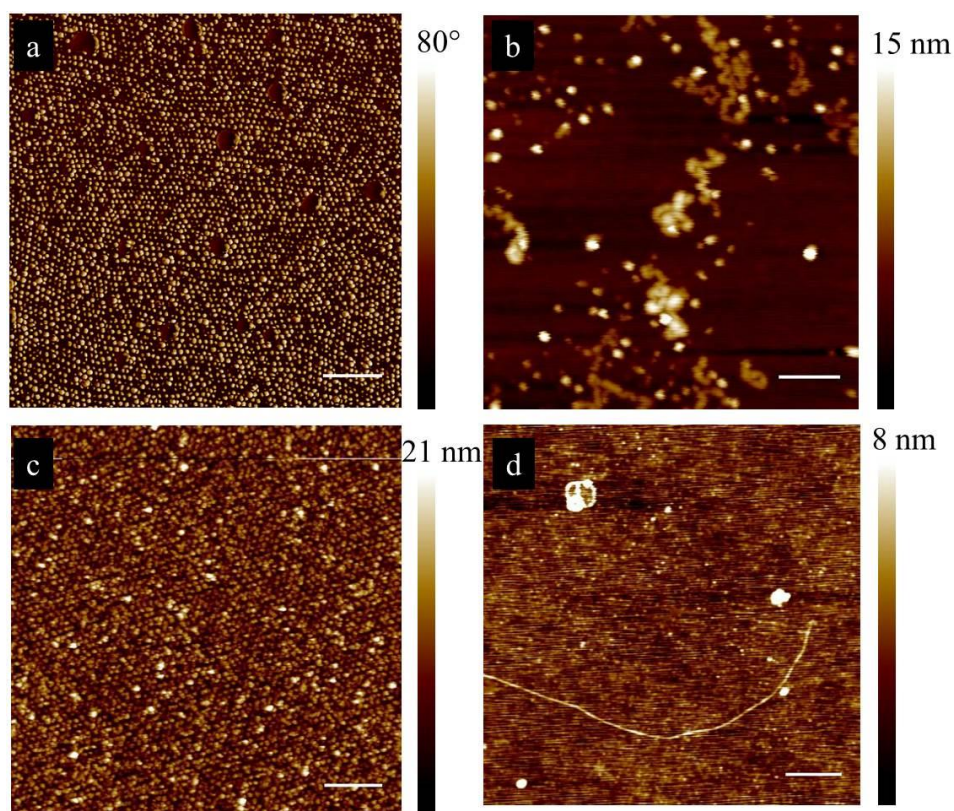


Figure 5.5: AFM phase image of (a) Fe<sub>2</sub>O<sub>3</sub> arrays, (b) carbon nanotubes grown using (a), (c) SnO<sub>2</sub> arrays, and (d) carbon nanotubes grown from (c). Nanotubes were grown by chemical vapor deposition. Scale bars represent 300 nm.

A minority of the dots was active and some of the nanotubes were parallel to the substrate. Also, the nanotubes from SnO<sub>2</sub> were noticeably straighter than the nanotubes from Fe<sub>2</sub>O<sub>3</sub>. For the purposes of generating high-surface area catalyst supports and light-harvesting films, it would be beneficial to refine the chemical vapor deposition process (*i.e.*, gas composition, flow rate, reaction time, and reactor temperature).

### 5.2.2.2 Pattern Propagation

Topographical patterning has been previously used to guide BP ordering.<sup>78,79</sup> The patterns demonstrated in 0 were limited to heights of 7 nm, which probably was too low to affect the self-assembly of subsequently deposited BP thin films;<sup>80</sup> effective topographical patterns typically have heights that are similar to the polymer film thickness.<sup>8,78,79,81,82</sup> However, metal and metal oxide patterns can be foundations for chemical patterns by employing complementary monolayers of silanes, thiols, carboxylic acids, or phosphonic acids.<sup>83,84</sup> Such “orthogonal self-assembly”<sup>85</sup> techniques create monolayers that can affect subsequently cast polymer thin films. Whereas previous investigations have used physical vapor deposition, electrodeposition in solution, or electroless deposition in solution to create substrate-material patterns,<sup>63</sup> the SPICE method could be used to create BP-templated substrate-material patterns. An example is illustrated in Figure 5.6. The SPICE-generated features are the basis for orthogonal self-assembly (Figure 5.6a). A self-assembled monolayer could be deposited in sequence or in parallel to differentiate the substrate chemistries of the features and the underlying silicon substrate (Figure 5.6b). The substrate chemistries would then influence subsequently cast BP film self-assembly (Figure 5.6d).

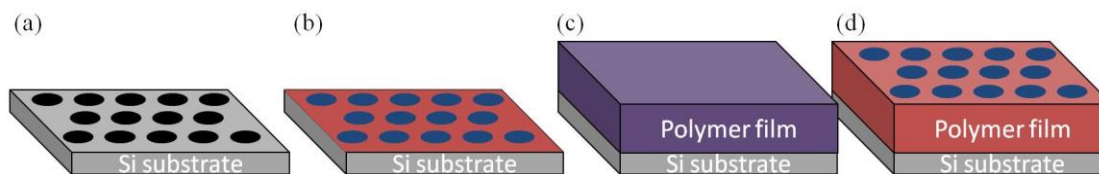


Figure 5.6: (a) SPICE-generated features are the basis for (b) an orthogonally self-assembled monolayer. (c) A subsequent BP film with similar domain sizes is cast on the modified substrate and (d) annealed to yield the substrate-propagated pattern through the film.

The advantage of this approach is that the original SPICE-based patterns could be propagated through numerous other BP systems. Pattern propagation is particularly relevant for systems that can be difficult to orient perpendicular to the substrate (*e.g.*, polystyrene-*b*-poly(dimethylsiloxane)). The disadvantage would be that pattern propagation would be limited to BPs with similarly sized domains. Further investigations would need to ascertain the tolerance window (*i.e.*, percentage difference in domain size and spacing) in which subsequently cast films could be influenced.

The first experiments should target thiol-silane monolayers on gold-silicon substrates. For example, *n*-hexanethiol and benzyldimethylchlorosilane could be used to influence a subsequently cast polyisoprene-*b*-polystyrene film. Phosphonic acid-silane analogues also could work for titania-silicon substrates. However, cross-contamination could occur because silanes also are used to modify metal oxide surfaces.<sup>86</sup> Therefore, sequential deposition of a phosphonic acid followed by a silane could help to maintain the spatial differentiation of substrate chemistries.

### 5.2.3 Pluronic™ Materials in SPICE

Pluronic block polymers from BASF are nonionic surfactants that are of the generic formula poly(ethylene oxide)-*b*-poly(propylene oxide)-*b*-poly(ethylene oxide). Pluronic polymers are available in varying compositions and molecular weights. Because they are inexpensive, nontoxic, and stable in laboratory conditions, Pluronics have found widespread adoption within the community of researchers that employ evaporation-induced self-assembly techniques to produce mesoporous inorganic materials.<sup>5,87,88</sup> Therefore, integrating Pluronic materials within the SPICE technique would be an economic way to achieve well-ordered arrays of nanodots. However, the immersion and metal-complexation steps would dissolve an ordered Pluronic film with the precursor solution. Whereas polystyrene, which was used in SPICE, was conveniently insoluble in the precursor solvents (*e.g.*, water, ethanol, or 2-propanol), Pluronic polymers are inconveniently soluble. To overcome this, a photo-induced crosslinking moiety could be incorporated at the hydroxyl termini of the Pluronic chains.<sup>89,90</sup> Therefore, one could feasibly achieve inexpensive templates by casting and annealing a Pluronic film, exposing the film to light, and continuing with the immersion, metal-complexation, and polymer etching.

### 5.2.4 Additional Catalytic Reactions

While the Au/TiO<sub>2</sub> samples in section 4.3 were effective at catalyzing the photodegradation of methylene blue, the ability to template numerous metal oxides opens the door to many other catalytic reactions. An immediate example is low-temperature CO-oxidation on the so-called Haruta catalyst (AuNP/TiO<sub>2</sub>).<sup>91</sup> The nanoscale array can be further tailored by incorporating multiple metal oxides. For

example, the following sample is of a ceria-zirconia array that was templated by the same process described in Section 4.2.2 (Figure 5.7).

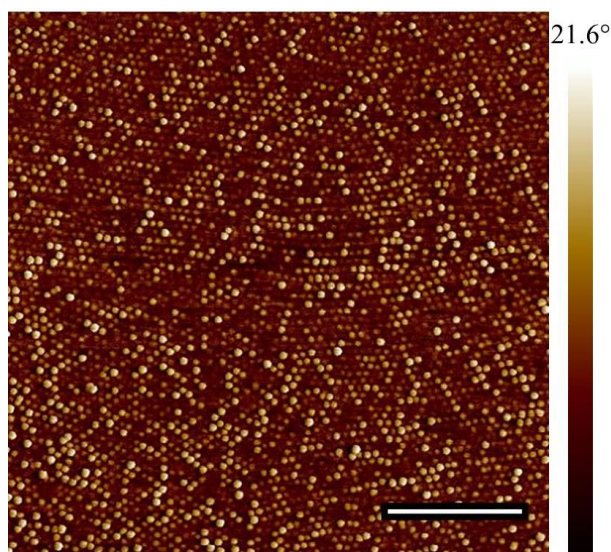


Figure 5.7: AFM phase image of a ceria-zirconia dot array made by the SPICE method. The scale bar represents 500 nm.

Ceria-zirconia is commonly used as a three-way catalyst in automotive exhaust: NO<sub>x</sub> reduction, CO oxidation, and hydrocarbon oxidation.<sup>92-95</sup> Low temperature CO-oxidation reactions over tin-manganese-cerium oxides also have received interest for applications in the automotive industry.<sup>96-98</sup> In fact, metal oxide combinations only are limited to their precursors' mutual solubility and ability to complex with the host polymer.<sup>33</sup> For example, vanadia arrays were unobtainable because the vanadium(IV) sulfate oxide hydrate precursor was soluble only in water; it was insoluble in methanol, ethanol, and 2-propanol, which were required in the SPICE method. In all cases, the ability to create well-ordered monodisperse oxides on flat substrates makes

the sample amenable to measurements using polarization-modulated infrared spectroscopy, which can be used to elucidate reaction pathways and mechanisms at relatively high pressures ( $> 10^{-3}$  torr).<sup>99</sup>

### **5.3 Conclusions**

Geometric control of templated inorganic materials is a limiting factor to the usefulness of nanometer-scaled patterns. The utilization of BPs represents a natural chemical progression towards smaller features. Future work should bolster the ability to manipulate the size, spacing, and composition of the employed composite templates and extend the usefulness of such templates in the aforementioned top-down and bottom-up schemes. The future studies proposed herein can be conducted in parallel. The easiest experiments that can be performed within the research groups are most likely the temperature-controlled ozone etching, pattern propagation using orthogonal self-assembly, and high-pressure CO oxidation studies on the Haruta catalyst.

### **5.4 Acknowledgements**

The author would like to acknowledge Sonia Eskandari for assistance with zinc oxide seed experiments, Dr. Cun Wen for assistance with the carbon nanotube growth experiments, and Professor Chuanbing Tang for use of the atomic force microscope.

## REFERENCES

1. Haryono, A.; Binder, W. H. *Small* **2006**, 2(5), 600-611.
2. Segalman, R. A. *Mater. Sci. Eng., R* **2005**, 48(6), 191-226.
3. Mayeda, M. K.; Kuan, W.-F.; Young, W.-S.; Lauterbach, J. A.; Epps III, T. H. *Chem. Mater.* **2012**, 24(14), 2627-2634.
4. Mayeda, M. K.; Hayat, J.; Epps, T. H.; Lauterbach, J. *J. Mater. Chem. A* **2015**.
5. Brinker, C. J. *MRS Bull.* **2004**, 29(9), 631-640.
6. Sun, Z. C.; Kim, D. H.; Wolkenhauer, M.; Bumbu, G. G.; Knoll, W.; Gutmann, J. S. *ChemPhysChem* **2006**, 7(2), 370-378.
7. Ortel, E.; Fischer, A.; Chuenchom, L.; Polte, J.; Emmerling, F.; Smarsly, B.; Kraehnert, R. *Small* **2012**, 8(2), 298-309.
8. Cheng, Y. J.; Gutmann, J. S. *J. Am. Chem. Soc.* **2006**, 128(14), 4658-4674.
9. Chang, S. W.; Chuang, V. P.; Boles, S. T.; Ross, C. A.; Thompson, C. V. *Adv. Funct. Mater.* **2009**, 19(15), 2495-2500.
10. Li, X. L. *Curr. Opin. Solid State Mat. Sci.* **2012**, 16(2), 71-81.
11. Narayanan, R.; El-Sayed, M. A. *J. Phys. Chem. B* **2005**, 109(26), 12663-12676.
12. Murray, C. B.; Kagan, C. R.; Bawendi, M. G. *Annu. Rev. Mater. Sci.* **2000**, 30, 545-610.
13. Homayoonfal, M.; Mehrnia, M. R.; Mojtahedi, Y. M.; Ismail, A. F. *Desalin. Water Treat.* **2013**, 51(16-18), 3295-3316.
14. Bell, A. T. *Science* **2003**, 299(5613), 1688-1691.
15. Huber, G. W.; Iborra, S.; Corma, A. *Chem. Rev.* **2006**, 106(9), 4044-4098.
16. Wicki, A.; Witzigmann, D.; Balasubramanian, V.; Huwyler, J. *J. Controlled Release* **2015**, 200, 138-157.
17. Chen, H. D.; Weiss, J. C.; Shahidi, F. *Food Technol* **2006**, 60(3), 30-36.

18. Weiss, J.; Takhistov, P.; McClements, D. J. *J. Food Sci.* **2006**, *71*(9), R107-R116.
19. Tao, A. R.; Habas, S.; Yang, P. D. *Small* **2008**, *4*(3), 310-325.
20. Melinon, P.; Begin-Colin, S.; Duvail, J. L.; Gauffre, F.; Boime, N. H.; Ledoux, G.; Plain, J.; Reiss, P.; Silly, F.; Warot-Fonrose, B. *Phys. Rep.-Rev. Sec. Phys. Lett.* **2014**, *543*(3), 163-197.
21. Toshima, N.; Yonezawa, T. *New J. Chem.* **1998**, *22*(11), 1179-1201.
22. Trindade, T.; O'Brien, P.; Pickett, N. L. *Chem. Mater.* **2001**, *13*(11), 3843-3858.
23. Grubbs, R. B. *Polym. Rev.* **2007**, *47*(2), 197-215.
24. Zhao, P. X.; Li, N.; Astruc, D. *Coord. Chem. Rev.* **2013**, *257*(3-4), 638-665.
25. Eckhardt, B.; Ortel, E.; Bernsmeier, D.; Polte, J.; Strasser, P.; Vainio, U.; Emmerling, F.; Kraehnert, R. *Chem. Mater.* **2013**, *25*(14), 2749-2758.
26. Gu, D.; Schuth, F. *Chem. Soc. Rev.* **2014**, *43*(1), 313-344.
27. Liu, Z. C.; Huang, H. Y.; He, T. B. *Small* **2013**, *9*(4), 505-510.
28. Zikalova, M.; Zikal, A.; Kavan, L.; Nazeeruddin, M. K.; Liska, P.; Gratzel, M. *Nano Lett.* **2005**, *5*(9), 1789-1792.
29. Cai, W. Q.; Yu, J. G.; Anand, C.; Vinu, A.; Jaroniec, M. *Chem. Mater.* **2011**, *23*(5), 1147-1157.
30. Jones, M. R.; Osberg, K. D.; Macfarlane, R. J.; Langille, M. R.; Mirkin, C. A. *Chem. Rev.* **2011**, *111*(6), 3736-3827.
31. Peng, J.; Li, X.; Kim, D. H.; Knoll, W. *Macromol. Rapid Commun.* **2007**, *28*(21), 2055-2061.
32. Bates, C. M.; Maher, M. J.; Janes, D. W.; Ellison, C. J.; Willson, C. G. *Macromolecules* **2014**, *47*(1), 2-12.
33. Lu, J. Q. *J. Phys. Chem. C* **2008**, *112*(28), 10344-10351.

34. Greene, L. E.; Law, M.; Tan, D. H.; Montano, M.; Goldberger, J.; Somorjai, G.; Yang, P. *Nano Lett.* **2005**, 5(7), 1231-1236.
35. Ghoshal, T.; Sentharamaikkannan, R.; Shaw, M. T.; Holmes, J. D.; Morris, M. A. *Adv. Mater.* **2014**, 26(8), 1207-1216.
36. Ghoshal, T.; Maity, T.; Sentharamaikkannan, R.; Shaw, M. T.; Carolan, P.; Holmes, J. D.; Roy, S.; Morris, M. A. *Sci. Rep.* **2013**, 3, 1-8.
37. Bang, B. M.; Kim, H.; Lee, J.-P.; Cho, J.; Park, S. *Energy Environ. Sci.* **2011**, 4(9), 3395-3399.
38. Huang, Z. P.; Geyer, N.; Werner, P.; de Boor, J.; Gosele, U. *Adv. Mater.* **2011**, 23(2), 285-308.
39. Dimova-Malinovska, D.; Sendova-Vassileva, M.; Tzenov, N.; Kamenova, M. *Thin Solid Films* **1997**, 297(1-2), 9-12.
40. Li, X.; Bohn, P. W. *Appl. Phys. Lett.* **2000**, 77(16), 2572-2574.
41. Kolasinski, K. W. *Curr. Opin. Solid State Mat. Sci.* **2005**, 9(1-2), 73-83.
42. Yae, S.; Kawamoto, Y.; Tanaka, H.; Fukumuro, N.; Matsuda, H. *Electrochem. Commun.* **2003**, 5(8), 632-636.
43. Koynov, S.; Brandt, M. S.; Stutzmann, M. *Appl. Phys. Lett.* **2006**, 88(20).
44. Branz, H. M.; Yost, V. E.; Ward, S.; Jones, K. M.; To, B.; Stradins, P. *Appl. Phys. Lett.* **2009**, 94(23), 231121.
45. Xiu, Y.; Zhu, L.; Hess, D. W.; Wong, C. P. *Nano Lett.* **2007**, 7(11), 3388-3393.
46. Huang, Z. P.; Zhang, X. X.; Reiche, M.; Liu, L. F.; Lee, W.; Shimizu, T.; Senz, S.; Gosele, U. *Nano Lett.* **2008**, 8(9), 3046-3051.
47. Tsujino, K.; Matsumura, M. *Adv. Mater.* **2005**, 17(8), 1045-1047.
48. Qu, Y. Q.; Liao, L.; Li, Y. J.; Zhang, H.; Huang, Y.; Duan, X. F. *Nano Lett.* **2009**, 9(12), 4539-4543.
49. Huang, Z. P.; Fang, H.; Zhu, J. *Adv. Mater.* **2007**, 19(5), 744-748.

50. Chartier, C.; Bastide, S.; Levy-Clement, C. *Electrochim. Acta* **2008**, *53*(17), 5509-5516.
51. Hadjersi, T.; Gabouze, N.; Kooij, E. S.; Zinine, A.; Ababou, A.; Chergui, W.; Cheraga, H.; Belhousse, S.; Djeghri, A. *Thin Solid Films* **2004**, *459*(1-2), 271-275.
52. Harada, Y.; Li, X. L.; Bohn, P. W.; Nuzzo, R. G. *J. Am. Chem. Soc.* **2001**, *123*(36), 8709-8717.
53. Hwang, T. Y.; An, G. H.; Lim, J. H.; Myung, N. V.; Choa, Y. H. *Jpn. J. Appl. Phys.* **2014**, *53*(5).
54. Lin, H.; Fang, M.; Cheung, H. Y.; Xiu, F.; Yip, S. P.; Wong, C. Y.; Ho, J. C. *RSC Adv.* **2014**, *4*(91), 50081-50085.
55. Yeom, J.; Ratchford, D.; Field, C. R.; Brintlinger, T. H.; Pehrsson, P. E. *Adv. Funct. Mater.* **2014**, *24*(1), 106-116.
56. Bechelany, M.; Berodier, E.; Maeder, X.; Schmitt, S.; Michler, J.; Philippe, L. *ACS Appl. Mater. Interfaces* **2011**, *3*(10), 3866-3873.
57. Wolfsteller, A.; Geyer, N.; Nguyen-Duc, T. K.; Das Anungo, P.; Zakharov, N. D.; Reiche, M.; Erfurth, W.; Blumtritt, H.; Werner, P.; Gosele, U. *Thin Solid Films* **2010**, *518*(9), 2555-2561.
58. Choi, W. K.; Liew, T. H.; Dawood, M. K.; Smith, H. I.; Thompson, C. V.; Hong, M. H. *Nano Lett.* **2008**, *8*(11), 3799-3802.
59. Shim, J.-H.; Lee, B.-J.; Cho, Y. W. *Surf. Sci.* **2002**, *512*(3), 262-268.
60. Maye, M. M.; Zheng, W.; Leibowitz, F. L.; Ly, N. K.; Zhong, C.-J. *Langmuir* **2000**, *16*(2), 490-497.
61. Tureau, M. S.; Kuan, W. F.; Rong, L. X.; Hsiao, B. S.; Epps, T. H. *Macromolecules* **2012**, *45*(11), 4599-4605.
62. Shan, L.; Punniyakoti, S.; Van Bael, M. J.; Temst, K.; Van Bael, M. K.; Ke, X.; Bals, S.; Van Tendeloo, G.; D'Olieslaeger, M.; Wagner, P.; Haenen, K.; Boyen, H.-G. *J. Mater. Chem. C* **2014**, *2*(4), 701-707.
63. Love, J. C.; Estroff, L. A.; Kriebel, J. K.; Nuzzo, R. G.; Whitesides, G. M. *Chem. Rev.* **2005**, *105*(4), 1103-1169.

64. Bockstaller, M. R.; Thomas, E. L. *Phys. Rev. Lett.* **2004**, *93*(16).
65. Xia, Y. N.; Xiong, Y. J.; Lim, B.; Skrabalak, S. E. *Angew. Chem.-Int. Edit.* **2009**, *48*(1), 60-103.
66. Niu, W. X.; Xu, G. B. *Nano Today* **2011**, *6*(3), 265-285.
67. Lohse, S. E.; Murphy, C. J. *Chem. Mater.* **2013**, *25*(8), 1250-1261.
68. Li, W. Z.; Xie, S. S.; Qian, L. X.; Chang, B. H.; Zou, B. S.; Zhou, W. Y.; Zhao, R. A.; Wang, G. *Science* **1996**, *274*(5293), 1701-1703.
69. Ren, Z. F.; Huang, Z. P.; Xu, J. W.; Wang, J. H.; Bush, P.; Siegal, M. P.; Provencio, P. N. *Science* **1998**, *282*(5391), 1105-1107.
70. Wang, X.; Summers, C. J.; Wang, Z. L. *Nano Lett.* **2004**, *4*(3), 423-426.
71. Joshi, R. K.; Schneider, J. J. *Chem. Soc. Rev.* **2012**, *41*(15), 5285-5312.
72. Sun, Y.; Fuge, G. M.; Fox, N. A.; Riley, D. J.; Ashfold, M. N. R. *Adv. Mater.* **2005**, *17*(20), 2477-2481.
73. Lu, J.; Yi, S. S.; Kopley, T.; Qian, C.; Liu, J.; Gulari, E. *J. Phys. Chem. B* **2006**, *110*(13), 6655-6660.
74. Takagi, D.; Homma, Y.; Hibino, H.; Suzuki, S.; Kobayashi, Y. *Nano Lett.* **2006**, *6*(12), 2642-2645.
75. Liu, Y.; Lor, C.; Fu, Q.; Pan, D.; Ding, L.; Liu, J.; Lu, J. *J. Phys. Chem. C* **2010**, *114*(13), 5767-5772.
76. Gonzalez-Valls, I.; Lira-Cantu, M. *Energy Environ. Sci.* **2009**, *2*(1), 19-34.
77. Cassell, A. M.; Franklin, N. R.; Tombler, T. W.; Chan, E. M.; Han, J.; Dai, H. *J. Am. Chem. Soc.* **1999**, *121*(34), 7975-7976.
78. Cheng, J. Y.; Ross, C. A.; Thomas, E. L.; Smith, H. I.; Vancso, G. J. *Adv. Mater.* **2003**, *15*(19), 1599-1602.
79. Xiao, S. G.; Yang, X. M.; Edwards, E. W.; La, Y. H.; Nealey, P. F. *Nanotechnology* **2005**, *16*(7), S324-S329.

80. Segalman, R. A.; Yokoyama, H.; Kramer, E. J. *Adv. Mater.* **2001**, *13*(15), 1152-1155.
81. Fitzgerald, T. G.; Borsetto, F.; O'Callaghan, J. M.; Kosmala, B.; Holmes, J. D.; Morris, M. A. *Soft Matter* **2007**, *3*(7), 916-921.
82. Bitá, I.; Yang, J. K. W.; Jung, Y. S.; Ross, C. A.; Thomas, E. L.; Berggren, K. K. *Science* **2008**, *321*(5891), 939-943.
83. Shabtai, K.; Rubinstein, I.; Cohen, S. R.; Cohen, H. *J. Am. Chem. Soc.* **2000**, *122*(20), 4959-4962.
84. Bauer, L. A.; Reich, D. H.; Meyer, G. J. *Langmuir* **2003**, *19*(17), 7043-7048.
85. Hickman, J. J.; Laibinis, P. E.; Auerbach, D. I.; Zou, C. F.; Gardner, T. J.; Whitesides, G. M.; Wrighton, M. S. *Langmuir* **1992**, *8*(2), 357-359.
86. Kailasam, K.; Natile, M. M.; Glisenti, A.; Muller, K. *J. Chromatogr. A* **2009**, *1216*(12), 2345-2354.
87. Mahoney, L.; Koodali, R. T. *Materials* **2014**, *7*(4), 2697-2746.
88. Soler-Illia, G.; Angelome, P. C.; Fuertes, M. C.; Grosso, D.; Boissiere, C. *Nanoscale* **2012**, *4*(8), 2549-2566.
89. Lee, S.-Y.; Tae, G. *J. Controlled Release* **2007**, *119*(3), 313-319.
90. Wu, C.-J.; Gaharwar, A. K.; Chan, B. K.; Schmidt, G. *Macromolecules* **2011**, *44*(20), 8215-8224.
91. Grunwaldt, J. D.; Baiker, A. *J. Phys. Chem. B* **1999**, *103*(6), 1002-1012.
92. Monte, R. D.; Kaspar, J. *J. Mater. Chem.* **2005**, *15*(6), 633-648.
93. Jen, H. W.; Graham, G. W.; Chun, W.; McCabe, R. W.; Cuif, J. P.; Deutsch, S. E.; Touret, O. *Catal. Today* **1999**, *50*(2), 309-328.
94. Gandhi, H. S.; Graham, G. W.; McCabe, R. W. *J. Catal.* **2003**, *216*(1-2), 433-442.
95. Kaspar, J.; Fornasiero, P.; Graziani, M. *Catal. Today* **1999**, *50*(2), 285-298.

96. Agüero, F. N.; Barbero, B. P.; Pereira, M. F. R.; Figueiredo, J. L.; Cadús, L. E. *Industrial & Engineering Chemistry Research* **2009**, *48*(6), 2795-2800.
97. Bedford, R. E.; LaBarge, W. J., Base metal automotive exhaust catalysts with improved activity and stability and method of making the catalysts. Google Patents: 1991.
98. Oh, S.-H.; Hoflund, G. B. *The Journal of Physical Chemistry A* **2006**, *110*(24), 7609-7613.
99. Bedenbaugh, J. E. Investigation of Catalytic Materials for Cracking of Military Aviation Fuel to Liquefied Petroleum Gas: High Throughput Experimentation. University of Delaware, Newark, 2012.

## Chapter 6

### OPTIMIZING A CATALYTIC FUEL CONVERTER

#### 6.1 Introduction

In the military battlefield, power is predominantly supplied by lithium ion batteries and jet fuel (JP-8).<sup>1</sup> The former is a mature technology that is convenient for portable applications such as communications, tracking, and illumination.<sup>2</sup> The latter is an energy dense kerosene-based fuel that is useful for high-power applications such as vehicles, generators, and heaters.<sup>3</sup> Because the military operates in desolate regions, soldiers and defense contractors necessarily spend more time away from stationary power sources. Therefore, portable devices require numerous replacement batteries to supply lengthy operations.<sup>4</sup> In fact, the Government Accountability Office estimated approximately \$2.1B was spent on power sources between 2006 and 2010; most of it was spent on batteries.<sup>5</sup> The added weight and heft of low energy density batteries is a hindrance for low-power mobile operations.<sup>6</sup> For example, battery-powered unmanned aerial vehicles (UAVs) can fly for only 1-2 h (*e.g.*, AeroVironment Raven or Lockheed Stalker). However, liquefied petroleum gas-powered fuel cells used in UAVs can provide longer operating times (up to 8 hours; Lockheed's Stalker XE). Energy dense fuel cells can reduce weight by a factor of ten (Table 6.1).<sup>7</sup> However, the high sulfur content and large average molecular mass of jet fuel precludes its use in fuel cells.<sup>8-10</sup> Furthermore, the single fuel forward policy precludes the distribution of non-JP-8 fuels into battle arena for the foreseeable future.<sup>11-13</sup> Therefore, a system that converted available JP-8 supplies into a suitable fuel, such as liquefied petroleum

gas (LPG), would enable longer missions and more mobile soldiers while circumventing the distribution limitation.<sup>14</sup>

Table 6.1. Approximate energy densities and power densities of battlefield power sources and civilian power sources for comparison.

<b>Power Source</b>	<b>Energy Density (W h kg<sup>-1</sup>)</b>	<b>Power Density (W kg<sup>-1</sup>)</b>
<b>Fuel cell</b>	200 <sup>15</sup>	10 <sup>15</sup>
<b>Li ion battery</b>	100 <sup>16,17</sup>	300 <sup>17</sup>
<b>Lead acid battery</b>	10 <sup>17</sup>	50 <sup>17</sup>

As was discussed in section 1.1.4, fuel reformation is typically accomplished using autothermal reformation (ATR), which is a mature reaction with an efficiency that is approximately 80% (energy basis).<sup>18,19</sup> Furthermore, ATR produces relatively high hydrogen concentrations using inexpensive catalysts like nickel and cerium oxides. Despite the benefits of ATR, its widespread adoption is prevented by problems with sulfur-induced catalyst poisoning, high temperature catalyst sintering, and coke formation.<sup>18,20</sup> For example, the average sulfur concentration in JP-8 is 714 ppm, but specifications allow up to 3,000 ppm.<sup>18</sup> Outside of the defense market, sulfur concentrations in diesel remain high in developing countries (Section 1.1.4.1, Figure 1.9).<sup>21</sup> For example, ultra-low sulfur diesel in the USA contains less than 15 ppm sulfur, but countries in sub-Saharan Africa and the Middle East allow over 5,000 ppm sulfur. Fuel sulfur strongly binds to active sites on catalyst surfaces, which decreases efficiency and reactor lifetime.<sup>22,23</sup> Also, high temperatures for ATR, above 750 °C, can lead to catalyst sintering.<sup>24</sup> Sintering decreases catalytic efficiency by decreasing the active surface area and loss of active catalyst surface sites.<sup>20,24</sup> Finally, aromatic

and olefin compounds within JP-8 contribute to catalyst deactivation *via* coke formation.<sup>25</sup> Catalyst deactivation by sulfur poisoning, sintering, and coke formation remain nontrivial obstacles to effective fuel reforming.<sup>18</sup>

The patent-pending fuel cracking technology, which was developed at the University of South Carolina, uses a novel catalyst to crack JP-8 down to a LPG mixture of hydrocarbons.<sup>14</sup> Catalytic cracking of diesel, gasoline and kerosene can be accomplished by the same approach. JP-8, diesel, gasoline, and kerosene all contain approximately equivalent paraffin concentrations, which is important because paraffins are the parent molecules for most of the LPG product yield.<sup>26</sup> The fuels differ in their concentrations of aromatic and sulfurous species concentrations; in countries outside of the Organization for Economic Co-operation and Development, diesel can contain upwards of 5,000 ppm of sulfur and 35% aromatics.<sup>21</sup> These differences will yield various coking and poisoning rates and change the optimal catalyst composition for low-temperature regeneration cycles. A previously developed zeolite-based catalyst was sulfur tolerant, active at low temperatures, and easily regenerated from coking.<sup>14</sup> Additionally, the LPG product was sulfur-free (< 10 ppm) and suitable for use in solid oxide fuel cells or commercial gas appliances. However, the catalyst is not a drop-in solution; the catalyst requires a comprehensive system that includes balance of plant components.

### **6.1.1 Past Project Objectives and Solutions**

The original project, which was funded by the Defense Advance Research Project Agency (DARPA), successfully demonstrated the conversion of JP-8 into C<sub>2</sub>-C<sub>4</sub> hydrocarbons (*i.e.*, ethane, ethylene, propane, propylene, etc.) *via* a heterogeneous catalytic cracking reaction.<sup>14</sup> Qualitative and quantitative goals were stipulated by

DARPA. Qualitative goals included minimizing reactant fuel pre-processing and maximizing safety and durability. The quantitative goals were previously discussed in detail but are briefly summarized in Table 6.2.<sup>26</sup> Previous work was focused on catalyst discovery and optimizing reaction conditions.<sup>14</sup> The first three objectives revolved around catalyst formulation and reaction conditions while the last objective sought to optimize the balance of plant.<sup>26</sup>

Table 6.2. Summary of quantitative objectives for converting JP-8 to C<sub>2</sub>-C<sub>4</sub> hydrocarbons. Adapted with permission from Bedenbaugh, J.E. Ph.D. Dissertation, University of Delaware, Newark, 2012.

Figure of Merit	Minimum	Ideal
Conversion (wt%)	> 5	> 30
Product sulfur content (ppm)	< 50	< 10
C <sub>2</sub> -C <sub>4</sub> production rate (kg/h)	> 0.2	> 10
Size (m <sup>3</sup> )	< 2	< 0.2

The project successfully demonstrated catalytic cracking of sulfur-containing JP-8 into a mixture of C<sub>2</sub>-C<sub>4</sub> hydrocarbons.<sup>14</sup> The process (Figure 6.1) employed a packed bed single reactor filled with a platinum- and gadolinium-decorated ZSM-5 zeolite catalyst.

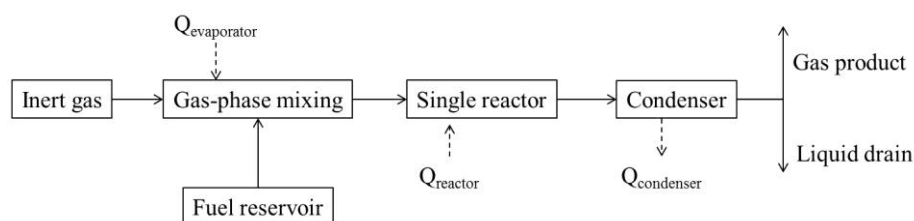


Figure 6.1: Flow diagram of jet fuel conversion system. An inert gas used to push the evaporated reactant fuel through a single reactor. Reaction products were separated from the unreacted fuel *via* condensation. The liquid product was discarded while the gaseous product was analyzed for purity.

Initial conversion efficiencies peaked at 20 wt%, which surpassed the minimum goal and approached the ideal goal (see Appendix C, Figure C.1).<sup>26</sup> In addition to being tolerant to fuel sulfur, the sulfur content of the product gas was below the detection limit (10 ppm) of the gas chromatography mass spectrometry (GC-MS) that was used; the cracking process was both a fuel converter and a sulfur removal tool. No further characterization of the sulfur content was performed because industry advisors recommended that 10 ppm was tolerable in commercially available solid oxide fuel cells.<sup>27,28</sup> The production rate hovered near 0.3 g/h, which was three orders of magnitude below the minimum goal. Finally, the overall size of the entire process was difficult to assess because characterization instrumentation, along with associated plumbing, power supplies, and controls, was embedded alongside the essential components. However, the essential components were approximately within the minimum size goal. Fundamental science research accomplished the objectives, but the current and future goals aim to transfer the technology from the laboratory into the field.

### **6.1.2 Current Project Objectives**

Given the promising catalyst discovery, current and future project objectives sought to facilitate scale up, technology transfer, and commercialization. While the catalytic reaction was proven within laboratory settings, a realistic device would need to be field-deployable, portable, and inexpensive. Therefore, the team outlined the following objectives: (1) maximize fuel conversion (2) streamline device design, and (3) minimize device cost.

Using a single reactor system, maximum fuel conversions hovered near 20 wt% (Appendix, Figure C.1).<sup>26</sup> While 20 wt% conversions topped the minimum goal

(Table 6.2), greater fuel utilizations would be required to provide fuel cells and commercial gas appliances enough competitive advantage against a combustion generator, which is the incumbent in-field power supply unit.<sup>15</sup> If the generator and solid oxide fuel cell are assumed to operate near 15% and 40% efficiency, respectively, fuel converters would need to surpass 37.5% to give the fuel cell the energetic advantage over an internal combustion generator. Therefore, 37.5% was used as a benchmark for the fuel conversion objective.

In its nascent stages, device design primarily referred to the balance of plant components and not to the physical appearance or component layout. Progress on streamlining the device design was made by focusing on the inert gas carrier system. Helium was used to push the reactant and product fuel through the system. The use of helium in the field would require an on-board tank that would be consumed and require periodic replacement. Another option was to switch to a commercially available air separator that would provide nitrogen as the system carrier gas. However, the additional bulk, complexity, parasitic energy losses, and safety concerns prohibited the inclusion of such a unit. Therefore, the team explored the possibility of entirely eliminating the carrier gas system by using the pressure of the superheated gaseous reactant to push through the catalyst bed. The lack of an inert gas would significantly streamline the device design by eliminating a carrier gas system and its associated tank, pump, regulator, and valves.

The components used to demonstrate the catalytic cracking were research-grade instruments with superfluous features, performance standards, and bulk. For example, a recirculating chiller was used to maintain the condenser temperature. Such a heavy piece of equipment added significant cost, size, complexity, and parasitic

losses. Similar over-performing components were used for the reactor furnace and liquid pump. Therefore, it was necessary to reconstruct the catalytic cracking process using commercially available components that could facilitate a realistic lab-to-field transition. Furthermore, such substitutions aimed to improve device performance or have minimal negative impacts. Efforts towards (1) maximizing fuel conversion, (2) streamlining the device design, and (3) minimizing device cost facilitated the lab-to-field transition of the proven catalytic fuel conversion process.

## 6.2 Experimental Section

JP-8 (~350 ppmw sulfur) was supplied by the U.S. military. **Care should be taken when handling JP-8 due to its flammability and toxicity.**<sup>29</sup> JP-8 should be handled away from ignition sources and oxidizers. In the following experiments, JP-8 was heated to well above its flash point ( $\approx 40$  °C) and even above its autoignition temperature ( $\approx 210$  °C).<sup>29</sup> Care was taken to minimize air leaks into the reaction tubing by using stainless steel tubing and compression fittings. A flashback arrestor (Concoa, 532 7005) was inserted between the fuel reservoir and the gas mixer (Figure 6.1) to prevent explosions. Solenoid valves (DudaDiesel, 2WJ04008N) isolated the reactor tubes in the event of a power interruption. In addition to flammability concerns, JP-8 contains known volatile carcinogenic components that can be inhaled and can subsequently affect balance and lung health.<sup>30-32</sup> **While dermal exposure was estimated to be relatively innocuous,<sup>33</sup> personal protective equipment should be worn at all times while working with JP-8.**

Fuel conversion reactions utilized a ZSM-5 catalyst that was augmented with platinum and gadolinium as was previously described in the literature.<sup>14</sup> Reactions were carried out at 450 °C and atmospheric pressure with a weight-hourly space

velocity of  $10 \text{ h}^{-1}$ . JP-8 was evaporated and passed over a fixed catalyst bed (350-500 °C); 150 mg of catalyst was loaded into a 0.5-in quartz tube reactor. The effluent gas flowed through a condenser and the remaining gaseous product was analyzed by GC-MS. Liquid samples labeled “condensed” were collected from the condenser after a single pass through the reformer. Liquid samples labeled “recycled” were collected from the condenser after implementing a recycle system with a constant volumetric ratio of fresh JP-8 and recycled liquid; reactions with fresh JP-8 were allowed to run for 30 min to accumulate enough condensed liquid for recycling. In all cases, the catalyst was regenerated using ambient air while holding the reactor temperature constant for 1 h. Regenerations were performed every 10 h.

Gaseous products downstream of the condenser were characterized by a Shimadzu QP2010 Plus GC-MS equipped with a HaySep-D capillary column (0.53 mm ID  $\times$  30 m, Agilent), which was calibrated using gas standards. Helium was injected in the effluent gas, after the reactor and condenser, to carry the product through the GC-MS.

Condensed and recycled liquids were characterized by GC-MS and nuclear magnetic resonance spectroscopy ( $^1\text{H}$  NMR).  $^1\text{H}$  NMR measurements were taken with a Bruker Avance III HD 300 using deuterated chloroform (7.26 ppm reference).

The gaseous product was tested in a commercially available solid oxide fuel cell for technology validation. Gas product was pumped (Hargraves H125B-13) into a liquid nitrogen-cooled lecture bottle (440 mL, Sigma Aldrich). The resulting product was tested in a P250i Power System (Ultra Electronics - AMI; Ann Arbor, MI), which was designed to consume commercial propane. Internal reforming took place within the fuel cell, converting the propane into readily usable hydrogen and carbon

monoxide. The fuel-to-electricity process occurred with a 31% gross efficiency (LHV, propane) under maximum fuel utilization conditions with commercial grade propane.<sup>34</sup> The LPG was connected in parallel with commercial propane to allow simple fuel gas switching during the test.

### **6.3 Results and Construction**

When designing a fuel converter, the conversion efficiency is one of its most important figures of merit. Previous work from our group consistently yielded maximum instantaneous conversions near 20 wt% over multiple catalyst regeneration cycles (see Appendix C, Figure C.1).<sup>26</sup> Although the conversion approached the ideal goal (Table 6.2), even higher conversions were expected because (1) it was previously known that paraffins were the primary source of LPG whereas aromatics and olefins contributed to catalyst coking<sup>20,35</sup> and (2) JP-8 is composed of approximately 70 vol% paraffins and only 20 vol% aromatics.<sup>18,36</sup> Therefore, it was hypothesized that higher yields could be achieved by recycling the condensed liquid through the converter for multiple passes (Figure 6.2). A 50:50 (fresh JP-8:condensed liquid) ratio was used during recycling experiments such that flow through the reactor remained constant as compared to a single-pass orientation.

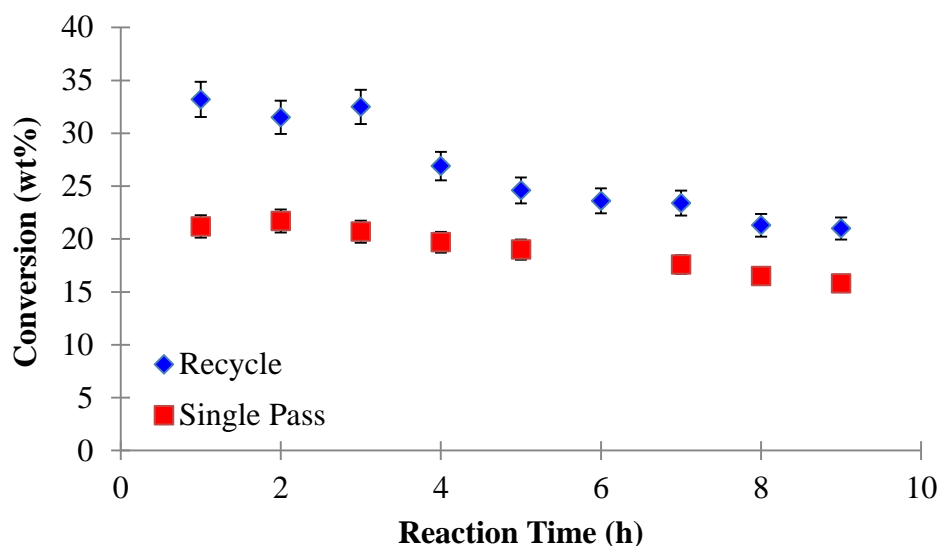


Figure 6.2: Fuel conversion efficiency as a function of time using a single-pass and a recycling approach. Reactions were performed at 450 °C using a 0.3 mL/h total liquid flowrate (*i.e.*, 0.15 mL<sub>JP-8</sub>/h and 0.15 mL<sub>condensed</sub>/h for recycling or 0.3 mL<sub>JP-8</sub>/h for single-pass). The author would like to acknowledge Dr. Sungtak Kim for performing the conversion experiments.

Indeed, recycling increased the time-averaged efficiency from 19.2 wt% to 27.1 wt% over the nine-hour period tested. The deactivation rates, which were approximated by the slope of the data, for recycling and single-pass were -1.7 and -0.7 percentage points per hour, respectively. The condensed liquid became noticeably darker yellow as the recycling continued (see Appendix C, Figure C.2). Such a discoloration suggested a gradual chemical composition change over time.

<sup>1</sup>H NMR was used to characterize the quality of the JP-8 before and after cracking and during recycle experiments (Figure 6.3). Integrated peak areas for <sup>1</sup>H NMR spectra are in Table 6.3.

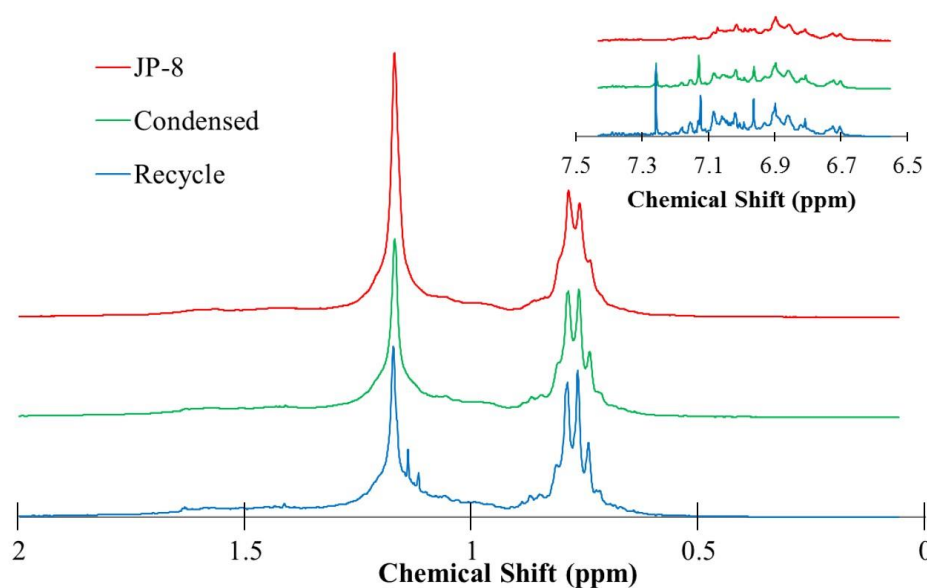


Figure 6.3:  $^1\text{H}$  NMR spectra of fresh JP-8, post-reaction condensed liquid, and post-recycle reaction condensed liquid. Spectra were normalized to the methyl proton peak near 0.75 ppm. The inset image shows a magnified view of the aromatic region (6.5 – 7.5 ppm). All spectra were vertically offset for comparison purposes. Intensity was measured in arbitrary units. The peak near 7.26 ppm is from the deuterated chloroform used in the measurement.

Table 6.3: Normalized integrated peak areas from  $^1\text{H}$  NMR spectra in Figure 6.3. Peak areas were normalized to the methyl proton peak near 0.75 ppm.

Peak	JP-8	Condensed liquid	Recycled liquid
<b>Methyl</b>	1.00	1.00	1.00
<b>Aliphatic</b>	1.43	1.21	1.16
<b>Aromatic</b>	0.09	0.10	0.12

For comparison purposes,  $^1\text{H}$  NMR spectra were normalized to the methyl proton peaks near 0.75 ppm. The peak near 1.2 ppm was attributed to aliphatic protons while peaks between 6.6 - 7.2 ppm represented aromatic compounds.<sup>37,38</sup> Fresh JP-8 exhibited a large aliphatic peak due to the large amount of paraffins. Qualitatively, the three spectra exhibit similar peak positions and peak shapes; overlaid spectra can be

seen in the Appendix (Figure C.3). Condensed- and after-recycling liquids exhibited aliphatic peak areas that decreased by 15% and 19%, respectively, compared to JP-8. The decrease in the aliphatic peak area compared to the methyl peak area suggested a decrease in the average carbon number after catalytic cracking.<sup>39</sup> On the other hand, peak areas associated with aromatic compounds increased by 11% and 33%, respectively. Without an internal standard, the changes in peak areas could be attributed to (1) an increased in aromatic hydrocarbon content and/or (2) a decrease in linear hydrocarbon content. Therefore, GC-MS measurements were used to augment the <sup>1</sup>H NMR results (Figure 6.4).

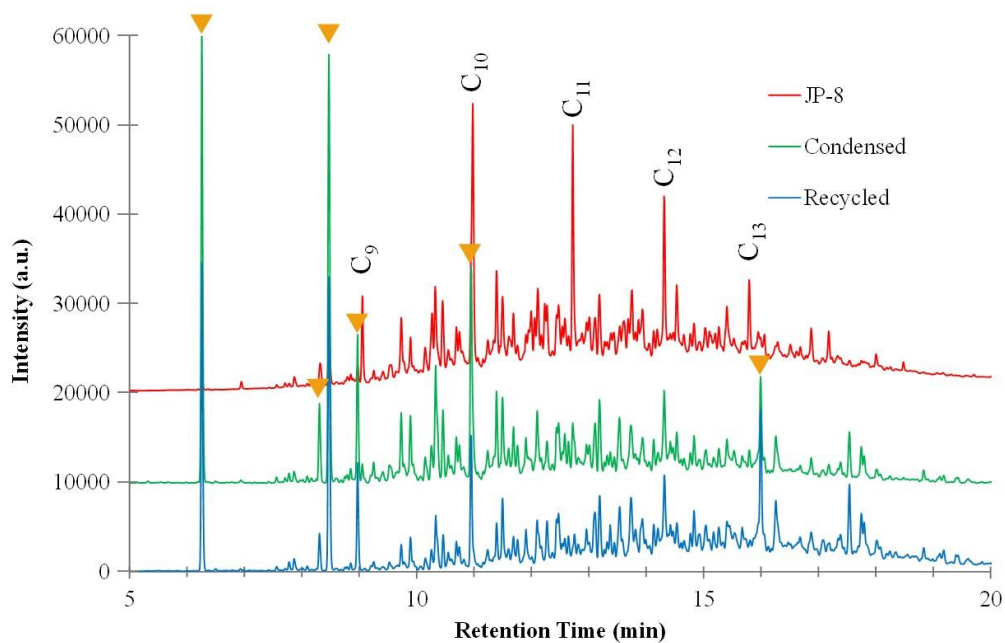


Figure 6.4: GC data of JP-8, condensed liquid after cracking JP-8, and condensed liquid after implementing a recycle loop while cracking JP-8. Spectra were vertically offset. Toluene and C<sub>9</sub>-C<sub>13</sub> *n*-paraffins are labeled; ▼ symbols mark aromatic hydrocarbons in the condensed and recycled liquid that are distinguishable from nearby linear hydrocarbons in JP-8.

GC-MS spectra show a dramatic decrease in *n*-paraffin components (*i.e.*, nonane, decane, undecane, dodecane, and tridecane) when comparing JP-8 (red trace) with the condensed liquid byproduct (green trace). Calibration curves (not shown) indicated that the JP-8 contained 20 wt% C<sub>9</sub>-C<sub>13</sub> *n*-paraffin compounds. From low retention times to high retention times in Figure 6.4, the ▼ symbols mark toluene ( $\approx$ 6:15), xylenes (8:00-9:00, three isomers), ethylbenzene ( $\approx$ 11:00), and polycyclic aromatics ( $\approx$ 16:00). Therefore, the condensed liquid and recycled liquid spectra exhibit significant increases for aromatic compounds. GC-MS spectra corroborate <sup>1</sup>H NMR spectra and indicate that aliphatic compounds were consumed and aromatic compounds were produced when JP-8 was recycled through the catalytic cracking reaction.

While previous experiments employed helium (120 standard cm<sup>3</sup>/min) to carry the reactant through the packed bed reactor (10 h<sup>-1</sup> weight hourly space velocity), helium is not readily available in most field environments. A fuel converter could feasibly utilize an air separator to supply nitrogen; but the added size, weight, and cost (both energetically and financially) would burden the system. Therefore, the system was tested without using any carrier gas in a single-pass fashion (Figure 6.5).

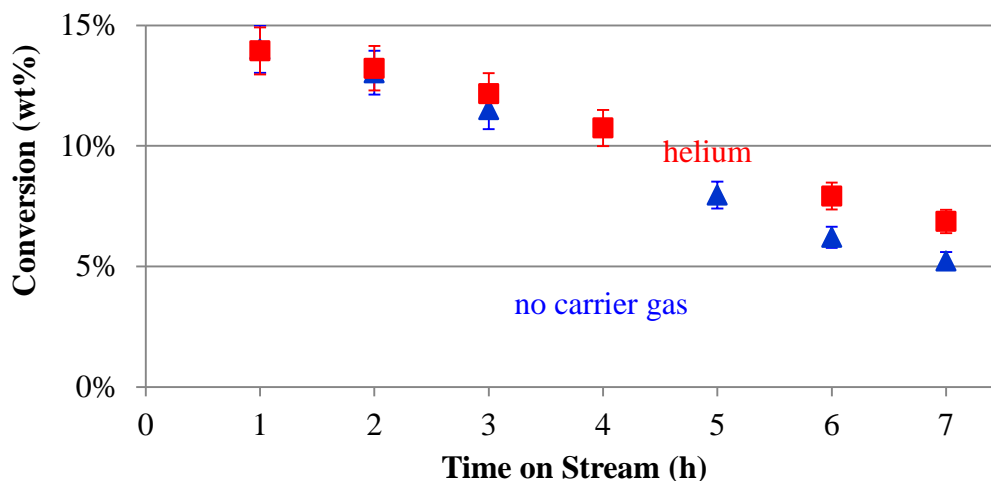


Figure 6.5: Fuel conversion efficiency with and without the carrier gas (helium). The author would like to acknowledge Dr. Sungtak Kim for performing the conversion experiments.

Conversions without carrier gas exhibited a 24% faster deactivation profile, which was possibly caused by increased coking due to an increase in residence time. The time-averaged conversions with and without helium were 11.1 wt% and 10.3 wt%, respectively.

One of the envisioned uses for a fuel converter was to be a fuel preprocessor for military solid oxide fuel cells.<sup>40</sup> To this end, the gaseous product was compressed into a lecture bottle and tested in an Ultra Electronics-AMI P250i solid oxide fuel cell system. While the P250i was designed to operate with commercial grade propane, the gaseous product was tested without any alterations to the solid oxide fuel cell system. Current-voltage curves from the P250i are shown in Figure 6.6.

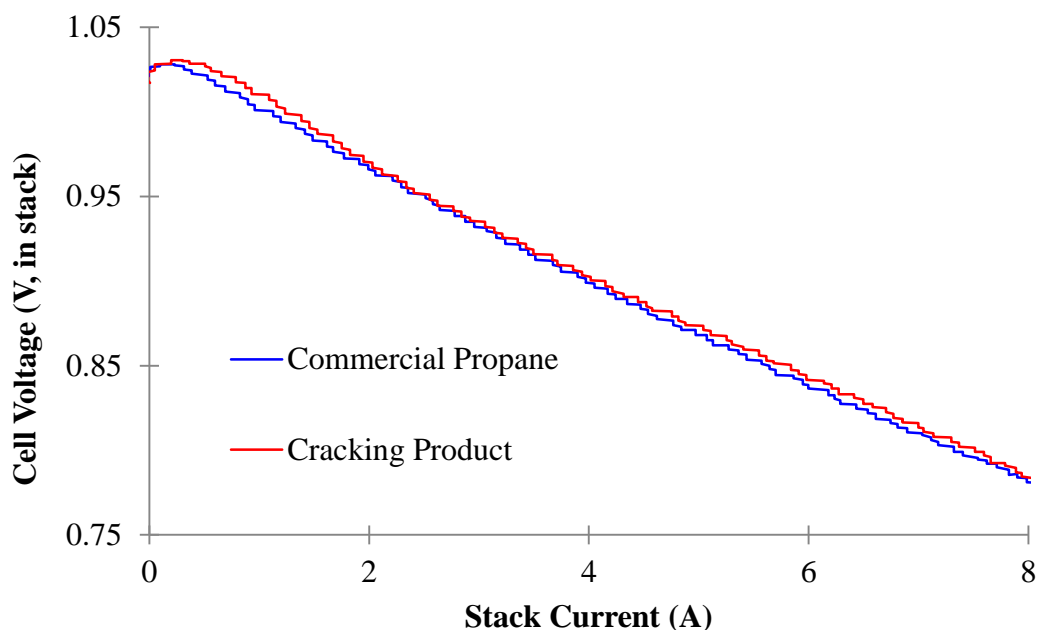


Figure 6.6: Current-voltage curves for the P250i solid oxide fuel cell stack performance on commercial propane and the gas product from gasoline conversion. The author would like to acknowledge Dr. Tom Westrich for performing the conversion experiments.

Differences between the two curves were small, which indicated that the cracking product was suitable for use in the solid oxide fuel cell. For the gaseous product curve, the slight increase in cell voltage was attributed to a small fraction of hydrogen that was present. The tests confirmed that the gaseous product could be used as a direct substitute to commercial propane in commercially available solid oxide fuel cells.

#### 6.4 Discussion

The catalytic cracking reaction converts JP-8 into a LPG-like gas mixture and a condensable organic liquid. Fuel reformation is a complicated reaction owing to the numerous different hydrocarbons present in the mixture.<sup>18</sup> Previous attempts to

optimize catalyst composition and reaction conditions yielded maximum weight conversions near 20%.<sup>26</sup> During previous investigations, no attention was given to the condensable organic liquid, which was discarded as waste (Figure 6.1). However, the results from recycling the byproduct organic liquid (Figure 6.2) clearly showed that more LPG product could be extracted from the condensed liquid. Higher conversions came at the expense of catalyst lifetime and production rate. The increased conversion efficiency was partially due to increased mixing between reactant and catalyst (*i.e.*, unreacted hydrocarbons can be recycled back through the reactor for more cracking). In a separate group of experiments, a decrease in the space velocity exhibited only incremental increases in time-averaged conversion efficiencies.<sup>41</sup> However, decreasing the space velocity also led to LPG production rates that were too low (< 300 g/h) for field deployment; a multitude of parallel reactors would be required to supply a 250-watt fuel cell.

<sup>1</sup>H NMR was used to qualitatively compare the composition of JP-8, condensed liquid (single-pass products), and recycled liquid (recycling products). The three spectra (Figure 6.3) exhibited a decrease in aliphatic chain lengths and increasing aromatic content relative to aliphatic content. The peak area ratios of aliphatic to methyl protons gradually decreased between JP-8 (1.43:1) to condensed liquid (1.21:1) to recycled liquid (1.16:1), which suggested that the hydrocarbon chain lengths were decreasing. Also, the peak area ratios of aromatic protons to aliphatic protons gradually increased between JP-8 (0.09:1) to condensed liquid (0.10:1) to recycled liquid (0.12:1), which suggested the aromatization of linear hydrocarbons. The trends were expected from previous investigations, which demonstrated that cracking, hydrogen transfer, and aromatization are all competing reactions.<sup>38,42,43</sup>

Therefore, recycled fuel proved to contain sufficient levels of aliphatic hydrocarbons that were cracked to produce additional LPG.

GC spectra (Figure 6.4) indicated that liquid byproducts exhibited a general decrease in paraffins, total consumption of *n*-paraffins, and an increase in aromatic hydrocarbons.<sup>37</sup> The *n*-paraffin compounds, which were approximately 20% of the JP-8 feed, were the main LPG precursors.<sup>41,44</sup> Indeed, *n*-paraffins were wholly consumed after a single pass (10 h<sup>-1</sup> WHSV) through the catalyst bed (Figure 6.4, green). <sup>1</sup>H NMR data showed an aliphatic peak area decrease of only 15% (Figure 6.3, green). However, due to the complexity of the solution, the ratio of paraffins to olefins could be easily ascertained. An improvement to 27.1% efficiency was obtained by recycling. The gain in conversion efficiency was achieved despite a dramatic decrease in *n*-paraffin (C<sub>9</sub>-C<sub>13</sub>) compounds after only one cracking pass (Figure 6.4, green), which further suggested the reusability of the organic liquid byproduct. The similarities in GC-MS spectra and <sup>1</sup>H NMR for condensed and recycled samples belied the increase in catalytic activity achieved by recycling. Therefore, in addition to *n*-paraffins, other hydrocarbon olefins and isoparaffins also must contribute to the LPG production.

When compared to commercially available propane fed into a solid oxide fuel cell, the LPG produced slightly higher voltages (Figure 6.6). The increase in open circuit voltage was attributed to a small amount of hydrogen in the LPG product as determined by gas chromatography measurements taken at Ultra Electronics.<sup>27,45</sup> The Shimadzu QP2010 GC-MS used within our labs was not sensitive to hydrogen; the amount of hydrogen in the gaseous product was below the quantifiable limits (but above the detection limit) of the gas chromatography instrument at Ultra Electronics. Most importantly, operating the P250i on the LPG product confirmed the absence of

sulfur-containing species, which would irreversibly poison the solid oxide fuel cell and result in lower voltages. Ultimately, the LPG product was proven to be an apt substitute for commercial grade propane.

One of the most important aspects of our fuel reformation technology was its sulfur tolerance.<sup>8,36,46</sup> Despite 556 ppm sulfur in the tested batch of JP-8, no sulfur was detected (LDL = 10 ppm) in the LPG product. In one test, a surrogate JP-8 was doped with 5,000 ppm dibenzothiophene; similar product distributions and activities and sulfur-free LPG were observed.<sup>41</sup> Although not proven, the sulfur likely remained bound to aromatic species in the condensed liquid phase. Because sulfur primarily exists as aromatic thiophenes (*e.g.* benzothiophene, dibenzothiophene, etc.),<sup>8</sup> which are inert over our catalyst, our catalyst remained unperturbed by sulfur content.<sup>47</sup> Low sulfur concentration was particularly important for solid oxide fuel cells,<sup>46</sup> because the nickel catalysts in SOFCs are poisoned by high sulfur concentrations (> 50 ppm).<sup>22,23</sup> Undetectable sulfur concentrations in the product LPG made the reformation technology suitable for use with a SOFC system.

## **6.5 Device Construction and Operation**

The absence of a carrier gas caused a slight decrease in conversion efficiency and a recycle loop caused an increase in conversion efficiency; together, the two modifications had a net-positive effect on the conversion efficiency. A proof-of-concept device was constructed that eliminated the use of a carrier gas and included a recycle loop. 80/20® aluminum 1” extrusions were used to create a rectangular frame (2’ x 2’ x 2.5’). Transparent impact-resistant polycarbonate panels were attached to the outsides of the frame. High density polyethylene bottles (Nalgene) were used as reservoirs for fresh fuel and condensed liquid. A peristaltic pump head and tubing

(Masterflex 7013-20 and 06401-13) were driven by a brushless stepper motor (Applied Motion, HT23-396). The stepper motor was controlled by an Applied Motion 1240i printed-circuit board. Fuel was fed to the custom-built evaporator (silica bead-packed 1-inch-diameter 314 stainless steel tube). The evaporator temperature was controlled with heating tape and a temperature controller (Omega CN76000). From the evaporator, reactant flow was split into two separate packed-bed quartz tube reactors, both of which were isolated with normally-closed solenoid valves (DudaDiesel, 2WJ04008N). Reactors were heated with tube furnaces (Omega CRFC-1256) and a temperature controller (Omega CSC32). Gaseous products passed through two aluminum cold plates in series (McMaster-Carr) that were lined with a total of four 2.5 W Peltier coolers and fans. Condensed liquid was fed back to the aforementioned polyethylene fuel reservoirs while gaseous products were collected in Kynar® gas sampling bags for later analysis or compression and storage.

## **6.6 Conclusions**

A fuel reformation unit was developed that accepts sulfurized JP-8 and produces desulfurized LPG. The catalyst was sulfur tolerant, active at low temperatures, and easy to regenerate. A reformation efficiency of 20% was achieved and recycling improved the instantaneous efficiency up to 35%. It was anticipated that further adjustments to the recycling system could improve the reformation efficiency to 45-50%. It was determined that LPG was primarily produced from linear paraffins while aromatics passed inertly over the catalyst or contributed to coking. The catalyst was regenerated by oxidizing the coke in ambient air. LPG product distributions remained self-consistent after regeneration steps.

The overarching goal for optimizing the catalytic fuel converter was to push the technology closer towards commercialization. To this end, the first objective of increasing the fuel conversion efficiency helped to minimize the amount of liquid byproduct. However, future work should assess the practical value of the hydrocarbon liquid byproduct. For example, it may be usable in an engine as a JP-8 blend. Although the goal of a time-averaged efficiency of 37% was not achieved, the author suspects that alterations to the recycling ratio could achieve the desired conversion efficiency.

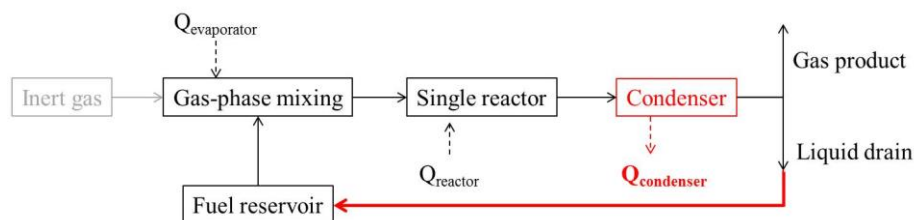


Figure 6.7: Current block diagram of the prototype fuel converter. Significant changes include the absence of a carrier gas, low-power condenser system, and a recirculating reactant feed.

Improvements made to the overall catalytic fuel cracking process has largely simplified and improved the balance of plant. Changes were engineering in nature; they did not alter the catalyst or reaction conditions. The components that were implemented in the prototype design were commercially available. Furthermore, ongoing work indicated that all of the components could be replaced with military-purposed analogues.

While additional engineering improvements are necessary before field testing can begin, it is important to maintain clarity on the end goal: commercialization.

Therefore, a market assessment with preliminary customer discovery is warranted prior to further expenditure of time and resources. Chapter 7 discusses envisioned market opportunities and potential-customer feedback that may guide the future development of the fuel converter.

## **6.7 Acknowledgements**

The author kindly acknowledges Dr. Jochen Lauterbach, Dr. Erdem Sasmaz, and Dr. Sungtak Kim for assistance with constructing and testing the apparatus. Also, the author acknowledges Dr. Tom Westrich (Ultra Electronics) for performing experiments with the solid oxide fuel cell. Finally, the author acknowledges the Columbia Fuel Cell Challenge for funding and support.

## REFERENCES

1. National Research, C., *Reducing the Logistics Burden for the Army After Next : Doing More with Less*. National Academy Press: Washington, D.C., 1999.
2. Rominiecki, A. [www.army.mil](http://www.army.mil): The Official Homepage of the United States Army.  
[http://www.army.mil/article/103583/Researchers\\_bring\\_standard\\_Army\\_battery\\_charger\\_into\\_the\\_21st\\_century\\_refine\\_conformal\\_battery/](http://www.army.mil/article/103583/Researchers_bring_standard_Army_battery_charger_into_the_21st_century_refine_conformal_battery/) (accessed October 12, 2014).
3. Korres, D. M.; Karonis, D.; Lois, E.; Linck, M. B.; Gupta, A. K. *Fuel* **2008**, 87(1), 70-78.
4. Szondy, D. US Army's new portable charger brings power to soldiers in the field. <http://www.gizmag.com/universal-battery-charger-us-army/27665/> (October 12, 2014).
5. Erwin, S. I. Army, Marines Face Uphill Battle To Lighten Troops' Battery Load.  
<http://www.nationaldefensemagazine.org/archive/2011/May/Pages/ArmyMarinesFaceUphillBattleToLightenTroops%E2%80%99BatteryLoad.aspx> (May 2012).
6. Thampan, T.; Shah, D.; Cook, C.; Novoa, J.; Shah, S. *J. Power Sources* **2014**, 259, 276-281.
7. Winter, M.; Brodd, R. J. *Chem. Rev.* **2004**, 104(10), 4245-4269.
8. Lee, I. C.; Ubanyionwu, H. C. *Fuel* **2008**, 87(3), 312-318.
9. Song, C. S. *Catal. Today* **2003**, 86(1-4), 211-263.
10. Song, C. S. *Catal. Today* **2002**, 77(1-2), 17-49.
11. Le Pera, M. E. *Army Logistician* **2005**, 37(2), 40-43.
12. Garrett, R. K., *Is a Single Fuel on the Battlefield Still a Viable Option?* ICAF-FAP: Fort McNair, 1993.
13. Weir, D. G., *Strategic Implications For A Single-Fuel Concept*. US Army War College: Carlisle Barracks, 1996.

14. Bedenbaugh, J. E.; Kim, S.; Sasmaz, E.; Lauterbach, J. *ACS Comb. Sci.* **2013**, *15*(9), 491-497.
15. Patil, A. S.; Dubois, T. G.; Sifer, N.; Bostic, E.; Gardner, K.; Quah, M.; Bolton, C. *J. Power Sources* **2004**, *136*(2), 220-225.
16. Abraham, K. M. *Electrochim. Acta* **1993**, *38*(9), 1233-1248.
17. Braun, P. V.; Cho, J.; Pikul, J. H.; King, W. P.; Zhang, H. *COSSMS Current Opinion in Solid State & Materials Science* **2012**, *16*(4), 186-198.
18. Xu, X. H.; Li, P. W.; Shen, Y. S. *Appl. Energy* **2013**, *108*, 202-217.
19. Brown, L. F. *Int. J. Hydrogen Energy* **2001**, *26*(4), 381-397.
20. Bartholomew, C. H. *Appl. Catal., A* **2001**, *212*(1-2), 17-60.
21. *Opening the Door to Cleaner Vehicles in Developing and Transition Countries: The Role of Lower Sulfur Fuels*; United Nations Environment Programme: Nairobi, 2014.
22. Klinghoffer, N. B.; Barraï, F.; Castaldi, M. J. *J. Power Sources* **2011**, *196*(15), 6374-6381.
23. Strohm, J. J.; Zheng, J.; Song, C. S. *J. Catal.* **2006**, *238*(2), 309-320.
24. Gudlavalleti, S.; Ros, T.; Lieftink, D. *Appl. Catal., B* **2007**, *74*(3-4), 251-260.
25. Shamsi, A.; Baltrus, J. R.; Spivey, J. J. *Appl. Catal., A* **2005**, *293*, 145-152.
26. Bedenbaugh, J. E. Investigation of Catalytic Materials for Cracking of Military Aviation Fuel to Liquefied Petroleum Gas: High Throughput Experimentation. University of Delaware, Newark, 2012.
27. Westrich, T., Interview with Tom Westrich, Project Engineer. In *NSF I-Corps*, Mayeda, M. K., Ed. Ultra Electronics AMI: Ann Arbor, MI, 2014.
28. Emley, B., Interview with Ben Emley, Director of Fuel Cell Technology. In *NSF I-Corps*, Mayeda, M. K.; Lauterbach, J.; Sasmaz, E.; Kim, S., Eds. Watt Fuel Cell: Port Washington, NY, 2014.
29. *JP-8 Safety Data Sheet*; Hess: 2012; pp 1-10.

30. Pleil, J. D.; Smith, L. B.; Zelnick, S. D. *Environ. Health Perspect.* **2000**, *108*(3), 183-192.
31. Smith, L. B.; Bhattacharya, A.; Lemasters, G.; Succop, P.; Puhala, E.; Medvedovic, M.; Joyce, J. *J. Occup. Environ. Med.* **1997**, *39*(7), 623-632.
32. Robledo, R. F.; Barber, D. S.; Witten, M. L. *Toxicol. Sci.* **1999**, *51*(1), 119-125.
33. McDougal, J. N.; Pollard, D. L.; Weisman, W.; Garrett, C. M.; Miller, T. E. *Toxicol. Sci.* **2000**, *55*(2), 247-255.
34. Portable Fuel Cells. AMI, U. E.-. Ed. Ultra Electronics - AMI: Ann Arbor, 2012; pp 1-2.
35. Guerzoni, F. N.; Abbot, J. *Appl. Catal., A* **1994**, *120*(1), 55-69.
36. Velu, S.; Ma, X. L.; Song, C. S. *Ind. Eng. Chem. Res.* **2003**, *42*(21), 5293-5304.
37. Mukherjee, S.; Kapur, G. S.; Chopra, A.; Sarpal, A. S. *Energy Fuels* **2004**, *18*(1), 30-36.
38. Qin, X. M.; Chi, H.; Fang, W. J.; Guo, Y. S.; Xu, L. *J. Anal. Appl. Pyrolysis* **2013**, *104*, 593-602.
39. Bansal, V.; Krishna, G. J.; Chopra, A.; Sarpal, A. S. *Energy Fuels* **2007**, *21*(2), 1024-1029.
40. Roychoudhury, S.; Lyubovsky, M.; Walsh, D.; Chu, D.; Kallio, E. *J. Power Sources* **2006**, *160*(1), 510-513.
41. Kim, S. Study of ZSM-5 based catalysts for conversion of JP-8 fuel and pentanediol to LPG-like fuel and BTEX. Ph.D., University of South Carolina, Columbia, 2015.
42. Andresen, J. M.; Strohm, J. J.; Sun, L. *Energy Fuels* **2001**, *15*(3), 714-723.
43. Jiang, R. P.; Liu, G. Z.; Zhang, X. W. *Energy Fuels* **2013**, *27*(5), 2563-2577.
44. Kubo, K.; Iida, H.; Namba, S.; Igarashi, A. *Microporous Mesoporous Mat.* **2012**, *149*(1), 126-133.

45. Miao, H.; Wang, W. G.; Li, T. S.; Chen, T.; Sun, S. S.; Xu, C. *J. Power Sources* **2010**, *195*(8), 2230-2235.
46. Trembly, J. P.; Marquez, A. I.; Ohrn, T. R.; Bayless, D. J. *J. Power Sources* **2006**, *158*(1), 263-273.
47. Lauterbach, J.; Glascock, M.; Bedenbaugh, J. E.; Chien, C.-Y.; Jangam, A.; Salim, S.; Kim, S.; Tilburg, R. Highly Active Decomposition Catalyst for Low Carbon Hydrocarbon Production from Sulfur Containing Fuel. U.S. Patent application 13/584,180, **2013**.

## Chapter 7

### SUMMARY AND FUTURE WORK FOR A FUEL CONVERTER

#### 7.1 Summary

Improvements were made to a fuel conversion process (developed at the University of South Carolina) that converted long-chain hydrocarbon fuels (*e.g.*, jet fuel, diesel, or gasoline) into liquefied petroleum gas (LPG). The improvements to the conversion process resulted in a portable proof-of-concept device using commercially available components. The first modification to the fuel conversion process was to incorporate a product recycle loop to extract more LPG from the reactant feed. By increasing the reaction yield, the proof-of-concept device reduced the required reactor size. The second modification was to eliminate a carrier gas and use the pressure of the vaporized reactant fuel to drive the reactant through the catalyst packed bed. Forgoing an inert carrier gas removed associated tanks, regulators, pumps, and consumables. Finally, by utilizing compact and inexpensive balance-of-plant components, the converter was portable enough for demonstrations independent of a laboratory setting. Ultimately, the fuel conversion process, which occupied multiple laboratory benches, was simplified into less than 8 ft<sup>3</sup> without sacrificing LPG quality or production rate.

Despite the improvements that were made to the fuel conversion process, the resulting device was far from ready for field deployment. Technical and non-technical questions remained about the context of its intended use and minimum viable performance specifications. Section 7.2 discusses the efforts made to define the

envisioned usage characteristics. Furthermore, recommendations for future development are outlined based on interviews with relevant managers, engineers, and technicians who would use the fuel converter.

## **7.2 Recommendations for Future Work in Commercializing a Fuel Converter**

During the nascent stages of the search for a catalyst that could convert jet fuel into liquefied petroleum gas, the intended market for the fuel conversion reaction was the defense industry. Objectives were defined by the Defense Advanced Research Projects Agency (DARPA) as summarized in section 6.1.1. The initial goals were defined with the purpose of establishing a proof-of-concept system. Because the concept was proven in the fume hood, current objectives (section 6.1.2) seek to optimize a system for lab-scale demonstrations. Future objectives seek to produce a system that is ready for field testing and eventually, deployment. This chapter will frame the foreseeable objectives in light of potential-customer feedback, which was acquired during the National Science Foundation Innovation Corps (I-Corps) program. It is anticipated that the future objectives must be accomplished before commercialization can be realized.

I-Corps was a 9-week program that immersed professors and graduate students in the process of identifying appropriate *customer segments* and *value propositions* of their respective scientific innovations. Customer segments are people who are important to the financial success of the fuel converter. As was emphasized during the I-Corps seminars, customer segments must be people and should not be abstracted to companies or organizations. Value propositions are statements that summarize the benefits of using a fuel converter. Typically, propositions start with phrases such as “Save money by...”, “Generate more revenues by...”, or “Save time by....” Customer

segments and value propositions were identified by incorporating feedback from over 100 self-networked contacts. The end of the I-Corps program culminated into a business “go/no-go” decision that summarized the team’s intuition given the feedback received from the aforementioned contacts. In the case of the fuel reforming technology, a no-go decision was made over multiple customer segments due to a lack of significant demand that could sustain a business. The no-go decision is in light of data collected throughout the I-Corps. Significant changes to the technology, customer segments, or government policy would warrant a reinvestigation of the no-go decision.

The following sections will describe the pre-program hypotheses and their evolution during the 9-week program. First, a summary of the perceived market opportunity will be used to justify the commercialization thrust. Section 7.2.1 describes the vetted customer segments and their respective value propositions. Given the feedback from customer segments, section 7.2.2 describes the requisite technical improvements. Section 7.2.3 summarizes other relevant obstacles to commercializing a fuel converter. Throughout the chapter, selected interviews will be used to corroborate market insights and proposed future work.

### **7.2.1 Customer Segment Development**

After initially developing a novel fuel conversion technology, it was important to initiate a market assessment by identifying the individuals that would use or purchase the fuel converter.<sup>1</sup> In particular, market assessments should be made prior to device optimization so as not to produce a “finished product” that would not satisfy the corresponding market requirements; inventors’ solutions may be incongruous to customers’ desired solutions.<sup>1</sup> To this end, discussions with potential customers and users have revealed valuable insights into the future development of a fuel converter

device. As was previously mentioned (section 1.1.4), it was believed that propane generation via fuel conversion would be valuable in environments that exhibited an extreme imbalance in supply and demand. Therefore, four customer archetypes were hypothesized to be appropriate targets to pursue: (1) sports game tailgaters, (2) disaster relief agencies, (3) military field kitchen providers, and (4) military fuel cell system integrators.

### **7.2.1.1 Tailgating at Sports Events**

Per the recommendation of the University of South Carolina's technology transfer office representative,<sup>2</sup> an investigation was conducted into the market feasibility of a fuel converter for tailgaters at sports events. The hypothesis was that a fuel converter would be purchased to either (1) streamline the tailgating planning process by eliminating the need to source propane and/or (2) providing a backup source of propane in case a propane tank was depleted or malfunctioned. The two hypotheses were tested by conducting interviews in-person (30, University of South Carolina *versus* East Carolina University, Sept. 6, 2014) and over-the-phone (18, Mechanical Turk). Interviews sought to qualitatively determine the stiffness of the propane supply and demand curves. Results indicated that while propane demand was stiff and *retail* supply was low, tailgaters did not see the value in a fuel converter because bartering and exchange were common alternative on-site propane supplies.

Tailgating events present interesting environments where the supply and demand of fuels are unusually low and high, respectively. For larger events, such as football games at the University of South Carolina, tailgating can be a long event (*e.g.*, > 12 h), regardless of the length of the actual sporting event. Because of the large influx of people, local traffic patterns commonly are manipulated to encourage

unidirectional vehicle flow towards and away from the event location before and after the event, respectively.<sup>3</sup> The asymmetric traffic patterns make repeated entering and leaving nearly impossible unless a person is traveling *via* non-motorized means (*e.g.*, by foot or bicycle). Interview results confirmed the inability to leave tailgating areas until after traffic flow was directed away from the event arena. The restrictions on vehicle mobility artificially depress the supply of retail propane by limiting a customer's access to a nearby commercial outlet.

As for fuel demand, tailgaters used gasoline and propane for electricity production, heating, and cooking. Gasoline usually was carried in portable 5 gallon containers, and it was used in generators. The most commonly employed generators were manufactured by Honda and Yamaha, both of which were small ( $\approx 2 \text{ ft}^3$  and 40 lbs) and quiet ( $< 55 \text{ dB}$  within 3 ft). The generated electricity was used to power televisions, fans, and sound systems. Propane was carried in 25 lb refillable tanks and 1 lb single-use tanks. At the time of interviewing (September – October 2014), propane was used for cooking but many tailgaters noted that propane would be used for heating during colder months. Demand for propane at tailgates is high; a majority of tailgating groups used propane while a minority of groups used charcoal grills or brought only prepared foods that did not require further heating or cooking.

According to interviewees, the top three recurring concerns for planning tailgating parties was having an adequate food/beverage supply, bringing enough fuel, and ensuring that equipment was properly functioning. When pressed on fuel issues, 52% of interviewees have experienced a shortage of propane while tailgating. Furthermore, 21% of interviewees have recurring shortages: at least once per season. In a common scenario for propane shortage, a tailgater would fail to check the propane

tank level prior to traveling to the destination. Upon arrival, the tailgater discovers a depleted tank and calls upon an incoming friend or relative, who has not yet been confined within the unidirectional traffic flow, to bring in a supplemental tank. The delay is usually less than an hour and negative consequences are limited to embarrassment and slight discomfort due to hunger. In the less common case that propane is depleted while cooking, tailgaters will seek a fuel tank from neighboring parties. Exchanging and borrowing goods in-kind is common, especially amongst tailgaters supporting the same team.

When asked about the perceived value of a fuel converter, tailgaters expressed three concerns. First, tailgaters did not like the added burden of checking the functionality of an additional device. Although a check would be prudent, it adds to existing preparation time and complexity. Furthermore, most people did not think they would use the fuel converter as a primary source of propane; therefore the importance of a converter would be marginal; it would only be useful in the event of a propane shortage. Second, tailgaters were concerned with the bulk of a fuel converter. Due to the relatively large number of items brought to a tailgate, a fuel converter would need to be compact so as not to displace more important items such as passengers, a grill, a cooler, or chairs. Finally, tailgaters were concerned that carcinogenic molecules might pass from the fuel, through the converter, and into the product propane. From the interviews, the existing solutions leave no room for a fuel converter as it is currently designed. Even if the fuel converter were substantially improved in terms of size and performance, a low-cost and low-maintenance on-site propane tank vending machine would likely better serve the tailgating community.

### 7.2.1.2 Disaster Relief Agencies

In a disaster, the affected zones frequently have damaged or inaccessible infrastructures including roads, gas lines, and utility lines. Recent domestic events include superstorm Sandy, Oso mudslide, South Carolina flooding, and various California wildfires. International events abound such as the Fukushima meltdown, typhoon Haiyan, and the Haitian earthquake. In all cases, the lack of infrastructure can hinder recovery and restoration efforts.<sup>4,5</sup> The hypothesis was that by eliminating the need to source propane, a fuel converter would save a disaster relief crew a minimum of 8-16 person-hours per day.<sup>6</sup> In interviews, representatives from disaster relief agencies were asked about existing problems and solutions associated with the distribution of propane and negative consequences during shortages. Responses were variable; some representatives expressed immediate need for a fuel converter while others had no use for propane at all. While customer discovery efforts found two early adopters, the existing market size was too small to sustain a startup.<sup>7,8</sup>

The response to a domestic disaster is a coordinated effort between the state's disaster management team, American Red Cross, Salvation Army, and Southern Baptist Convention.<sup>3,6,9-11</sup> Of the major organizations involved, the Southern Baptist Conventions (SBC) are instrumental for providing hot food and showers to disaster-hit residents. Meals are provided by the American Red Cross, cooked by the SBCs, and delivered by the American Red Cross or the Salvation Army.<sup>9</sup> While some feeding organizations (*e.g.*, Texas Baptist Men) utilize electric-powered appliances,<sup>12</sup> the vast majority of feeding units use propane-powered tray ration heaters, water heaters, and tilt skillets.<sup>13-16</sup> Feeding units vary in size; the smallest units can provide approximately 1,000 meals per day while the larger units can handle 25,000 meals per day.<sup>7</sup> According to the State Directors of Disaster Relief that were interviewed, most

disasters occur in the southeast and mid-west due to hurricanes from the Gulf of Mexico and tornadoes, respectively.<sup>7,8,13,15-17</sup> For example, the Alabama SBC owns and operates five 25,000 meals-per-day feeding units and a separate feeding unit that can be airlifted, which is dispatched internationally.<sup>7</sup> Of the disaster relief organizations, the SBC heavily relies on propane to fulfill its objectives.

Every disaster is unique. When responding to a disaster, state directors do not depend on a single method to establish resupply methods. Because disaster scenarios pose challenges that the SBC must hurdle in the midst of chaotic or even violent atmospheres, arriving to the affected area and creating a cooking base are non-trivial tasks. There are two disasters that many state directors referred to when illustrating the unique difficulties of delivering propane: hurricane Katrina and super storm Sandy. During hurricane Katrina, the vastness of the devastation meant that fuels were delivered into the New Orleans area from over a hundred miles away, which created time delays between requests and deliveries.<sup>17</sup> Although delays could be avoided by anticipating propane usage, even momentary interruptions in cooking could lead to violent situations; SBC units sometimes travel under armed guard.<sup>7</sup> In the aftermath of super storm Sandy, sub-freezing temperatures and the lack of power increased the demand for propane, especially around Manhattan.<sup>6</sup> Unfortunately, local laws and policies prohibited the transport of propane over bridges and through tunnels.<sup>15</sup> The result was a dearth of on-site propane in the disaster zone. In one case, a relief director called upon a Virginia-based propane vendor to circumvent the City of New York laws to deliver propane to the SBC feeding units.<sup>13</sup> The difficulties in propane distribution for the Katrina and Sandy storms were indicative of the daunting logistics that were encountered by SBC state directors.

Despite the previously discussed high demand and low supply, the vast majority of state directors did not want to purchase a fuel converter and felt that their existing fuel delivery solutions were adequate. Interestingly, although nearly all state directors had perceived hurricane Katrina and super storm Sandy as being particularly difficult to address, neither the Louisiana nor the New York state directors thought that a fuel converter would provide enough value to justify a purchase. In fact, only two SBC state directors indicated that they would need a fuel converter. Mel Johnson (Alabama) and Gaylon Moss (North Carolina) approximated their need to be a total of less than fifty fuel converters (\$2,000/converter).<sup>7,8</sup> Figure 7.1 illustrates the results from interviewing state directors. It should be noted that despite the 50 states on the map, there are only 42 SBCs because some states with lower populations combine into a single convention.

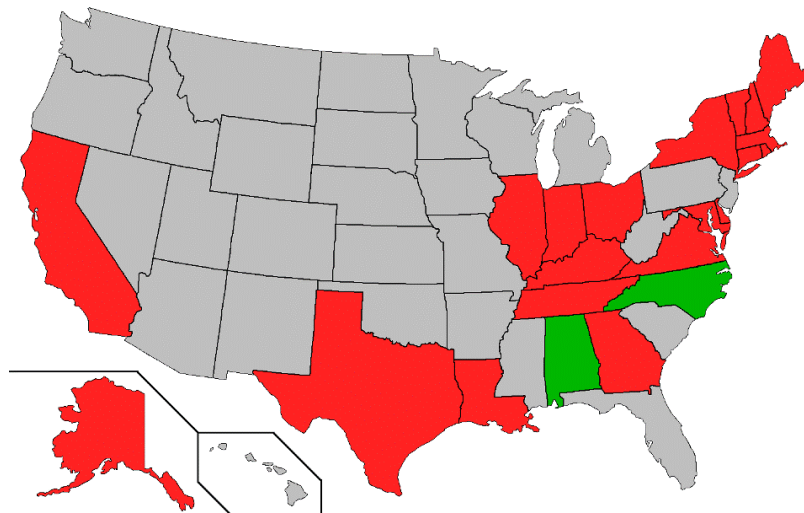


Figure 7.1: Map of the US indicating the responses from state directors of disaster relief. Grey states did not respond, red states indicated “no,” and green states indicated “yes.”

Every SBC state director that was interviewed stated that their feeding units traveled with a 2-3 day supply of propane. In most cases, fuel logisticians were able to create and manage an *ad hoc* propane resupply network within the 2-3 day time constraint. However, because larger feeding units consume propane at higher rates, there is less time to set up a propane resupply network in wider-spread disaster areas. The North Carolina and Alabama SBC state directors command the largest-capacity feeding units and regularly stress their fuel logisticians.<sup>7,8</sup> It would be reasonable to pursue interviews with the state directors of Mississippi and Florida, too. However, even if their needs were similar to those of North Carolina and Alabama, the market demand for a fuel converter would remain small.

In summary, the demand for fuel converters used with field kitchen units by disaster relief agencies is too small to sustain a startup. Although results would likely be similar, it may be prudent to investigate the use of propane by water heaters in field showering units. Furthermore, future work should look into international disaster relief agencies. Whereas domestic disasters are mostly limited to natural causes, international political events can create large numbers of displaced refugees in addition to victims of natural disasters. Ultimately, a substantial market demand was not found for domestic uses of a fuel converter; however, further investigation is warranted.

### **7.2.1.3 Military Field Kitchens**

In the Fall of 2013, the US Army issued a small-business innovation research (SBIR) solicitation entitled “Battle Fuel Conditioner (BFC) for Commercial Gas Appliances in Field Kitchens,” which sought to “develop a technological solution for safely, reliably, and effectively utilizing [JP-8] in commercial off the shelf gas-fired

appliances in military field kitchens.”<sup>18</sup> By replacing military-specific appliances with commercially available analogs, the military could reduce costs of procurement and maintenance. Therefore, it was hypothesized that the fuel converter would help to realize the aforementioned cost reductions. Representatives from the Defense Logistics Agency,<sup>19-21</sup> Army SBIR office,<sup>22</sup> Army kitchen procurement office,<sup>23</sup> Sotera Defense Solutions,<sup>24</sup> Babington Technologies,<sup>25,26</sup> Creare Inc.,<sup>27</sup> and Proheat were interviewed about the current problems related to military field kitchens.<sup>28</sup> The results revealed that technological solutions exist, primarily in the form of atomizers,<sup>25-27</sup> which are less complicated and more efficient than the proposed fuel converter. Despite alternative technology solutions, the incumbent technology (*i.e.*, modern burner units from Proheat) remains the only technology used in military field kitchens.<sup>28</sup> One source claimed that the existing monopoly is attributable to non-technical aspects;<sup>25</sup> Proheat would not elaborate on their monopoly.<sup>28</sup>

While US civilians use commercially available systems that consume lightweight hydrocarbons (*e.g.*, appliances from Coleman, MSR, Ozark Trail, Jetboil, etc.), military personnel are confined to military-specific systems that consume field-available fuels, which excludes bottled lightweight hydrocarbons. Before 1990, the standard heat source was a M2 burner, which consumed gasoline. The M2 burner was prone to catastrophically explode because the gasoline was relatively volatile and the u-shaped fuel tank was located directly under the heat source (Figure 7.2).



Figure 7.2: The M2 military burner viewed from the (a) side and (b) underside, which clearly shows the u-shaped fuel tank. Images are reproduced with permission from the photographer. Images were originally posted on [www.spiritburner.com](http://www.spiritburner.com).

Due to the explosive hazards and the single fuel forward policy (section 6.1), the M2 was promptly replaced by the modern burner unit (MBU), which was exclusively produced and sold by Proheat.<sup>28</sup> The MBU is a military-specific burner that minimizes explosions by using JP-8 in a non-pressurized fuel tank.<sup>29</sup> JP-8 is a low volatility fuel (BP = 156 - 260 °C) compared to gasoline (BP = 85 °C).<sup>30,31</sup> Also, the non-pressurized JP-8 fuel tank is fitted with a pressure relief valve that prevents over pressurization during operation. The success of the MBU is evidenced by its service for 25 years with minimal modifications.<sup>28</sup>



Figure 7.3: The modern burner unit produced by Proheat. Image was adapted and reproduced with permission from Marine Canada Acquisition Inc., doing business as SeaStar Solutions.

However, per the SBIR solicitation and industry contact interviews,<sup>18,23,24</sup> drawbacks of the MBU include its unvented exhaust heat, excessive noise, and military-specific design. When MBUs are used in field kitchens, cooks are rotated into and out of the cooking area to minimize their exposure to the heat and exhaust gases that are built up within the structure.<sup>24</sup> Regarding the noise, during a demonstration of a MBU, the author could not hear himself talking to interviewees when standing within 10 ft of the operating MBU.<sup>25,26</sup> Finally, the military-specific MBU is sole-sourced, which presents cost inefficiencies; replacement parts also are sole-sourced from Proheat.<sup>23,28</sup> While the MBU has solved the safety concerns associated its predecessor M2 burner, performance and cost concerns have pushed the military to investigate the possibility of using commercial gas appliances.

The advantage of using a fuel converter would be to produce propane that can be used in commercially available appliances. Because propane appliances are used in commercial markets, the devices are time-tested for reliability, efficiency, and performance. Furthermore, a plethora of suppliers offer a myriad of appliances that range in size and function. Therefore, by converting field-available JP-8 into propane,

the military could feasibly deploy commercially available stoves, ovens, lamps, space heaters, and water heaters while maintaining budgetary constraints. However, the major drawback to chemically converting JP-8 into propane is the relatively low efficiency of the reaction (30-50 wt%).<sup>32</sup>

Engineers at Babington Technologies and Creare, Inc. are producing efficient JP-8 burners by implementing an atomization step prior to fuel ignition.<sup>25-27</sup> Atomization creates fine particles that can be efficiently combusted.<sup>33</sup> The technical details of their atomization processes are beyond the scope of this discussion;<sup>33</sup> it is sufficient to say that minimal fuel is wasted in the atomization process and the resulting nebulized fuel can be used in gas appliances.<sup>27</sup> Indeed, it was discovered that one of the companies that was awarded the A13-045 SBIR Phase 1 and Phase 2 solicitations is using an atomization approach (Novatio Engineering, Inc., Waltham, MA).<sup>18,22</sup> Furthermore, interviews indicated that the problems associated with excessive heat and noise were associated with the burner enclosure, not the flame combustion characteristics. The biggest technical hurdle was to make a JP-8 flame that was similar to a propane flame.<sup>22,23</sup> Therefore, until the chemical yield of the fuel converter is drastically improved, mechanical solutions to burning JP-8 will remain the favored approach towards improving military field kitchens.

In addition to the technical hurdle of improving the fuel conversion efficiency above 30-50 wt%, interviews indicated that ending the Proheat monopoly would be a significant political hurdle. Babington Technologies is the most mature company competing against Proheat for the military field kitchen contract. Indeed, the atomization process that is employed by Babington Technologies has been field-proven and implemented in field kitchens sold to the Virginia Southern Baptist

Convention.<sup>15,25</sup> Furthermore, the atomization technology has long been in the public domain; the patent was issued in 1969.<sup>33</sup> Other companies can design, produce, and sell similar devices and interchangeable parts.<sup>26</sup> Nevertheless, Proheat maintains a successful monopoly on the military field kitchen burner market. Therefore, it would be unreasonable to expect that a startup company, with an inferior chemical technology, could achieve significant market penetration.

#### **7.2.1.4 Military Portable-Fuel Cell System Integrators**

As discussed in section 6.1, the initial objective of designing a fuel converter was to support the use of solid oxide fuel cells in unmanned aerial vehicles (UAV). The inherently larger energy density of a fuel cell enabled longer flight times (8 h) than a battery-powered equivalent UAV (2 h).<sup>34</sup> However, owing to the high sulfur content in JP-8, no SOFC system can operate on untreated JP-8.<sup>35,36</sup> The most developed SOFC system was designed to consume commercial propane and is currently being sold into commercial markets for applications in the rail industry (Figure 7.4).<sup>37</sup> We hypothesized that a JP-8-to-propane fuel converter would help to generate additional revenue for system integrators by repurposing commercial propane-powered fuel cells for military applications.

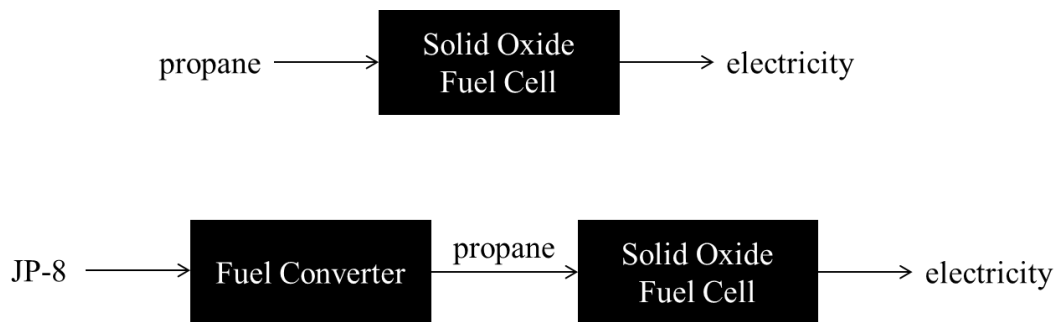


Figure 7.4: Commercial SOFC systems have been designed to operate on propane (top). Without propane in the battlefield, a fuel converter would be necessary to utilize field-available JP-8 (bottom).

As of this writing, there are only a few companies that have portable (< 1 kW) solid oxide fuel cells in their product portfolio; they include Watt Fuel Cell (Port Washington, NY),<sup>38</sup> Ultra Electronics AMI (Ann Arbor, MI),<sup>37</sup> Acumentrics (Westwood, MA),<sup>39</sup> NexTech Materials (Lewis Center, OH),<sup>40-42</sup> and Protonex (Southborough, MA).<sup>43</sup> While the aforementioned companies claim to be able to feed JP-8 into their SOFC, all have expressed skepticism towards their respective competitors' claims on JP-8 compatibility. Multiple interviewees agreed that Ultra Electronics – AMI has developed a system with the highest technology readiness level; it uses propane.<sup>35,44-46</sup> On the other hand, Protonex sells their systems to special operations forces, but the larger US Army remains free of portable SOFC systems. All interviewees have expressed concerns with crack formation in ceramic electrolytes under thermal cycling which occurs during system startup and shutdown transients.<sup>37,42,43,47</sup>

In addition to problems with fuel utilization, total-system reliability has yet to be proven; engineering teams design and optimize the fuel processor or the fuel cell, not both (Figure 7.4).<sup>42</sup> Currently, the most proven means to enable SOFCs in the

battlefield is to employ autothermal reformation (ATR) followed by gas-phase desulfurization.<sup>35,36,48,49</sup> While ATR methods can consistently achieve 80% energetic yield,<sup>50,51</sup> the requisite desulfurization system can treble the fuel-to-electricity system size.<sup>36,47</sup> Finally, when powering fuel cells with fuel reformation products, the reformat is usually simulated or obtained from controlled fuels, both of which lack sulfurous compounds.<sup>52-55</sup> Therefore, there exist significant technical hurdles to building a fully integrated JP-8-to-electricity system.

Despite the feasibility of a JP-8-to-propane fuel converter (Chapter 6, Figure 6.7), interviews yielded consistently mediocre enthusiasm primarily due to a lack of financial support. Fuel cell design teams rely heavily on military spending to develop military-purposed technology. In fact, many companies first confirm commercial market feasibility and then repurpose commercial products for military applications.<sup>25,37,38</sup> While nearly all fuel cell-developing interviewees have expressed interest in a JP-8-to-propane fuel converter, no companies had internal funding to license, purchase, or otherwise develop such a conversion technology. Conversely, some interviewees expressed interest in forming collaborations to co-write proposals that would be submitted to private and federal funding agencies. To this end, letters of support were garnered from SAFCell, Ultra Electronics - AMI, and the US Army Corps of Engineers. Therefore, continued development of a fuel converter could occur with third party support (*e.g.*, Army, Navy, Office of the Secretary of Defense, Office of Naval Research, Defense Advanced Research Projects Agency, or in the case of South Carolina, the South Carolina Research Authority) in the form of Small Business Innovation Research (SBIR) or Small Business Technology Transfer (STTR) funds. It should be noted that approximately fewer than half of relevant awardees in the past ten

years remain in business; the survival rate was estimated based on over fifty calls made to awardees found from an online search.<sup>56</sup> Furthermore, interviewees estimated that the lead time to military market penetration is 5 years.<sup>25,37,38</sup> It is a daunting task to continuously raise enough funds to support a startup for the lead time without generating revenues.

Ultimately, a fuel converter has mediocre interest within the military fuel cell community. Existing fuel cell systems cannot operate on field-available fuels. However, the technology readiness level of the proposed fuel converter is too low; the converter must be further developed to prove system-level reliability during in-field testing. Potential customers' are interested in the technical aspects of the converter but do not see enough immediate value to purchase or license the technology. If the converter is to be further developed, it would likely occur under the auspices of third party financial support from federal organizations. It is the author's opinion that work on the fuel converter project should continue; however, expectations need to be tempered by the reality of a tepid customer client base and the political and financial difficulties of entering the military market.

#### **7.2.1.5 Other Customer Segments**

During the NSF I-Corps period, the team did not have enough time to investigate two other potential customer segments that were brainstormed. The first potential customer segment includes owners of high-value recreational vehicles (RV) and boats. Off-grid vehicles typically use diesel or gasoline for their engines and propane for their on-board appliances like an oven, stove, water heater, and refrigerator. Therefore, an on-board fuel converter would eliminate the need for filling and monitoring a propane tank. It is hypothesized that owners place value on time

saved from filling and monitoring only a single fuel. Furthermore, if coupled with an on-board fuel cell system, owners would value the ability to produce electricity from their on-board fuels without using a noisy internal combustion generator. To test the hypothesis, it would be beneficial to speak with owners, producers, and dealers. Interviews should yield information on current electricity production methods, any problems associated with refueling, and desires for noise abatement.

The second potential customer segment includes residents of developing countries (section 1.1.4.1). Owing to its geographic separation and region-specific problems, an international rural market segment would require significant focus. Generally, developing countries have fuel distribution infrastructures that are less developed than those in the West. While heavier hydrocarbon fuels like kerosene, diesel, and gasoline are commonly used to operate generators and vehicles, cleaner lightweight hydrocarbon fuels are eschewed for cheaper and widely available biowaste and charcoal. Interviews would need to identify the socioeconomic barriers to fuel distribution and usage characteristics within a given town, region, and country. For example, the Indian government subsidizes the cost of petroleum in India; the result is an artificially deflated cost of diesel but a relatively high cost of propane.<sup>57</sup> However, the existing political regime has indicated it would reduce fuel subsidies; fuel price turmoil will play an important role in the market feasibility of a fuel converter. Conversely, customers of a fuel converter may be Western individuals and organizations operating in developing regions, not residents. For example, the Alabama Southern Baptist Convention has an airlift kitchen that has been deployed in Haiti and Iran. While abroad, sourcing propane can be significantly more difficult with additional political, language, and currency complications.<sup>7</sup> A fuel converter may be

valuable to logisticians with the US Agency for International Development, World Health Organization, or the Peace Corps. To test the hypothesis, a visit to the targeted locale would yield the best insights into the problems and potential solutions to fuel distribution and propane supply. However, to minimize costs and logistics, the first interviews should be with agency regional representatives and local consultants.<sup>58</sup>

## **7.2.2 Future Technical Considerations**

While the technical capabilities of the current fuel converter shows progress from its initial development in the fume hood, there exist significant shortcomings that need to be addressed before field testing can begin. In general, future designs of the fuel converter need to increase operational safety, optimize thermal management, and achieve military specifications.

### **7.2.2.1 Safety**

There are four main hazards associated with operating the fuel converter: (1) reactant and product flammability and corrosiveness, (2) high temperatures, (3) over pressurization, and (4) exhaust gas toxicity. The minimum flashpoint of JP-8 is 38 °C, and it has an autoignition temperature of 210 °C.<sup>30</sup> Flammable products and reactants necessitate the use of electronics that eliminate arcing: pumps should be driven by brushless motors instead of brushed motors and switches should be accomplished using relays instead of mechanical devices. To prevent corrosion, stainless steel should be used everywhere that comes in contact with the reactant and product streams. Aluminum and brass are prone to corrosion and should not be used despite weight and cost savings, respectively. One exception can be the use of Tygon® tubing in the

peristaltic fuel pumps. The hazards associated with the reactants and products necessitate a careful selection of components and materials to build a converter.

The combination of flammable reactants and products with temperatures in excess of their autoignition point presents a precarious situation. Furthermore, it is likely that an open-flame on-board burner will need to be implemented in order to provide adequate heating to the endothermic reaction (section 7.2.2.2). Air leakage could result in catastrophic failure; compression tube fittings should be used at all possible junctions and Viton® o-rings should be used everywhere else. O-rings should be inspected before each operation. In addition to eliminating undesirable air leaks, the design of the system needs to carefully consider desirable air flow, which will be used for regenerating spent catalyst beds. After a bed has been exposed to air it should be depleted of oxygen. An on-board air separation unit that purges the bed with nitrogen would be too heavy, bulky, and costly. Therefore, the bed can be evacuated with a pump or purged with exhaust gases from the burner (section 7.2.2.2). Evacuation could require an additional pump, incur parasitic electric losses, and introduce complications with reactant- and product-flow due to pressure swings. Further research should investigate the effects of a pressure swing in the reactor bed. On the other hand, purging the reactor bed with exhaust gases from a burner may adversely affect the catalyst lifetime, introduce unwanted gaseous species (*i.e.*, sulfurous compounds) in the product stream, and add complicated plumbing. Further research should characterize the durability of the catalyst when exposed to exhaust gases and characterize the effective concentration of sulfur-containing species in the nominal propane product gas. Finally, flashback arrestors need to isolate the reactors, fuel

reservoir, and condensed fuel reservoir to avoid catastrophic combustion. The aforementioned measures should be used to minimize the risk of explosion.

The current system operates slightly above ambient pressure (< 10 psig). Vented fuel tanks should be used to prevent over-pressurization in both reservoirs. Pressure-release valves also should be included after the evaporator and after the reactor. Vents should be directed away from heat sources, electronics, or open flames.

Use of a fuel burner to provide heat will produce toxic exhaust gases. Exhaust gases should be vented away from the “cold” parts of the converter (*i.e.*, fuel reservoirs, condenser, and electronics). Further research will have to identify the pertinent military specification on exhaust gases. A catalytic converter, similar to those used for automotive exhausts, may be required.

Advances in the conversion process may cause significant deviations from the current design. Therefore, a failure-mode analysis should be conducted after each iteration to keep safety at the fore.

#### **7.2.2.2 Thermal Management**

The fuel conversion process requires a substantial amount of heat input to evaporate the liquid reactant (BP = 180-255 °C)<sup>59</sup> and drive the endothermic fuel conversion reaction (operating temperature  $\approx$  450 °C). After the reaction, heat needs to be removed from the product stream so as to separate the gaseous products (BP < 25 °C) from the liquid products (BP > 25 °C). In total, the fuel conversion reaction requires a large amount of thermal inputs and extractions.

The first setup used heating tape to heat the evaporator, a benchtop tube furnace to heat the reactor, and a recirculating chiller to cool the reaction products. Modifications in the current proof of concept uses a compact tube furnace for heating

the reactor and two cold plates in series with four mounted Peltier coolers (section 6.5). The next iteration of a fuel converter should (1) recycle heat from the product gas stream into the liquid reactant and (2) include an internal heat source for heating the evaporator and reactor during startup. Recycling heat will reduce the energy required to evaporate the reactant and condense the product. An internal heat source will need to be used when starting the system from “cold” and sustaining the evaporator and reactor temperatures. For now, it is unknown as to whether the waste heat from a solid oxide fuel cell can sustain the endothermic fuel conversion. In any case, demonstrations of the fuel converter should be successfully proven without a fuel cell.

A tube-shell heat exchanger should be designed to accept the hot product gas (450 °C) and room-temperature reactant fuel (25 °C). The geometry of the heat exchanger should accommodate phase changes (*i.e.*, evaporation or condensation) in both streams. Condensed fuel from the product gas should be collected and recycled through the reaction process to improve yields. Heat exchanger design will require information on the reactant and product: thermal properties, operating temperature, and flow rates. While it is difficult to know the thermal properties of JP-8 because of its variations per batch, *n*-dodecane is a commonly used surrogate and should be relied on for initial modeling. The product gas can be modeled using propane. Unless there are significant changes in the catalyst, the hot gas operating temperature should be 450 °C. Reactant and product flow rates will be dictated by the size of the intended partnered solid oxide fuel cell. A heat exchanger should largely improve the thermal management of the fuel converter by recycling heat from the product gas into the reactant fuel.

It is estimated that 500 W of waste heat from a 250 W solid oxide fuel cell is above 400 °C.<sup>37</sup> However, the exact profile of the heat is proprietary knowledge and specific to the solid oxide fuel cell design. Even if the quality and quantity of the heat were high enough to sustain the fuel converter, an on-board system would be required to heat the evaporator and reactor during startup. An electric system would likely require a significantly large battery bank, which would reduce the portability of the fuel converter and incur parasitic electric losses. To achieve a lightweight and compact system, a fuel burner should be used; because of the high energy content of the reactant fuel ( $\approx 35$  MJ/L), a relatively small mass of fuel would need to be burned per mass of fuel reacted. When designing a burner, the aforementioned safety considerations are the most important (section 7.2.2.1). Additionally, the burner should have a wide turndown ratio to provide the shortest possible startup time (high power) and sustain reactor and evaporator temperatures (low power). A nozzle-type burner would be a likely first choice and thus the existing fuel pumps should be selected to provide adequate pressure over the designed turndown ratio. A low-pressure atomizer from Babington or Creare may prove to be more beneficial if pressurizing the fuel becomes a safety hazard or is too difficult to achieve with the existing fuel pumps.

### **7.2.2.3 Military Specifications**

As discussed in section 7.2.1.4, the most promising market application is as a fuel preconditioner for military fuel cell systems. Therefore, the fuel converter would eventually need to meet military specifications (mil-spec) in terms of field stress tests. The most applicable mil-spec code would be 810G and 801C.<sup>37,60</sup> All iterations of the fuel converter must include, or potentially upgrade to, components that are mil-spec

approved. Owing to the unusual usage characteristics in the battlefield, mil-specs seek to provide performance and safety for soldiers. Therefore, designing a system that cannot meet mil-spec would meet significant resistance.<sup>35,60</sup>

### **7.2.3 Obstacles and Recommendations for Commercialization**

The defense industry has been identified as the most promising market to buy a fuel converter. Although the defense industry can be credited with many successful innovations, the inherent tie to federal programs, budgeting, and bureaucracy drastically increase the time-to-sale. Estimates from the NSF I-Corps team indicated that an accelerated timeline could see fuel converter device sales after three years; five years is more realistic. Therefore, one of the biggest obstacles to realizing any sales and profits is the lack of funding to adequately run the daily operations of designing, constructing, and marketing a fuel converter. Unless an immediate commercial market is discovered, a self-sustaining startup is unrealistic.

Continued efforts to commercialize the fuel converter should be done in partnership with existing defense-related companies and organizations. As of this writing, a Cooperative Research and Development Agreement (CRADA) has been drafted with the Army Corps of Engineers (Nicholas Josefik, Champaign, IL) and letters of support were acquired from SAFCell (Calum Chisolm, Pasadena, CA) and Ultra Electronics – AMI (Tom Westrich, Ann Arbor, MI). Furthermore, additional funding could be garnered from the recently announced collaboration between the South Carolina Research Authority and their Israeli counterpart. Partnerships should be forged with relevant organizations including the Communications-Electronics Research, Development and Engineering Center (CERDEC), Precision Combustion (Subir Roychoudhury, North Haven, CT), and Lockheed Martin. Researchers within

CERDEC have yielded results that bode well for field-ready solid oxide fuel cells.<sup>61</sup> Although Precision Combustion can be viewed as a direct competitor, a synergistic partnership could leverage their expertise with fuel conversion and system design. Finally, while interest from any prime contractor would be desirable, further research should investigate the progress of the Lockheed Martin Stalker XE, which was a drone that used a propane-powered solid oxide fuel cell from Ultra Electronics - AMI.

The successful commercialization of a fuel converter largely depends on the ability to demonstrate its feasibility and secure funds for further development. The author recommends simultaneously designing the converter and forging partnerships with relevant individuals and organizations by presenting at conferences or making on-site visits when economically feasible. As of this writing, assistance with the fuel converter design was graciously provided by Alan Grier at Midlands Technical College and Bob Stewart at Trulite. Ramy Harik of the McNair Aerospace Center also has expressed support by offering to simulate the thermal, chemical, and mechanical phenomena of the fuel converter.

### **7.3 Conclusions**

The feasibility of commercializing a fuel converter was ascertained by augmenting existing academic literature knowledge with interviews from industrially relevant contacts. The four explored applications were sports event tailgating, disaster relief, military field kitchen feeding, and military portable solid oxide fuel cells. The four applications were investigated because of a hypothesized supply-demand imbalance for propane. In all cases, interviews revealed that supply-demand imbalances indeed limited access to propane. However, in the former three cases, existing solutions sufficiently met the customers' needs and price points. It was only

in the case of military portable solid oxide fuel cells that potential value was discovered; existing solutions were not proven and prices were not clear owing to the immaturity of the market. However, because the market is so immature, it would be presumptuous to confirm market feasibility.

#### **7.4 Acknowledgements**

The author would like to acknowledge the members of SAGE Energy Solutions, LLC (Dr. Jochen Lauterbach, Dr. Erdem Sasmaz, and Dr. Sungtak Kim) and Mr. Tyler Tatum (Ripple Management in Atlanta, GA) for support and the NSF I-Corps (NSF-1449506) for funding.

## REFERENCES

1. Blank, S.; Dorf, B., *The Startup Owner's Manual: The Step-by-Step Guide for Building a Great Company*. K&S Ranch, Inc.: Pescadero, 2012.
2. Hardaway, C., Interview with Chad Hardaway, Associate Director of Innovation. In *NSF I-Corps*, Mayeda, M. K., Ed. Faber Entrepreneurship Center, University of South Carolina: Columbia, SC, 2014.
3. Allen, T., Interview with Tom Allen, Director of Emergency Support Function. In *NSF I-Corps*, Mayeda, M. K., Ed. South Carolina Office of Regulatory Staff: Columbia, SC, 2014.
4. Bono, F.; Gutiérrez, E. *J. Transp. Geogr.* **2011**, *19*(6), 1443-1455.
5. Mahmoudabadi, A.; Seyedhosseini, S. M. *Trans. Policy* **2014**, *36*(0), 34-45.
6. Patterson, M., Interview with Mike Patterson, Emergency Disaster Services Director. In *NSF I-Corps*, Mayeda, M. K., Ed. Salvation Army: Columbia, SC, 2014.
7. Johnson, M., Interview with Mel Johnson, State Director for Disaster Relief. In *NSF I-Corps*, Mayeda, M. K., Ed. Alabama Southern Baptist Convention: Montgomery, AL, 2014.
8. Moss, G., Interview with Gaylon Moss, NC State Director of Disaster Relief. In *NSF I-Corps*, Mayeda, M. K., Ed. Southern Baptist Convention - NC: Cary, NC, 2014.
9. Lim, M., Interview with Mark Lim, Logistics Manager. In *NSF I-Corps*, Mayeda, M. K.; Tatum, T., Eds. Emergency & Disaster Response Red Cross: Los Angeles, CA, 2014.
10. Braddock, K., Interview with Ken Braddock, Chief of Preparedness. In *NSF I-Corps*, Mayeda, M. K., Ed. South Carolina Emergency Management Division: Columbia, SC, 2014.
11. Hutton, A., Interview with Ann Hutton, Natural Disaster Program Manager. In *NSF I-Corps*, Mayeda, M. K.; Lauterbach, J.; Tatum, T., Eds. Army Corps of Engineers: Los Angeles, CA, 2014.
12. Gann, R., Interview with Raymond Gann, Feeding Unit Director. In *NSF I-Corps*, Mayeda, M. K., Ed. Texas Baptist Men: Dallas, TX, 2014.

13. Miller, D., Interview with Dean Miller, VA State Director of Disaster Relief. In *NSF I-Corps*, Mayeda, M. K., Ed. Virginia Baptist Convention: Richmond, VA, 2014.
14. Page, A., Phone Interview with Al Page, Disaster Relief Coordinator. In *NSF I-Corps*, Mayeda, M. K., Ed. New Hampshire Baptist Association: Manchester, NH, 2014.
15. Noble, J., Phone Interview with Jack Noble, State Director of Disaster Relief. In *NSF I-Corps*, Mayeda, M. K., Ed. Virginia Southern Baptist Convention: Richmond, VA, 2014.
16. Alexander, R., Interview with Rex Alexander, State Director of Disaster Relief. In *NSF I-Corps*, Mayeda, M. K., Ed. Illinois Southern Baptist Convention: Springfield, IL, 2014.
17. McMillan, G., Phone Interview with Gibbie McMillan, State Director of Disaster Relief. In *NSF I-Corps*, Mayeda, M. K., Ed. Louisiana Southern Baptist Convention: Alexandria, LA, 2014.
18. Knowlton, L., Battle Fuel Conditioner (BFC) for Commercial Gas Appliances in Field Kitchens. In *A13-045*, Army-SBIR, Ed. 2013.
19. Hardy, R., Interview with Randy Hardy, Deputy Chief of Operations. In *NSF I-Corps*, Mayeda, M. K., Ed. Defense Logistics Agency: Fort Belvoir, VA, 2014.
20. Brown, J., Interview with Jeff Brown, Customer Relations Officer. In *NSF I-Corps*, Mayeda, M. K., Ed. Defense Logistics Agency: Fort Belvoir, VA, 2014.
21. Smith, I., Interview with Irene Smith, Public Affairs Officer. In *NSF I-Corps*, Mayeda, M. K., Ed. Defense Logistics Agency: Fort Belvoir, VA, 2014.
22. Knowlton, L., Interview with Leigh Knowlton, SBIR Program Manager. In *NSF I-Corps*, Mayeda, M. K., Ed. Department of Defense - US Army Small Business Innovation Research Program: Natick, MA, 2014.
23. Jordan, J., Phone Interview with Joe Jordan, Food Service & Equipment life cycle manager. In *NSF I-Corps*, Mayeda, M. K., Ed. US Army - Food Service Equipment & Field Feeding: Natick, MA, 2014.

24. Weiss, J., Phone Interview with Joe Weiss, Vice President of Mission Programs and Engineering. In *NSF I-Corps*, Mayeda, M. K., Ed. Sotera Defense Solutions: Herndon, VA, 2014.
25. Hague, W., Interview with Bill Hague, Senior Director of Military Sales. In *NSF I-Corps*, Mayeda, M. K., Ed. Babington Technologies: Rocky Mount, NC, 2014.
26. Lemus, J. C., Interview with Carlos Lemus, Project Engineer. In *NSF I-Corps*, Mayeda, M. K., Ed. Babington Technologies: Rocky Mount, NC, 2014.
27. Knaus, D., Interview with Darin Knaus, Engineer. In *NSF I-Corps*, Mayeda, M. K., Ed. Creare, Inc.: Hanover, NH, 2014.
28. Christoff, K., Phone Interview with Kirsti Christoff, MBU Product Manager. In *NSF I-Corps*, Mayeda, M. K., Ed. Proheat: Richmond, British Columbia, 2014.
29. Modern Burner Unit. Proheat, Ed. Proheat: Richmond, B.C. Canada, 2012.
30. *JP-8 Safety Data Sheet*; Hess: 2012; pp 1-10.
31. *Gasoline Safety Data Sheet*; Hess: 2012; pp 1-16.
32. Bedenbaugh, J. E.; Kim, S.; Sasmaz, E.; Lauterbach, J. *ACS Comb. Sci.* **2013**, 15(9), 491-497.
33. Babington, R. S. Method of Atomizing Liquids. U.S. Patent application 3421692, December 29, 1966, **1969**.
34. Hambling, D., Longer-Lasting Drones Powered by Fuel Cells. *Popular Mechanics* May 3, 2013, 2013.
35. Thampan, T., Phone Interview with Tony Thampan, engineer. In *NSF I-Corps*, Mayeda, M. K., Ed. Army - CERDEC: Aberdeen Proving Ground, MD, 2014.
36. Poshusta, J., Skype Interview with Joe Poshusta, R&D Engineer. Mesoscopic Devices (now Protonex): Broomfield, CO, 2014.
37. Westrich, T., Interview with Tom Westrich, Project Engineer. In *NSF I-Corps*, Mayeda, M. K., Ed. Ultra Electronics AMI: Ann Arbor, MI, 2014.

38. Emley, B., Interview with Ben Emley, Director of Fuel Cell Technology. In *NSF I-Corps*, Mayeda, M. K.; Lauterbach, J.; Sasmaz, E.; Kim, S., Eds. Watt Fuel Cell: Port Washington, NY, 2014.
39. Schmidt, D., Interview with Doug Schmidt, Director of Liquid Fuel Systems. In *NSF I-Corps*, Mayeda, M. K., Ed. Acumentrics: Westwood, MA, 2014.
40. Arkenberg, G., Phone Interview with Gene Arkenberg, SOFC Technology Group Leader. In *NSF I-Corps*, Mayeda, M. K., Ed. NexTech Materials: Lewis Center, OH, 2014.
41. Kimbrell, R., Interview with Robin Kimbrell, Technical sales. In *NSF I-Corps*, Mayeda, M. K., Ed. NexTech Materials: Lewis Center, OH, 2014.
42. Swartz, S., Interview with Scott Swartz, Co-Founder & CTO. In *NSF I-Corps*, Mayeda, M. K., Ed. NexTech Materials: Lewis Center, OH, 2014.
43. Robinson, P., Interview with Phil Robinson, Project Engineer. In *NSF I-Corps*, Mayeda, M. K., Ed. Protonex: Southborough, MA, 2014.
44. Namazian, M., Phone Interview with Mehdi Namazian, Vice President. In *NSF I-Corps*, Mayeda, M. K., Ed. Altex Technologies: Sunnyvale, CA, 2014.
45. Johnson, S., Interview with Stephen Johnson, Propulsion System Analyst. In *NSF I-Corps*, Mayeda, M. K.; Lauterbach, J., Eds. Northrop Grumman: Torrance, CA, 2014.
46. Breit, J., Phone Interview with Joe Breit, Associate Technical Fellow. In *NSF I-Corps*, Mayeda, M. K., Ed. The Boeing Company: Huntington Beach, CA, 2013.
47. Elangovan, S., Phone Interview with "Elango" Elangovan, SOFC Project Manager. In *NSF I-Corps*, Mayeda, M. K., Ed. Ceramatec: Salt Lake City, UT, 2014.
48. Roychoudhury, S.; Lyubovsky, M.; Walsh, D.; Chu, D.; Kallio, E. *J. Power Sources* **2006**, *160*(1), 510-513.
49. Josefik, N., Phone Interview with Nick Josefik, Contracting Officer Representative. In *NSF I-Corps*, Mayeda, M. K.; Sasmaz, E., Eds. US Army Corps of Engineers: Champaign, IL, 2014.

50. Chen, C.-H., Phone Interview with Chien-Hua Chen, R&D Engineer. In *NSF I-Corps*, Mayeda, M. K., Ed. Advanced Cooling Technologies, Inc.: Lancaster, PA, 2014.
51. Xu, X. H.; Li, P. W.; Shen, Y. S. *Appl. Energy* **2013**, *108*, 202-217.
52. Yi, Y. F.; Rao, A. D.; Brouwer, J.; Samuelsen, G. S. *J. Power Sources* **2005**, *144*(1), 67-76.
53. Lamp, P.; Tachtler, J.; Finkenwirth, O.; Mukerjee, S.; Shaffer, S. *Fuel Cells* **2003**, *3*(3), 146-152.
54. Kromp, A.; Leonide, A.; Weber, A.; Ivers-Tiffée, E. *J. Electrochem. Soc.* **2011**, *158*(8), B980-B986.
55. Chen, F. Z.; Zha, S. W.; Dong, J.; Liu, M. L. *Solid State Ion.* **2004**, *166*(3-4), 269-273.
56. DoD SBIR/STTR Awards. <http://www.dodsbir.net/awards/> (October 15, 2014).
57. Bajjuri, P., Phone Interview with Pranay Bajjuri, Investor/Engineer. In *NSF I-Corps*, Mayeda, M. K.; Lauterbach, J.; Sasmaz, E.; Kim, S., Eds. John Deere: Moline, IL, 2014.
58. Fitzgerald, W., Interview with Bill Fitzgerald, Senior Vice President for Government Affairs. In *NSF I-Corps*, Mayeda, M. K., Ed. Vanu-Africa: Columbia, SC, 2013.
59. Smith, B. L.; Bruno, T. J. *Energy Fuels* **2007**, *21*(5), 2853-2862.
60. Stewart, R., Interview with Bob Stewart, Director of Engineering. In *NSF I-Corps*, Mayeda, M. K., Ed. Trulite: Columbia, SC, 2014.
61. Thampan, T.; Shah, D.; Cook, C.; Novoa, J.; Shah, S. *J. Power Sources* **2014**, *259*, 276-281.

## Appendix A

### SUPPORTING INFORMATION FOR CHAPTER 3

#### A.1 Ligand Exchanges

Table A.1. Molar and mass feed ratios for ligand exchange reactions

$\text{Au}_\infty\text{NP:PS-SH}$ mass feed ratio	$\text{C}_{12}\text{SH:PS-SH}$ molar ratio
$0.70 \pm 0.05$	$2.7 \pm 0.2$
$1.31 \pm 0.05$	$2.8 \pm 0.2$
$1.38 \pm 0.05$	$3.1 \pm 0.2$
$2.20 \pm 0.05$	$4.1 \pm 0.2$
$2.4 \pm 0.1$	$4.5 \pm 0.2$
$2.6 \pm 0.1$	$4.8 \pm 0.2$
$2.8 \pm 0.1$	$5.1 \pm 0.2$
$3.4 \pm 0.1$	$6.6 \pm 0.2$

Mass feed ratios ( $\text{Au}_\infty\text{NP:PS-SH}$ ) were calculated using mass measurements taken from reagents dried under roughing pump vacuum for at least 8 h. Molar ratios ( $\text{C}_{12}\text{SH:PS-SH}$ ) were calculated using integrated peaks from  $^1\text{H}$  NMR spectra (see Figure A.1).

## A.2 $^1\text{H}$ NMR Spectra

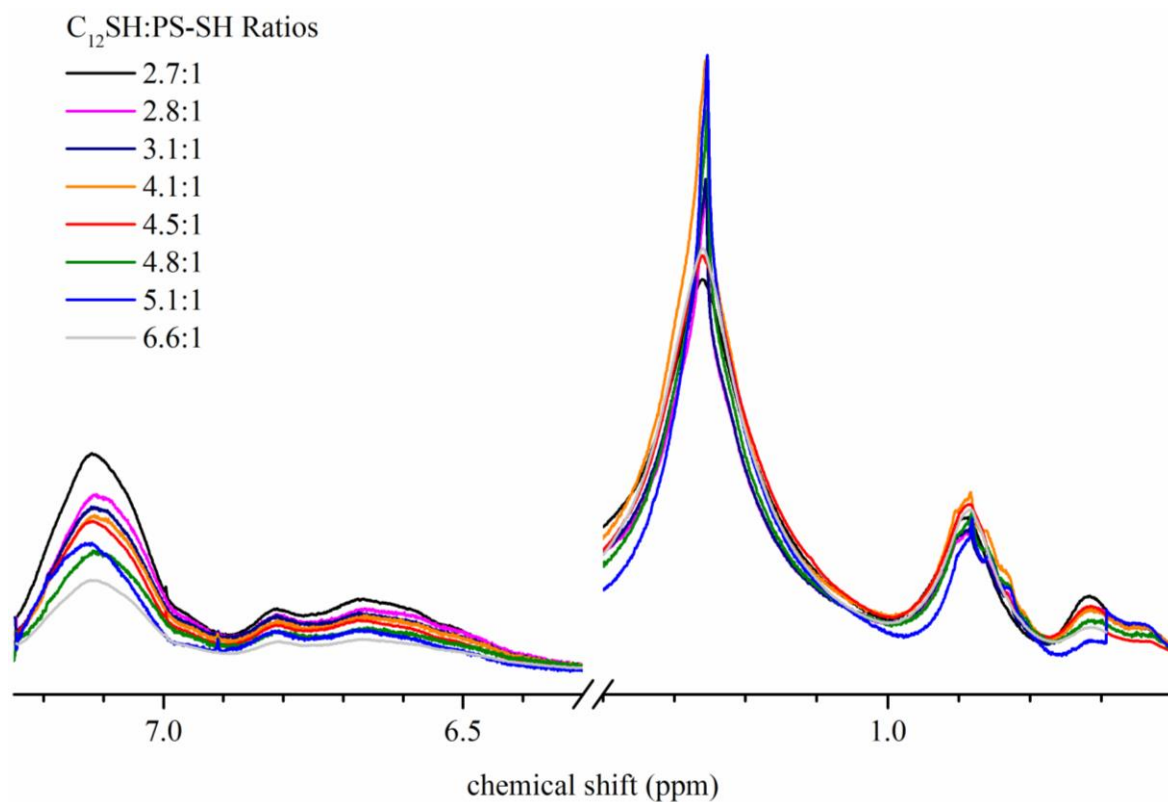


Figure A.1:  $^1\text{H}$  NMR spectroscopy of ligand exchange products in deuterated chloroform. Spectra were normalized to integrated areas associated with  $\text{C}_{12}\text{SH}$  between 1 - 1.4 ppm. Peaks between 6.3 - 7.3 ppm, associated with the phenyl group in PS-SH, grow with decreasing  $\text{C}_{12}\text{SH}:\text{PS-SH}$  ratios while the peak between 1.0 - 1.4 ppm, associated with the  $\text{C}_{12}\text{SH}$  hydrocarbon chain, remains relatively constant.  $\text{C}_{12}\text{SH}:\text{PS-SH}$  ratios of the spectra shown were 2.7:1, 2.8:1, 3.1:1, 4.1:1, 4.8:1, 5.1:1, and 6.6:1. Reprinted with permission from Mayeda *et al.*, *Chemistry of Materials*, 2012, 24(14), 2627-2634.

### A.3 $^1\text{H}$ MAS-NMR Spectra

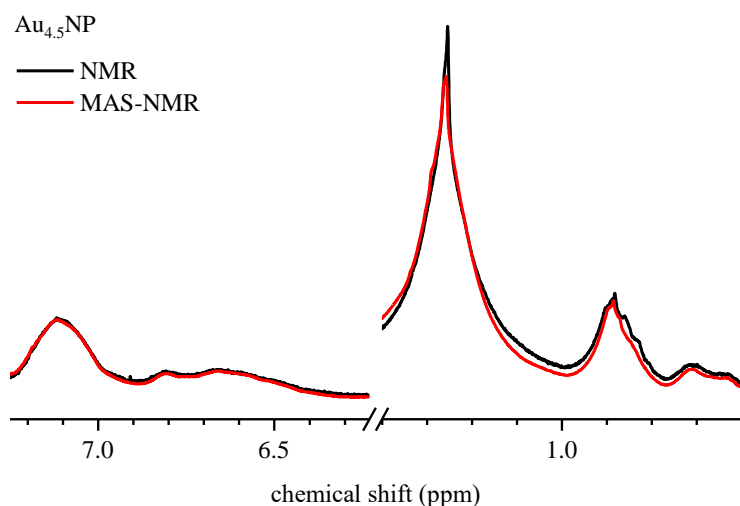


Figure A.2: Comparison of  $^1\text{H}$  spectra obtained via conventional NMR (black line) and MAS-NMR (red line). Reprinted with permission from Mayeda *et al.*, *Chemistry of Materials*, 2012, 24(14), 2627-2634.

$\text{Au}_{4.5}\text{NP}$  ligand exchange products were suspended in deuterated chloroform. The  $^1\text{H}$  NMR spectrum was obtained using a Bruker AV400. The  $^1\text{H}$  MAS-NMR spectrum was obtained using a Varian Inova 500 fitted with a Doty Scientific 4 mm XC MAS probe, spinning the sample at 1 kHz in 40  $\mu\text{L}$  Kel-F sealing cells provided by Doty, and acquiring 32 transients with a 3.5 s recycle delay. Full widths at half max (FWHM) were 0.11 ppm in both cases for the broad hydrocarbon chain peak at  $\delta 1.26$ . The constant FWHM between the two experimental techniques suggests that the line broadening is induced by chain confinement and tethering to the AuNP surface.

#### A.4 Gold Nanoparticle Size Characterization

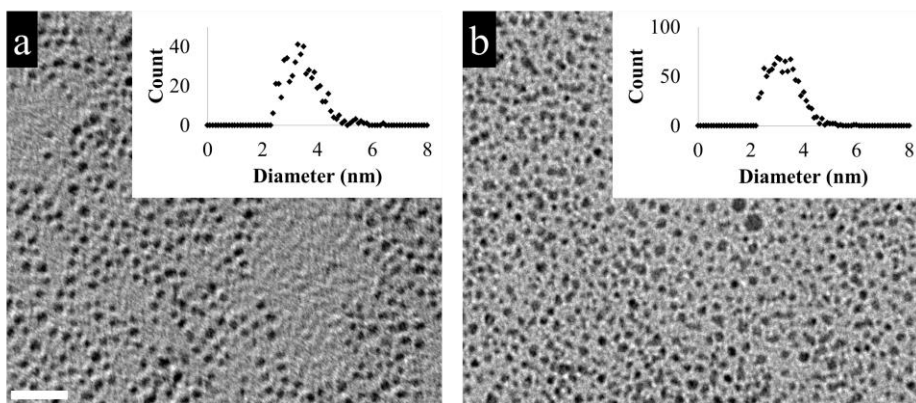


Figure A.3: TEM micrographs of AuNPs (a) as-synthesized and (b) after a typical ligand exchange with PS-SH. The AuNPs were mounted on a lacey carbon grid for imaging. Insets present histograms generated using ImageJ. Histograms indicate that AuNPs do not appreciably change size ( $3.5 \pm 0.6$  nm) following ligand exchange. The scale bar corresponds to 20 nm. Reprinted with permission from Mayeda *et al.*, *Chemistry of Materials*, 2012, 24(14), 2627-2634.

## A.5 Thermally Annealed Nanocomposites

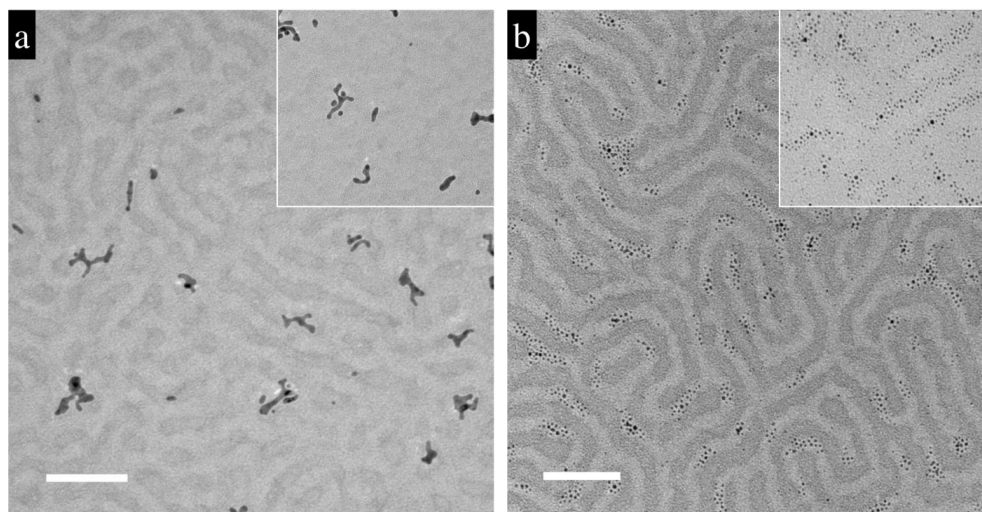


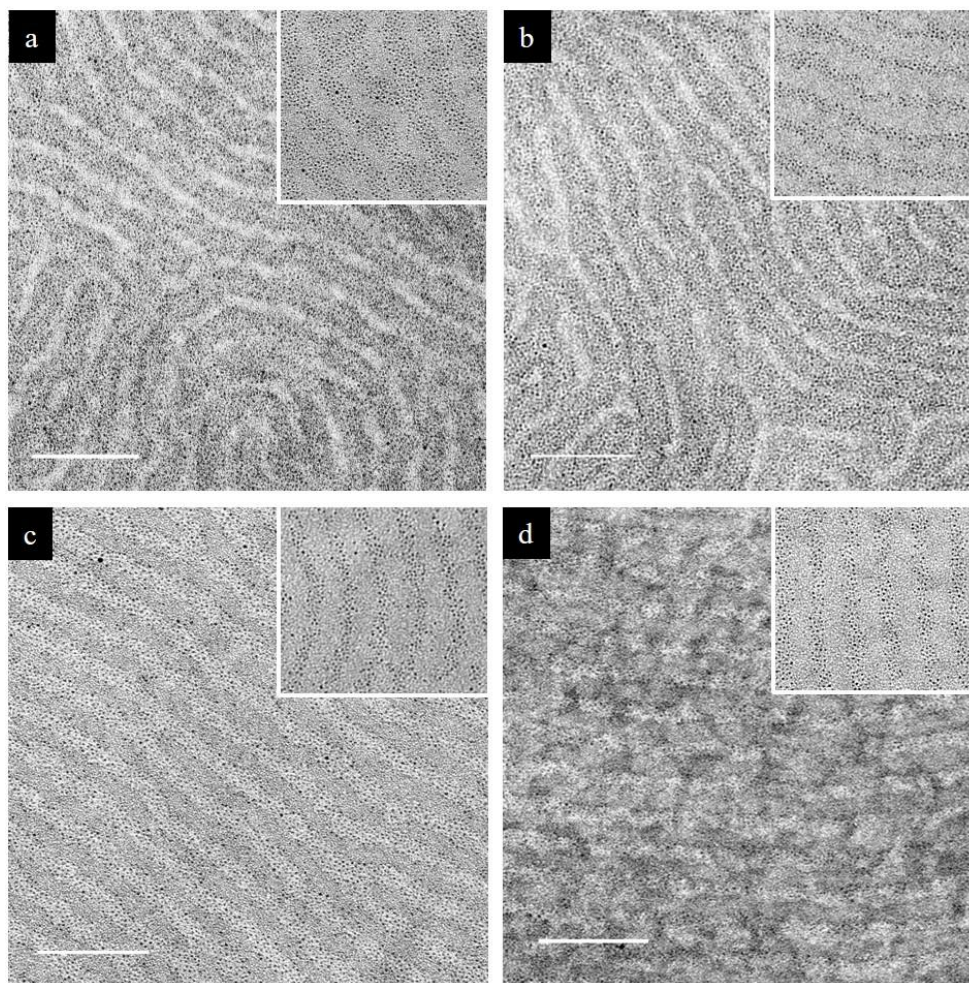
Figure A.4: Transmission electron micrographs of OsO<sub>4</sub> stained and unstained (insets) nanocomposite thin films after thermal annealing at 120 °C for 4 hours, (a) Au<sub>∞</sub>NP/SIS and (b) Au<sub>2.7</sub>NP/SIS. Scale bars correspond to 100 nm; insets are presented at the same magnification. The micrograph in (a) contain globular gold aggregates with affinities for the PI domains. The micrograph in (b) contains AuNP aggregates ( $4 \pm 2$  nm) that preferentially segregate to the PS domains. Reprinted with permission from Mayeda *et al.*, *Chemistry of Materials*, 2012, 24(14), 2627-2634.

Samples were thermally annealed at 120 °C, which is above the glass transition temperatures for PS and PI, under roughing pump vacuum for 2, 4, 6, and 12 h. In general, results from thermal annealing exhibit decreased polymer domain order and aggregated gold particulates as compared to solvent vapor annealed equivalents. Despite aggregation of AuNPs, the preferential segregation of the resulting agglomerates exhibits the same domain preference as if solvent vapor annealed; thermally annealed Au<sub>∞</sub>NP/SIS and Au<sub>2.7</sub>NP/SIS samples yielded Au agglomerates that preferentially resided in PI and PS domains, respectively.

In the case of the Au<sub>∞</sub>NP/SIS, sample results were invariant across annealing times (Figure A.4a). Longer annealing times did not appreciably increase the parallel-oriented grain sizes.

In the case of the Au<sub>2.7</sub>NP/SIS, samples that were annealed for less than 2 h showed poor ordering, and the Au<sub>2.7</sub>NPs did not preferentially segregate to either polymer domain. Samples that were annealed for 4 h or longer yielded PS-segregating Au<sub>2.7</sub>NPs and grain sizes large enough to show inhomogeneous distributions of Au<sub>2.7</sub>NPs in the PS domains (Figure A.4b).

## A.6 TEM Micrographs



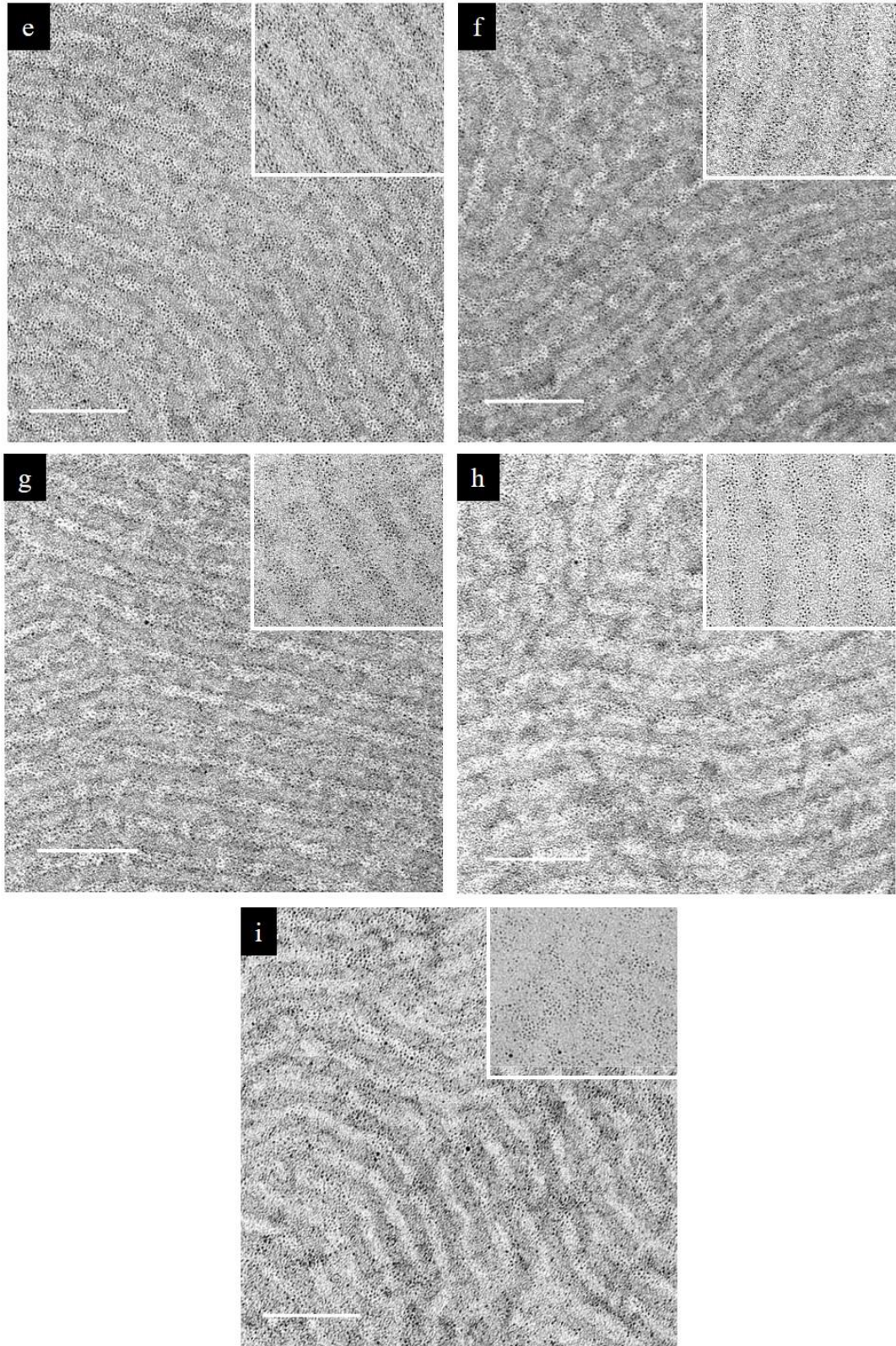


Figure A.5: TEM micrographs of OsO<sub>4</sub> stained (a) Au<sub>6.6</sub>NP/SIS, (b) Au<sub>5.1</sub>NP/SIS, (c) Au<sub>4.8</sub>NP/SIS, (d) Au<sub>4.5</sub>NP/SIS, (e) Au<sub>4.1</sub>NP/SIS, (f) Au<sub>3.1</sub>NP/SIS, (g) Au<sub>2.8</sub>NP/SIS, (h) Au<sub>2.7</sub>NP/SIS, (i) Au<sub>∞</sub>NP/Au<sub>2.7</sub>NP/SIS. Scale bars correspond to 100 nm. Inset images are unstained and at the same magnification. In micrographs a-h, unstained images confirm AuNP segregation. AuNPs do not show preference for one polymer domain in (i), which highlights the stability of the gold-thiol bond. Reprinted with permission from Mayeda *et al.*, *Chemistry of Materials*, 2012, 24(14), 2627-2634.

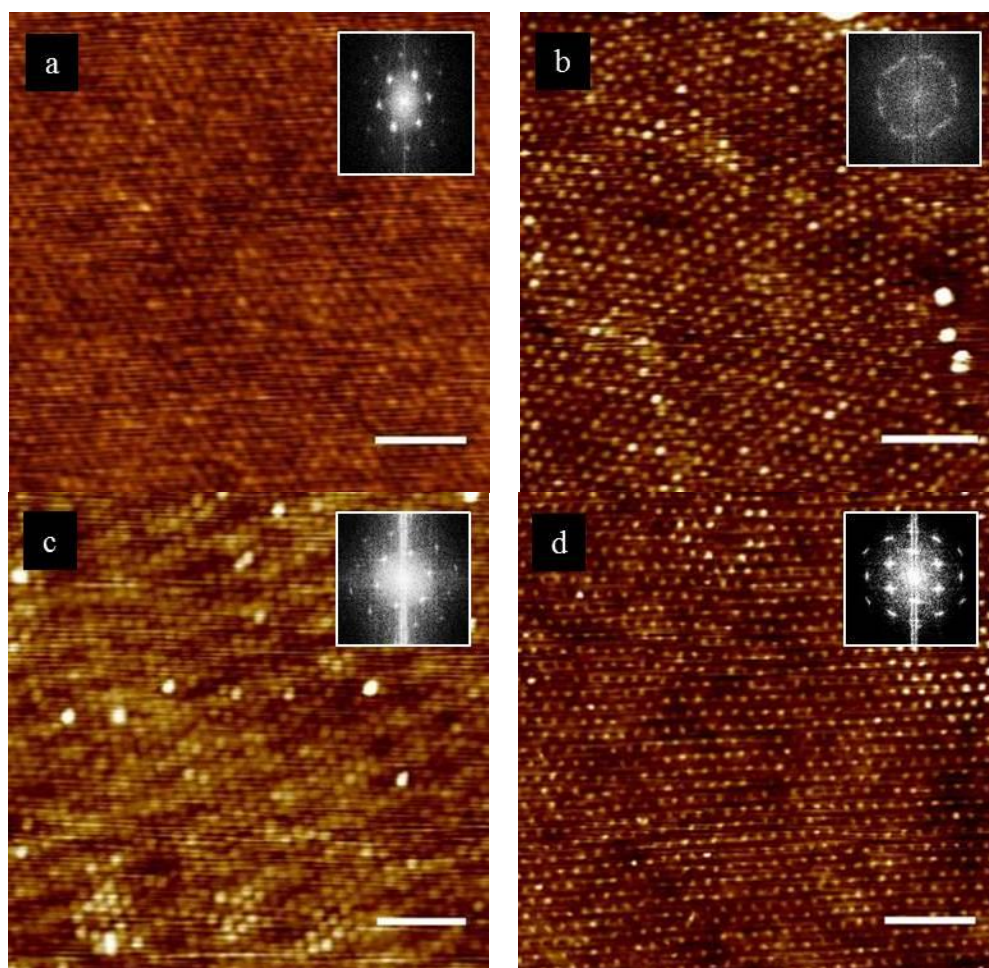
### A.7 Tomogram Movie

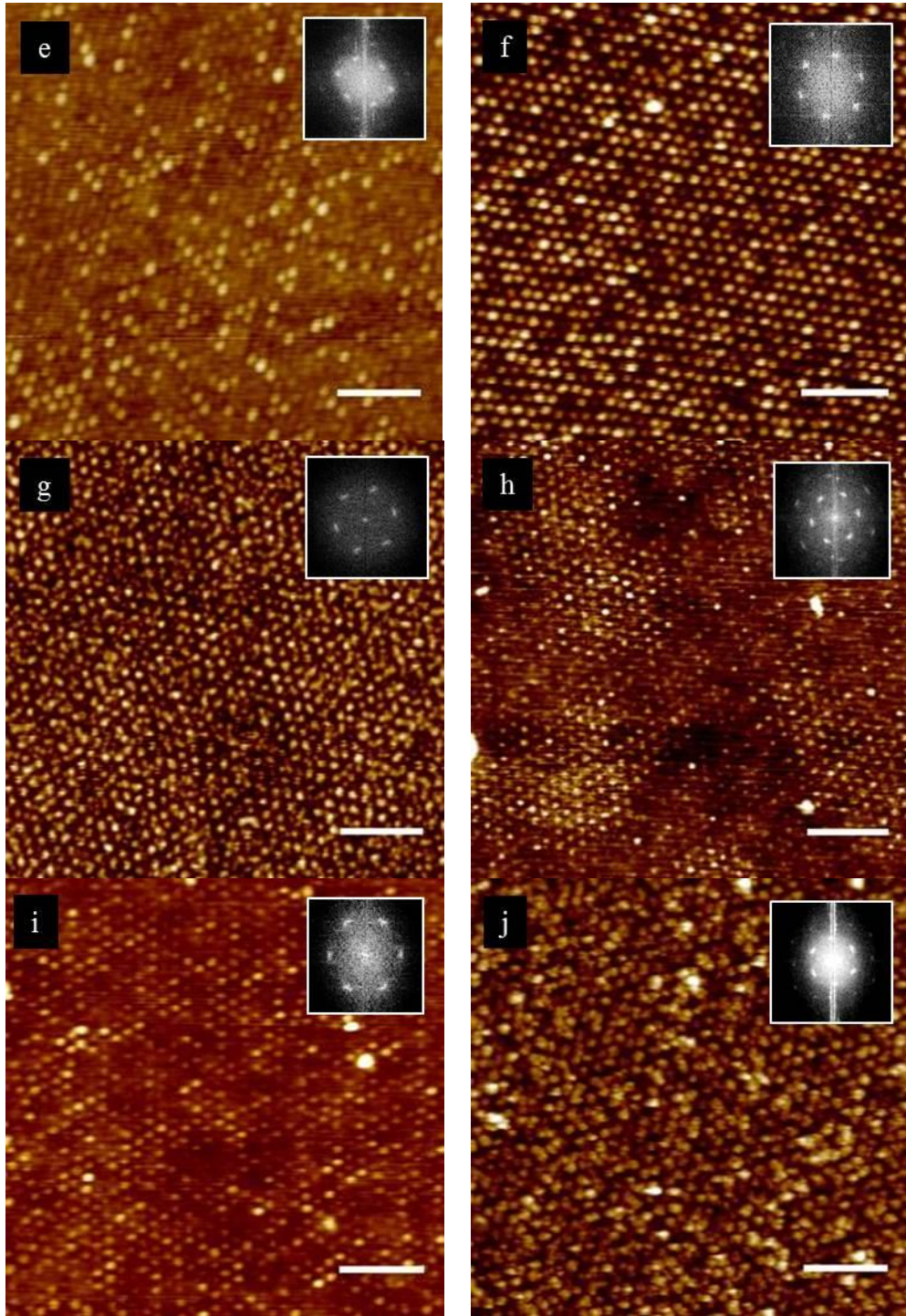
The tomogram movie (Mayeda\_tomogram.mpg) cycles through Z-slices of the reconstructed tomogram of Au<sub>4.5</sub>NP/SIS. The composite sample contains 0.4 vol% nanoparticle loading; the sample was THF annealed and is not stained. Au<sub>4.5</sub>NPs come into and out of focus as one might expect of particles clustered into a specific polymer domain.

## Appendix B

### SUPPORTING INFORMATION FOR CHAPTER 4

#### B.1 AFM of Metal Oxides





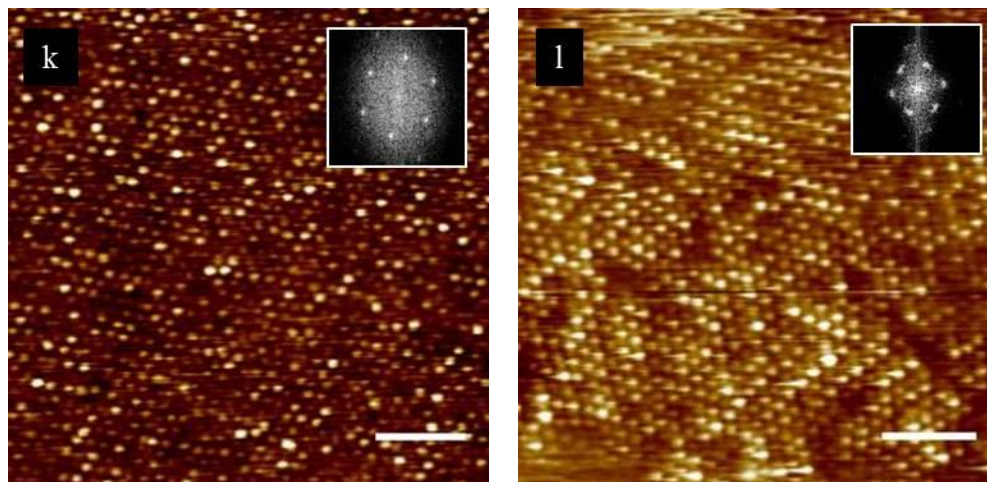


Figure B.1: AFM height images of metal oxides templated by the SPICE method: (a) MgO, (b) Al<sub>2</sub>O<sub>3</sub>, (c) MnO<sub>2</sub>, (d) Fe<sub>2</sub>O<sub>3</sub>, (e) Co<sub>3</sub>O<sub>4</sub>, (f) NiO, (g) CuO, (h) ZnO, (i) ZrO<sub>2</sub>, (j) SnO<sub>2</sub>, (k) Ce<sub>2</sub>O<sub>3</sub>, and (l) RuO<sub>2</sub>. Insets are FFTs of the entire image. Scale bars represent 200 nm. Reprinted with permission from Mayeda *et al.*, *Journal of Materials Chemistry A*, 2015, 3(15), 7822-7829.

The SPICE method was used to template MgO, Al<sub>2</sub>O<sub>3</sub>, TiO<sub>2</sub>, MnO<sub>2</sub>, Fe<sub>2</sub>O<sub>3</sub>, Co<sub>3</sub>O<sub>4</sub>, NiO, CuO, ZnO, ZrO<sub>2</sub>, RuO<sub>2</sub>, SnO<sub>2</sub>, and Ce<sub>2</sub>O<sub>3</sub>. Representative AFM height images are shown in Figure B.1. FFTs of the image are shown in the insets. The 6-spot pattern is characteristic of hexagonal packing.

## B.2 XPS of Metal Oxides

Table B.1. XPS peak positions and associated full width half maxima (FWHM).

Metal oxide	Position (eV)	FWHM (eV)	Metal oxide	Position (eV)	FWHM (eV)
MgO 2p	50.8	1.7	ZnO 2p <sub>3/2</sub>	1022.7	1.8
RuO <sub>2</sub> 3d <sub>5/2</sub>	280.7	1.8	TiO <sub>2</sub> 2p <sub>3/2</sub> 2p <sub>1/2</sub>	458.9 464.6	1.3 2.3
Al <sub>2</sub> O <sub>3</sub> 2p	74.6	1.8	Fe <sub>2</sub> O <sub>3</sub> 2p <sub>3/2</sub> shake-up 2p <sub>1/2</sub> shake-up	711.2 718.6 724.9 728.2	2.8 5.1 4.0 13.3
CeO <sub>2</sub> 3d <sub>3/2</sub>	916.5	4.4			
MnO <sub>2</sub> 2p <sub>3/2</sub> shake-up 2p <sub>1/2</sub> shake-up	642.2 645.6 654.0 655.3	2.7 5.5 2.5 9.1	NiO 2p <sub>3/2</sub> shake-up 2p <sub>1/2</sub> shake-up	856.7 861.6 874.3 880.0	2.0 7.8 2.6 6.9
Co <sub>3</sub> O <sub>4</sub> 2p <sub>3/2</sub> shake-up 2p <sub>1/2</sub> shake-up	781.7 786.2 797.2 802.9	2.7 8.1 3.5 7.2	Ce <sub>2</sub> O <sub>3</sub> 3d <sub>5/2</sub> 3d <sub>5/2</sub> 3d <sub>3/2</sub> 3d <sub>3/2</sub>	882.0 885.8 900.0 904.2	3.0 3.9 3.5 5.2
CuO 2p <sub>3/2</sub> shake-up 2p <sub>1/2</sub> shake-up	932.9 942.4 952.6 962.4	1.3 5.9 1.8 3.7	ZrO <sub>2</sub> 3d <sub>5/2</sub> 3d <sub>3/2</sub>	182.7 185	1.4 1.5
Cu(OH) <sub>2</sub> 2p <sub>3/2</sub> 2p <sub>1/2</sub>	934.7 954.6	3.7 3.1	SnO <sub>2</sub> 3d <sub>5/2</sub> 3d <sub>3/2</sub>	487.3 495.7	1.4 1.4

XPS data were fit using CasaXPS to determine peak positions and FWHM. Metal oxide signatures were evident in all spectra. No evidence of precursor salts or metals was noted.

### B.3 Titania Loading

By comparing the PEO cylinder volume ( $V_{PEO}$ ) to the  $TiO_2$  volume ( $V_{TiO_2}$ ), a loading ratio can be calculated. The measured height of titania dots, which has a density ( $\rho_{TiO_2}$ ) and formula weight ( $FW_{TiO_2}$ ), was  $5.4 \pm 1.4$  nm when using PS-*b*-PEO films, which had a PEO density ( $\rho_{PEO}$ ) and monomer formula weight ( $FW_{PEO\ unit}$ ), that were 30 nm thick. PEO cylinders and  $TiO_2$  radii were  $8.7 \pm 0.8$  nm and  $8.5 \pm 1.9$  nm, respectively.

$$\left(\frac{\text{mol}_{Ti}}{\text{mol}_{PEO\ unit}}\right) = \left(\frac{V_{TiO_2} \cdot \rho_{TiO_2}}{FW_{TiO_2}}\right) \left(\frac{FW_{PEO\ unit}}{V_{PEO} \cdot \rho_{PEO}}\right) \quad \text{B-1}$$

$$\left(\frac{\text{mol}_{Ti}}{\text{mol}_{PEO\ unit}}\right) = \left(\frac{1.3 \times 10^{-24} \text{m}^3 \cdot 4230 \text{kg} \cdot \text{m}^{-3}}{0.079 \text{kg} \cdot \text{mol}^{-1}}\right) \cdot \left(\frac{0.044 \text{kg} \cdot \text{mol}^{-1}}{7.1 \times 10^{-24} \text{m}^3 \cdot 1130 \text{kg} \cdot \text{m}^{-3}}\right) \quad \text{B-2}$$

$$\left(\frac{\text{mol}_{Ti}}{\text{mol}_{PEO\ unit}}\right) = 0.38 \quad \text{B-3}$$

The loading ratio ( $\text{mol}_{Ti}:\text{mol}_{PEO\ unit} = 0.38$ ) is less than traditional EISA methods, which can reach up to 2 by employing micelles. However, the precursor loading mechanisms for EISA and SPICE are different. A disparity in the precursor loading mechanism is exemplified by EISA-templated  $TiO_2$  dots, which exhibited larger radii (10 nm) despite being templated from a smaller molecular weight BP ( $\bar{M}_n = 5,000 \text{g mol}^{-1}$  PEO domain).<sup>37</sup> If the loading mechanisms were similar, the smaller molecular weight BP would be expected to accommodate fewer precursors and thus

produce smaller dots. Instead, loading ratios by the SPICE method should be compared to work by Shan *et al.*; they achieved well-ordered arrays by complexing precursors with homopolymers prior to blending with a BP solution.<sup>51</sup> Their reported loading ratios were 0.18-0.30; however, the ratios were calculated based on the homopolymer solution and not the final precursor/homopolymer/BP solution. In the case of the latter, the loading ratios would have been closer to 0.12-0.20. Therefore, the SPICE method uses relatively large precursor loading ratios and thus minimizes consumed polymer material.

#### B.4 Methylene Blue Catalysis

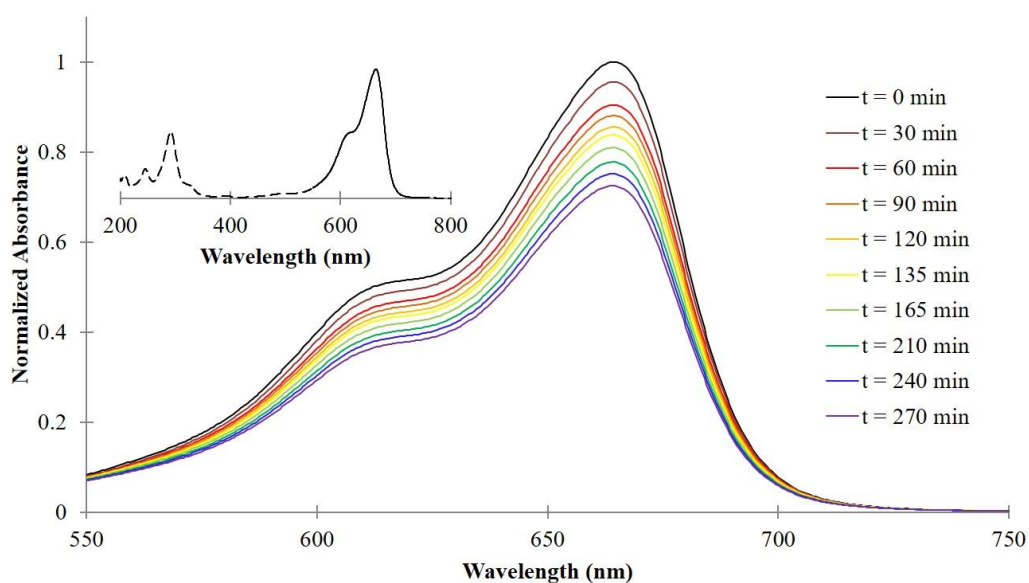


Figure B.2: Representative UV-vis spectra of MB photocatalytically degraded by SPICE TiO<sub>2</sub>. MB solutions were exposed to catalyst and UV irradiation in UV-transparent cuvettes. Spectra were collected in two hour intervals. Inset contains the entire UV-vis spectra of a MB aqueous solution. The peaks between 550-750 nm (solid) were used to evaluate the photocatalytic activity of SPICE TiO<sub>2</sub>, EISA TiO<sub>2</sub>, and Au/SPICE-TiO<sub>2</sub> surfaces. Reprinted with permission from Mayeda *et al.*, *Journal of Materials Chemistry A*, 2015, 3(15), 7822-7829.

MB was used to demonstrate the improved photocatalytic activity of SPICE TiO<sub>2</sub> over traditional EISA TiO<sub>2</sub>. The peaks between 550-750 nm were used to monitor the photocatalytic degradation of MB. Instrument drift was monitored by analyzing a stock MB solution that was not exposed to UV irradiation (Figure B.2 inset) prior to each measurement. Time-lapse data clearly exhibit decreases in peak intensity. MB solution concentrations, which were based on integrated peak areas, were fit to first-order kinetics to determine rate constants (Figure 4.4). By monitoring the UV-vis spectra, it was shown that SPICE TiO<sub>2</sub> was 16% more effective than EISA TiO<sub>2</sub>.

## B.5 TiO<sub>2</sub> Dispersion

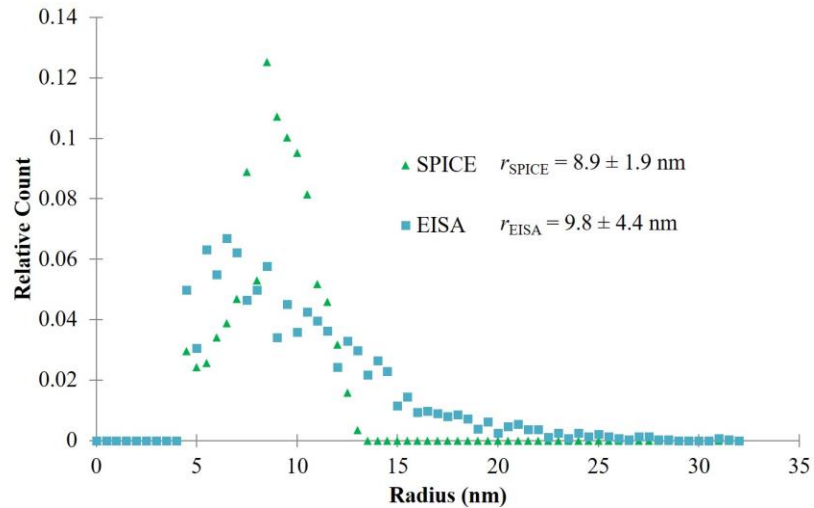


Figure B.3: Size distributions of EISA and SPICE TiO<sub>2</sub> were measured according to the AFM images in Figure 4.2c and Figure 4.2d, respectively. Radii were calculated using ImageJ and binned in 0.5 nm increments. Counts (y-axis) were normalized for the purposes of comparison. Radii ( $r_x$ ) represent the average and standard deviation of each data set. The data represent over 2700 measurements for each AFM image. Reprinted with permission from Mayeda *et al.*, *Journal of Materials Chemistry A*, 2015, 3(15), 7822-7829.

The SPICE method produced a narrower distribution of TiO<sub>2</sub> than the EISA method. The narrower distribution was qualitatively evident by the line scan in Figure 4.2f, but it is quantified here. The variance ( $\sigma$ ) within the distribution of radii were  $\sigma_{\text{SPICE}} = 3.5 \text{ nm}$  and  $\sigma_{\text{EISA}} = 19.6 \text{ nm}$ . With  $\mu$  representing the number average of the distribution, the index of dispersion ( $D$ ) was calculated by the following expression:

$$D = \frac{\sigma^2}{\mu} \quad \text{B-4}$$

The indices of dispersion were  $D_{SPICE} = 1.5$  nm and  $D_{EISA} = 39.2$  nm. A narrower size distribution is one of the key benefits of the SPICE method over the traditional EISA method.

## Appendix C

### SUPPORTING INFORMATION FOR CHAPTER 5

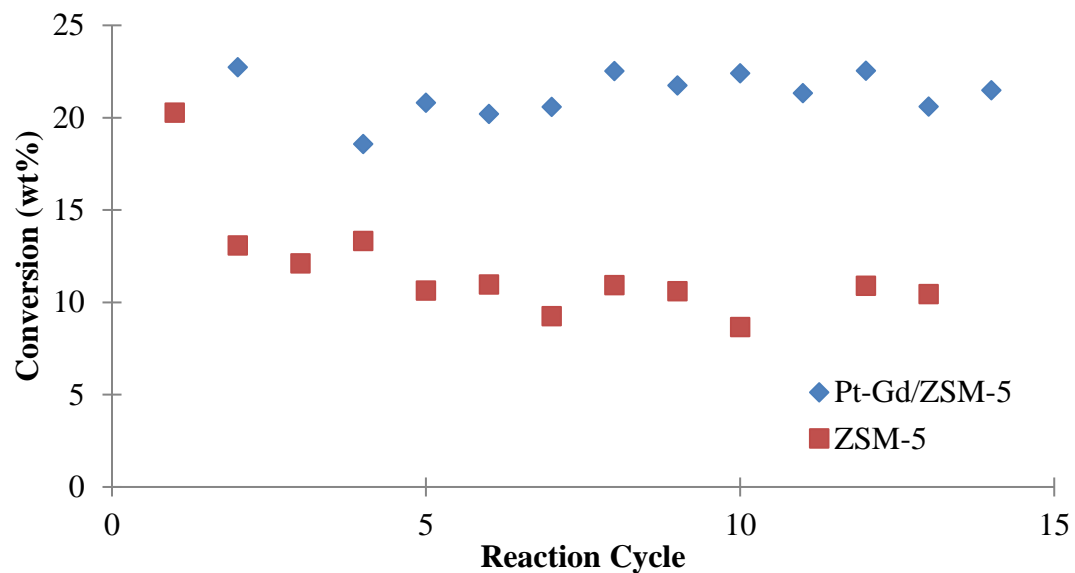


Figure C.1: Weight conversions (determined by GC) as a function of reaction cycle. One reaction cycle is 10 h of reaction followed by 1 h of regeneration. Adapted with permission from Bedenbaugh, J.E. Ph.D. Dissertation, University of Delaware, Newark, 2012.

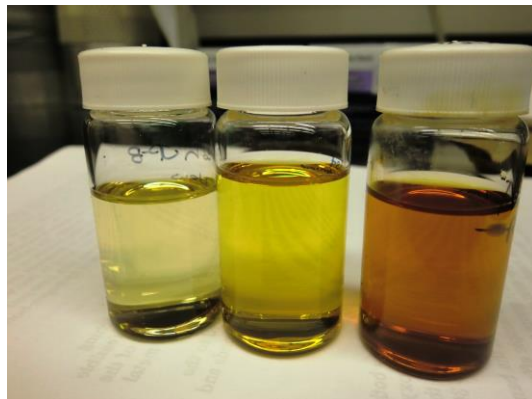


Figure C.2: Picture of (left to right) JP-8, condensed liquid, and recycled liquid. JP-8 is shown with a light yellow hue whereas condensed liquid is bright yellow and recycled liquid is nearly brown.

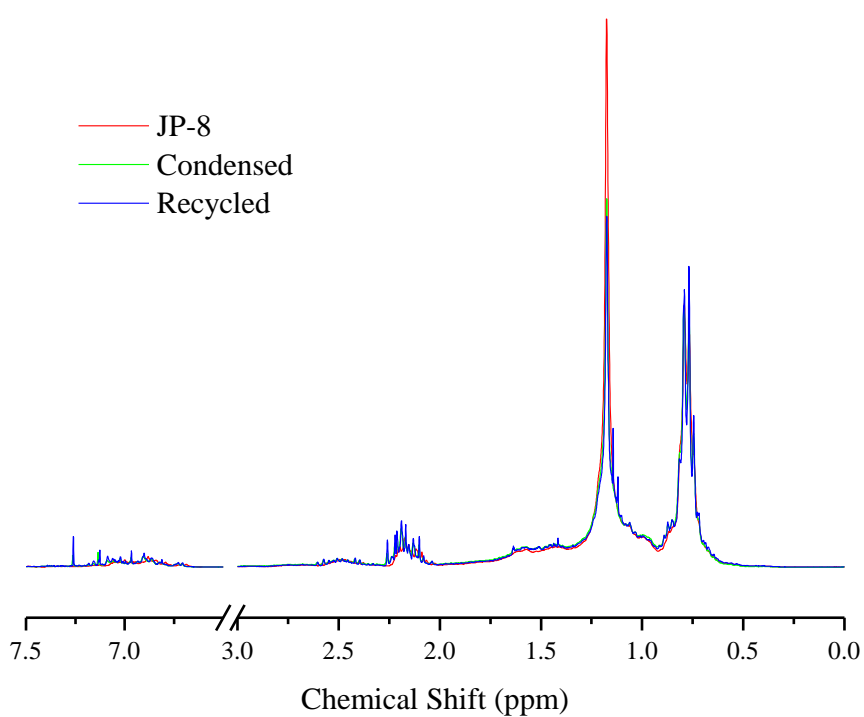
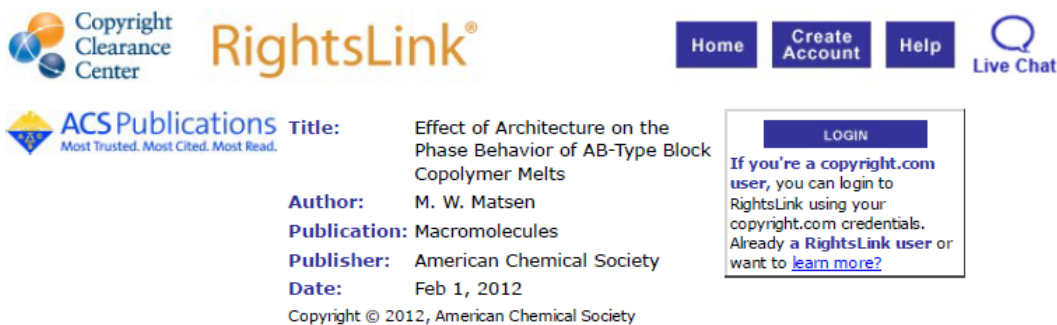


Figure C.3: Overlaid <sup>1</sup>H NMR spectra for JP-8 (red), condensed liquid after cracking (green), and condensed liquid after recycling (blue). Spectra are normalized to the methyl proton peak (0.75 ppm). All spectra show peaks associated with aromatics (6.5-7.5 ppm), unsaturated bonds (2-2.5 ppm), and aliphatics (0.5-1.5 ppm).

## Appendix D

### COPYRIGHT PERMISSIONS

Permission for Figure 1.2



The screenshot shows the Copyright Clearance Center RightsLink interface. At the top left is the Copyright Clearance Center logo. To its right is the RightsLink logo. Further right are navigation buttons for Home, Create Account, and Help, and a Live Chat icon. Below the logos is the ACS Publications logo with the tagline "Most Trusted. Most Cited. Most Read." To the right of the ACS logo, the following information is displayed:

**Title:** Effect of Architecture on the Phase Behavior of AB-Type Block Copolymer Melts  
**Author:** M. W. Matsen  
**Publication:** Macromolecules  
**Publisher:** American Chemical Society  
**Date:** Feb 1, 2012  
Copyright © 2012, American Chemical Society

To the right of this information is a LOGIN button and a text box that reads: "If you're a copyright.com user, you can login to RightsLink using your copyright.com credentials. Already a RightsLink user or want to [learn more?](#)"

#### PERMISSION/LICENSE IS GRANTED FOR YOUR ORDER AT NO CHARGE

This type of permission/license, instead of the standard Terms & Conditions, is sent to you because no fee is being charged for your order. Please note the following:

- Permission is granted for your request in both print and electronic formats, and translations.
- If figures and/or tables were requested, they may be adapted or used in part.
- Please print this page for your records and send a copy of it to your publisher/graduate school.
- Appropriate credit for the requested material should be given as follows: "Reprinted (adapted) with permission from (COMPLETE REFERENCE CITATION). Copyright (YEAR) American Chemical Society." Insert appropriate information in place of the capitalized words.
- One-time permission is granted only for the use specified in your request. No additional uses are granted (such as derivative works or other editions). For any other uses, please submit a new request.

If credit is given to another source for the material you requested, permission must be obtained from that source.

BACK

CLOSE WINDOW

Copyright © 2016 Copyright Clearance Center, Inc. All Rights Reserved. [Privacy statement](#). [Terms and Conditions](#).  
Comments? We would like to hear from you. E-mail us at [customercare@copyright.com](mailto:customercare@copyright.com)

## Permission for Figure 1.3

# NATURE PUBLISHING GROUP LICENSE TERMS AND CONDITIONS

Mar 11, 2016

This is an Agreement between Michael K Mayeda ("You") and Nature Publishing Group ("Nature Publishing Group"). It consists of your order details, the terms and conditions provided by Nature Publishing Group, and the payment terms and conditions.

**All payments must be made in full to CCC. For payment instructions, please see information listed at the bottom of this form.**

License Number	3824491354241
License date	Mar 08, 2016
Licensed Content Publisher	Nature Publishing Group
Licensed Content Publication	Nature
Licensed Content Title	Epitaxial self-assembly of block copolymers on lithographically defined nanopatterned substrates
Licensed Content Author	Sang Ouk Kim, Harun H. Solak, Mark P. Stoykovich, Nicola J. Ferrier, Juan J. de Pablo et al.
Licensed Content Date	Jul 24, 2003
Volume number	424
Issue number	6947
Type of Use	reuse in a dissertation / thesis
Requestor type	academic/educational
Format	print and electronic
Portion	figures/tables/illustrations
Number of figures/tables /illustrations	1
High-res required	no
Figures	Figure 2c
Author of this NPG article	no
Your reference number	None
Title of your thesis / dissertation	TEMPLATING INORGANIC MATERIALS WITH BLOCK POLYMER THIN FILMS AND CATALYZING MILITARY JET FUEL TO LIQUEFIED PETROLEUM GAS
Expected completion date	Jan 2016
Estimated size (number of pages)	250
<b>Total</b>	<b>0.00 USD</b>
Terms and Conditions	

### Terms and Conditions for Permissions

Nature Publishing Group hereby grants you a non-exclusive license to reproduce this material for this purpose, and for no other use, subject to the conditions below:

1. NPG warrants that it has, to the best of its knowledge, the rights to license reuse of this material. However, you should ensure that the material you are requesting is original to Nature Publishing Group and does not carry the copyright of another entity (as credited in the published version). If the credit line on any part of the material you have requested indicates that it was reprinted or adapted by NPG with permission from another source, then you should also seek permission from that source to reuse the material.
2. Permission granted free of charge for material in print is also usually granted for any electronic version of that work, provided that the material is incidental to the work as a whole and that the electronic version is essentially equivalent to, or substitutes for, the print version. Where print permission has been granted for a fee, separate permission must be obtained for any additional, electronic re-use (unless, as in the case of a full paper, this has already been accounted for during your initial request in the calculation of a print run). NB: In all cases, web-based use of full-text articles must be

authorized separately through the 'Use on a Web Site' option when requesting permission.

3. Permission granted for a first edition does not apply to second and subsequent editions and for editions in other languages (except for signatories to the STM Permissions Guidelines, or where the first edition permission was granted for free).
4. Nature Publishing Group's permission must be acknowledged next to the figure, table or abstract in print. In electronic form, this acknowledgement must be visible at the same time as the figure/table/abstract, and must be hyperlinked to the journal's homepage.
5. The credit line should read:  
Reprinted by permission from Macmillan Publishers Ltd: [JOURNAL NAME] (reference citation), copyright (year of publication)  
For AOP papers, the credit line should read:  
Reprinted by permission from Macmillan Publishers Ltd: [JOURNAL NAME], advance online publication, day month year (doi: 10.1038/sj.[JOURNAL ACRONYM].XXXXX)

**Note: For republication from the *British Journal of Cancer*, the following credit lines apply.**

Reprinted by permission from Macmillan Publishers Ltd on behalf of Cancer Research UK: [JOURNAL NAME] (reference citation), copyright (year of publication)For AOP papers, the credit line should read:

Reprinted by permission from Macmillan Publishers Ltd on behalf of Cancer Research UK: [JOURNAL NAME], advance online publication, day month year (doi: 10.1038/sj.[JOURNAL ACRONYM].XXXXX)

6. Adaptations of single figures do not require NPG approval. However, the adaptation should be credited as follows:

Adapted by permission from Macmillan Publishers Ltd: [JOURNAL NAME] (reference citation), copyright (year of publication)

**Note: For adaptation from the *British Journal of Cancer*, the following credit line applies.**

Adapted by permission from Macmillan Publishers Ltd on behalf of Cancer Research UK: [JOURNAL NAME] (reference citation), copyright (year of publication)

7. Translations of 401 words up to a whole article require NPG approval. Please visit <http://www.macmillanmedicalcommunications.com> for more information. Translations of up to a 400 words do not require NPG approval. The translation should be credited as follows:

Translated by permission from Macmillan Publishers Ltd: [JOURNAL NAME] (reference citation), copyright (year of publication).

**Note: For translation from the *British Journal of Cancer*, the following credit line applies.**

Translated by permission from Macmillan Publishers Ltd on behalf of Cancer Research UK: [JOURNAL NAME] (reference citation), copyright (year of publication)

are certain that all parties will benefit from this agreement and wish you the best in the use of this material. Thank you.  
cial Terms:

ons? [customer care@copyright.com](mailto:customer care@copyright.com) or +1-855-239-3415 (toll free in the US) or +1-978-646-2777.

## Permission for Table 1.2



RightsLink®

Home

Create Account

Help



ACS Publications  
Most Trusted. Most Cited. Most Read.

**Title:** Complexation and form of poly(vinylpyridine) derivatives with copper(II) in aqueous solution  
**Author:** Hiroshi Nishikawa, Eishun Tsuchida  
**Publication:** The Journal of Physical Chemistry B  
**Publisher:** American Chemical Society  
**Date:** Sep 1, 1975  
Copyright © 1975, American Chemical Society

LOGIN

If you're a **copyright.com user**, you can login to RightsLink using your copyright.com credentials. Already a **RightsLink user** or want to [learn more?](#)

### PERMISSION/LICENSE IS GRANTED FOR YOUR ORDER AT NO CHARGE

This type of permission/license, instead of the standard Terms & Conditions, is sent to you because no fee is being charged for your order. Please note the following:

- Permission is granted for your request in both print and electronic formats, and translations.
- If figures and/or tables were requested, they may be adapted or used in part.
- Please print this page for your records and send a copy of it to your publisher/graduate school.
- Appropriate credit for the requested material should be given as follows: "Reprinted (adapted) with permission from (COMPLETE REFERENCE CITATION). Copyright (YEAR) American Chemical Society." Insert appropriate information in place of the capitalized words.
- One-time permission is granted only for the use specified in your request. No additional uses are granted (such as derivative works or other editions). For any other uses, please submit a new request.

If credit is given to another source for the material you requested, permission must be obtained from that source.

BACK

CLOSE WINDOW

Copyright © 2016 [Copyright Clearance Center, Inc.](#) All Rights Reserved. [Privacy statement.](#) [Terms and Conditions.](#)  
Comments? We would like to hear from you. E-mail us at [customercare@copyright.com](mailto:customercare@copyright.com)

## Permission for Figure 1.5a

# ELSEVIER LICENSE TERMS AND CONDITIONS

Mar 11, 2016

This is an Agreement between Michael K Mayeda ("You") and Elsevier ("Elsevier"). It consists of your order details, the terms and conditions provided by Elsevier, and the payment terms and conditions.

**All payments must be made in full to CCC. For payment instructions, please see information listed at the bottom of this form.**

Supplier	Elsevier Limited The Boulevard, Langford Lane Kidlington, Oxford, OX5 1GB, UK
Registered Company Number	1982084
Customer name	Michael K Mayeda
Customer address	4501 Bentley Drive COLUMBIA, SC 29210
License number	3824500171265
License date	Mar 08, 2016
Licensed content publisher	Elsevier
Licensed content publication	Chemical Engineering Journal
Licensed content title	Block copolymer-templated synthesis of highly organized mesoporous TiO <sub>2</sub> -based films and their photoelectrochemical applications
Licensed content author	Jia Hong Pan, X.S. Zhao, Wan In Lee
Licensed content date	1 June 2011
Licensed content volume number	170
Licensed content issue number	2-3
Number of pages	18
Start Page	363
End Page	380
Type of Use	reuse in a thesis/dissertation
Intended publisher of new work	other
Portion	figures/tables/illustrations
Number of figures/tables/illustrations	1
Format	both print and electronic
Are you the author of this Elsevier article?	No
Will you be translating?	No
Original figure numbers	Figure 2
Title of your thesis/dissertation	TEMPLATING INORGANIC MATERIALS WITH BLOCK POLYMER THIN FILMS AND CATALYZING MILITARY JET FUEL TO LIQUEFIED PETROLEUM GAS
Expected completion date	Jan 2016
Estimated size (number of pages)	250
Elsevier VAT number	GB 494 6272 12

Price	0.00 USD
VAT/Local Sales Tax	0.00 USD / 0.00 GBP
<b>Total</b>	<b>0.00 USD</b>
<a href="#">Terms and Conditions</a>	

#### INTRODUCTION

1. The publisher for this copyrighted material is Elsevier. By clicking "accept" in connection with completing this licensing transaction, you agree that the following terms and conditions apply to this transaction (along with the Billing and Payment terms and conditions established by Copyright Clearance Center, Inc. ("CCC"), at the time that you opened your Rightslink account and that are available at any time at <http://myaccount.copyright.com>).

#### GENERAL TERMS

2. Elsevier hereby grants you permission to reproduce the aforementioned material subject to the terms and conditions indicated.
3. Acknowledgement: If any part of the material to be used (for example, figures) has appeared in our publication with credit or acknowledgement to another source, permission must also be sought from that source. If such permission is not obtained then that material may not be included in your publication/copies. Suitable acknowledgement to the source must be made, either as a footnote or in a reference list at the end of your publication, as follows:  
"Reprinted from Publication title, Vol /edition number, Author(s), Title of article / title of chapter, Pages No., Copyright (Year), with permission from Elsevier [OR APPLICABLE SOCIETY COPYRIGHT OWNER]." Also Lancet special credit - "Reprinted from The Lancet, Vol. number, Author(s), Title of article, Pages No., Copyright (Year), with permission from Elsevier."
4. Reproduction of this material is confined to the purpose and/or media for which permission is hereby given.
5. Altering/Modifying Material: Not Permitted. However figures and illustrations may be altered/adapted minimally to serve your work. Any other abbreviations, additions, deletions and/or any other alterations shall be made only with prior written authorization of Elsevier Ltd. (Please contact Elsevier at [permissions@elsevier.com](mailto:permissions@elsevier.com))
6. If the permission fee for the requested use of our material is waived in this instance, please be advised that your future requests for Elsevier materials may attract a fee.
7. Reservation of Rights: Publisher reserves all rights not specifically granted in the combination of (i) the license details provided by you and accepted in the course of this licensing transaction, (ii) these terms and conditions and (iii) CCC's Billing and Payment terms and conditions.
8. License Contingent Upon Payment: While you may exercise the rights licensed immediately upon issuance of the license at the end of the licensing process for the transaction, provided that you have disclosed complete and accurate details of your proposed use, no license is finally effective unless and until full payment is received from you (either by publisher or by CCC) as provided in CCC's Billing and Payment terms and conditions. If full payment is not received on a timely basis, then any license preliminarily granted shall be deemed automatically revoked and shall be void as if never granted. Further, in the event that you breach any of these terms and conditions or any of CCC's Billing and Payment terms and conditions, the license is automatically revoked and shall be void as if never granted. Use of materials as described in a revoked license, as well as any use of the materials beyond the scope of an unrevoked license, may constitute copyright infringement and publisher reserves the right to take any and all action to protect its copyright in the materials.
9. Warranties: Publisher makes no representations or warranties with respect to the licensed material.
10. Indemnity: You hereby indemnify and agree to hold harmless publisher and CCC, and their respective officers, directors, employees and agents, from and against any and all claims arising out of your use of the licensed material other than as specifically authorized pursuant to this license.
11. No Transfer of License: This license is personal to you and may not be sublicensed, assigned, or transferred by you to any other person without publisher's written permission.
12. No Amendment Except in Writing: This license may not be amended except in a writing signed by both parties (or, in the case of publisher, by CCC on publisher's behalf).
13. Objection to Contrary Terms: Publisher hereby objects to any terms contained in any purchase order, acknowledgment, check endorsement or other writing prepared by you, which terms are inconsistent with these terms and conditions or CCC's Billing and Payment terms and conditions. These terms and conditions, together with CCC's Billing and Payment terms and conditions (which are incorporated herein), comprise the entire agreement between you and publisher (and CCC) concerning this licensing transaction. In the event of any conflict between your obligations established by these terms and conditions and those established by CCC's Billing and Payment terms and conditions, these terms and conditions shall control.
14. Revocation: Elsevier or Copyright Clearance Center may deny the permissions described in this License at their sole discretion, for any reason or no reason, with a full refund payable to you. Notice of such denial will be made using the contact information provided by you. Failure to receive such notice will not alter or invalidate the denial. In no event will Elsevier or Copyright Clearance Center be responsible or liable for any costs, expenses or damage incurred by you as a result of a denial of your permission request, other than a refund of the amount(s) paid by you to Elsevier and/or Copyright Clearance Center for denied permissions.

#### LIMITED LICENSE

The following terms and conditions apply only to specific license types:

15. **Translation:** This permission is granted for non-exclusive world **English** rights only unless your license was granted for translation rights. If you licensed translation rights you may only translate this content into the languages you requested. A professional translator must perform all translations and reproduce the content word for word preserving the integrity of the article.

16. **Posting licensed content on any Website:** The following terms and conditions apply as follows: Licensing material from an Elsevier journal: All content posted to the web site must maintain the copyright information line on the bottom of each image; A hyper-text must be included to the Homepage of the journal from which you are licensing at <http://www.sciencedirect.com/science/journal/xxxxx> or the Elsevier homepage for books at <http://www.elsevier.com>; Central Storage: This license does not include permission for a scanned version of the material to be stored in a central repository such as that provided by Heron/XanEdu. Licensing material from an Elsevier book: A hyper-text link must be included to the Elsevier homepage at <http://www.elsevier.com>. All content posted to the web site must maintain the copyright information line on the bottom of each image.

**Posting licensed content on Electronic reserve:** In addition to the above the following clauses are applicable: The web site must be password-protected and made available only to bona fide students registered on a relevant course. This permission is granted for 1 year only. You may obtain a new license for future website posting.

17. **For journal authors:** the following clauses are applicable in addition to the above:

**Preprints:**

A preprint is an author's own write-up of research results and analysis, it has not been peer-reviewed, nor has it had any other value added to it by a publisher (such as formatting, copyright, technical enhancement etc.). Authors can share their preprints anywhere at any time. Preprints should not be added to or enhanced in any way in order to appear more like, or to substitute for, the final versions of articles however authors can update their preprints on arXiv or RePEc with their Accepted Author Manuscript (see below).

If accepted for publication, we encourage authors to link from the preprint to their formal publication via its DOI. Millions of researchers have access to the formal publications on ScienceDirect, and so links will help users to find, access, cite and use the best available version. Please note that Cell Press, The Lancet and some society-owned have different preprint policies. Information on these policies is available on the journal homepage.

**Accepted Author Manuscripts:** An accepted author manuscript is the manuscript of an article that has been accepted for publication and which typically includes author-incorporated changes suggested during submission, peer review and editor-author communications.

Authors can share their accepted author manuscript:

- immediately
  - via their non-commercial person homepage or blog
  - by updating a preprint in arXiv or RePEc with the accepted manuscript
  - via their research institute or institutional repository for internal institutional uses or as part of an invitation-only research collaboration work-group
  - directly by providing copies to their students or to research collaborators for their personal use
  - for private scholarly sharing as part of an invitation-only work group on commercial sites with which Elsevier has an agreement
- after the embargo period
  - via non-commercial hosting platforms such as their institutional repository
  - via commercial sites with which Elsevier has an agreement

In all cases accepted manuscripts should:

- link to the formal publication via its DOI
- bear a CC-BY-NC-ND license - this is easy to do
- if aggregated with other manuscripts, for example in a repository or other site, be shared in alignment with our hosting policy not be added to or enhanced in any way to appear more like, or to substitute for, the published journal article.

**Published journal article (JPA):** A published journal article (PJA) is the definitive final record of published research that appears or will appear in the journal and embodies all value-adding publishing activities including peer review co-ordination, copy-editing, formatting, (if relevant) pagination and online enrichment.

Policies for sharing publishing journal articles differ for subscription and gold open access articles:

**Subscription Articles:** If you are an author, please share a link to your article rather than the full-text. Millions of researchers have access to the formal publications on ScienceDirect, and so links will help your users to find, access, cite, and use the best available version.

Theses and dissertations which contain embedded PJAs as part of the formal submission can be posted publicly by the awarding institution with DOI links back to the formal publications on ScienceDirect.

If you are affiliated with a library that subscribes to ScienceDirect you have additional private sharing rights for others' research

accessed under that agreement. This includes use for classroom teaching and internal training at the institution (including use in course packs and courseware programs), and inclusion of the article for grant funding purposes.

**Gold Open Access Articles:** May be shared according to the author-selected end-user license and should contain a [CrossMark logo](#), the end user license, and a DOI link to the formal publication on ScienceDirect.

Please refer to Elsevier's [posting policy](#) for further information.

18. **For book authors** the following clauses are applicable in addition to the above: Authors are permitted to place a brief summary of their work online only. You are not allowed to download and post the published electronic version of your chapter, nor may you scan the printed edition to create an electronic version. **Posting to a repository:** Authors are permitted to post a summary of their chapter only in their institution's repository.

19. **Thesis/Dissertation:** If your license is for use in a thesis/dissertation your thesis may be submitted to your institution in either print or electronic form. Should your thesis be published commercially, please reapply for permission. These requirements include permission for the Library and Archives of Canada to supply single copies, on demand, of the complete thesis and include permission for Proquest/UMI to supply single copies, on demand, of the complete thesis. Should your thesis be published commercially, please reapply for permission. Theses and dissertations which contain embedded PJAs as part of the formal submission can be posted publicly by the awarding institution with DOI links back to the formal publications on ScienceDirect.

#### **Elsevier Open Access Terms and Conditions**

You can publish open access with Elsevier in hundreds of open access journals or in nearly 2000 established subscription journals that support open access publishing. Permitted third party re-use of these open access articles is defined by the author's choice of Creative Commons user license. See our [open access license policy](#) for more information.

#### **Terms & Conditions applicable to all Open Access articles published with Elsevier:**

Any reuse of the article must not represent the author as endorsing the adaptation of the article nor should the article be modified in such a way as to damage the author's honour or reputation. If any changes have been made, such changes must be clearly indicated.

The author(s) must be appropriately credited and we ask that you include the end user license and a DOI link to the formal publication on ScienceDirect.

If any part of the material to be used (for example, figures) has appeared in our publication with credit or acknowledgement to another source it is the responsibility of the user to ensure their reuse complies with the terms and conditions determined by the rights holder.

#### **Additional Terms & Conditions applicable to each Creative Commons user license:**

**CC BY:** The CC-BY license allows users to copy, to create extracts, abstracts and new works from the Article, to alter and revise the Article and to make commercial use of the Article (including reuse and/or resale of the Article by commercial entities), provided the user gives appropriate credit (with a link to the formal publication through the relevant DOI), provides a link to the license, indicates if changes were made and the licensor is not represented as endorsing the use made of the work. The full details of the license are available at <http://creativecommons.org/licenses/by/4.0>.

**CC BY NC SA:** The CC BY-NC-SA license allows users to copy, to create extracts, abstracts and new works from the Article, to alter and revise the Article, provided this is not done for commercial purposes, and that the user gives appropriate credit (with a link to the formal publication through the relevant DOI), provides a link to the license, indicates if changes were made and the licensor is not represented as endorsing the use made of the work. Further, any new works must be made available on the same conditions. The full details of the license are available at <http://creativecommons.org/licenses/by-nc-sa/4.0>.

**CC BY NC ND:** The CC BY-NC-ND license allows users to copy and distribute the Article, provided this is not done for commercial purposes and further does not permit distribution of the Article if it is changed or edited in any way, and provided the user gives appropriate credit (with a link to the formal publication through the relevant DOI), provides a link to the license, and that the licensor is not represented as endorsing the use made of the work. The full details of the license are available at <http://creativecommons.org/licenses/by-nc-nd/4.0>. Any commercial reuse of Open Access articles published with a CC BY NC SA or CC BY NC ND license requires permission from Elsevier and will be subject to a fee.

Commercial reuse includes:

- Associating advertising with the full text of the Article
- Charging fees for document delivery or access
- Article aggregation
- Systematic distribution via e-mail lists or share buttons

Posting or linking by commercial companies for use by customers of those companies.

#### **20. Other Conditions:**

v1.8

Questions? [customer-care@copyright.com](mailto:customer-care@copyright.com) or +1-855-239-3415 (toll free in the US) or +1-978-646-2777.

## Permission for Figure 1.5b



RightsLink®

Home

Account  
Info

Help



ACS Publications  
Most Trusted. Most Cited. Most Read.

**Title:**

Ordered Mesoporous Silicas and  
Carbons with Large Accessible  
Pores Templated from  
Amphiphilic Diblock Copolymer  
Poly(ethylene oxide)-  
b-polystyrene

Logged in as:

Michael Mayeda

Account #:

3000810933

LOGOUT

**Author:**

Yonghui Deng, Ting Yu, Ying  
Wan, et al

**Publication:**

Journal of the American  
Chemical Society

**Publisher:**

American Chemical Society

**Date:**

Feb 1, 2007

Copyright © 2007, American Chemical Society

### PERMISSION/LICENSE IS GRANTED FOR YOUR ORDER AT NO CHARGE

This type of permission/license, instead of the standard Terms & Conditions, is sent to you because no fee is being charged for your order. Please note the following:

- Permission is granted for your request in both print and electronic formats, and translations.
- If figures and/or tables were requested, they may be adapted or used in part.
- Please print this page for your records and send a copy of it to your publisher/graduate school.
- Appropriate credit for the requested material should be given as follows: "Reprinted (adapted) with permission from (COMPLETE REFERENCE CITATION). Copyright (YEAR) American Chemical Society." Insert appropriate information in place of the capitalized words.
- One-time permission is granted only for the use specified in your request. No additional uses are granted (such as derivative works or other editions). For any other uses, please submit a new request.

If credit is given to another source for the material you requested, permission must be obtained from that source.

BACK

CLOSE WINDOW

Copyright © 2016 Copyright Clearance Center, Inc. All Rights Reserved. [Privacy statement](#). [Terms and Conditions](#).  
Comments? We would like to hear from you. E-mail us at [customecare@copyright.com](mailto:customecare@copyright.com)

Permission for Figure 1.6a and Figure 1.6b

**ROYAL SOCIETY OF CHEMISTRY LICENSE  
TERMS AND CONDITIONS**

Mar 09, 2016

---

---

This Agreement between Michael K Mayeda ("You") and Royal Society of Chemistry ("Royal Society of Chemistry") consists of your license details and the terms and conditions provided by Royal Society of Chemistry and Copyright Clearance Center.

License Number	3825010274362
License date	Mar 09, 2016
Licensed Content Publisher	Royal Society of Chemistry
Licensed Content Publication	Journal of Materials Chemistry C
Licensed Content Title	Homopolymers as nanocarriers for the loading of block copolymer micelles with metal salts: a facile way to large-scale ordered arrays of transition-metal nanoparticles
Licensed Content Author	Lianchen Shan,Sathya Punniyakoti,Margriet J. Van Bael,Kristiaan Temst,Marlies K. Van Bael,Xiaoxing Ke,Sara Bals,Gustaaf Van Tendeloo,Marc D'Olieslaeger,Patrick Wagner,Ken Haenen,Hans-Gerd Boyen
Licensed Content Date	Nov 11, 2013
Licensed Content Volume Number	2
Licensed Content Issue Number	4
Type of Use	Thesis/Dissertation
Requestor type	academic/educational
Portion	figures/tables/images
Number of figures/tables /images	1
Format	print and electronic
Distribution quantity	100
Will you be translating?	no
Order reference number	None
Title of the thesis/dissertation	TEMPLATING INORGANIC MATERIALS WITH BLOCK POLYMER THIN FILMS AND CATALYZING MILITARY JET FUEL TO LIQUEFIED PETROLEUM GAS
Expected completion date	Jan 2016
Estimated size	250
Requestor Location	Michael K Mayeda 4501 Bentley Drive #1024  COLUMBIA, SC 29210 United States Attn: Michael K Mayeda

Billing Type	Invoice
Billing Address	Michael K Mayeda 4501 Bentley Drive #1024  COLUMBIA, SC 29210 United States Attn: Michael K Mayeda
Total	0.00 USD

#### Terms and Conditions

This License Agreement is between {Requestor Name} ("You") and The Royal Society of Chemistry ("RSC") provided by the Copyright Clearance Center ("CCC"). The license consists of your order details, the terms and conditions provided by the Royal Society of Chemistry, and the payment terms and conditions.

#### RSC / TERMS AND CONDITIONS

##### INTRODUCTION

The publisher for this copyrighted material is The Royal Society of Chemistry. By clicking "accept" in connection with completing this licensing transaction, you agree that the following terms and conditions apply to this transaction (along with the Billing and Payment terms and conditions established by CCC, at the time that you opened your RightsLink account and that are available at any time at .

##### LICENSE GRANTED

The RSC hereby grants you a non-exclusive license to use the aforementioned material anywhere in the world subject to the terms and conditions indicated herein. Reproduction of the material is confined to the purpose and/or media for which permission is hereby given.

##### RESERVATION OF RIGHTS

The RSC reserves all rights not specifically granted in the combination of (i) the license details provided by your and accepted in the course of this licensing transaction; (ii) these terms and conditions; and (iii) CCC's Billing and Payment terms and conditions.

##### REVOCATION

The RSC reserves the right to revoke this license for any reason, including, but not limited to, advertising and promotional uses of RSC content, third party usage, and incorrect source figure attribution.

##### THIRD-PARTY MATERIAL DISCLAIMER

If part of the material to be used (for example, a figure) has appeared in the RSC publication with credit to another source, permission must also be sought from that source. If the other source is another RSC publication these details should be included in your RightsLink request. If the other source is a third party, permission must be obtained from the third party. The RSC disclaims any responsibility for the reproduction you make of items owned by a third party.

##### PAYMENT OF FEE

If the permission fee for the requested material is waived in this instance, please be advised that any future requests for the reproduction of RSC materials may attract a fee.

##### ACKNOWLEDGEMENT

The reproduction of the licensed material must be accompanied by the following acknowledgement:

Reproduced ("Adapted" or "in part") from {Reference Citation} (or Ref XX) with

permission of The Royal Society of Chemistry.

If the licensed material is being reproduced from New Journal of Chemistry (NJC), Photochemical & Photobiological Sciences (PPS) or Physical Chemistry Chemical Physics (PCCP) you must include one of the following acknowledgements:

For figures originally published in NJC:

Reproduced ("Adapted" or "in part") from {Reference Citation} (or Ref XX) with permission of The Royal Society of Chemistry (RSC) on behalf of the European Society for Photobiology, the European Photochemistry Association and the RSC.

For figures originally published in PPS:

Reproduced ("Adapted" or "in part") from {Reference Citation} (or Ref XX) with permission of The Royal Society of Chemistry (RSC) on behalf of the Centre National de la Recherche Scientifique (CNRS) and the RSC.

For figures originally published in PCCP:

Reproduced ("Adapted" or "in part") from {Reference Citation} (or Ref XX) with permission of the PCCP Owner Societies.

#### **HYPertext LINKS**

With any material which is being reproduced in electronic form, you must include a hypertext link to the original RSC article on the RSC's website. The recommended form for the hyperlink is <http://dx.doi.org/10.1039/DOI> suffix, for example in the link <http://dx.doi.org/10.1039/b110420a> the DOI suffix is 'b110420a'. To find the relevant DOI suffix for the RSC article in question, go to the Journals section of the website and locate the article in the list of papers for the volume and issue of your specific journal. You will find the DOI suffix quoted there.

#### **LICENSE CONTINGENT ON PAYMENT**

While you may exercise the rights licensed immediately upon issuance of the license at the end of the licensing process for the transaction, provided that you have disclosed complete and accurate details of your proposed use, no license is finally effective unless and until full payment is received from you (by CCC) as provided in CCC's Billing and Payment terms and conditions. If full payment is not received on a timely basis, then any license preliminarily granted shall be deemed automatically revoked and shall be void as if never granted. Further, in the event that you breach any of these terms and conditions or any of CCC's Billing and Payment terms and conditions, the license is automatically revoked and shall be void as if never granted. Use of materials as described in a revoked license, as well as any use of the materials beyond the scope of an unrevoked license, may constitute copyright infringement and the RSC reserves the right to take any and all action to protect its copyright in the materials.

#### **WARRANTIES**

The RSC makes no representations or warranties with respect to the licensed material.

#### **INDEMNITY**

You hereby indemnify and agree to hold harmless the RSC and the CCC, and their respective officers, directors, trustees, employees and agents, from and against any and all claims arising out of your use of the licensed material other than as specifically authorized pursuant to this licence.

#### **NO TRANSFER OF LICENSE**

This license is personal to you or your publisher and may not be sublicensed, assigned, or transferred by you to any other person without the RSC's written permission.

#### **NO AMENDMENT EXCEPT IN WRITING**

This license may not be amended except in a writing signed by both parties (or, in the case of "Other Conditions, v1.2", by CCC on the RSC's behalf).

#### **OBJECTION TO CONTRARY TERMS**

You hereby acknowledge and agree that these terms and conditions, together with CCC's Billing and Payment terms and conditions (which are incorporated herein), comprise the entire agreement between you and the RSC (and CCC) concerning this licensing transaction, to the exclusion of all other terms and conditions, written or verbal, express or implied (including any terms contained in any purchase order, acknowledgment, check endorsement or other writing prepared by you). In the event of any conflict between your obligations established by these terms and conditions and those established by CCC's Billing and Payment terms and conditions, these terms and conditions shall control.

#### **JURISDICTION**

This license transaction shall be governed by and construed in accordance with the laws of the District of Columbia. You hereby agree to submit to the jurisdiction of the courts located in the District of Columbia for purposes of resolving any disputes that may arise in connection with this licensing transaction.

#### **LIMITED LICENSE**

The following terms and conditions apply to specific license types:

##### **Translation**

This permission is granted for non-exclusive world English rights only unless your license was granted for translation rights. If you licensed translation rights you may only translate this content into the languages you requested. A professional translator must perform all translations and reproduce the content word for word preserving the integrity of the article.

##### **Intranet**

If the licensed material is being posted on an Intranet, the Intranet is to be password-protected and made available only to bona fide students or employees only. All content posted to the Intranet must maintain the copyright information line on the bottom of each image. You must also fully reference the material and include a hypertext link as specified above.

##### **Copies of Whole Articles**

All copies of whole articles must maintain, if available, the copyright information line on the bottom of each page.

##### **Other Conditions**

###### **v1.2**

Gratis licenses (referencing \$0 in the Total field) are free. Please retain this printable license for your reference. No payment is required.

If you would like to pay for this license now, please remit this license along with your payment made payable to "COPYRIGHT CLEARANCE CENTER" otherwise you will be invoiced within 48 hours of the license date. Payment should be in the form of a check or money order referencing your account number and this invoice number {Invoice Number}.

Once you receive your invoice for this order, you may pay your invoice by credit card.

Please follow instructions provided at that time.

Make Payment To:

Copyright Clearance Center

Dept 001

P.O. Box 843006

Boston, MA 02284-3006

For suggestions or comments regarding this order, contact Rightslink Customer Support: [customercare@copyright.com](mailto:customercare@copyright.com) or +1-855-239-3415 (toll free in the US) or +1-978-646-2777.

**Questions? [customercare@copyright.com](mailto:customercare@copyright.com) or +1-855-239-3415 (toll free in the US) or +1-978-646-2777.**

---

---

## Permission for Figure 1.6c

### ROYAL SOCIETY OF CHEMISTRY LICENSE TERMS AND CONDITIONS

Mar 08, 2016

This Agreement between Michael K Mayeda ("You") and Royal Society of Chemistry ("Royal Society of Chemistry") consists of your license details and the terms and conditions provided by Royal Society of Chemistry and Copyright Clearance Center.

License Number	3824500314328
License date	Mar 08, 2016
Licensed Content Publisher	Royal Society of Chemistry
Licensed Content Publication	Journal of Materials Chemistry
Licensed Content Title	Precise placements of metal nanoparticles from reversible block copolymer nanostructures
Licensed Content Author	Heesook Cho,Hyungmin Park,Thomas P. Russell,Soojin Park
Licensed Content Date	May 10, 2010
Licensed Content Volume Number	20
Licensed Content Issue Number	24
Type of Use	Thesis/Dissertation
Requestor type	academic/educational
Portion	figures/tables/images
Number of figures/tables /images	1
Format	print and electronic
Distribution quantity	100
Will you be translating?	no
Order reference number	None
Title of the thesis/dissertation	TEMPLATING INORGANIC MATERIALS WITH BLOCK POLYMER THIN FILMS AND CATALYZING MILITARY JET FUEL TO LIQUEFIED PETROLEUM GAS
Expected completion date	Jan 2016
Estimated size	250
Requestor Location	Michael K Mayeda 4501 Bentley Drive #1024  COLUMBIA, SC 29210 United States Attn: Michael K Mayeda
Billing Type	Invoice
Billing Address	Michael K Mayeda 4501 Bentley Drive #1024

COLUMBIA, SC 29210  
United States  
Attn: Michael K Mayeda

Total 0.00 USD

#### Terms and Conditions

This License Agreement is between {Requestor Name} ("You") and The Royal Society of Chemistry ("RSC") provided by the Copyright Clearance Center ("CCC"). The license consists of your order details, the terms and conditions provided by the Royal Society of Chemistry, and the payment terms and conditions.

### RSC / TERMS AND CONDITIONS

#### INTRODUCTION

The publisher for this copyrighted material is The Royal Society of Chemistry. By clicking "accept" in connection with completing this licensing transaction, you agree that the following terms and conditions apply to this transaction (along with the Billing and Payment terms and conditions established by CCC, at the time that you opened your RightsLink account and that are available at any time at .

#### LICENSE GRANTED

The RSC hereby grants you a non-exclusive license to use the aforementioned material anywhere in the world subject to the terms and conditions indicated herein. Reproduction of the material is confined to the purpose and/or media for which permission is hereby given.

#### RESERVATION OF RIGHTS

The RSC reserves all rights not specifically granted in the combination of (i) the license details provided by your and accepted in the course of this licensing transaction; (ii) these terms and conditions; and (iii) CCC's Billing and Payment terms and conditions.

#### REVOCAION

The RSC reserves the right to revoke this license for any reason, including, but not limited to, advertising and promotional uses of RSC content, third party usage, and incorrect source figure attribution.

#### THIRD-PARTY MATERIAL DISCLAIMER

If part of the material to be used (for example, a figure) has appeared in the RSC publication with credit to another source, permission must also be sought from that source. If the other source is another RSC publication these details should be included in your RightsLink request. If the other source is a third party, permission must be obtained from the third party. The RSC disclaims any responsibility for the reproduction you make of items owned by a third party.

#### PAYMENT OF FEE

If the permission fee for the requested material is waived in this instance, please be advised that any future requests for the reproduction of RSC materials may attract a fee.

#### ACKNOWLEDGEMENT

The reproduction of the licensed material must be accompanied by the following acknowledgement:

Reproduced ("Adapted" or "in part") from {Reference Citation} (or Ref XX) with permission of The Royal Society of Chemistry.

If the licensed material is being reproduced from New Journal of Chemistry (NJC), Photochemical & Photobiological Sciences (PPS) or Physical Chemistry Chemical

Physics (PCCP) you must include one of the following acknowledgements:

For figures originally published in NJC:

Reproduced ("Adapted" or "in part") from {Reference Citation} (or Ref XX) with permission of The Royal Society of Chemistry (RSC) on behalf of the European Society for Photobiology, the European Photochemistry Association and the RSC.

For figures originally published in PPS:

Reproduced ("Adapted" or "in part") from {Reference Citation} (or Ref XX) with permission of The Royal Society of Chemistry (RSC) on behalf of the Centre National de la Recherche Scientifique (CNRS) and the RSC.

For figures originally published in PCCP:

Reproduced ("Adapted" or "in part") from {Reference Citation} (or Ref XX) with permission of the PCCP Owner Societies.

#### **HYPertext LINKS**

With any material which is being reproduced in electronic form, you must include a hypertext link to the original RSC article on the RSC's website. The recommended form for the hyperlink is <http://dx.doi.org/10.1039/DOI> suffix, for example in the link <http://dx.doi.org/10.1039/b110420a> the DOI suffix is 'b110420a'. To find the relevant DOI suffix for the RSC article in question, go to the Journals section of the website and locate the article in the list of papers for the volume and issue of your specific journal. You will find the DOI suffix quoted there.

#### **LICENSE CONTINGENT ON PAYMENT**

While you may exercise the rights licensed immediately upon issuance of the license at the end of the licensing process for the transaction, provided that you have disclosed complete and accurate details of your proposed use, no license is finally effective unless and until full payment is received from you (by CCC) as provided in CCC's Billing and Payment terms and conditions. If full payment is not received on a timely basis, then any license preliminarily granted shall be deemed automatically revoked and shall be void as if never granted. Further, in the event that you breach any of these terms and conditions or any of CCC's Billing and Payment terms and conditions, the license is automatically revoked and shall be void as if never granted. Use of materials as described in a revoked license, as well as any use of the materials beyond the scope of an unrevoked license, may constitute copyright infringement and the RSC reserves the right to take any and all action to protect its copyright in the materials.

#### **WARRANTIES**

The RSC makes no representations or warranties with respect to the licensed material.

#### **INDEMNITY**

You hereby indemnify and agree to hold harmless the RSC and the CCC, and their respective officers, directors, trustees, employees and agents, from and against any and all claims arising out of your use of the licensed material other than as specifically authorized pursuant to this licence.

#### **NO TRANSFER OF LICENSE**

This license is personal to you or your publisher and may not be sublicensed, assigned, or transferred by you to any other person without the RSC's written permission.

#### **NO AMENDMENT EXCEPT IN WRITING**

This license may not be amended except in a writing signed by both parties (or, in the case of "Other Conditions, v1.2", by CCC on the RSC's behalf).

## OBJECTION TO CONTRARY TERMS

You hereby acknowledge and agree that these terms and conditions, together with CCC's Billing and Payment terms and conditions (which are incorporated herein), comprise the entire agreement between you and the RSC (and CCC) concerning this licensing transaction, to the exclusion of all other terms and conditions, written or verbal, express or implied (including any terms contained in any purchase order, acknowledgment, check endorsement or other writing prepared by you). In the event of any conflict between your obligations established by these terms and conditions and those established by CCC's Billing and Payment terms and conditions, these terms and conditions shall control.

## JURISDICTION

This license transaction shall be governed by and construed in accordance with the laws of the District of Columbia. You hereby agree to submit to the jurisdiction of the courts located in the District of Columbia for purposes of resolving any disputes that may arise in connection with this licensing transaction.

## LIMITED LICENSE

The following terms and conditions apply to specific license types:

### Translation

This permission is granted for non-exclusive world English rights only unless your license was granted for translation rights. If you licensed translation rights you may only translate this content into the languages you requested. A professional translator must perform all translations and reproduce the content word for word preserving the integrity of the article.

### Intranet

If the licensed material is being posted on an Intranet, the Intranet is to be password-protected and made available only to bona fide students or employees only. All content posted to the Intranet must maintain the copyright information line on the bottom of each image. You must also fully reference the material and include a hypertext link as specified above.

### Copies of Whole Articles

All copies of whole articles must maintain, if available, the copyright information line on the bottom of each page.

### Other Conditions

#### v1.2

Gratis licenses (referencing \$0 in the Total field) are free. Please retain this printable license for your reference. No payment is required.

If you would like to pay for this license now, please remit this license along with your payment made payable to "COPYRIGHT CLEARANCE CENTER" otherwise you will be invoiced within 48 hours of the license date. Payment should be in the form of a check or money order referencing your account number and this invoice number {Invoice Number}.

Once you receive your invoice for this order, you may pay your invoice by credit card.

Please follow instructions provided at that time.

### Make Payment To:

Copyright Clearance Center

Dept 001

P.O. Box 843006

Boston, MA 02284-3006

For suggestions or comments regarding this order, contact Rightslink Customer Support: [customer care@copyright.com](mailto:customer care@copyright.com) or +1-855-239-3415 (toll free in the US) or +1-978-646-2777.

**Questions? [customer care@copyright.com](mailto:customer care@copyright.com) or +1-855-239-3415 (toll free in the US) or +1-978-646-2777.**

---

---

## Permission for Chapter 3



RightsLink®

Home

Account  
Info

Help



**Title:**

Controlling Particle Location with  
Mixed Surface Functionalities in  
Block Copolymer Thin Films

Logged in as:

Michael Mayeda

Account #:

3000810933

**Author:**

Michael K. Mayeda, Wei-Fan  
Kuan, Wen-Shiue Young, et al

LOGOUT

**Publication:** Chemistry of Materials

**Publisher:** American Chemical Society

**Date:** Jul 1, 2012

Copyright © 2012, American Chemical Society

### PERMISSION/LICENSE IS GRANTED FOR YOUR ORDER AT NO CHARGE

This type of permission/license, instead of the standard Terms & Conditions, is sent to you because no fee is being charged for your order. Please note the following:

- Permission is granted for your request in both print and electronic formats, and translations.
- If figures and/or tables were requested, they may be adapted or used in part.
- Please print this page for your records and send a copy of it to your publisher/graduate school.
- Appropriate credit for the requested material should be given as follows: "Reprinted (adapted) with permission from (COMPLETE REFERENCE CITATION). Copyright (YEAR) American Chemical Society." Insert appropriate information in place of the capitalized words.
- One-time permission is granted only for the use specified in your request. No additional uses are granted (such as derivative works or other editions). For any other uses, please submit a new request.

BACK

CLOSE WINDOW

Copyright © 2016 Copyright Clearance Center, Inc. All Rights Reserved. [Privacy statement](#). [Terms and Conditions](#).  
Comments? We would like to hear from you. E-mail us at [customercare@copyright.com](mailto:customercare@copyright.com)

Permission for Chapter 4

## **Metal oxide arrays from block copolymer thin film templates**

M. K. Mayeda, J. Hayat, T. H. Epps and J. Lauterbach, *J. Mater. Chem. A*, 2015, **3**, 7822  
DOI: 10.1039/C5TA00117J

This article is licensed under a [Creative Commons Attribution 3.0 Unported Licence](#). Material from this article can be used in other publications provided that the correct acknowledgement is given with the reproduced material.

Reproduced material should be attributed as follows:

- For reproduction of material from NJC:  
[Original citation] - Published by The Royal Society of Chemistry (RSC) on behalf of the Centre National de la Recherche Scientifique (CNRS) and the RSC.
- For reproduction of material from PCCP:  
[Original citation] - Published by the PCCP Owner Societies.
- For reproduction of material from PPS:  
[Original citation] - Published by The Royal Society of Chemistry (RSC) on behalf of the European Society for Photobiology, the European Photochemistry Association, and RSC.
- For reproduction of material from all other RSC journals:  
[Original citation] - Published by The Royal Society of Chemistry.

Information about reproducing material from RSC articles with different licences is available on our [Permission Requests page](#).

Permission for Table 5.2

**JOHN WILEY AND SONS LICENSE  
TERMS AND CONDITIONS**

Mar 11, 2016

This Agreement between Michael K Mayeda ("You") and John Wiley and Sons ("John Wiley and Sons") consists of your license details and the terms and conditions provided by John Wiley and Sons and Copyright Clearance Center.

License Number	3826131238094
License date	Mar 11, 2016
Licensed Content Publisher	John Wiley and Sons
Licensed Content Publication	Advanced Materials
Licensed Content Title	Metal-Assisted Chemical Etching of Silicon: A Review
Licensed Content Author	Zhipeng Huang,Nadine Geyer,Peter Werner,Johannes de Boor,Ulrich Gösele
Licensed Content Date	Sep 21, 2010
Pages	24
Type of use	Dissertation/Thesis
Requestor type	University/Academic
Format	Print and electronic
Portion	Figure/table
Number of figures/tables	1
Original Wiley figure/table number(s)	Figure 6
Will you be translating?	No
Title of your thesis / dissertation	TEMPLATING INORGANIC MATERIALS WITH BLOCK POLYMER THIN FILMS AND CATALYZING MILITARY JET FUEL TO LIQUEFIED PETROLEUM GAS
Expected completion date	Jan 2016
Expected size (number of pages)	250
Requestor Location	Michael K Mayeda 4501 Bentley Drive #1024  COLUMBIA, SC 29210 United States Attn: Michael K Mayeda
Billing Type	Invoice
Billing Address	Michael K Mayeda 4501 Bentley Drive #1024  COLUMBIA, SC 29210 United States Attn: Michael K Mayeda

Total

0.00 USD

[Terms and Conditions](#)

### TERMS AND CONDITIONS

This copyrighted material is owned by or exclusively licensed to John Wiley & Sons, Inc. or one of its group companies (each a "Wiley Company") or handled on behalf of a society with which a Wiley Company has exclusive publishing rights in relation to a particular work (collectively "WILEY"). By clicking "accept" in connection with completing this licensing transaction, you agree that the following terms and conditions apply to this transaction (along with the billing and payment terms and conditions established by the Copyright Clearance Center Inc., ("CCC's Billing and Payment terms and conditions"), at the time that you opened your RightsLink account (these are available at any time at <http://myaccount.copyright.com>).

#### Terms and Conditions

- The materials you have requested permission to reproduce or reuse (the "Wiley Materials") are protected by copyright.
- You are hereby granted a personal, non-exclusive, non-sub licensable (on a stand-alone basis), non-transferable, worldwide, limited license to reproduce the Wiley Materials for the purpose specified in the licensing process. This license, **and any CONTENT (PDF or image file) purchased as part of your order**, is for a one-time use only and limited to any maximum distribution number specified in the license. The first instance of republication or reuse granted by this license must be completed within two years of the date of the grant of this license (although copies prepared before the end date may be distributed thereafter). The Wiley Materials shall not be used in any other manner or for any other purpose, beyond what is granted in the license. Permission is granted subject to an appropriate acknowledgement given to the author, title of the material/book/journal and the publisher. You shall also duplicate the copyright notice that appears in the Wiley publication in your use of the Wiley Material. Permission is also granted on the understanding that nowhere in the text is a previously published source acknowledged for all or part of this Wiley Material. Any third party content is expressly excluded from this permission.
- With respect to the Wiley Materials, all rights are reserved. Except as expressly granted by the terms of the license, no part of the Wiley Materials may be copied, modified, adapted (except for minor reformatting required by the new Publication), translated, reproduced, transferred or distributed, in any form or by any means, and no derivative works may be made based on the Wiley Materials without the prior permission of the respective copyright owner. **For STM Signatory Publishers clearing permission under the terms of the [STM Permissions Guidelines](#) only, the terms of the license are extended to include subsequent editions and for editions in other languages, provided such editions are for the work as a whole in situ and does not involve the separate exploitation of the permitted figures or extracts**, You may not alter, remove or suppress in any manner any copyright,

trademark or other notices displayed by the Wiley Materials. You may not license, rent, sell, loan, lease, pledge, offer as security, transfer or assign the Wiley Materials on a stand-alone basis, or any of the rights granted to you hereunder to any other person.

- The Wiley Materials and all of the intellectual property rights therein shall at all times remain the exclusive property of John Wiley & Sons Inc, the Wiley Companies, or their respective licensors, and your interest therein is only that of having possession of and the right to reproduce the Wiley Materials pursuant to Section 2 herein during the continuance of this Agreement. You agree that you own no right, title or interest in or to the Wiley Materials or any of the intellectual property rights therein. You shall have no rights hereunder other than the license as provided for above in Section 2. No right, license or interest to any trademark, trade name, service mark or other branding ("Marks") of WILEY or its licensors is granted hereunder, and you agree that you shall not assert any such right, license or interest with respect thereto
- NEITHER WILEY NOR ITS LICENSORS MAKES ANY WARRANTY OR REPRESENTATION OF ANY KIND TO YOU OR ANY THIRD PARTY, EXPRESS, IMPLIED OR STATUTORY, WITH RESPECT TO THE MATERIALS OR THE ACCURACY OF ANY INFORMATION CONTAINED IN THE MATERIALS, INCLUDING, WITHOUT LIMITATION, ANY IMPLIED WARRANTY OF MERCHANTABILITY, ACCURACY, SATISFACTORY QUALITY, FITNESS FOR A PARTICULAR PURPOSE, USABILITY, INTEGRATION OR NON-INFRINGEMENT AND ALL SUCH WARRANTIES ARE HEREBY EXCLUDED BY WILEY AND ITS LICENSORS AND WAIVED BY YOU.
- WILEY shall have the right to terminate this Agreement immediately upon breach of this Agreement by you.
- You shall indemnify, defend and hold harmless WILEY, its Licensors and their respective directors, officers, agents and employees, from and against any actual or threatened claims, demands, causes of action or proceedings arising from any breach of this Agreement by you.
- IN NO EVENT SHALL WILEY OR ITS LICENSORS BE LIABLE TO YOU OR ANY OTHER PARTY OR ANY OTHER PERSON OR ENTITY FOR ANY SPECIAL, CONSEQUENTIAL, INCIDENTAL, INDIRECT, EXEMPLARY OR PUNITIVE DAMAGES, HOWEVER CAUSED, ARISING OUT OF OR IN CONNECTION WITH THE DOWNLOADING, PROVISIONING, VIEWING OR USE OF THE MATERIALS REGARDLESS OF THE FORM OF ACTION, WHETHER FOR BREACH OF CONTRACT, BREACH OF WARRANTY, TORT, NEGLIGENCE, INFRINGEMENT OR OTHERWISE (INCLUDING, WITHOUT LIMITATION, DAMAGES BASED ON LOSS OF PROFITS, DATA, FILES, USE, BUSINESS OPPORTUNITY OR CLAIMS OF THIRD PARTIES), AND WHETHER OR NOT THE PARTY HAS BEEN ADVISED OF THE POSSIBILITY OF SUCH DAMAGES. THIS LIMITATION SHALL APPLY NOTWITHSTANDING ANY FAILURE OF ESSENTIAL PURPOSE OF ANY

#### LIMITED REMEDY PROVIDED HEREIN.

- Should any provision of this Agreement be held by a court of competent jurisdiction to be illegal, invalid, or unenforceable, that provision shall be deemed amended to achieve as nearly as possible the same economic effect as the original provision, and the legality, validity and enforceability of the remaining provisions of this Agreement shall not be affected or impaired thereby.
- The failure of either party to enforce any term or condition of this Agreement shall not constitute a waiver of either party's right to enforce each and every term and condition of this Agreement. No breach under this agreement shall be deemed waived or excused by either party unless such waiver or consent is in writing signed by the party granting such waiver or consent. The waiver by or consent of a party to a breach of any provision of this Agreement shall not operate or be construed as a waiver of or consent to any other or subsequent breach by such other party.
- This Agreement may not be assigned (including by operation of law or otherwise) by you without WILEY's prior written consent.
- Any fee required for this permission shall be non-refundable after thirty (30) days from receipt by the CCC.
- These terms and conditions together with CCC's Billing and Payment terms and conditions (which are incorporated herein) form the entire agreement between you and WILEY concerning this licensing transaction and (in the absence of fraud) supersedes all prior agreements and representations of the parties, oral or written. This Agreement may not be amended except in writing signed by both parties. This Agreement shall be binding upon and inure to the benefit of the parties' successors, legal representatives, and authorized assigns.
- In the event of any conflict between your obligations established by these terms and conditions and those established by CCC's Billing and Payment terms and conditions, these terms and conditions shall prevail.
- WILEY expressly reserves all rights not specifically granted in the combination of (i) the license details provided by you and accepted in the course of this licensing transaction, (ii) these terms and conditions and (iii) CCC's Billing and Payment terms and conditions.
- This Agreement will be void if the Type of Use, Format, Circulation, or Requestor Type was misrepresented during the licensing process.
- This Agreement shall be governed by and construed in accordance with the laws of the State of New York, USA, without regards to such state's conflict of law rules. Any legal action, suit or proceeding arising out of or relating to these Terms and Conditions or the breach thereof shall be instituted in a court of

competent jurisdiction in New York County in the State of New York in the United States of America and each party hereby consents and submits to the personal jurisdiction of such court, waives any objection to venue in such court and consents to service of process by registered or certified mail, return receipt requested, at the last known address of such party.

#### **WILEY OPEN ACCESS TERMS AND CONDITIONS**

Wiley Publishes Open Access Articles in fully Open Access Journals and in Subscription journals offering Online Open. Although most of the fully Open Access journals publish open access articles under the terms of the Creative Commons Attribution (CC BY) License only, the subscription journals and a few of the Open Access Journals offer a choice of Creative Commons Licenses. The license type is clearly identified on the article.

##### **The Creative Commons Attribution License**

The [Creative Commons Attribution License \(CC-BY\)](#) allows users to copy, distribute and transmit an article, adapt the article and make commercial use of the article. The CC-BY license permits commercial and non-

##### **Creative Commons Attribution Non-Commercial License**

The [Creative Commons Attribution Non-Commercial \(CC-BY-NC\) License](#) permits use, distribution and reproduction in any medium, provided the original work is properly cited and is not used for commercial purposes. (see below)

##### **Creative Commons Attribution-Non-Commercial-NoDerivs License**

The [Creative Commons Attribution Non-Commercial-NoDerivs License](#) (CC-BY-NC-ND) permits use, distribution and reproduction in any medium, provided the original work is properly cited, is not used for commercial purposes and no modifications or adaptations are made. (see below)

##### **Use by commercial "for-profit" organizations**

Use of Wiley Open Access articles for commercial, promotional, or marketing purposes requires further explicit permission from Wiley and will be subject to a fee. Further details can be found on Wiley Online Library <http://olabout.wiley.com/WileyCDA/Section/id-410895.html>

#### **Other Terms and Conditions:**

**v1.10 Last updated September 2015**

Questions? [customercare@copyright.com](mailto:customercare@copyright.com) or +1-855-239-3415 (toll free in the US) or +1-978-646-2777.

---

---